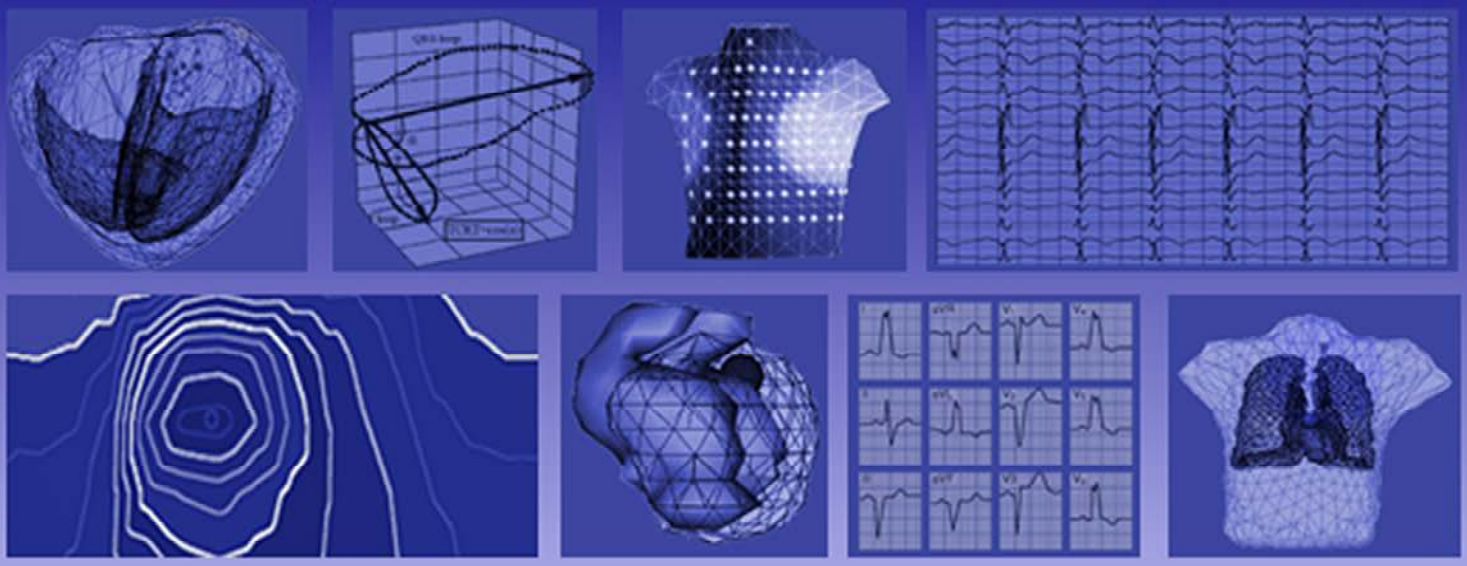

41st International Congress on Electrocardiology
June 4 -7, 2014, Bratislava, Slovakia

ELECTROCARDIOLOGY 2014

Proceedings

Editors:
Milan Tysler
Jana Svehlikova
Ljuba Bacharova
Katarina Kozlikova

ELECTROCARDIOLOGY 2014

PROCEEDINGS

of the 41st International Congress on Electrocardiology

June 4 - 7, 2014, Bratislava, Slovakia

Editors:

Milan Tyšler

Jana Švehlíková

Ljuba Bachárová

Katarína Kozlíková

ELECTROCARDIOLOGY 2014
Proceedings of the 41st International Congress on Electrocardiology

Editors: Milan Tyšler, Jana Švehlíková, Ljuba Bachárová, Katarína Kozlíková
Publisher: Institute of Measurement Science
Slovak Academy of Sciences
Dúbravská cesta 9, 841 04 Bratislava
Slovakia

ISBN 978-80-969-672-7-8

Printed in Slovakia
by VEDA, Publishing House of the Slovak Academy of Sciences

Congress organisers:

International Society of Electrocardiology
Slovak Heart Rhythm Association
Slovak Society of Cardiology
Institute of Measurement Science, Slovak Academy of Sciences

The 41st International Congress on Electrocardiology was organised under the auspices of the International Society of Electrocardiology.

President:	**C. Pastore (Brazil)**
Past President:	**M. Hiraoka (Japan)**
President-Elect:	**W. Zareba (USA)**
Secretary:	**L. Bacharova (Slovakia)**
Treasurer:	**P. W. Macfarlane (UK)**
Council members:	**A. Baranchuk (Canada)**
	L. De Ambroggi (Italy)
	P. Dorostkar (USA)
	B. Gorenek (Turkey)
	T. Ikeda (Japan)
	G. Kozmann (Hungary)
	J. Liebman (USA)
	R. MacLeod (USA)
	P. Platonov (Sweden)
	M. Potse (The Netherlands)
	A. Ribeiro (Brazil)
	M. Roshchevsky (Russia)
	M. Sobieszczanska (Poland)
	M. Tysler (Slovakia)
	A. van Oosterom (The Netherlands)
	G. S. Wagner, ex officio (USA)
Founding Members:	**I. Ruttkay-Nedecky (Slovakia)**
	E. Schubert (Germany)
Honorary Members:	**H. Abel (Germany)**
	R. Selvester (USA)
Executive Committee:	**C. Pastore, M. Hiraoka, W. Zareba,**
	P.W. Macfarlane, L. De Ambroggi, J. Liebman
Membership Board:	**M. Hiraoka, R. MacLeod, M. Sobieszczanska**

Congress President:	**M. Tysler**
Scientific Secretary:	**L. Bacharova**
Program Committee:	**K. Kozlikova** **V. Szathmary** **R. Hatala** **S. Filipova** **I. Simkova** **N. Tribulova** **T. Ravingerova** **L. Gaspar**
Local Organising Committee:	**J. Svehlikova** **E. Bukovenova** **P. Kalavsky**

Preface

The 41st International Congress on Electrocardiology (ICE 2014) will be held in Bratislava, Slovakia from 4th to 7th June 2014. After the successful events in 1983 and 1997, Bratislava will host the congress for the third time in its history. In Bratislava there is a long tradition and high concentration of research and educational activities in the field of electrocardiology. They include the National Institute of Cardiovascular Diseases, Faculty of Medicine of the Comenius University, Slovak Medical University, several institutes of the Slovak Academy of Sciences. All these also contributed to the Congress organisation and their co-workers will present their latest results.

Traditionally, the Congress will offer an opportunity to exchange expertise on latest results of the research, recent technologies, and diagnostic approaches in the field of electrocardiology. The scientific programme includes pre-conference workshop on QRST morphology and a special session on interatrial block as anatomical-electrical substrate for atrial arrhythmias that is devoted to Professor Dr.Antonio Bayès de Luna. Invitation to deliver plenary lectures on selected topics, such as the current role of electrocardiology, cardiac resynchronization therapy or the role of modelling in electrocardiology, accepted Professors Luigi De Ambroggi, Wojciech Zareba, Mark Potse and Jose F. Rodriguez Matas.

The participants submitted more than 120 contributions on their results and finally almost 100 of them are included in the Congress program and abstract book. They will be presented within 15 oral and 2 poster sessions. More than 50 papers are also included in extended form in these proceedings, and we have made an effort to have the proceedings prepared at the time of the Congress. Eleven oral presentations included in the proceedings were submitted also for the traditional Young Investigator Award competition that will be evaluated by a jury chaired by Professor Parvin Dorostkar.

Besides the scientific program, within the three days we will offer the participants also an insight into Slovak culture, history and the life in Slovakia. We hope that they will enjoy the few social events we prepared for them and for the accompanying persons.

We would also like to take this opportunity to thank all of those who were involved in preparing the Congress, namely the people from the local organising committee and the program committee who spent much time for the Congress success but also the reviewers that helped us to select and improve the papers.

We hope that all those who decided to attend the meeting in Bratislava will enjoy both the scientific value and the social program of the Congress.

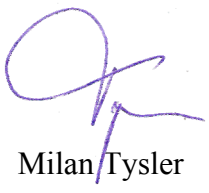

Milan Tysler
Congress President

Ljuba Bacharova
Scientific Secretary

CONTENTS

YIA SESSION II: ECG MARKERS FOR CARDIAC DIAGNOSTICS

ECG IN DIAGNOSTICS OF CARDIAC DISEASES

CARDIAC ELECTROPHYSIOLOGY

MODELING IN ELECTROCARDIOLOGY

HEART RATE VARIABILITY

BODY SURFACE POTENTIAL MAPPING

ATRIAL FIBRILLATIONS

POSTERS: EXPERIMENTAL AND CLINICAL ELECTROCARDIOLOGY

POSTERS: NEW METHODS AND TECHNOLOGIES IN ELECTROCARDIOLOGY

The Rijlant Paper

The Role of Electrocardiography Today

Luigi De Ambroggi

Arrhythmias and Electrophysiology Center,
IRCCS Policlinico San Donato, Milan, Italy
Email: luigi.deambroggi@unimi.it

1. Introduction

The electrocardiography is an old technique born more than one hundred years ago. Augustus Waller published the first human electrocardiographic recording in 1887. In subsequent years, the technique was developed mainly by Einthoven: he invented the string galvanometer, proposed the limb leads and the terminology of the electrocardiographic waves (P, Q, R, S, T).

During the past century the ECG became an indispensable tool for diagnosis and management of patients with varying heart diseases. As pointed out by Fisch [1] the main merit of ECG is to be a non-invasive technique, simple, easily available, reproducible, inexpensive.

Despite the widespread clinical use of electrocardiography, in the last decades the ECG has lost some of its diagnostic importance with the emerging and growing clinical use of newer sophisticated imaging techniques. In fact, anatomic and functional information on several heart conditions (e.g., hypertrophy, location and extension of myocardial infarction, and so on) that in the past were obtained, with various degree of accuracy, almost exclusively by means of electrocardiographic techniques, today can be more precisely and directly obtained by other techniques such as echocardiography, nuclear imaging, magnetic resonance, multislice computed tomography. Nevertheless, still today the ECG provides useful diagnostic and prognostic information in every type of heart disease. It maintains a unique, primary role not only in the field of arrhythmias and conduction disturbances, in which no other technique can provide relevant insights, but also in other clinical settings such as in the ischemic heart disease, particularly during the acute phase.

For the sake of brevity, this presentation will be confined to focus only few most important contributions given by the electrocardiographic technique in the daily cardiology practice and the newer development of ECG imaging.

2. Acute Coronary Syndrome

In this field the ECG is essential for classification of acute myocardial infarction on the basis of the presence or absence of ST elevation (the term STEMI is today commonly used by cardiologists) [2] and hence for the treatment. In patients presenting with symptoms of acute myocardial ischemia a rapid decision-making is mandatory. In this situation the ECG provides essential information on the extent and severity of myocardial ischemia. Moreover the continuous ECG monitoring provides “in real time” the evolution of the ischemic/necrotic process. All these data are important for the choice of treatment and specifically for indicating the need of coronary reperfusion procedures.

3. Cardiac Arrhythmias and Conduction Disturbances

In supraventricular arrhythmias the ECG often allows the correct identification of different types of tachyarrhythmias (atrial tachycardias, flutter, fibrillation) and their arrhythmogenic substrate (e.g.: ectopic focus, A-V nodal re-entry, accessory AV pathway).

In ventricular tachycardias the ability of the ECG to identify the site of origin of the arrhythmias can be poor in presence of extensive myocardial damage (myocardial infarction, scar), but the localization is easier in idiopathic VT (for instance, aortic or pulmonary root).

In genetic arrhythmias, specifically long and short QT syndromes, Brugada syndrome, catecholaminergic polymorphic VT, right ventricular arrhythmogenic cardiomyopathy, the 12- lead ECG plays a paramount diagnostic and prognostic role.

In conduction disturbances the ECG has obviously a primary role in the diagnosis of the various types of AV and intraventricular blocks, indicating the need of different device implantation. Moreover, today it has become also essential in specific situations, such as in ventricular dysfunction/heart failure for selecting patients who can benefit from cardiac resynchronization therapy (biventricular pacing) and for the optimization of the LV lead position [3].

4. Electrocardiografic Markers of Arrhythmias Vulnerability

In addition to the use of ECG for the diagnosis of specific arrhythmias and conduction disturbances, the ECG has gained an important role in the identification of subjects prone to malignant ventricular arrhythmias and sudden cardiac death (SCD), which is still an unsolved problem. In fact, different indices of vulnerability to arrhythmias have been studied, but no marker has proved sufficiently sensitive in predicting high risk. Various methods of analysis of short or long periods of electrocardiographic recordings have been proposed in order to detect information not deducible by the traditional analysis of the standard 12-lead ECG, specifically, signal averaging ECG (ventricular late potentials), T wave alternans, RR/QT relation variations, heart rate variability, heart rate turbulence and others.

Many investigations have focused on the key role of ventricular repolarization abnormalities in the genesis of cardiac arrhythmias. Schematically, vulnerability to arrhythmias can arise from two conditions of repolarization process. 1) Dynamic (beat to beat) variation of repolarization sequence. This condition can be detected exceptionally by visual inspection of routine ECG (for instance in cases of long QT syndrome), because the beat to beat variations of the ST-T waves are usually very subtle (in the order of microvolts) and sophisticated computerized analyses of multiple beats of an ECG tracing have to be used (analysis of T wave alternans,). The prognostic significance of micro T wave alternans was demonstrated by several studies, mainly in patients with ischemic heart disease, and heart failure [4]. 2) State of heterogeneity of repolarization, i.e. a greater than normal dispersion of recovery times. This condition can be detected by analyzing even a single beat, using the 12-lead ECG or body surface potential maps.

Various methods for quantification of repolarization heterogeneity from the standard 12-lead ECG have been proposed: a) QT dispersion: the measurement of 12-lead QT interval dispersion was widely used as an index of repolarization heterogeneity mainly because of its semplicity, but it has several methodological and theoretical limitations, which can explain the controversial results reported in the literature [5]; b) principal component analysis: PCA has been originally applied on body surface potential maps (BSPM) and subsequently also on the 12-lead ECG waveforms. The method defines several independent components, which

contain all the information of the T waves of the ECGs recorded; an increased PCA ratio in the 12-lead ECG was reported to be an independent predictor of cardiovascular mortality [6]; c) T wave morphology descriptors: a set of variables has been proposed [7,8], which measure the spatial and temporal variations of T wave morphology, the difference of the mean wavefront direction between ventricular depolarization and repolarization, the non-dipolar component (total cosine R-to-T, spatial QRS-T angle, T wave residuum).

5. ECG-Imaging

Beyond the traditional clinical use of 12-lead ECG, it is worth mentioning a new modality of electrocardiology which has been developed and applied in humans in the last decade, called ECG-imaging (ECG-I) [9]. The ECG-I, based on mathematical studies and experimental investigations in animal models started in the seventies of the last century and aimed at the solution of the so called "inverse problem of electrocardiography", requires 2 sets of data: the electrocardiographic potentials over the entire thoracic surface (BSPM usually from 250 electrodes) and the geometries of the heart and torso surface obtained by a computed tomography (CT). The recorded torso potential and CT-derived geometric information provide the input data for the ECG-I algorithm, which reconstructs on the heart surface electrograms, potential distributions, activation sequences (isochrones) and repolarization patterns. The ECG-I gives also the possibility to identify, with sufficient degree of accuracy, transmural reentry and intramural focal arrhythmias, and to define ischemic or necrotic areas within the myocardium.

Recently improvements to the inverse solution method were made by van Oosterom and coworkers [10].The required computation time and the quality of the results obtained should facilitate the applications of this inverse procedure in a clinical setting.

The ECG-I has been successfully applied in humans in different situations including the normal heart, hearts with conduction disorders, ventricular pre-excitation, focal activation initiated by right or left ventricular pacing, ventricular tachycardias, focal atrial tachycardia, flutter and atrial fibrillation [11,12]. Recently, the ECG-I was used by other research groups in elctrophysiology laboratory to identify in each patient the different mechanisms initiating and maintaining AF (localization of active sources, rotors, re-entry circuits). These findings were validate by endocardial recordings and catheter ablation results [13, 14].

6. Conclusion

The ECG, in its second century of life, is still quite "vital". In fact, the continuing research in the field of electrocardiology has provided new knowledge that gives the possibility, in clinical setting, to gain from the analysis of the 12-lead ECG more information than in the past for the diagnosis and prognosis of various heart diseases.

Moreover the tremendous advance in technology allows to merge electrical information from ECG with anatomic, functional and metabolic information provided by other imaging modalities. This results in new clinical applications enabling an accurate localization of arrhythmias mechanisms, with respect to cardiac anatomy, useful for catheter ablation guidance.

References

[1] Fish C. The clinical electrocardilogram: a classic. Circulation 62: III-1-4,1989.

[2] Thygesen K, Alpert JS, Jaffe AS, et al. Third universal definition of myocardial infarction. *Circulation* 126: 2020-35, 2012

[3] Van Deursen CJ, Blaauw Y, Witjens MI, Debie L, Wecke L, Crijns HJ, Prinzen FW, Vernooy K. The value of the 12-lead ECG for evaluation and optimization of cardiac resynchronization therapy in daily clinical practice. *Journal of Electrocardiology* 47: 202-11, 2014.

[4] Merchant FM, Ikeda T, Pedretti RF, Salerno-Uriarte JA, Chow T, Chan PS, Bartone C, Hohnloser SH, Cohen RJ, Armoundas AA. Clinical utility of microvolt T-wave alternans testing in identifying patients at high or low risk of sudden cardiac death. *Heart Rhythm* 9:1256-64, 2012

[5] Malik M, Batchvarov VN. Measurement, interpretation and clinical potential of QT dispersion. *Journal of American College of Cardiology* 36:1749-66, 2000.

[6] Okin PM, Devereux RB, Fabsitz RR, et al. Principal component analysis of the T wave and prediction of cardiovascular mortality in american Indians. The strong heart study. *Circulation* 105: 714-719, 2002

[7] Zabel M, Acar,B, Klingenheben T, et al. Analysis of T wave morphology for risk stratification after myocardial infarction. *Circulation* 102: 1252-1257, 2002.

[8] Kardys I, Kors JA, van der Meer IM, Hofman A, van der Kuip DA, Witteman JC. Spatial QRS-T angle predicts cardiac death in a general population. *European Heart Journal* 24: 1357-1364, 2003.

[9] Ramanatham C, Ghanem RN, Jia P, Ryu K, Rudy Y. Noninvasive electrocardiographic imaging for cardiac electrophysiology and arrhythmias. *Nature Medicine* 10: 422-28, 2004.

[10] Van Dam P.M., Oostendorp T.F., Linnenbank A.C., and van Oosterom A. Non-invasive imaging of cardiac activation and recovery. *Annals of Biomedical Engineering* 37: 1739-56, 2009.

[11] Ghanem RN, Jia P, Ramanatham C, Ryu K, Markowitz A, Rudy Y. Noninvasive electrocardiographic imaging (ECGI): comparison to intraoperative mapping in patients. *Heart Rhythm* 2: 339-54, 2005.

[12] Rudy Y. Noninvasive electrocardiographic imaging of arrhythmogenic substrates in humans. Circulation Research 112: 863-74, 20013.

[13] Haissaguerre M, Hocini M, Shah AJ, Derval N, Sacher F, Jais P, Dubois R. Noninvasive panoramic mapping of human atrial fibrillation mechanisms: a feasibility report. *Journal Cardiovascular Electrophysiology* 24: 711-7, 2013.

[14] Cochet H, Dubois R, Sacher F, Derval N, Sermesant M, Hocini M, Montaudon M, Haïssaguerre M, Laurent F, Jaïs P. Cardiac Arrythmias: Multimodal Assessment Integrating Body Surface ECG Mapping into Cardiac Imaging. *Radiology* 271: 239-47, 2014.

ECG in Hypertension, Ischemia and MI

Defining QT/QTc Prolongation During ST-Elevation Myocardial Infarction and Reperfusion

[1]C. Green, [2]W. Kuijt, [1]D. Hegland, [1]B. Atwater, and [1]M. Krucoff

[1]Duke University Medical Center, Durham, NC, USA,
[2]Academic Medical Center, University of Amsterdam, Amsterdam, The Netherlands
Email: cindy.green@duke.edu

Abstract. *Before novel drugs are approved, the US FDA mandates an adequate safety evaluation, including evaluation of measurable QT interval changes. Defining the safety profile of drugs for patients in disease states is a particular challenge, including patients suffering ST-elevation myocardial infarction (STEMI). Although STEMI therapies are effective in restoring perfusion at the epicardial level, ongoing cellular injury "downstream" can result in adverse arrhythmic events and remains an area of active research. To determine if therapies administered during STEMI create an increased safety risk, QT behavior from the disease itself needs to be quantified sufficiently to define boundary conditions evaluative of acute arrhythmic risk. We conducted a feasibility study to define the expected QT range during STEMI and reperfusion. Four cardiologists each measured QT and RR in a random sample of 44 subjects selected from a larger database of 24-hour, continuously recorded, 12-lead electrocardiograms (ECG) previously analyzed for ST-segment deviation. Seven pre-specified time points related to ST deviation were utilized. QTcF mean estimates were computed at each time point using repeated measures analysis, demonstrating the range, accuracy, and variation across different periods of ST deviation and the consistency across readers. More than 1,400 ECGs were measured with mean QTcF estimates by decreasing ST deviation from 416±5.2 to 431±5.2 msec, demonstrating a significant negative correlation between ST-segment deviation and QTcF ($p=0.02$). Intra-observer correlation among each pair of readers ranged from 0.87 to 0.94 and 0.90 to 0.99 for QT and RR, respectively. Study results could provide a global first-in-kind reference standard for patients in a disease state, complementing the existing standards utilized for thorough QT studies in normal volunteers. This STEMI ST-QT reference standard would further inform drug safety research and development paths in actual population of use STEMI studies. Boundaries around the mean QT for risk related to drugs given during STEMI would enable outliers to be characterized as safety concerns for proarrhythmic risk.*

Keywords: ST-segment; QT interval; STEMI; reperfusion

1. Introduction

While QT prolongation is an imperfect biomarker for proarrhythmic risk, a qualitative relationship exists between prolonged QT and the development of arrhythmias such as torsade de point (TdP). The United States (US) Food and Drug Administration (FDA) uses this biomarker as the gold standard for cardiac safety evaluation of new molecular entities (NME). QT studies for FDA submission are routinely performed in healthy volunteers, limiting the information available on cardiovascular safety in actual populations of use. Even more complex is the interpretation of drug-induced QT changes in a population of use whose disease state independently effects repolarization measured as QT interval, such as patients treated with drugs targeting reperfusion injury during ST elevation MI (STEMI). A reliable standard of the disease's impact on QT would be valuable for understanding whether NME exposure during STEMI promotes more QT prolongation than would be expected for STEMI alone. Such a standard would be a first in kind, and if available in the public domain, could be useful to the cardiac safety evaluation of NMEs intended for STEMI care.

Before a NME can be approved for clinical use, the FDA and the International Congress on Harmonisation (ICH) guidelines mandate an appropriate cardiac safety evaluation, including evaluation of such "off-target" effects as prolongation of myocellular action potentials leading to measurable changes in the QT or heart rate-corrected (QTc) interval. The evaluation of a novel drug's effect on cardiac repolarization is usually performed during early clinical development after pharmacokinetics of the drug are known in healthy volunteers to assess cardiac risk and determine if the effect of a novel drug on the QT/QTc interval in target patient populations should be studied further, with optimal designs including exposure to a range of NME doses with confirmed serum drug concentrations mapped against QT prolongation. Based on current ICH E14 guidelines, this positive- and placebo-controlled "thorough QT/QTc study" (TQT) designed to detect a 5 to 10 milliseconds (msec) alteration in the QT/QTc interval is required before new drugs are approved and has stimulated much debate over the best way to measure efficacy of novel drugs while still protecting the public and actual populations of use from potentially harmful treatments.

Defining the safety profile of NMEs in actual patient populations has many challenges compared to the controlled conditions of TQT studies, particularly in populations in which the disease can affect the QT interval. Patients suffering from ST elevation myocardial infarction (STEMI) are one such group. More than 300,000 (21%) of the 1.57 million annual US hospital admissions are due to acute coronary syndromes. [1] Mortality rates in STEMI have been reduced to less than 5% through advances in reperfusion therapies such as thrombolytics and percutaneous coronary intervention (PCI). [2-3] Although therapies for STEMI are effective in restoring perfusion at the epicardial level, ongoing cellular injury "downstream," which can result in heart failure and arrhythmic events, remains an area of active drug research. [4-5]

Establishing if a new treatment administered during the acute phase of a STEMI creates a proarrhythmic safety risk, such as QT/QTc prolongation, requires the development of a reference standard quantifying the natural history of the QT behaviour from the disease itself. Such a standard would need to define boundary conditions of expected QT/QTc changes related to key aspects of the STEMI, such as amplitude, infarct location, and potential interaction with descriptors such as age, sex and diabetes. Such a reference standard provided in the public domain would be a first-in-kind and could significantly promote cardiac safety assessment in these vulnerable and complex patients.

To this end, we performed a retrospective analysis using data randomly selected from a large, existing warehouse of continuously recorded, 12-lead electrocardiograms (ECGs) collected during STEMI and reperfusion available at the ECG Core Laboratory at the Duke Clinical Research Institute (DCRI) to determine the feasibility of creating a public domain reference standard that defines the expected range of dynamic QT/QTc change during STEMI and reperfusion. QT measurements were performed using specialized core laboratory software at time points related to varying degrees of ST elevation and recovery to develop a disease-related boundary for QT/QTc interval behaviour in STEMI before, during, and after reperfusion. If successful, the results of the proposed study could be used to design a larger retrospective study to establish an accurate model for safety evaluation of drugs used as adjuncts to STEMI care and potentially establish a population-of-use standard in the public domain for short term QT exposure for evaluation of the proarrhythmic safety of NMEs in the actual STEMI setting.

2. Subject and Methods

A retrospective analysis using 44 subjects randomly selected from an existing larger database of three primary PCI clinical trials previously analyzed for ST-segment changes were used to investigate temporal fluctuations of the QT/QTc interval during STEMI and following reperfusion. [6] Continuous ECG data were collected using a 12-lead, digital, 24-hour, high-

fidelity NEMON (Northeast Monitoring, Maynard, MA, USA) Holter monitor which acquires and stores a standard 12-lead median beat ECG every 60 seconds for 24 hours. ECG data were analysed at an independent ECG core laboratory (Duke Clinical Research Institute, Durham, NC, USA) blinded to treatment and clinical outcomes.

The QT interval was defined as the duration in milliseconds (msec) from the initial deflection of the Q-wave through the end of the T-wave upon return to isoelectricity using a global superimposed median beat. The end of the T-wave was defined as the intersection of a tangent to the steepest slope of the last limb of the T-wave and the baseline in lead II or lead V5. The global QT measure is not an average, but rather a measure obtained from superimposing all 12 leads onto the joint isoelectric line. This is a standard method used by core laboratories for FDA submissions and is more consistent and reproducible than a lead-specific approach. Four readers were used to confirm reliability and reproducibility of results, while inter- and intra-observer reliability statistics were used to determine agreement among readers based on already existing ECG core laboratory standards. Neither the QT intervals nor ST deviation were measured during conduction abnormalities, such as U-waves or bundle branch block.

Continuous QT interval measurements were made at time points previously labelled for ST-segment deviation during periods of ischemia and subsequent reperfusion. These time points included monitor initiation (ECG prior to PCI), the start and end of each ischemic event, peak ST deviation, first 50% reperfusion, first and last contrast injection, 30 minutes post-PCI, stable reperfusion (reperfusion lasting > 4 hours), and baseline (most normal ECG). Each subject had at least two measurements (monitor initiation and baseline), while most subjects had more than 7 measurements, depending on the number of ischemic episodes and peak ST location. The Fridericia formula (QTcF) was used to obtain a QT measure corrected for heart rate.

A repeated measures linear mixed-effects model was used to estimate the least squares mean QT/QTc effect and QT/QTc variation with associated 95% confidence intervals. Confidence intervals were constructed for the QT/QTc mean estimate using the residual error of the ANCOVA regression model at varying degrees of ST-segment deviation. A p-value < 0.05 was considered statistically significant, and SAS version 9.2 was used all statistical analyses.

3. Results

Four cardiologists each measured QT and RR intervals in 44 randomly selected subjects at seven pre-specified time points previously labelled during ST-segment analyses, giving us 1,413 ECGs for this feasibility exercise. Using repeated measures analysis, QTcF mean estimates with confidence intervals were computed for each time point demonstrating the range, accuracy, and variation across time points that can be obtained from just a small number of the ECGs in our database across different periods of ST elevation and reperfusion. Mean QTcF estimates by decreasing ST deviation ranged from 416±5.2 to 431±5.2 msec, demonstrating a significant negative correlation between ST-segment deviation and QTcF ($p=0.02$).

Intra-observer correlation statistics were computed across all 4 readers and among each possible pair of readers using Shrout-Fleiss methodology. [7] The QT reliability ranged from 0.87 to 0.94 when a single QT measure was considered, while reliability ranged from 0.90 to 0.97 when the average of at least 2 readers was considered demonstrating the stability and consistency of the measures. RR reliability ranged from 0.90 to 0.99.

4. Discussion

Our goal is to create a public domain reference standard that defines the expected range of QT/QTc changes in the setting of dynamic ST-segment changes associated with STEMI and reperfusion. This model would be used to develop a disease-related boundary for QT/QTc

interval behaviour across a range of ST amplitudes and vector locations using a sufficient number of patients to show variability across other descriptors such as age, sex, and diabetes. We propose to establish boundaries for STEMI subjects by defining the expected QT/QTc ranges and boundary conditions within 2-3 standard deviations around the mean effect on QT/QTc for risk related to NMEs given during an acute STEMI. These proposed boundary conditions would enable outliers to be characterized as safety concerns for proarrhythmic risk.

We have previously described ST-elevation and recovery patterns in STEMI patients from more than 12 clinical trials, all using continuous 12-lead ECG monitors. [8] Using this larger dataset, we propose to retrospectively validate our feasibility study findings and quantify QT/QTc at varying degrees of ST deviation. Establishing boundaries in actual STEMI patients will significantly enhance cardiac safety evaluation for novel therapies in these vulnerable patients.

5. Conclusions

We have demonstrated the range, accuracy and variation of QT/QTc estimates across time points related to ST deviation that can be obtained from a small number of the ECGs. The QT-ST negative correlation implies that a relationship exists, and validation of these results in a larger study could provide a global first-in-kind reference standard for actual STEMI patients to complement the existing standards utilized for thorough QT studies in normal volunteers.

References

[1] Antman EM, Hand M, Armstrong, PW, et al. 2008 Focused Update of the ACC/AHA 2004 Guidelines for the Management of Patients with ST-elevation Myocardial Infarction: A Report of the American College of Cardiology/American Heart Association Task Force on Practice Guidelines. *Journal of the American College of Cardiology*, 51 (235), 2008.

[2] Kleiman NS, White HD, Ohman EM, et al. Mortality within 24 Hours of Thrombolysis for Myocardial Infarction. The Importance of Early Reperfusion. The GUSTO Investigators, Global Utilization of Streptokinase and Tissue Plasminogen Activator for Occluded Coronary Arteries. *Circulation*, 90 (6): 2658-65, 1994.

[3] Stone GW, Webb J, Cox DA, et al. Distal Microcirculatory Protection During Percutaneous Coronary Intervention in Acute ST-segment Elevation Myocardial Infarction: A Randomized Controlled Trial. *Journal of the American Medical Association*, 293 (9): 1063-72, 2005.

[4] Cura FA, Escudero A, Berrocal O, et al. Protection of Distal Embolization in High-Risk Patients with Acute ST-segment Elevation Myocardial Infarction (PREMIAR). *American Journal of Cardiology*, 99 (3): 357-63, 2007.

[5] Kandzari DE, Chu A, Brodie BR, et al. Feasibility of Endovascular Cooling as an Adjunct to Primary Percutaneous Coronary Intervention (Results of the LOWTEMP Pilot Study). American Journal of Cardiology, 93 (5): 636-9, 2004.

[6] Bar FW, Tzivoni D, Dirksen MT, et al. Results of the First Clinical Study of Adjunctive CAldaret (MCC-135) in Patients Undergoing Primary Percutaneous Coronary Intervention for ST-elevation Myocardial Infarction: The Randomized Multi-centre CASTEMI study. *European Heart Journal*, 27 (21): 2516-23, 2006.

[7] Shrout PE and Fleiss JL. Intraclass Correlations: Uses in Assessing Rater Reliability. *Psychological Bulletin*, 86: 420-28, 1979.

[8] Krucoff MW, Johanson P, Baeza R, et al. Clinical Utility of Serial and Continuous ST-segment Recovery Assessment in Patients with Acute ST-elevation Myocardial Infarction: Assessing the Dynamics of Epicardial and Myocardial Reperfusion. *Circulation*, 110 (25): 533-9, 2004.

Advance Methods for ECG Evaluation

Excitation Specificity of Repolarization Parameters

[1,2]J. Halamek, [1,2]P. Jurak, [2]P. Leinveber, [2]P. Vesely

[1]Institute of Scientific Instruments AS CR, Brno, Czech Republic
[2]St. Anne's University Hospital, ICRC, Brno, Czech Republic
Email: josef@isibrno.cz

Abstract. *QT/RR coupling was analyzed in two groups of subjects (healthy and hypertensive) with two protocols (exercise and tilt). A dynamic model of QT/RR coupling with 3 optimized parameters was used to analyze dynamic properties (memory and restitution) and to eliminate QT hysteresis. Linear and nonlinear models were used to analyze static properties. Parameter reproducibility was tested by a bootstrap methodology. The linear model is better with the tilt test, the nonlinear model is better in hypertensive patients with the exercise test. QT memory differs significantly between the exercise and tilt test in both groups. The QT/RR slope is steeper in the exercise test and QT adaptation faster with the tilt test. The excitation specificity of QT parameters may explain genetic dependent triggers of arrhythmias and QT/RR nonlinearity.*

Keywords: Repolarization analysis; QT/RR slope; QT restitution; Excitation specificity

1. Introduction

The measurement and analysis of ventricular repolarization began in 1920, when Bazett's correction was originated, though it remains a matter of debate. A number of recommendations exist [1], though unanswered questions remain in all areas (analyzed measurement, QT detection, QT-RR model, and QT parameters). The subject specificity of QT-RR coupling is generally accepted [2-7], and corresponding analysis of QT-RR coupling must be based on measurements with sufficient heart rate changes. Discussion of the type of heart rate stress used and the level of heart rate changes needed to obtain reproducible results is mostly neglected, even though it is known that QT-RR coupling is excitation specific [8,9]. QTc, as QT equivalent for 60 bpm, is used as the basic QT parameter. It should be analyzed after QT hysteresis elimination. Various models of QT-RR coupling and various algorithms of hysteresis elimination are used [2-7]. QT hysteresis is given by the dynamic properties of coupling, and physiological parameters – QT restitution and memory – may be analyzed with the proper model [6]. Analysis of QT parameter dependency on the two types of heart rate stress (exercise and tilt) was our aim.

2. Subjects and Methods

Healthy subjects (21 subjects, age 40±17) and non-medicated hypertensive subjects (21 subjects, age 43±11) were studied with two types of heart stress: exercise and a tilt-table test. Exercise: subject in supine position during three intervals of about 5 minutes each according to the sequence: 1) rest, 2) pedalling at a constant speed with a load of about 1 W/kg, 3) rest. Tilt: subject in supine position for 7 minutes, then tilted to 75° for 10 minutes and returned to the supine position for the last 5 minutes. The lead with the maximal T wave was analyzed with our custom-designed ScopeWin software. The end of the T wave was defined as the crossing between the isoelectric line and the tangent to the descending T wave. The results were visually controlled and distorted parts or parts with a low amplitude of the T wave were marked as non-detectable. A dynamic linear model (Eq. 1) was used to analyze dynamic properties of QT-RR coupling and to eliminate QT hysteresis:

$$qtxm(i) = b_2 rrx(i-1) + b_3 rrx(i-2) - a_1 qtxm(i-1) \quad (1)$$

where rrx(i), qtx(i) and qtxm(i) are i-th values of RR, QT and QTm without mean levels. QTm is model QT and a_1, b_2, b_3 are fitted parameters to achieve the best agreement between QT and QTm.

The parameters a_1, b_2, b_3 define the QT reaction on RR change (Fig. 1a) and the shape of response corresponds extremely well with the known QT response measured in patients with a pacemaker (Fig. 1b). The parameters a_1, b_2, b_3 and mean levels of RR and QT define QT static and dynamic QT parameters. The dynamic parameters are: i) $Gain_S$, i.e. the gain of QT-RR coupling for slow variability of HR, i.e. QT/RR slope; ii) $Gain_F$, i.e. the gain for fast variability of HR, i.e. the QT immediate response, i.e. QT restitution; and τ, i.e. the time constant of QT adaptation. $Gain_S$ and τ describe QT memory, i.e. QT slow adaptation. A more detailed description of the methodology used can be found in [6].

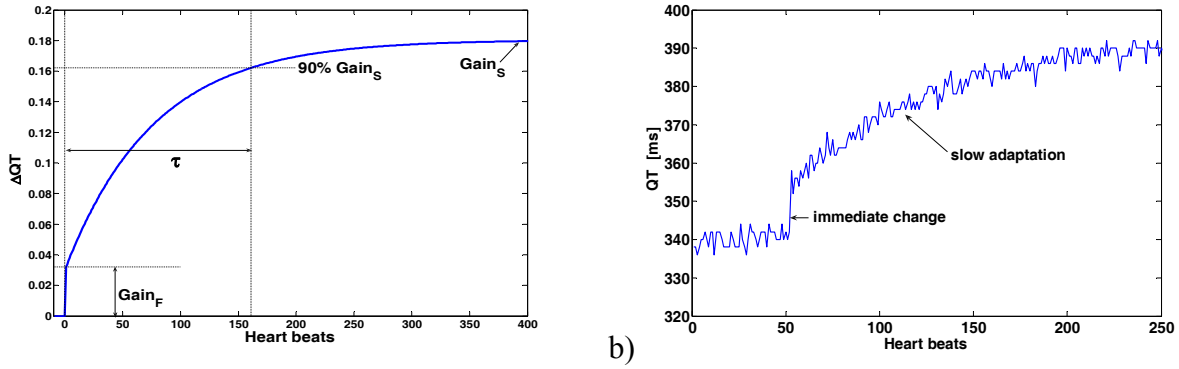

a) b)

Fig. 1. a) QT response on sudden change of RR according to supposed model. b) QT response measured in patient with a pacemaker as the reaction on sudden change of RR.

Parameters a_1, b_2, b_3 may be used to eliminate QT hysteresis, i.e. dynamic properties of QT-RR coupling [3, 5, 6]. Static QT properties (QTc, QT/RR slope, QT nonlinearity) are analyzed using the RRf (filtered RR) that is given by Eq. 2.

$$RRf = filter(b, a, RR - mean(RR)) / GainS + mean(RR) \quad (2)$$

where *filter* and *mean* are Matlab functions and *b, a* are parameters *a1, b2, b3*. An example of hysteresis elimination is given in Fig. 2. Two models of coupling between QT and RRf were tested. The linear (QTL), Eq. 3a, and nonlinear (QTN), Eq. 3b, presented in [4].

$$QTLm = a0 + a1 \times RRf, \quad (3a)$$

$$QTNm = a0 - (\delta/\gamma) \times (1 - RRf^{\gamma}) \quad (3b)$$

where a0, a1, δ and γ are optimized parameters according to the agreement of QTLm or QTNm with QT. The decision on the linearity/nonlinearity of coupling is mostly based on minimal RMS, though this is not sufficient proof. The RMS of QTNm must always be lower, as this model has 3 optimized parameters, as compared to 2 in QTLm. QTc reproducibility is more important than RMS and we tested this reproducibility with a bootstrap methodology [10].

3. Results

QT hysteresis elimination with a dynamic model is presented in Fig. 2. The QT parameters are shown in Tab. 1. The mean levels and STD, together with the statistical significance of differences between exercise and the tilt test, are given in Tab. 1.

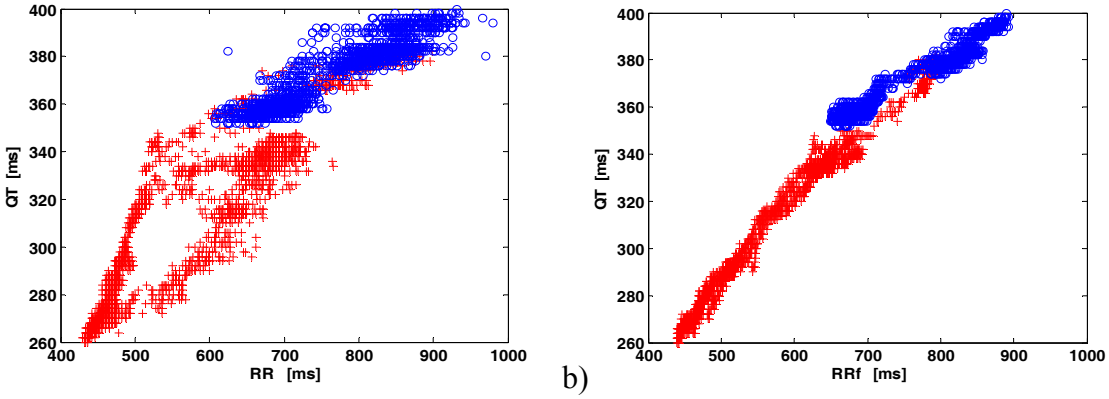

Fig. 2. Healthy subject, red marks '+' exercise test, blue marks 'o' tilt test. a) Raw detected QT and RR intervals. b) Raw QT intervals and filtered RR intervals to eliminate QT hysteresis.

Table 1. Mean levels ± STD. The inaccuracy of parameters, given by a bootstrap methodology and defined as STD/mean in %, is shown after the slash '/'. HY_E, HY_T are hypertensive subjects with exercise and tilt test respectively, CN_E and CN_T are healthy subjects with exercise and tilt test. QTcL and QTcN are QTc given by the linear and nonlinear models respectively, $Gain_S$, $Gain_F$ and τ are QT dynamic parameters, δ/γ is the QT/RR slope of the nonlinear model. The statistical significance of differences between exercise and the tilt test, given by a nonparametric paired t test is: *...P<0.05; **...P<0.01; ***...P<0.001; †...P<0.0001.

	QTcL [ms]	QTcN [ms]	$Gain_S$ [n.u.]	$Gain_F$ [n.u.]	τ [beats]	δ/γ [n.u.]
HY_E	423±30	394±29	0.24±0.06	0.047±0.024	127±41	0.09±0.06
	NS / 0.16 %	NS / 0.14 %	** / 0.93 %	NS / 23 %	* / 6 %	** / 3 %
HY_T	409±35	409±46	0.19±0.06	0.037±0.016	94±57	0.20±0.17
	/ 2.2 %	/ 2.2%	/ 7.2 %	/ 29 %	/ 9 %	/ 9 %
CT_E	395±24	381±20	0.21±0.05	0.040±0.020	161±42	0.12±0.04
	NS / 0.13 %	NS / 0.14 %	*** / 0.8 %	NS / 16 %	† / 4 %	** / 1.6 %
CT_T	386±22	388±23	0.15±0.04	0.032±0.014	75±24	0.17±0.10
	/ 0.06 %	/ 0.4 %	/ 1.2 %	/ 21 %	/ 11 %	/ 8 %

4. Discussion

Two groups of subjects, with two types of heart stress, were analyzed with two QT-RR models. Not all combinations can be discussed. With the tilt test, the QTc does not depend on the model used. With the exercise test, QTcN is shorter than QTcL, P<0.05. This corresponds with the downward shape of the QT-RR curvature and is probably the result of the increased oxygen demand of the working muscles. Some differences, not significant, exist between QTc during tilt and exercise. The sign of the differences depends on the model used. QTcL is longer with exercise, QTcN shorter than with tilt. The increased inaccuracy of QTc with tilt is the result of the lower span of heart rate. The accuracy of QT parameters significantly depends on the level of heart rate changes and on the position of 60 bpm relative to heart rate changes. These results were not presented due to the limited size of the paper.

QT memory, defined by $Gain_S$ and τ, is significantly different in the exercise and tilt tests in both groups. With exercise, the QT/RR slope ($Gain_S$) is significantly steeper and QT adaptation (τ) is significantly longer than with the tilt test. The QT/RR slope given by the nonlinear model (δ/γ) is also significantly different in the exercise and tilt tests, though it is steeper with the tilt test. This is given by definition, as δ/γ defines the slope in the narrow area of 60 bpm and $Gain_S$ defines the slope over the entire span of RR changes.

The excitation specificity of QT parameters may explain different genetic triggers of arrhythmias [8] and QT/RR nonlinearity. The linear model is better with the tilt test; the nonlinear model is better with exercise, where markers corresponding to ischemia occur in some subjects. Dynamic parameters significantly depend on the type of heart rate stress. They define the QT evolution during heart rate changes; they significantly differ between controls and LQT1 subjects [11], and may explain triggers of arrhythmias [8]. On the other hand, insight into the physiological background of QT dynamic parameters, i.e. restitution and memory, together with dependency on type of heart rate stress, is lacking. Extremely well controlled studies with defined provocations will be needed.

Acknowledgements

Research supported by project no. P102/12/2034 from the Grant Agency of the Czech Republic and by the European Regional Development Fund - Project FNUSA-ICRC No. CZ.1.05/1.1.00/02.0123.

References

[1] E14 Clinical evaluation of QT/QTc interval prolongation and proarrhythmic potential for nonantiarrhythmic drugs. Guidance to industry. Fed Regist 2005; 70:61134-61135.

[2] Malik M, Hnatkova K, Kowalski D, et al. Importance of subject-specific QT/RR curvatures in the design of individual heart rate corrections of the QT interval. *Journal of Electrocardiology*, 45: 571-581, 2012.

[3] Malik M. QT/RR hysteresis. *Journal of Electrocardiology,* 47: 236–239, 2014.

[4] Malik M, Hnatkova K, Kowalski D, Keirns JJ, van Gelderen EM. QT/RR Curvatures in healthy subjects: sex differences and covariates. *American Journal of Physiology – heart and circulatory physiology,* 305: H1798-H1806, 2013.

[5] Jacquemet V, Dube B, Knight R, et al. Evaluation of a subject-specific transfer-function-based nonlinear QT interval rate-correction method. *Physiological Measurement*, 6: 619-635, 2011.

[6] J. Halamek, P. Jurak, T. Bunch, et al. Use of a novel transfer function to reduce repolarization interval hysteresis. *Journal of Interventional Cardiac Electrophysiology*, 29: 23–32, 2010.

[7] Jacquemet V, Gonzalez C, Sturmer M, et al. QT interval measurement and correction in patients with atrial flutter: a pilot study. *Journal of Electrocardiology*, 47: 228-235, 2014.

[8] Schwartz PJ, Priori SG, Spazzolini C, et al. Genotype-Phenotype Correlation in the Long-QT Syndrome: Gene-Specific Triggers for Life-threatening Arrhythmias. *Circulation*, 103: 89-95, 2001.

[9] Huysduyen B.H, Swenne C.A, Eck HJ, et al. Hypertensive stress increases dispersion of repolarization. *Pace*, 27: 1603–1609, 2004

[10] Efron B. Bootstrap methods: Another look at the Jackknife. *The Annals of Statistic*, 7:1-26, 1979

[11] Halamek J, Couderc JP, Jurak P, et al. Measure of the QT–RR Dynamic Coupling in Patients with the Long QT Syndrome. *Annals of Noninvasive Electrocardiology*, 17:323–330, 2012

Chaos Theory and Non-linear Dynamics in Hypertensive Cardiopathy and Heart Failure

[1]V.D. Moga, [2]I. Kurcalte, [3]M. Moga, [3]F. Vidu, [4]C. Rezus, [5]I. Cotet, [1]R. Avram

[1]University of Medicine and Pharmacy "V.Babes" Cardiology Clinic Emergency County Hospital Timisoara, Romania
[2]Riga Stradins University, Riga Eastern Clinical University Hospital, Latvia
[3]IT Department of the of the Emergency County Hospital Timisoara
[4]University of Medicine and Pharmacy "Gr.T.Popa" Iasi, Romania
[5]Emergency County Hospital Arad, Romania
Email: moga.victor@gmail.com

Abstract. *Heart failure is worldwide cause for increased morbidity and mortality. High sympathetic activity is a potential factor for ventricular arrhythmias. Depressed heart rate variability (HRV) in heart failure is associated with increased mortality. Nonlinear analysis may quantify abnormalities in RR intervals series based on fractal analysis (chaos theory). Approximate entropy (ApEn) was applied to quantify the regularity and complexity of time series, as well as unpredictability of fluctuations in time series.*
Dynamic analysis based on chaos theory points out the multifractal time series in heart failure patients who loss normal fractal characteristics and regularity in HRV.
Hypertension is a risk factor for the development of heart failure (HF), both because hypertension increases cardiac work, which leads to the development of left ventricular hypertrophy, and because hypertension is a risk factor for the development of coronary heart disease. Knowing the role of the autonomic nervous system (ANS) in the mechanism of hypertension, the challenge is to evaluate the arrhythmic risk of hypertensive patients. Disturbances in the activity of the autonomic nervous system (ANS) also significantly influence the outcome of patients with chronic heart failure (CHF).
A subject open to debate is to compare heart rate variability (HRV) parameters and the chaos theory methods for the assessment of the clinical status and the outcome in hypertensive cardiopathy. Also we consider that it is necessary to improve ventricular arrhythmia prophylaxis in patients with preserved left ventricular left ejection fraction heart failure.

Keywords: Hypertension, heart failure, nonlinear analysis

1. Background

Rhythmic changes of blood pressure, heart rate, and other cardiovascular measures have drawn the attention of several investigators, since these oscillations can shed light onto the activity of the underlying control network [6].

Cardiovascular function is regulated by the autonomic nervous system (ANS). ANS is a neural network that operates at the subconscious level and regulates the visceral functions of the body. The main aim of autonomic cardiovascular regulation is to control cardiac output and the distribution of blood at the central and peripheral levels. Heart rate (HR) and the contractile properties of the myocardium, which contribute to cardiac output, are modulated by the main components of ANS: the parasympathetic and sympathetic nervous systems. The activity of these two ANS branches with opposite effects on HR causes continuous fluctuations in HR, which is called heart rate variability [3, 4].

Heart rate variability (HRV) has become a universal tool to study the neural control of the heart i.e. the delicate interaction between sympathetic and vagal influences on heart rate in

health and disease. HRV can be quantified by the simple calculation of the mean and standard deviation of RR-intervals in the time domain. Furthermore, in the frequency domain, spectral analysis of HRV reveals two distinct frequency regions in the modulation of heart rate in humans. A high frequency region (0.15-0.4 Hz) which is a marker of vagal modulation, and a low frequency region (0.04-0.15 Hz), which reflects predominantly sympathetic tone andbaroreflex activity [2]. A variety of linear, non-linear, periodical and nonperiodical oscillation patterns are present in heart rate fluctuations [1].

Detrended fluctuation analysis (DFA) has been introduced to evaluate the fractal correlation properties of R-R interval dynamics and to characterize the features of HR dynamics that may not be easily detectable by traditional methods of analysis. Breakdown of fractal organization into beat-to-beat R-R interval dynamics indicates increased cardiac vulnerability and a higher risk of mortality in patients with and without structural heart disease [5].

Hypertension represents an important condition that affects the adult population worldwide; it contributes significantly to morbidity and mortality from stroke, heart failure, coronary heart disease and renal failure [7]. The sympatho-vagal balance is altered in the resting conditions of numerous pathophysiological processes. It is the case of essential arterial hypertension (Guzzetti et al. 1988), even in the presence of arterial pressure values still in the high normal range (Lucini et al. 2002). The ability of decreased heart rate variability to predict incident hypertension has not been well studied, and there are no studies of whether hypertension leads to changes in heart rate variability [8].

The purpose of this study was to assess the physiological basis of methods evaluating beat-to-beat R-R interval dynamics and to assess new methods in the evaluation of ventricular arrhythmia and sudden cardiac death in congestive heart failure patients [7]. Finding and analysing hidden dynamical structures of these signals are of basic and clinical interest [2].

2. Method

The study was performed at the Cardiology Clinic of the Emergency County Hospital Timis, University of Medicine and Pharmacy “V. Babes “Timisoara. The study group has included hypertensive patients (n: 47, men: 23, women: 24, mean age: 54.2 yrs.) with hypertension stage II and III WHO classification and patients (n: 61) with heart failure with history of ischaemic heart disease (mean age: 61.3 yrs., M: 42, W: 19).

ECG signal analysis and blood pressure measurements were done using a EC-3H/ABP Combined Holter System, Labtech Ltd. The system performs simultaneously recording of the ECG signal and measurements of the blood pressure.

Twenty four hours of combined ECG and blood pressure monitoring was performed and more than 90 % of the signals and measurements were eligible for the study. Artefacts and noise was manually removed from the signals.

All ECG analysed signals were in sinus rhythm and analysis of heart rate variability was performed in time domain, mean RR intervals (ms.), standard deviation of all RR intervals ms) and frequency domain, very low frequency (VLF, 0.01-0.05 Hz), low frequency (LF, 0.05 -0.15 Hz) and high frequency (HF, 0.15-0.50 Hz), LF/HF ratio. Kubios v. 2.1, Finland (http://kubios.uku.fi/) was used for the measurement of the nonlinear parameters of the RR series. Approximate Sample entropy, detrended fluctuation analysis, and Poincare plots, have been used for the study of the behaviour of the heart rate dynamics.

Trends of heart rate (b/min) and blood pressure (mmHg) were recorded. Left ventricular ejection fraction (LVEF, %) was measured echocardiographic by an independent member of the team.

All patients included in the study underwent noninvasive evaluation comprising a physical examination, 12-lead ECG, chest radiography, M-mode and B-mode echocardiography, and 24-h Holter ECG. Following the left ventricular ejection fraction (LVEF) below 45% and above 45% we subdivided the heart failure group in altered LVEF (< 45%) and preserved LVEF (> 45%) subgroups.

The mean of all RR intervals (NN), standard deviation of all normal–normal RR intervals (SDNN), the nonlinear dynamics parameters, as detrended fluctuation analysis short-term α1 (DFA α1), Poincaré plot analysis, and sample entropy analysis were performed for all ECG signals. From the Poincaré plot analysis, using Kubios HRV 2.0 software, we obtained automatically the values of the short-term scaling exponent (α1).

Spectral power was quantified by fast-Fourier transformation analysis (FFT 256 points, Welch) and by autoregressive method, model 20 in 2 frequency bands: low frequency (0.05 – 0.15 Hz) and high frequency (0.15 – 0.4 Hz). We quantified several time domain HRV parameters: mean HR, standard deviation of normal HR data (SDNN) and the spectral analysis was performed on linearly resampled (1 Hz) time series using Welch's method. The 256-point fast Fourier transform was repeatedly computed with 50% overlap between adjacent segments. [6]. Low-to-high frequency ratio was considered as marker of the autonomic tone.

3. Statistical analysis

For the statistical analysis we used Graph Pad Prism. All numeric variables were expressed as mean and the statistical analysis was performed using Student's t-test and correlation analysis by Pearson method. A p value < 0.05 was considered statistically significant.

4. Results

The characteristics of the study population are presented in Table 1.

Table 1 Characteristics of the study population

Parameters	LVEF > 45 %	LVEF < 45 %	Arrhythmia	Control
No patients	27	29	29	15
Male/Female	15 / 12	22 / 7	22 /7	8 / 7
Age (yrs.)	58.7	63.8	64.8	44.7
LVEF (%)	54.4	37.9	44.3	71.3
NYHA III-IV	12	23	24	0
NSVT	14	16	29	0

The mean age of the patients subgroup with altered LVEF (A) was significant lower compared with the mean age of patients subgroup with preserved LVEF (B), 58.7 vs 63.8 yrs., $p<0.05$. The patients subgroup with altered LVEF was characterized by a higher NYHA functional classes (NYHA III-IV, n: 23) compared to the patients subgroup with preserved LVEF (NYHA III-IV, n: 12). The LVEF was significant lower in subgroup A compared to subgroup B (54 % vs 38 %, $p<0.001$). The subgroup A had a higher incidence of ventricular arrhythmias compared to the subgroup B. The patients subgroup with altered LVEF had a lower heart rate compared to the patients subgroup with preserved LVEF (77 b/min vs 87 b/min), probably as a response to β-blockade, but significant higher compared to the control group.

The SDNN (ms) was significantly lower in the subgroup with altered LVEF when compared to the preserved LVEF group and to control (118 ms vs 141ms vs 167 ms, $p < 0.001$). A high sympathetic tone was noticed in the heart failure group compared to control, expressed as

heart rate or LF/HF ratio (Table 2). Patients with altered LVEF had a high sympathetic tone characterized by a higher heart rate, high LF/HF ratio and depressed high frequency power spectrum density (figure 1). This was correlated with a higher incidence of ventricular arrhythmias.

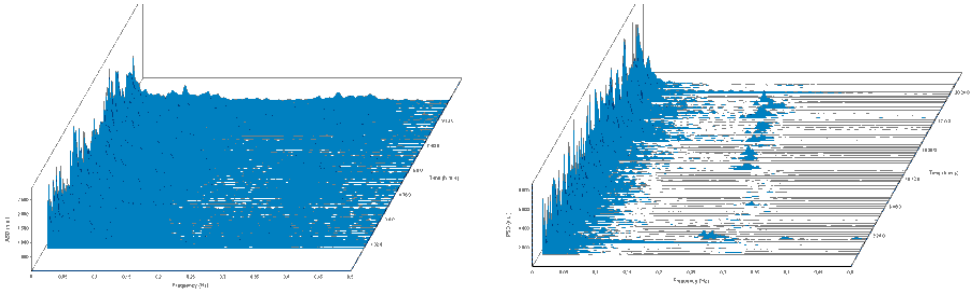

Fig. 1 Power spectral analysis in control group (a) and in the heart failure group (b)

The values of the nonlinear dynamic parameters, like DFA α1 and the Poincaré plots showed altered values (figure 2). DFA α1 was significant lower in the subgroup A compared to the entire heart failure group or to the control group (0.63 vs 0.97, $p < 0.001$).

Analysing the heart failure group, from the perspective of the presence or absence of acute coronary syndrome, we noticed that the most vulnerable patients group was characterized by high heart rate, high LF/HF ratio and low DFA α1, independently to the values of left ventricular ejection fraction (Table 2).

Table 2 HRV and Nonlinear dynamic parameters in heart failure group

	LVEF < 45 %	LVEF > 45 %	Heart Failure	Control Group
N	29	27	56	15
SDNN (ms)	118	141	128.9	167
Heart rate (b/min)	77	87	83.5	72.9
LVEF (%)	37.9	54.4	45.7	71.3
LF/HF	1.74	1.59	1.67	0.85
DFA α1	0.63	0.71	0.68	0.97
DFA α2	0.79	0.87	0.78	0.98
ApEN	0.97	1	0.96	1.21
SamEn	0.87	0.95	0.87	1.15

In the hypertensive group the gender distribution was almost equal, suggesting a higher incidence of essential hypertension in the women population and probably that the men were much earlier hypertensive than women. In the study group, women had mean age: 57 yrs. compared to men mean age: 50.4 yrs. ($p< 0.005$). Differences were noticed also in relation to the mean heart rate. Women were more tachycardic than the men hypertensive population (mean heart rate: 87 b/min vs. 80 b/min), but the differences were statistically significant. Considering only the gender aspects, in the hypertensive group, the left ventricular ejection fraction (LVEF %) seemed to be preserved, LVEF: 60 %, mean LVEF in the men population: 58 % compared to the women mean value: 61 %. In the hypertensive group, those with events had a lower left ventricular ejection compared with the events free hypertensive population (LVEF: 48 % vs. 68 %, $p< 0.005$). All the clinical data are resumed in Table 3.

Table 3 Main clinical characteristics of the hypertensive and the control group.

	Hypertension	Control	P

N	47	20	0.05
Age (yrs.)	54.2	46	0.05
Mean heart rate (b/min)	86	73	0.05
LVEF (%)	60	72	0.05
Systolic Blood Pressure (mmHg)	160	127	< 0.005
Diastolic Blood Pressure (mmHg)	105	75	< 0.005

Analysing the hypertensive group, we noticed differences between the dynamics of heart rate and systolic blood pressure as a measure of the circadian rhythm. The difference between day/night heart rate and blood pressure was considered a useful parameter of the influence of the circadian rhythm (Table 4).

Table 4 The influence of arrhythmic events and heart failure in the hypertensive group

	Hypertension + events	Hypertension - events	P
N	**18**	29	
Age (yrs)	**60.5**	49.7	0.05
Mean heart rate (b/min)	**85**	84	Ns
LVEF (%)	**48**	68	0.005
SBP (mmHg)	**163**	160	Ns
DBP (mmHg)	**97**	107	Ns
Δ HR (b/min)	**9.65**	15.62	0.005
ΔSBP (mmHg)	**27.8**	23.72	0.05

During the study we did not observed significant differences between the absolute values of the systolic blood pressure inside the hypertensive group. Despite this fact some parameters like the difference between day and night mean heart rate could suggest important modulations of the tone autonomic tone in hypertension. More of this, ΔHR (b/min) and ΔSBP (mmHg), the later as expression of the day-night differences in systolic blood pressure, seemed to correlate. The role of the autonomic tone in essential hypertension was assessed using linear and nonlinear parameters. Heart rate variability and nonlinear dynamic parameters like entropy and detrended fractal analysis was applied to the ECG signals obtained from hypertensive patients. Even in a limited and selected group of patients it was difficult to identify vulnerable hypertensive patients. It seemed adequate to perform nonlinear analysis of the RR intervals in hypertensive patients to identify vulnerable patients.

5. Discussion

Heart failure remains nowadays one of the most important clinical condition. This observation is sustained by the high number of patients with heart failure worldwide. Despite numerous studies, the mortality in heart failure remains high. The incidence of ventricular arrhythmias, mainly ventricular tachycardia or ventricular fibrillation represents the most important conditions for sudden cardiac death. Comparing to control group or to patients without heart failure, like in hypertension, our study group was characterized by a high sympathetic tone, expressed by a high heart rate, high LF/HF ratio and altered nonlinear dynamic parameters (figure 2).

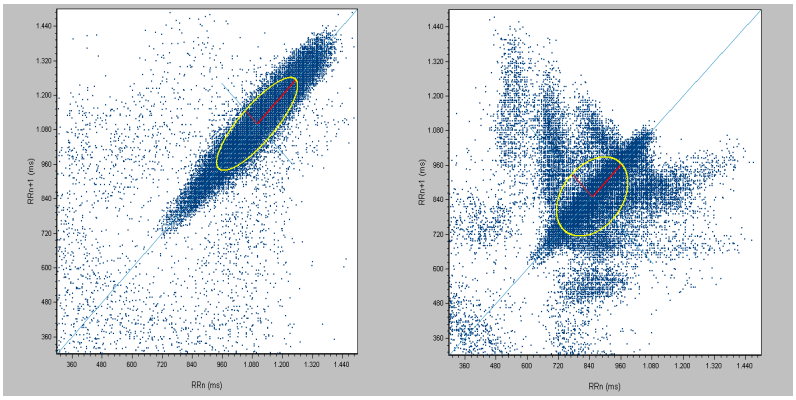

a b

Fig. 2 Nonlinear Dynamic Analysis in control group (a) and heart failure group (b)

We noticed an important association between variability and complexity organization of heart beat fluctuations that might be specific for the process of autonomic imbalance in heart failure and suggests that there are alterations in the cardiac control mechanism associated with ischaemic heart failure.

The aim of the study was to offer significant data about the complex mechanisms involved in heart failure and hypertension. The most important aspect of this study is that even in the presence of early stages of heart diseases the autonomic tone mechanisms are involved in the outcome and prognosis and are detectable by noninvasive methods.

References

[1] AE Aubert, F Beckers, B Seps: Non-linear Dynamics of Heart Rate Variability in Athletes: Effect of Training. *Computers in Cardiology* 2002;29:441−444

[2] Ahsan H Khandoker et all: Identifying diabetic patients with cardiac autonomic neuropathy by heart rate complexity analysis.*BioMedical Engineering OnLine* 2009, 8:3

[3] Akselrod S, Gordon D, Ubel FA, Shannon DC,Berger AC, Cohen RJ: Power spectral analysis of heart rate fluctuation: a quantitative probe of beat to beat cardiovascular control. *Science* 1981; 213:220-222.

[4] Kiviniemi, Antti: Measurement of cardiac vagal outflow by beat-to-beat R-R interval dynamics. *Acta Univ. Oul. D* 887, 2006 Oulu, Finland

[5] Sirkku M. Pikkujamsa, Timo H. Makikallio, K. E. Juhani Airaksinen, Heikki V. Huikuri: Determinants and interindividual variation of R-R interval dynamics in healthy middle-aged subjects.*Am J Physiol Heart Circ Physiol* 280: H1400–H1406, 2001.

[6] Claus D. Wagner, Pontus B. Persson: Chaos in the cardiovascular system: an update. *Cardiovascular Research* 40 (1998) 257–264

[7] Marek Malik, A. John Camm: Heart Rate Variability. Futura Publishing Company, Inc, 1995

[8] Melillo et al.: Heart rate variability and target organ damage in hypertensive patients. *BMC Cardiovascular Disorders* 2012, 12:105

Fractal Dimension of In-vivo and Ex-vivo Rabbit HRV Series

[1,2]O. Janoušek, [1,2]M. Ronzhina, [1,2]J. Kolářová, [1,2]I. Provazník, [3]T. Stračina, [3]V. Olejníčková, [2,3]M. Nováková

[1]Brno University of Technology, Brno, Czech Republic,
[2]International Clinical Research Center, St. Anne´s University Hospital Brno, Czech Republic,
[3]Masaryk University, Brno, Czech Republic
Email: janouseko@feec.vutbr.cz

Abstract. *Fractal dimensions of beat-to-beat series have been estimated by box-count algorithm in five New Zealand white rabbits and five isolated New Zealand rabbit hearts. In-vivo hearts beat-to-beat series have fractal dimension value equal to 1.49±0.03, whereas fractal dimension for ex-vivo hearts series is equal to 1.45±0.14. The fractal dimension of in-vivo hearts beat-to-beat series does not statistically differ ($\alpha = 0.05$) from those of the isolated hearts, indicating that fractal features of heart rate variability are probably predominantly affected by intrinsic behaviour of the heart.*

Keywords: HRV, box-count, fractal dimension, in-vivo and ex-vivo, rabbit heart

1. Introduction

The variability of RR-interval duration in beat-to-beat series has been recognized as characteristic attribute of vital heart [1]. The variability of RR-interval duration is affected by joint influence of sympathetic and parasympathetic branches of autonomous nervous system. Besides sympathetic-parasympathetic system activity, numerous intrinsic mechanisms of the heart may influence RR-interval duration, too. Cooperation of all abovementioned mechanisms gives rise to complex course of beat-to-beat time series.

There is a significant amount of variability in beat-to-beat series of isolated heart despite its complete denervation. Intrinsic mechanisms of the heart maintain the existence of beat-to-beat variability; however, the character of *ex-vivo* variability differs from the *in-vivo* one. The *ex-vivo* beat-to-beat series contain more quaziperiodic oscillations in comparison with *in-vivo* ones, resulting in a wavy shape of tachograms. Although the total amount of oscillations in *ex-vivo* tachogram is highly individual, one can visually differentiate *in-vivo* and *ex-vivo* beat-to-beat series by assessing of tachogram shape. Examples of *in-vivo* and *ex-vivo* tachograms are shown in Fig. 1.

In this article, the tachogram shape has been quantified by fractal dimension. We hypothesize that fractal dimension computed from sets of tachogram may be associated with influence of autonomous nervous system on heart rate variability (HRV). We investigated difference of fractal dimension between *in-vivo* and *ex-vivo* rabbit HRV series to discover, whether fractal dimension may serves as an indicator of autonomous nervous system activity.

2. Methods

The *in-vivo* ECG signals have been recorded from five New Zealand rabbits by SEIVA recording system. Body surface wire electrodes were attached to the skin with miniature clips. Location of electrodes did not restrict free posturing of the animal in sitting position.

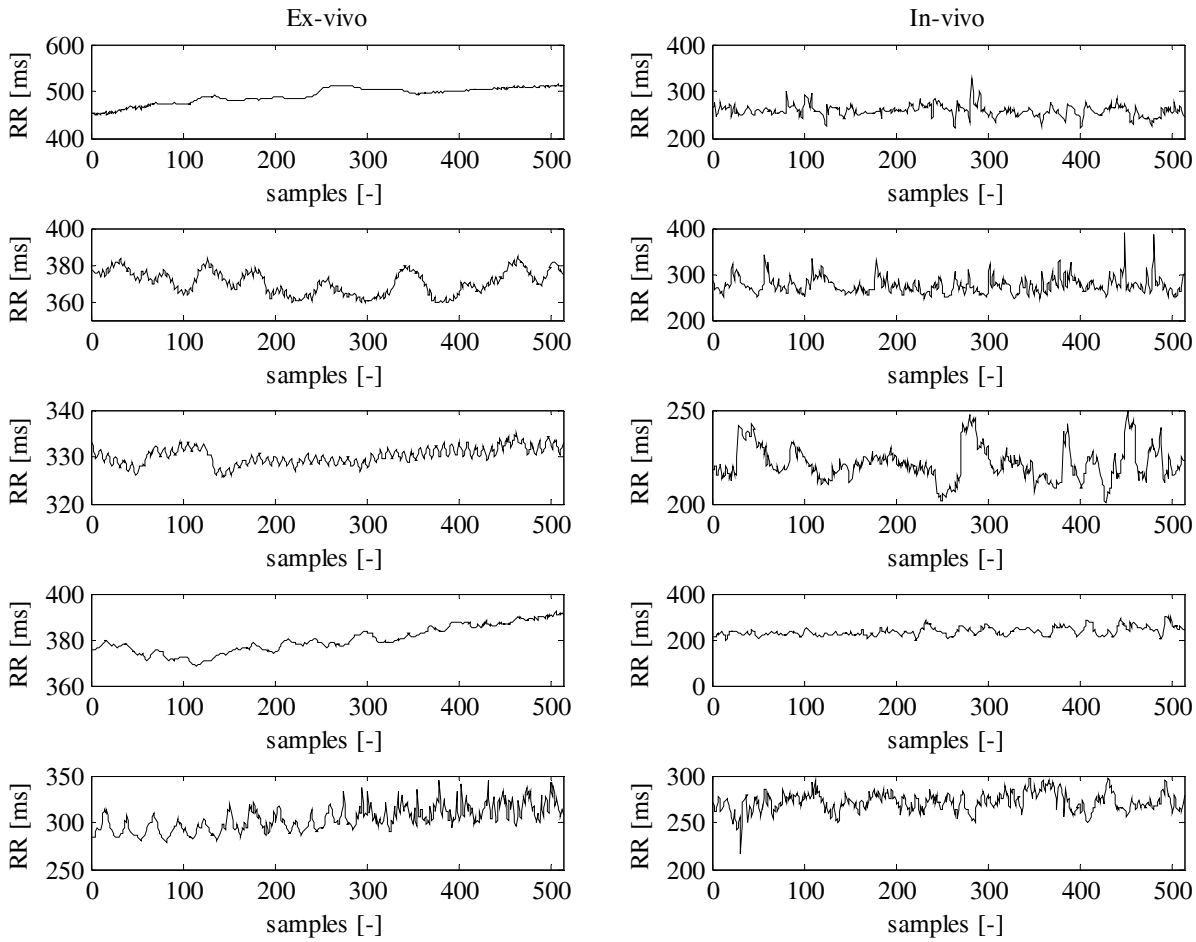

Fig. 1. Tachograms of *ex-vivo* (left) and *in-vivo* (right) hearts beat-to-beat series. Wavy shape of *ex-vivo* tachograms visually differs from sharp-edged shape of *in-vivo* tachograms.

The *ex-vivo* ECG signals have been recorded from isolated hearts perfused according to Langendorff in the mode of constant perfusion pressure (85mmHg). In deep anaesthesia with xylasin and ketamin, the hearts were excised and fixed on perfusion apparatus filled with Krebs-Henseleit solution (1.25mMCa^{2+}, 37°C) and placed in a thermostatically-controlled bath. After 30 minutes long stabilization period, the five minutes long ECG signals were recorded by touch-less method [2].

ECG signals degraded by arrhythmias were excluded from further processing. R-peaks were detected automatically by own R-wave detector designed in Matlab R2012b (MathWorks, USA). The results of automatic detection were reviewed and errors were corrected manually.

The fractal dimension has been estimated by box-count algorithm in custom made software in Matlab R2012b (MathWorks, USA). The box-count algorithm covers a beat-to-beat series with boxes of predefined size and the number of boxes required to cover the series is counted. In each subsequent step, the size of boxes is reduced, and the process of box counting is repeated [3]. Situation is illustrated in Fig. 2, where the tachograms covered by boxes of size 128 (upper part of figure), and 64 (middle part of figure), are shown. At each step, the number of boxes required to cover the curve and the size of box is kept in memory. When box size is reduced by factor of two in each step, resulting fractal dimension can be estimated as slope of ordinary least square regression fit of log(BoxCount) on log(BoxSize), where the BoxCount represents number of boxes required to cover the series, and BoxSize represents box size. The process of fractal dimension estimation is illustrated in bottom part of Fig. 2.

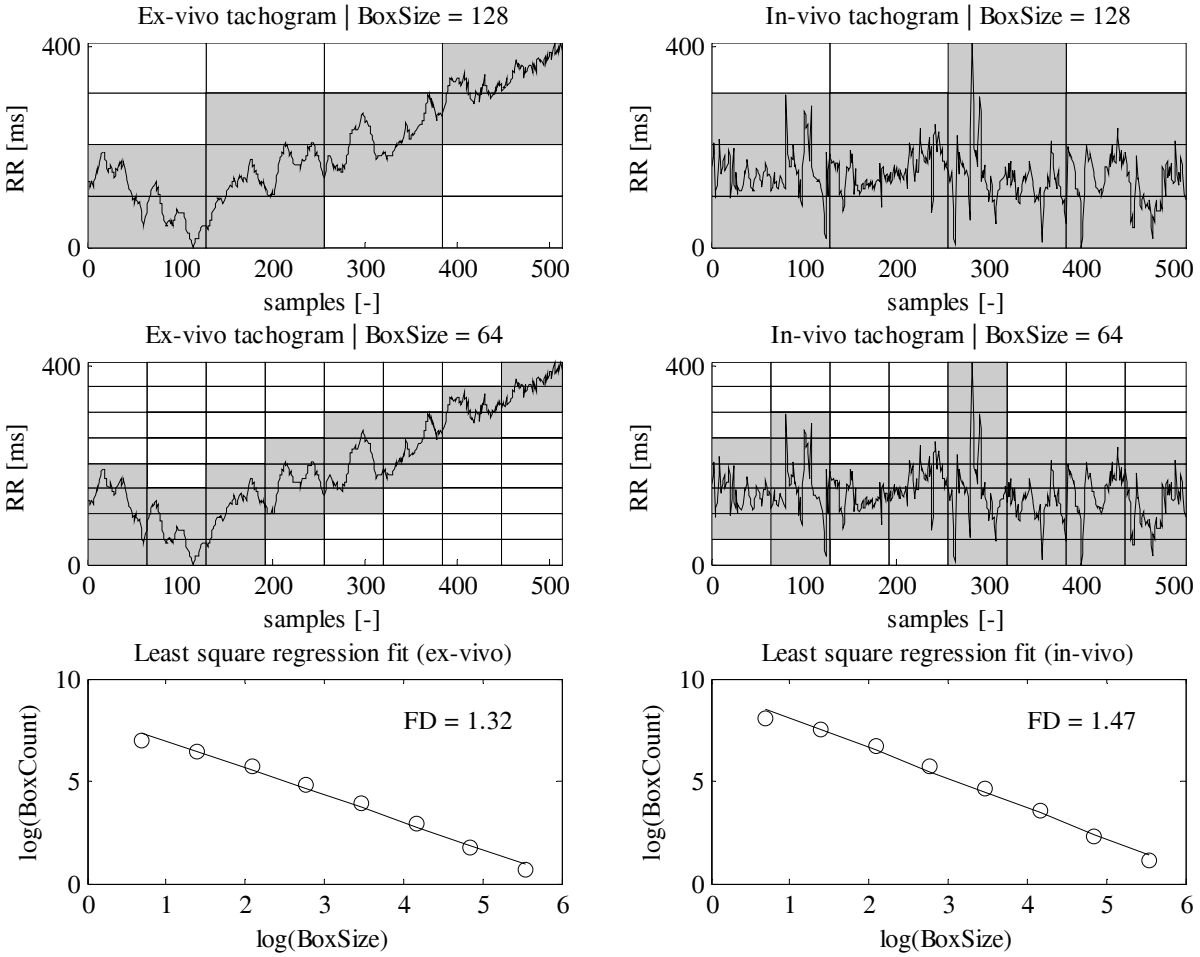

Fig. 2. Illustration of box-count algorithm. Upper part: tachogram is covered by boxes of size 128 and the number of boxes is counted. Middle part: the same situation with boxes of size 64. Bottom part: fractal dimension is estimated as the slope of least square regression fit of log(BoxCount) on log(BoxSize).

Wilcoxon rank sum test with $\alpha = 0.05$ has been used for evaluation of statistical significance of difference between in-vivo and ex-vivo fractal dimensions.

3. Results

Fractal dimension of *in-vivo* and *ex-vivo* beat-to-beat series has been estimated by box-count algorithm. The average value of estimated fractal dimension equals to 1.49±0.03 in *in-vivo* and 1.45±0.14 in *ex-vivo* beat-to-beat series. The difference between *in-vivo* and *ex-vivo* beat-to-beat series groups is not statistically significant. The least square regression fits of *ex-vivo* and *in-vivo* beat-to-beat series and the boxplot illustrating difference between *in-vivo* and *ex-vivo* groups are shown in Fig. 3.

The fractal dimension values of individual beat-to-beat series are close to each other in the *in-vivo* group. On the contrary, intra-individual value of fractal dimension in *ex-vivo* group is substantial.

4. Conclusions

The fractal dimension of *in-vivo* hearts beat-to-beat series is almost the same as of *ex-vivo* ones, indicating that the fractal features of HRV are probably predominantly affected by intrinsic behaviour of heart, not by sympathetic-parasympathetic branches of autonomous nervous system.

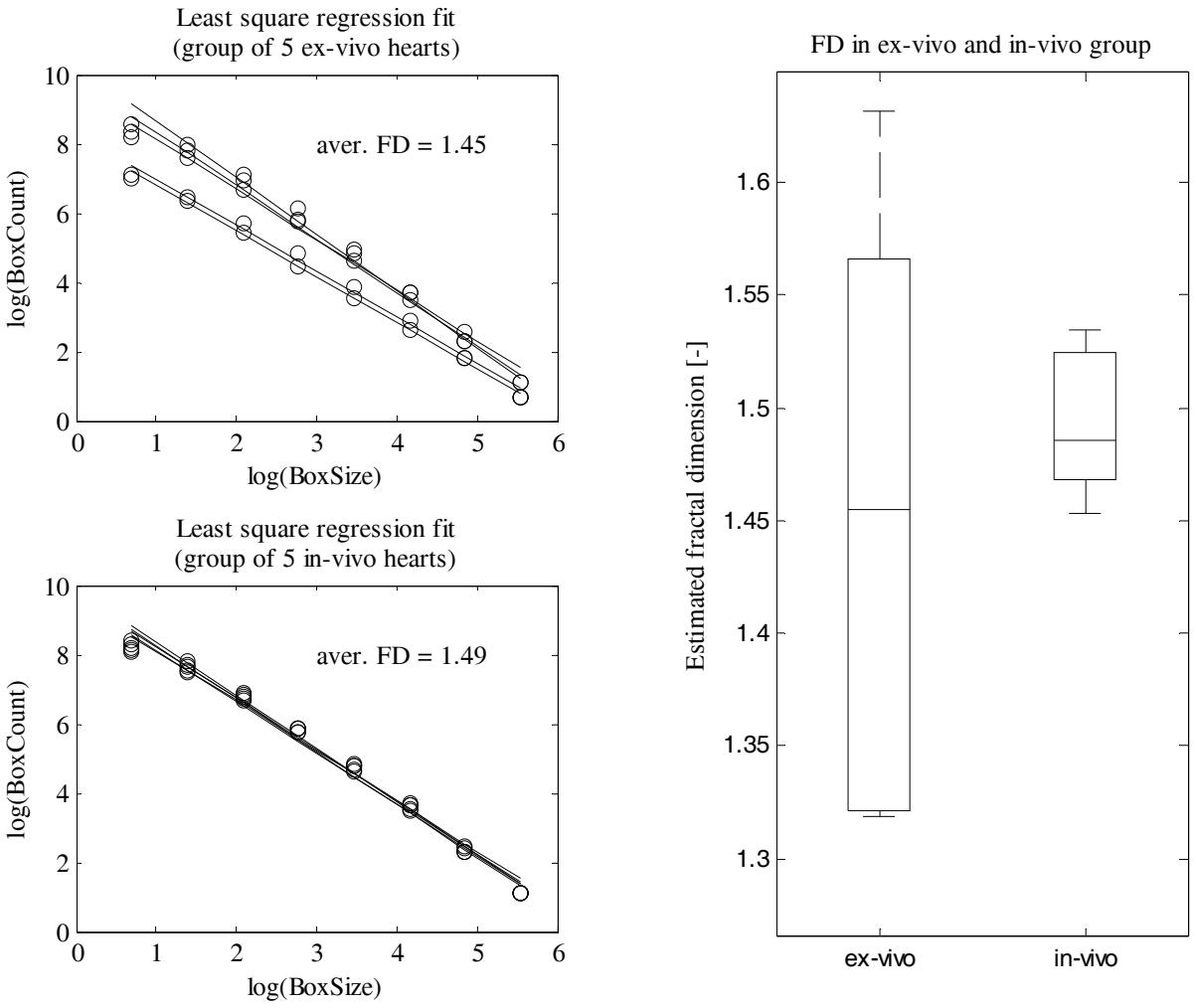

Fig. 3. Left: Slope of individual least square regression fits in *ex-vivo* (upper) and *in-vivo* (bottom) hearts. Right: boxplots of estimated fractal dimensions (FD) in *ex-vivo* and *in-vivo* heart groups.

Acknowledgements

The work was supported by European Regional Development Fund - Project FNUSA-ICRC (No. CZ.1.05/1.1.00/02.0123), grant projects of the Grant Agency GACR 102/12/2034, and MUNI/A/0957/2013.

References

[1] Berntson GG, Bigger JT Jr, Eckberg DL, Grossman P, Kaufmann PG, Malik M, Nagaraja HN, Porges SW, Saul JP, Stone PH, van der Molen MW. Heart rate variability: origins, methods, and interpretive caveats. *Psychophysiology*, 34(6): 623-48, 1997.

[2] Kolářová J, Fialová K, Janoušek O, Nováková M, Provazník I. Experimental methods for simultaneous measurement of action potentials and electrograms in isolated heart. *Physiological Research*, 59(S1): 71-80, 2010.

[3] Gneiting T, Ševčíková H, Percival DB. Estimators of Fractal Dimension: Assessing the Roughness of Time Series and Spatial Data. *Statistical Science*, 27(2): 247–277, 2012.

Interatrial Block as Anatomical – Electrical Substrate for Atrial Arrhythmias:

A Recognition to Prof. Dr. Antonio Bayès de Luna

The Long Journey to Interatrial Block Discovery

A. Bayés de Luna

Fundació Investigació Cardiovascular, ICCC, Barcelona, Spain
Email: abayes@csic-iccc.org

1. Introduction

To begin, I feel it is important to point out that before our publications on interatrial block starting in the mid-1970s, a number of papers had already discussed, with isolated cases or short series, different aspects of so-called blocks at atrial levels and specifically of interatrial or intraatrial block (IAB) [1-8], that is the topic that we will comment in this paper. Although there is some discrepancy in different papers [1-4] about the significance of the concept of interatrial or intraatrial block, usually this represents an impaired propagation of the stimulus between two portions of the atria, with enlarged P waves greater than or equal to 110-120 ms, and normally accompanied by left atrial enlargement. In a few articles [5-8] written in Latin languages, also was considered that if the stimulus was completely blocked at the upper part of the Bachmann zone, the activation of the left atrium would take place retrogradely, originating a long P wave (≥ 120ms) together with a ± morphology in II, III and VF. However, there are many aspects that are not well explained or discussed in these publications, as outlined below.

1. In no publication did it state that these ECG patterns of interatrial (intraatrial) block (IAB) are in fact a pattern of block based on the presence of the following 3 conditions: a) the pattern may appear suddenly and may be transient, b) the pattern may exist without associated enlargement of involved chambers. In fact, the term "left atrial abnormality" was coined and widely used to encompass both "atrial enlargement" and "interatrial block" [9, 10] and c) the ECG pattern may be reproduced experimentally.
2. Furthermore, no paper discussed at any time any possible clinical implications of these ECG patterns. We, therefore, cannot know if these cases were associated with supraventricular tachyarrhythmias, mortality or other problems.
3. There was no clear definition and classification of block at the atrial level, specifically of interatrial block (IAB) this means block between two atria. There was no mention that IAB may be, as other types of block, of partial (first-degree block), transient (second-degree block) or advanced (third-degree block) types.
4. There were no data about the prevalence of these blocks, and its etiological aspects.
5. There were no clear ECG-VCG criteria for advanced IAB, based on long series of patients.
6. The concept of IAB is not frequently used in cardiology. The P wave still remains "The Cinderella of the ECG". In a review of 76 books on ECG in English, Spanish, French and Italian languages, from the beginning of ECG study (Lewis' books) to present day, we have only found a clear reference to interatrial block in our books since the first edition [11] and in Piccolo and Oreto's book [12, 13]. For example, Te-Chuan Chou [14] states that "in P-wave changes, conduction defects may be present." A less specific term such as *atrial abnormality* is found in other books. Macfarlane [15], while discussing the concept of intra-atrial block, only defines it following the criteria of WHO/ISFC [16] that corresponds to partial interatrial block (IAB). In terms of general cardiology, the textbook by Braunwald [17] includes "all anomalies of P wave" under the term "*atrial abnormalities"*, which is also the case in the chapter on ECG of the previous editions of the textbook "The heart", by Fuster et al [18], except the last edition written by our group.

2. Our studies on interatrial block

Our dedication to the study of blocks at the atrial level, and especially to interatrial blocks (IAB), has been one of our favourite topics throughout the last 40 years. The following is a summary of the most important successive studies performed by our group.

Identification and classification of blocks at atrial level

We classified blocks at atrial level [19-22] in interatrial and other types of atrial blocks that includes right atrial block and atrial aberrancy. For the remainder of this paper we will focus on interatrial block (IAB). This is the block between the right and left atria in the zone of the Bachmann bundle and may be of first-degree (partial), when the stimulus pass through the Bachmann bundle but with delay the ECG criterion of which is P wave ≥ 120ms (≥ 110 for others); third-degree (advanced), when the stimulus is blocked in the zone of Bachmann bundle, and left atrium is retrogradely conducted to left atrium (RCLA) (Fig.1-3); the ECG criteria of which are P wave ≥ 120ms and ± morphology in II, III and VF. Second-degree, IAB is a transient pattern of partial or advanced IAB, a form of atrial aberrancy (Fig.4).

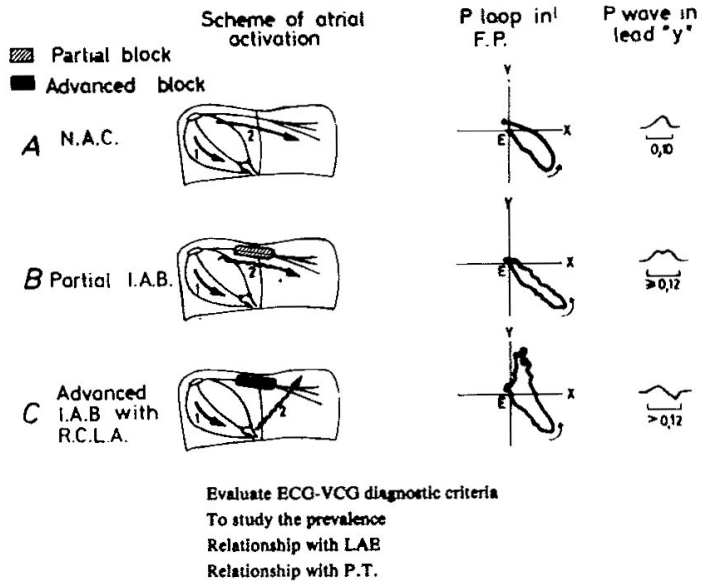

Fig. 1. Left: Scheme of atrial activation in a normal case (A), in presence of partial IAB (B), and of IAB with LARA (C). Right: Characteristics of the P loop and P wave in each case.

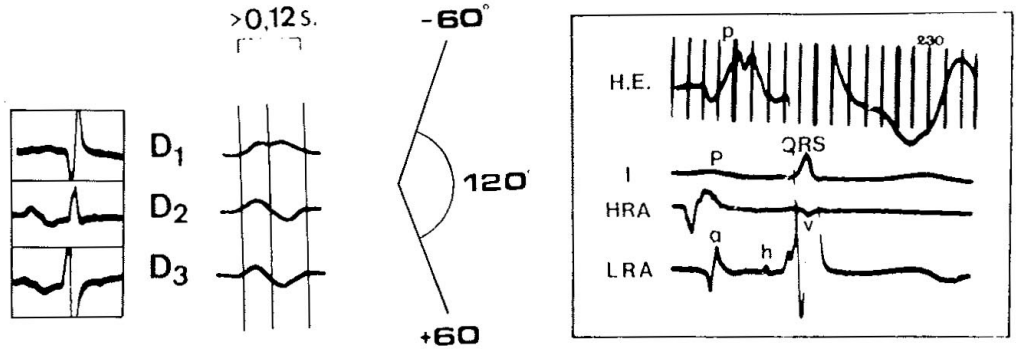

Fig. 2. Left: Characteristics of the P wave in the three bipolar limb leads. Note the existence of an open angle between the vector of the 1st part and of the 2nd. Right: Electrophysiological study that demonstrates the retrograde activation of the left atrium. HE: High esophageal lead. HRA: High right atrium. LRA: Low right atrium. In HE the morphology is -+ because the electrode first face the tale of activation and later the head of the vector. The way of activation is HRA-LRA-Second part (positive) in HE.

Although we published this classification already in the 70's [19-22] and in all editions of our ECG books published since the mid 1970s, this concept has not become popular. Very recently, we published a consensus paper on IAB under the auspices of ISHNE in the Journal of Electrocardiology [23] and a new edition of my book [30], and we hope this will help to further disseminate all these concepts.

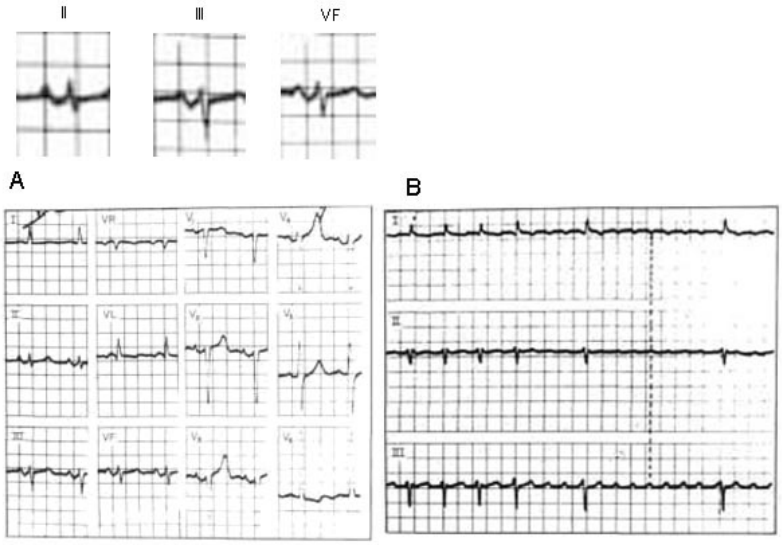

Fig. 3. A. Typical morphology of advanced interatrial conduction block and retrograde activation of the left atrium, in sinus rhythm. B. The polarity of the flutter wave indicates that the flutter is an atypical flutter.

These patterns may correspond to block.
Evidence consisted of the following: a) we found cases of partial and advanced IAB without LAE [21, 22]; b) we found cases of intermittent and progressive partial and advanced IAB [22]; and c) in the 1970s Waldo and others demonstrated that the pattern of advanced IAB may be reproduced experimentally [24] (Fig.5).

Definition of ECG-VCG diagnostic criteria
In 1976 and 1978 we published, our first abstract and paper on advanced interatrial block (19,20). Later, a larger series was published in 1985 (22) (Figs. 1-3) (Table 1).

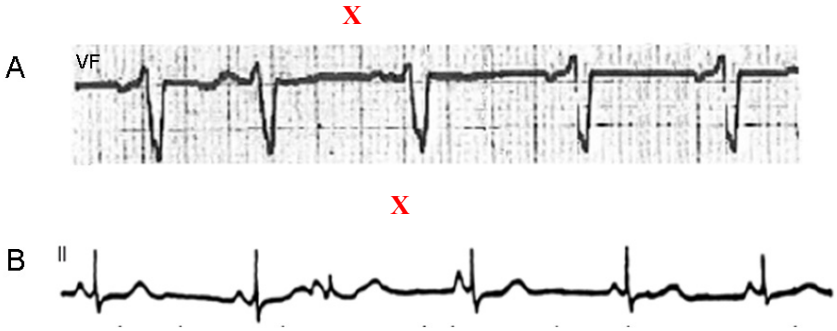

Fig. 4. Two cases of atrial aberrancy. The first one **A** is a case of second degree interatrial block. This is a case of a patient with basal advanced interatrial block (P± with first part isoelectric that mimics AV junction rhythm) that presents aberrant atrial conduction, ectopically induced by premature atrial complex, with a pattern, in this case, of first degree interatrial block **(x). B**. A patient with aberrant atrial conduction also ectopically induced by a premature atrial complex. After this premature complex, a transitory P wave with a different morphology, but not with a pattern of first or third interatrial block appear **(x).** The PR interval is equal to previous PR intervals. Other explanations to this change (atrial escape, artifact, etc.) are unlikely (see Bayés de Luna 2014 [30]).

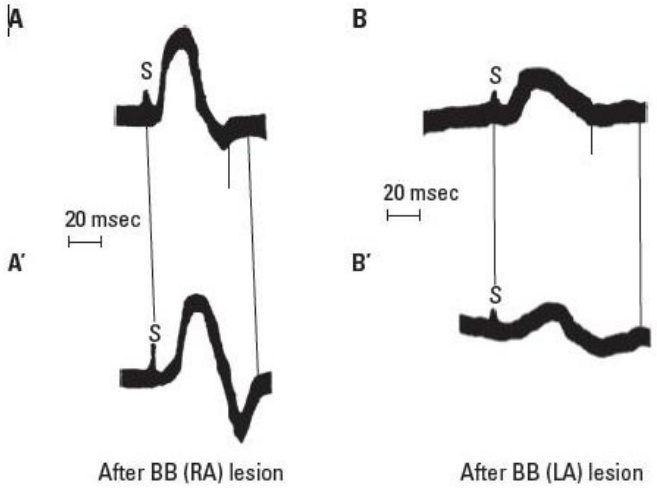

Fig. 5. Adapted from experimental Bachmann's bundle block (Waldo et al. 1971). (A) Control P wave recorded in ECG lead II when the atria were paced from the right atrium. See the change of morphology after Bachmann's bundle lesion in the right side. (B) P wave recorded in lead II after the creation of a lesion in the left atrial (LA) portion of Bachmann's bundle (BB). In both cases the changes in conduction time and morphology after block are shown.

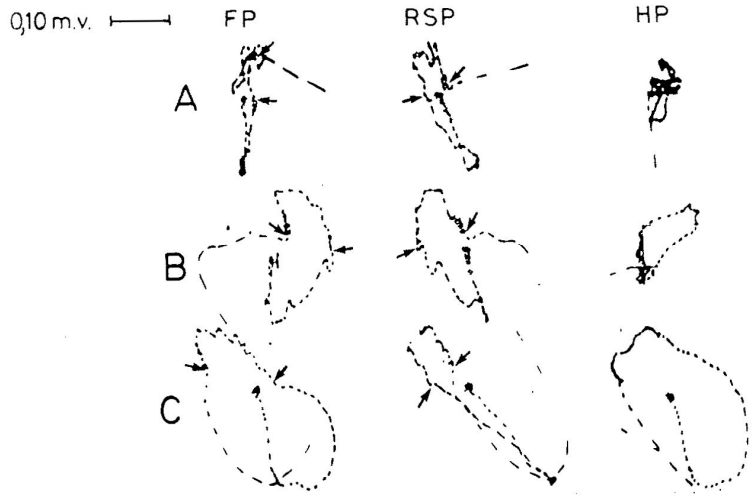

Fig. 6. Examples of the P loops in presence of advanced IAB. A) Closed loop. B) Open loop with a left final part. C) Open loop with a right final part.

Of the 81.000 ECGs, we collected, 83 cases that fulfilled the criteria of advanced IAB (P ± in II, III and VF with P width ≥ 120 ms.). We presented a detailed study of 35 cases with surface ECG and VCG and 29 cases with orthogonal ECG leads (Table I and fig. 2, 3, 6, 7). The results were then compared against 2 control groups: patients with heart disease (30 cases) and those without heart disease (25 cases). The prevalence of advanced IAB was nearly 1% in the global population, and 2% among patients with valvular heart disease.

The diagnostic criteria for advanced IAB included (Fig.6, 7 and Table I); 1) ECG: P ± in II, III and VF and P ≥ 120 ms, with an open angle (usually >90°) between the first and second parts of the P wave; 2) orthogonal ECG: P ± in the Y lead with a negative mode > 40 ms; 3) VCG: more than 50 ms above the X or Z axis, duration of the P loop ≥ 110 ms, with an open angle between the 2 parts of the P loop in both frontal (131.3° ± 32.3°) and right saggital planes (171.2° ± 15.1°), and the presence of notches and slurrings in the last part of the P loop.

TABLE I

Diagnostic Criteria of advanced IAB

1) Surface ECG:
   - P ± II, III, VF (in II can be only + with isodiphasic last part)
   - P ⩾ 120 msec.
   - Open angle (usually >90 °) between the 2 parts of the P wave

2) Orthogonal ECG:
   - P ± in Y lead with a negative mode duration ⩾ 40 msec.

3) VCG:
   - More than 40 msec. above X or Z axis
   - P loop duration ⩾ 110 msec.
   - Open angle in FP and RSP
   - Slurrings and delays in the last part of the loop

4) Oesophageal ECG:
   - H.O.L. = P wave ∓ with delayed inscription
   - L.O.L. = P wave ±

5) Interacavitary ECG:
   - C raneocaudal sequence in RA
   - C audocraneal sequence in LA (combined with oesophageal ECG)

HOL: High oesophageal lead. LOL: Low oesophageal lead. RA: Right atrium. LA: Left atrium.

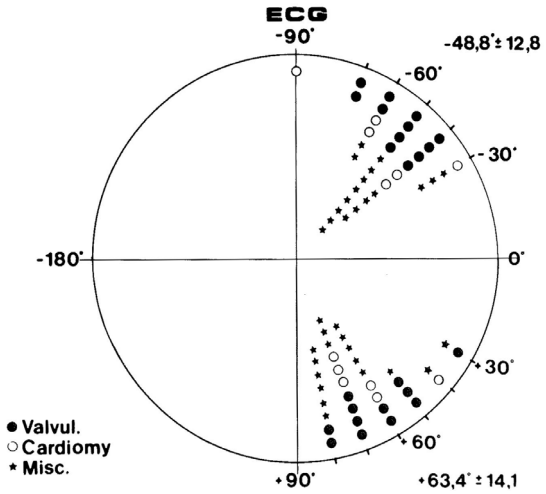

Fig. 7. Direction of the vectors of the first and second parts of the P wave in presence of advanced IAB in the three groups studied.

We have found that the pattern of interatrial block, not only may be transient (second degree) (Fig. 4A) but also may appear progressively (Fig. 8). In these papers [22, 23] we had already emphasized that the diagnosis of advanced IAB is not only of academic interest but may also have clinical implications due to the following:

a) This is a very specific sign of LAE that is present in ≈ 90% of cases.

b) In the absence of preventive treatment there is a high incidence of supraventricular paroxysmal arrhythmia (96 %) (flutter and fibrillation) within 1 year. Incidence is 100 % in valvular disease and cardiomyopathic groups.

c) Paroxysmal arrhythmia appears to be due to IACD-LARA rather than atrial enlargement; in the control groups of valvular disease and cardiomyopathies with similar LAE the incidence of paroxysmal tachyarrhythmia is much lower (20 % vs 100 %).

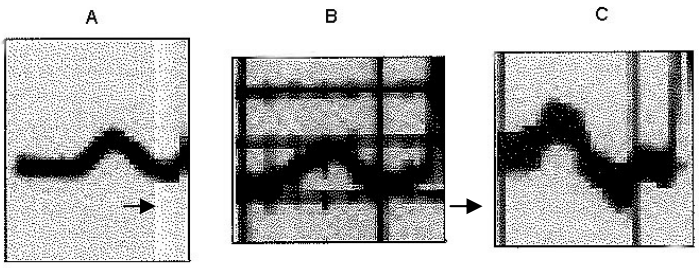

Fig. 8. Progressive interatrial block: P wave patterns in VF from a patient with mitro-aortic valve disease. (A) P wave with normal atrial duration (P = 105ms), (B) An intermediate morphology that corresponds to a first-degree interatrial block (P = 135ms). (C) Advanced interatrial block appearing after 5 years with P ± morphology in II, III, and VF (P = 145ms).

Identification of the syndrome [25]

We proceeded to study a series of patients with a long-term follow-up to better determine the true incidence of supraventricular arrhythmias in these groups of patients when compared with patients of the same clinical and echocardiographic characteristics. We studied 16 patients with electrocardiographic evidence of advanced IAB and retrograde activation of the left atrium ($P \geq 0.12$ s and dysphasic (±) P waves in leads II, III and VF). Eight patients had valvular heart disease, 4 had dilated cardiomyopathy and 4 had other forms of heart disease. Patients were compared with a control group of 22 patients with similar clinical and echocardiographic characteristics but who presented partial instead of advanced IAB.

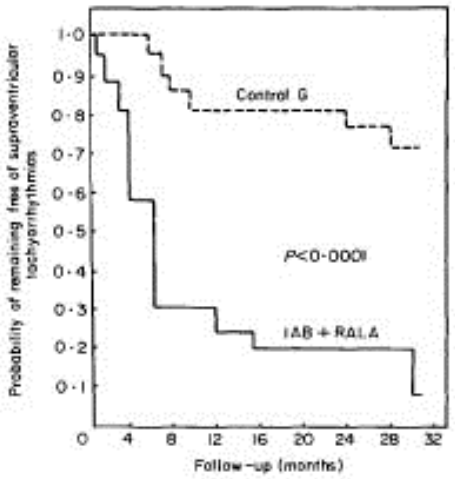

Fig. 9. Life table analysis of the probability of remaining free of supraventricular tachyarrhythmias in patients with advanced interatrial block (IAB) and controls. Taken from [26].

Patients with advanced IAB and retrograde activation of the left atrium had a much higher incidence of paroxysmal supraventricular tachyarrhythmias (93.7 %) during follow-up when compared to the control group with partial IAB, (27.7 %) ($P < 0.001$) (Fig.9). Eleven of the 16 patients (68.7 %) with advanced IAB and retrograde activation of left atrium had atrial flutter (atypical in 7 cases, typical in 2 cases, and with 2 or more morphologies in 2 cases). Six patients from the control group (27.7 %) had sustained atrial tachyarrhythmias (5 with atrial fibrillation and 1 with typical atrial flutter) (Fig.3 and Table II). The atrial tachyarrhythmias were due more to advanced IAB and retrograde activation of the left atrium with frequent atrial extrasystoles than to left atrial enlargement, because the control group of patients with a left atrium of the same size, but with partial IAB instead of advanced IAB and less incidence of atrial extrasystoles, had a much lower incidence of paroxysmal tachycardia.

Prevention of the syndrome and recurrences [26]

Having found a strong relationship between the presence of advanced IAB and the incidence of atrial flutter or atrial fibrillation when compared with a control group (93.7 % vs. 27.7 %), along with a high incidence of an uncommon type of atrial flutter (4), we decided to study the role of preventive antiarrhythmic treatment for this disorder.

Fifteen of the 16 consecutive patients we studied, who did not have preventive antiarrhythmic treatment (93.75 %), presented at least 1 crisis of paroxysmal supraventricular tachyarrhythmia requiring emergency treatment over a follow-up of 10 ± 6.1 months.

In view of the confirmation of high incidence of paroxysmal supraventricular tachyarrhythmias in this type of patient, and especially in valvular disease and cardiomyopathic patients, we decided to institute preventive antiarrhythmic treatment in subsequent patients.

With the use of preventive antiarrhythmic treatment in our 16 subsequent patients, once diagnosed of advanced IAB, the incidence of paroxysmal supraventricular tachyarrhythmia was greatly lowered (25 %) even with longer follow-up (18 ± 10.2 months) (Fig.10). Because of the high risk of embolism in valvular and cardiomyopathic disease, we now consider it advisable to start preventive antiarrhythmic treatment in such patients, prior to the onset of tachyarrhythmia.

It is extremely important to corroborate these results in a greater series of patients. We are therefore preparing a larger trial for this purpose.

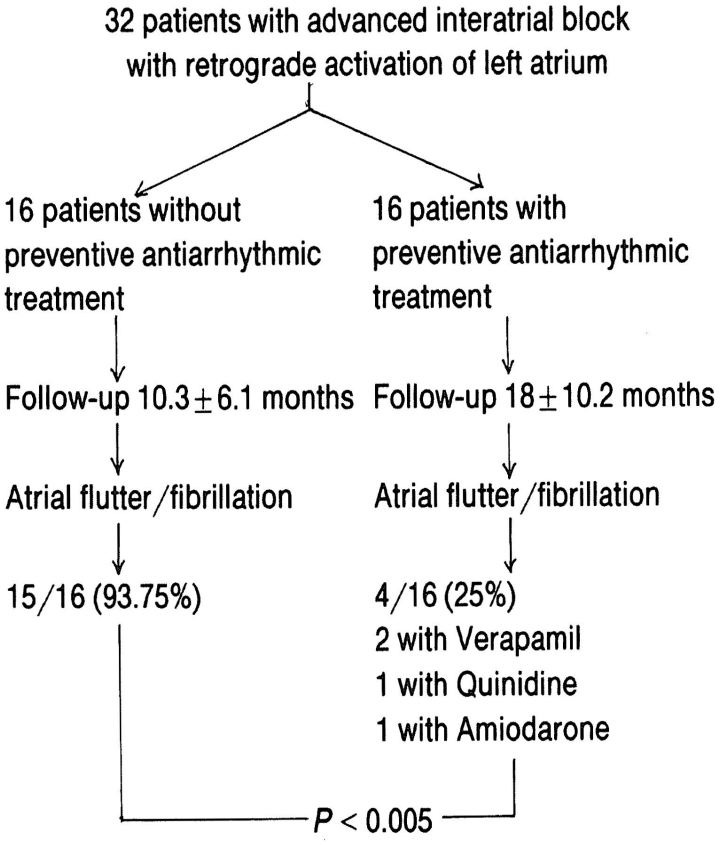

Fig. 10. Follow-up of 32 patients with advanced interatrial block with retrograde activation of left atrium with and without antiarrhythmic treatment

Table II. Characteristics of the sustained paroxysmal tachyarrhythmias

Group with interatrial block (16 patients; 15 with tachyarrhythmia during the follow-up) (93,7%)	
Atrial flutter	7 / 15 cases
Atrial fibrillation	4 / 15 cases
Atrial flutter with fibrillation	4 / 15 cases
MRV 133 ± 42 beats min $^{-1}$	
Characteristics of the atrial flutter (11 cases)	
Typical form (AR 276 ± 21 min -1)	2 cases
Atypical form (AR 252 ± 36 min -1)	7 cases
Two or more morphologies	2 cases
Control group (22 patients; 6 with tachyarrhythmia at follow-up) (27,7%)	
Typical atrial flutter (AR 270 min -1)	1 case
Atrial fibrillation	5 cases
MRV 127 ± 28 beats min-1	

AR, atrial rate; MVR, mean ventricular rate during crises.

3. Our most recent papers

In 1999 we published [27] a review paper in Europace commenting"The syndrome of advanced interatrial block and supraventricular arrhythmia" in which we summarized all previous research by our group and confirmed our view that this association most certainly constituted a syndrome.

We also published a review paper on block at atrial level [21], including the possible diagnosis of right atrial block in case of clockwise rotation of P loop in FP. Also we publish several papers on atrial aberrancy [28, 29], concept that, if the change of P wave is a pattern of partial or advanced IAB, corresponds to a second degree IAB [30] (Fig.4).

We emphasized as we stated in papers and books on ECG [11, 22, 30] and in the latest consensus paper on IAB [23] that these ECG patterns described as patterns of partial and advanced IAB are due to a block, not to atrial enlargement because a) it may be transient and progressive (Fig.7) , b) it may exist without associated left atrial enlargement and c) it may be reproduced experimentally [24] (Fig.12).

4. Conclusion

a) We have defined the ECG-VCG criteria of advanced IAB and its etiological aspects and prevalence.

b) We have observed that supraventricular arrhythmias appear very often in a short follow-up in patients with ECG pattern of advanced IAB, if left untreated, and that when are in front of a patient with atypical flutter we can be nearly certain that in sinus rhythm the patient will have the ECG pattern of advanced IAB.

c) We have demonstrated that if we treat with antiarrhythmic drugs the patients with advanced IAB, the incidence of supraventricular tachyarrhythmic in the future is much lower.

d) Therefore, we may conclude that this association should be considered a syndrome.

5. The recognition and the future

Thanks to all this information, a select group of cardiologists have manifested their agreement by writing with our view and are convinced that the association of advanced IAB together with supraventricular arrhythmias is a syndrome. This includes Braunwald [31], Daubert [32], and Brugada [33]. Furthermore some groups especially the ones of Daubert [34], Spodick [35, 36], Platonov [37, 38] Garcia-Cossio [39] and Baranchuk and Conde [40-43] have also published different and important aspects on this topic. However, in all these decades it has never occurred to me that one might consider the name *Bayés syndrome*. Therefore, it was with great surprise that I learned of the generosity of Adrian Baranchuk, seconded by Diego Conde, and many other colleagues when I received the first paper on the proposed name for this syndrome, which appeared recently in *Revista Instituto de México* [40], and later other articles in *Revista Argentina Cardiología* [12], the American Journal of Cardiology [42], ANE [43], among others. What is truly important, however, is that the physicians have to be awarded that the association of advanced IAB plus supraventricular arrhythmias is a syndrome. Really the ECG pattern of advanced IAB is an extremely strong marker of supraventricular tachyarrhythmias in a short period of time, much more so than the presence of partial IAB (only $P \geq 120$ msec), which already presents a high incidence of arrhythmia [26, 28], although to a lesser degree when compared with advanced IAB pattern, as we have already shown. The other speakers of this symposium will explain other very important aspects of the electrophysiology of the atria, and Adrian Baranchuk, the father of this symposium will outline the many possibilities for research that still exist with this syndrome, whatever its name may be in the future.

I would like to express my gratitude to Dr. L. Bacharova President of the meeting (ICE-2014), and International Society of Electrocardiology (ISE) President Dr.C.Pastore, for giving to me the opportunity to explain this story to so many friends. It was extremely generous of her. My special thanks go to all other members of this round table for your friendship and for attending this symposium. I also have to thank the support and intellectual challenge provided by several cardiologists working in this field in different aspects, who have been exchanging ideas with me from the beginning: P. Puech, JC. Daubert, D. Spodick, P. Platonov, A. Waldo, F. Garcia-Cossio, A. Baranchuk, D. Conde and the friendly support of B. Olson, E. Braunwald, P. Chiale, M. Elizari, A. Perez-Riera, R. Barbosa, C. Pastore, Hnos. Brugada, X. Viñolas, W. Zareba, I. Cygankiewicz, R. Baranowski, R. Villuendas, A. Bayés Genís, and of course each and every member of my team. Thank you all so very much.

References

[1] Bachmann G. The significance of splitting of the P-wave in the ECG. *Am.Int.Med*.1941;14:1707.
[2] Cohen J, Scharf D. Complete interatrial and intraatrial block (atrial demonstration). *American Heart* Journal 1965;70:24
[3] Legato MJ, Ferrer MI. Intermitent intra-atrial block: its diagnosis, incidence, and implications. *Chest* 1974;65:243
[4] Zoneraich O, Zoneraich S. Atrial tachycardia with high degree intraatrial block. *J.Electricardiol*. 1971;4:369.
[5] Puech P. L'activite electrique auriculaire normal et pathologique. *Maron* 1956 p.206.
[6] Castillo A, Vernant P. Troubes de la conduction interauriculaire par bloc du fascion de Bachmann. Estude de 3 cas per ECG endoauriculaire. *Arch. Mal. Coeur* 1973;4:31
[7] D.Biase M, Rizzon P. Blocco interatriale con activatione retrograde dell'atrio sinistro. *Giornale Italiano Card.* 1975;5:323.
[8] Garcia Civera R, Llinus A, Benages A, et al. Estúdio de la activación auricular y de la conducción AV en el bloqueo del Haz de Bachmann en el corazón humano. *Rev.Esp. Card*. 1972;24:341
[9] Lee K, Appleton C, Lester S, et al. Relation of ECG criteria for LAE in two-dimensional echocardiographic left atrial volume measurements. *American Journal Card*. 2007;99:113.
[10] Tsao CW, Josepson ME, Hauser TH. Accuraces of ECG criteria for LAE. J. Cardio. *Mag. Resonance* 2002;10:7.

[11] Bayés de Luna A, et al. Curso de Electrocardiografia y vectorcardiografia. *Edit. Cientifico Médica.*1975.
[12] Piccolo E. Electrocardiografic e veto cardiografic. *Edit. Piccin* 1981 p.88.
[13] Oreto G. L'elletrocardiogramma: a mosaico a 12 tessere. *Centro Scientifico Editore* 2009.
[14] T-Chuan Chou. Electrocardiography in clinical practice. *Grune-Stratton* 1979
[15] Marfarlane P, et al. Editors. Comprehensive Electrocardiology. *Springer* 2011.
[16] Willems JL, Robles de Medina EO, Bernard R, et al. Criteri for intraventricular conduction disturbances and pre-excittion: WHO/ISFC Task Force Ad Hoc. *J Am Coll Cardiol* 1985;5:1261.
[17] Mirivis D, Gordberger. Electrocardiography Chapter V.Braunwald textbook.Heart disease. *Saunders.* 2001
[18] Fuster V, et al, Editors. The heart 13th Edition. Mc-Graw Hill 2011.
[19] Bayés de Luna A, Ferrer S, Vilaplana J, et al. Interatrial block with left atrial retrograde activation . *Abstract in Eu.Con.Card*. Book II p.369. 1976.
[20] Bayés de Luna A. Bloqueo a nivel auricular. *Rev.Esp.Cardiol*.1979;39:5.
[21] Bayés de Luna A, Bailén JL, Guindo, et al. Blocks at the atrial level. *New Trends in Arrhythmias* 1987;3:219.
[22] Bayés de Luna A, Fort de Ribot R, Trilla E, et al. Electrocrdiographic and vectorcardiographic study of interatrial conduction disturbances with left atrial retrograde activation . *J Electrocardiology* 1985;18:1.
[23] Bayés de Luna A, Platonov P, Cossio FG, et al. Interatrial blocks. A separate entity from left atrial enlargement: a consensus report. *Journal of Electrocardilogy* 2012;45:445-451.
[24] Waldo A, Harry L, Bush Jr, et al. Effects on the canine P wave of descrete lesions in the specialized atrial tracts. *Circulation Res* 1971;29:452.
[25] Bayés de Luna A, Cladellas R, Oter P, et al. Interatrial conduction block and retrograde activation of the lerf atrium and paroxysmal supraventricular tachyarrhythmia. *European Heart Journal* 1988;9:1112.
[26] Interatrial conduction block with retrograde activation of the left atrium and paroxysmal supraventricular tachyarrhythmias: influence of preventive antiarrhythmic treatment. *International Journal of Cardiol*.1989;22:147-150.
[27] Bayés de Luna A, Guindo J, Viñolas X, et al. Third-degree inter-atrial block and supraventricular tachyarrhythmias.*Europace* 1999;1:43.
[28] Bayés de Luna A, Julià J, Lopez J. ECG-VCG study of atrial aberrancy. *Book V International Congress in ECG*. Glasgow 1978.
[29] Julià J, Bayés de Luna A, Candell J, et al. Aberrancia auricular. A proposito de 21 casos. *Rev. Esp. Cardiologia* 1978;31:207.
[30] Bayés de Luna A. The ECG for beginners. *Wiley-Blackwell* 2014.
[31] Braunwald E. Foreword. In: Bayés de Luna A, Clinical Electrocardiography: a textbook. Chichester, West Sussex, UK: *Wiley-Blackwell*;2012.
[32] Daubert JC. Atrial flutter and interatrial conduction block. In: Waldo A, Touboul P, editors. Atrial Flutter. Armonk, NY: *Futura Publisihing;* 1966. p.33.
[33] Brugada P, Brugada J, Brugada R. Sindromes arritmologicos en Cardiologia clinica. Bayés de Luna et al, editors.p.478. *Masson* 2003.
[34] Daubert JC, Pavin D, Jauvert G, et al. Intra and interatrial conduction delay: implications for cardiac pacing. *Pacing Clin Electrophysiol* 2004;27:507.
[35] Spodick DH, Ariyarah V. Interatrial block. The pandemic remains poorly perceived. *Pacing Clin Electrophisiol* 2009;32:662.
[36] Spodick DH, Ariyarah V. Interatrial block; a prevalent, widely neglected and portentous anormality. *J Electrocardiol* 2008;41:61.
[37] Platonov P. Atrial conduction and atrial fibrillation. What can we learn form ECG? *Cardiol J* 2008;15:402.
[38] Platonov P, Mitrofanova L, Ivanov V, et al. Substrates for intra-atrial and interatrial conduction in the atrial septum: anatomical study on 84 humans hearts. *Heart Rhythm* 2008;5:1189.
[39] Cosio FG, Martín-Peñato A, Pastor A, et al. Atrial activation zapping in sinus rhythm in the clinical electrophysiology laboratory. Observations in Bachmann's bundle block. *J Cardiovasc Electrophysiol* 2004;15:524.
[40] Conde D, Baranchuk A. Bloqueo interauricular como sustrato anatómico-eléctrico de arritmias supraventriculares: syndrome de Bayés.*Archivos de Cardiología de México.*2013.
[41] Conde D, Baranchuk A. Síndrome de Bayés: lo que un cardiologo no debe dejar de saber. *Revista Argentina de Cardiologia*.2014. in press.
[42] Enriquez A, Conde D, Baranchuk A, et al. Relation of interatrial block to new-onset atrial fibrillation in patients with chagas cardiomyopathy and implantable cardioverter-defibrillators. *AJC impress.* DOI: 10.1016/j.amjcard.2014.02.036.
[43] Baranchuk A, Conde D, Enriquez A, et al. P-wave duration or Pwave morphology? Interatrial block: seeking for the holy grail to predict AF recurrence. Ann Noninvasive Electrocardiol 2014;00:1-3.

ECG Methods and Technologies

Lead Selection for Maximal QT Interval Duration Measurement in Patients with Heart Failure and Stroke

I.Mozos

"Victor Babes" University of Medicine and Pharmacy, Timisoara, Romania
Email: ioanamozos@yahoo.de

Abstract. *A prolonged QT interval is a predictor of sudden cardiac death. QT interval is prolonged in heart failure and stroke patients. Interlead variability of the QT interval is considerable, but its measurement is laborious in all 12 standard ECG leads. The objective of the present study was to find the leads with the longest QT interval duration in patients with stroke and heart failure. A total of 122 patients, 43 with heart failure, 61 with stroke and 18 healthy controls, underwent standard 12-lead ECG, and the QT interval was measured in each lead and corrected for heart rate using the Bazett formula (QTc). Maximal QT interval duration (QTmax) was measured most often in the precordial leads: V2, V4, and V3. Considering limb leads, QTmax was measured most often in DII. The highest QTc and QTmax values were recorded in stroke and heart failure patients, respectively. The precordial leads are the most reliable leads for assessment of maximal QT interval duration. DII is the most reliable limb lead for QT interval measurements in patients with stroke and heart failure.*

Keywords: Electrocardiography, QT interval, Heart Failure, Stroke

1. Introduction

The QT interval, including ventricular depolarization and repolarization, begins at the initiation of the Q wave and ends where the T wave returns to the isoelectric line, and reflects the summed ventricular action potential durations [1, 2]. Prolonged QT interval duration continues to be a reliable predictor of syncope, torsades de pointes, ventricular arrhythmia and sudden cardiac death. Significant spontaneous variability in the QT interval duration appears within standard 12-lead ECG leads [1]. Measurement of the QT interval is laborious in all 12 standard ECG leads, the selection of the optimal ECG lead for QT interval measurement may be crucial for further therapy [3], which justifies the objective of the present study to find the leads with maximal QT intervals. With improved survival after major cardiovascular events and aging of the population, stroke, myocardial infarction and arrhythmias will be increasing clinical entities in the coming decades [4].

2. Subject and Methods

Study Design and Population
An observational retrospective study was performed including 122 participants with stroke, heart failure and healthy controls. The investigations conformed to the principles outlined in the Declaration of Helsinki (Cardiovascular Research 1997; 35:2-4) and were approved by the Ethics Committee of the university. Patients with heart failure, diagnosed according to the ACCF/AHA Guidelines [5] and stroke, according to the AHA criteria [6], were included. The most important exclusion criteria were atrial fibrillation and electrolyte imbalances.

Standard 12 Lead ECG
The participants underwent standard 12-leadECG and QT interval was assessed in each lead, according to a previously described methodology [7]. QT interval duration was prolonged if >450 ms in men and >460 ms in women [8]. Borderline QT interval was considered for QT interval

durations of 430-450 ms in men and 450-460 ms in women [9]. The Bazett formula was used for heart rate correction of the QT interval [10].

3. Results

The study population included 122 participants, aged 60±16 years, 54% female, 43 with heart failure stage A, B and C (27 with an old myocardial infarction, 16 hypertensive), 61 with ischemic stroke and 18 healthy controls. QTmax, QTc, HR and QT interval duration in all standard ECG leads are included in Table 1. QTc was prolonged in 73 patients (60%). Borderline QTc values were measured in 15 patients (12%).

Table 1. Maximal QT interval duration (QTmax), heart rate corrected QTmax (QTc), heart rate (HR) and QT interval duration in each of the 12 standard ECG leads.

Variable	Results (Means±SD)
QTmax	421±55 ms
QTc	483±65 ms
HR	81±20 beats/min
QT in DI	380±56 ms
QT in DII	377±59 ms
QT in DIII	363±56 ms
QT in aVL	382±61 ms
QT in aVF	377±55 ms
QT in aVR	376±54 ms
QT in V1	370±54 ms
QT in V2	393±48 ms
QT in V3	393±49 ms
QT in V4	387±52 ms
QT in V5	388±55 ms
QT in V6	387±55 ms

Leads with Maximal QT Interval Duration

Maximal QT was measured more frequent in leads V2 (in 18% of the patients), V4 (15%) and V3 (14%). Considering only patients with a prolonged QTc, QTmax was measured most often in V3 (16%), followed by leads DI, aVL and V2 (14%) and DII, aVF, V4 and V5 (12%), and most seldom in lead aVR (5%). In heart failure patients, maximal QT interval duration was found most frequently in leads V2 (28%), aVF and V4 (21%), and V3 (19%). QT interval duration was frequently found prolonged in DII (20%), V3 and V5 (18%) and V4 (16%), in stroke patients. V3 (33%), V6 (28%) and DII and V2 (22%) were most often the leads with the maximal QT interval duration in the healthy control group.

Interlead variability

The leads proving the closest approximation to QTmax were: V3 (26%), V2 (21%), V6 and DII (20%). In patients with a prolonged QTc, the leads providing the closest approximation to QTmax were: V3 (23%), V2 and V6 (21%) and DI and V4 (15%); V5 (35%), DII, V3 and V6 (28%) and aVL (23%) in patients with heart failure; V3 (26%), V6 (20%) and DI (18%) in stroke patients; V2 (28%), DII, aVF, V3 and V4 (22%) and DI, aVR and V6 (17%) in the control group. DIII, DI, aVR and aVL were the leads with the highest deviation from the QTmax value. Considering only the patients with a prolonged QTc, the leads with the highest deviation from the maximal QT interval value were as follows: V1 (23%), DIII (22%) and aVR (18%). In patients with heart failure, DIII (33%), aVR (21%) and DI, DII were the leads with the highest deviation from the maximal QT interval. V1 (25%), DIII (23%) and DI (18%) were the leads with the highest deviation from the maximal QT interval in stroke patients, and aVL (44%), V1 (22%) and DIII (17%) in the control group.

ANOVA

The highest QTc and QTmax values were recorded in stroke and heart failure patients, respectively (Table 2). Heart rate showed no significant differences between the patients of the 3 groups (p=0.462).

Table 2. Maximal QT interval duration (QTmax), heart rate corrected QT interval (QTc) and heart rate (HR) in patients with heart failure, stroke and the control group

Variable	Heart failure group (n=43)	Stroke group (n=61)	Control group (n=18)	p values by ANOVA
QTc (ms)	490±61	494±69	429±25	0.00054
QTmax (ms)	434±57	424±57	382±19	0.003
HR (beats/minute)	79±21	83±21	76±9	0.462

QT interval duration and QTc in different leads was further compared in 30 participants with measurable QT intervals in all leads. The differences were not statistically significant (p by ANOVA = 0.232 and 0.355 for QT and QTc, respectively) (Table 3). The highest QT and QTc values were also

Table 3. QT interval duration in different leads for 30 study participants with measurable QT interval in all leads

Lead	**QT** (ms)	**QTc** (ms)
DI	368±50	429±61
DII	385±51	448±66
DIII	364±51	423±71
aVR	370±48	431±48
aVF	361±54	420±55
aVL	381±50	440±51
V1	367±49	427±42
V2	385±38	445±51
V3	388±42	448±46
V4	385±40	445±50
V5	384±53	443±57
V6	387±58	447±52

recorded in the precordial leads, especially V3, V6 and V4. QTc in lead DII was also very high. Table 1 also shows the highest QT interval durations in leads V2 and V3 for all study participants.

4. Discussion

The present study found the precordial leads as the most reliable leads for maximal QT interval measurements, especially: V3, V2, and V4 in patients with heart failure, stroke, prolonged QT intervals and healthy controls. Considering limb leads, QTmax was measured most often in DII.

It is known that the measured QT interval is influenced by the leads available for analysis [2]. The projections of the electrical activity on the various leads [11] are, probably, responsible for the QT interval differences in different leads. Electrical activity needs a longer period to travel from the heart to the peripheral electrodes [11], which explains the differences noticed in the limb leads. Lead DII is used for QT measurements in pharmacological studies [1]. The precordial leads are known to contribute significantly to the diagnostic utility of standard 12-lead ECG. Cowan et al demonstrated previously, in patients with anterior and inferior myocardial infarction, that V2 and V3 provide the closest approximation to QTmax [12], and interlead variability is, mainly, due to variation in QRS onset and T wave offset [11, 12]. There is a need for standardization of lead selection for QT interval duration measurement [12]. Sylven at al. suggested the possibility of uniform repolarization abnormalities throughout the ventricular myocardium, in patients with QT prolongation [13], which would explain why QTmax was often measured in several precordial and limb leads in the present study. Yeragani et al. found a highly significant difference between QT variability measures in leads V5 and V1 compared to V3 [14]. Monnig et al. recommended lead DII as a first choice and V5 as a second choice for clinical management of patients with congenital long QT syndrome, considering the risk of syncope and sudden cardiac death [3]. Yamaki et al. demonstrated that the sites of prolonged QT intervals corresponded to the sites of infracted areas in patients with anterior and postero-inferior myocardial infarction [15]. Alvarado-Serrano et al. observed that the QTpeak and JTpeak intervals prolong in old myocardial infarction patients when these intervals are measured in the infarct related leads [16].

The risk of sudden death is high in patients with heart failure, even with aggressive therapy, especially in decompensated heart disease with left ventricular dysfunction, postischemic heart failure, and use of diuretics [17]. Cardiac arrhythmias and ECG cerebrogenic abnormalities are frequent after acute cerebrovascular events [18], mainly due to an autonomic nervous system dysregulation, catecholamine storm, concomitant myocardial ischemia or necrosis, heart failure, cardiovascular risk factors, elevated serum uric acid, inflammation, reactive oxygen species, electrolyte imbalances, especially hypokalemia, and the structural and electrophysiological changes of the senescent heart [18, 19].

The present study is, as far as we know, the first attempt to find the leads with the longest QT interval duration in patients with stroke and heart failure, demonstrating the precordial leads as most reliable. Considering that patients with stroke and congestive heart failure are very often difficult to mobilize, it is very useful to know which ECG leads to select. The leads proving the closest approximation to QTmax were: V3, V6, V2 and DII. Considering that no statistically significant differences were found between the QT intervals in different leads in

patients with a measurable QT interval in all leads, any lead is useful for QT interval measurement, especially if the precordial leads are not available. The last choice for QT interval measurement should be: DIII and aVR, considering that in those leads the highest deviations from QTmax were obtained.

Concluding, the precordial leads are the most reliable leads for assessment of QT interval duration, especially V3, V2 and V4, so QTc should be obtained in one of these leads, in patients with heart failure, stroke, or healthy controls. DII, the inferolateral lead, is the most reliable limb lead for QT interval measurements.

References

[1] Lanjewar P, et al. Issues in QT interval measurement. *Indian Pacing Electrophysiol J*, 4(4): 156-161, 2004.

[2] Goldberger JJ, et al. AHA/ACCF/HRS Scientific Statement on Noninvasive Risk Stratification Techniques for Identifying Patients at Risk for Sudden Cardiac Death: A Scientific Statement from the AHA Council on Clinical Cardiology Committee on Electrocardiography and Arrhythmias and Council on Epidemiology and Prevention. *Circulation*, 118: 1497-1518, 2008.

[3] Monnig G, et al. Electrocardiographic risk stratification in families with congenital long QT syndrome. *Eur Heart J,* 27(17): 2074-80, 2006.

[4] Basile AM, et al. Selective risk factors profiles and outcomes among patients with stroke and history of prior myocardial infarction. The European Community Stroke Project. *J Neurol Sci*, 264: 87-92, 2008.

[5] Yancy CW, et al. 2013 ACC/AHA Guideline for the management of heart failure. *Circulation*, 128(16): e240-e327, 2013.

[6] Sacco RL, et al. An updated definition of stroke for the 21st century: A statement for healthcare professionals from the AHA/ASA. *Stroke*, 44: 2064-2089, 2013.

[7] Mozos I, et al. Factors associated with a prolonged QT interval in liver cirrhosis patients. *J Electrocardiol*, 44: 105-108, 2011.

[8] Rautaharju PM, et al. AHA/ACC/HRS recommendations for the standardization and interpretation of the electrocardiogram. Part IV: The ST segment, T and U waves, and the QT interval: A scientific statement from the AHA Electrocardiography and Arrhythmias Committee, Council on Clinical Cardiology; the ACCF; and the HRS; Endoresed by the ISCE. *Circulation*, 119: e241-e250, 2009.

[9] Goldenberg I, et al. QT interval: How to measure it and what is "normal". *J Cardiovasc Electrophysiol,* 17: 333-336, 2006.

[10] Bazett HC. An analysis of the time-relations of electrocardiograms. *Heart*, 7: 353-70, 1920.

[11] Macfarlane PW, et al. Influence of lead selection and population on automated measurement of QT dispersion. *Circulation*, 98:2160-2167, 1998.

[12] Cowan JC, et al. Importance of lead selection in QT interval measurement. *Am J Cardiol*, 61(1): 83-7, 1988.

[13] Sylven JC, et al. QT interval variability on the body surface. *J Electrocardiol*, 17(2): 179-88, 1984.

[14] Yeragani VK, et al. Significant difference in beat-to-beat QT interval variability among different leads. *Heart Dis*, 4(6): 344-8, 2002.

[15] Yamaki M, et al. The body surface distribution of the QT interval in patients with previous myocardial infarction and normal subjects. *Jpn Circ J*, 51(11): 1289-95, 1987.

[16] Alvarado-Serrano C, et al. Novel indices of ventricular repolarization to screen post myocardial infarction patients. *Comput Biol Med,* 36: 507-515, 2006.

[17] Ferrari R, et al. 150 questions and answers. 2nd edition. IME, Baume-les-Dames, France, 2011.

[18] Katsanos AH, et al. Electrocardiographic abnormalities and cardiac arrhythmias in structural brain lesions. *Int J Cardiol*, 167:328-334, 2013.

[19] Aronow WS. Cardiac arrhythmias. Mechanisms, pathophysiology, and treatment. InTech, Rijeka, Croatia, 2014.

YIA Session I:
New ECG Methods and Animal Experiments

Removing Ventricular Far Field Artifacts in Intracardiac Electrograms during Stable Atrial Flutter using the Periodic Component Analysis – Proof of Concept Study

[1]T. G. Oesterlein, [1]G. Lenis, [2]A. Luik, [1]B. Verma, [2]C. Schmitt, [1]O. Dössel

[1]Institute of Biomedical Engineering, Karlsruhe Institute of Technology, Germany,
[2]Städtisches Klinikum Karlsruhe, Karlsruhe, Germany
Email: publications@ibt.kit.edu

Abstract. *Post-ablation atrial flutter (AF) is a frequently occurring arrhythmia after treatment for persistent atrial fibrillation. However, mapping the flutter circuit using intracardiac electrograms is often challenging due to low signal voltage and scar areas caused by prior substrate modification. In addition, signals are frequently compromised by ventricular far field (VFF) artifacts, which obscure atrial activity (AA). This work introduces a new approach for VFF removal, which is based on the Periodic Component Analysis (πCA). It utilizes the stable temporal relationship between AA and VFF, which poses a problem for other techniques like Principal Component Analysis (PCA) when both components superpose. A benchmark using simulated electrograms demonstrated significantly better correlation for this case when comparing pure AA to the reconstructed data using πCA instead of PCA (0.98 vs. 0.90, p<0.001). Its benefit for diagnosis is demonstrated on clinical data.*

Keywords: Intracardiac Electrograms; Ventricular Far Field; Periodic Component Analysis; Atrial Flutter; Signal Processing

1. Introduction

Atrial flutter (AF) following catheter ablation of atrial fibrillation (AFib) poses a major problem since it occurs in about 36-40 % of cases and is highly symptomatic due to dominant 2:1 conduction [1]. For diagnosis, atrial activity (AA) is the most important component of intracardiac electrograms (EGM), since it indicates the flutter circuit. However, scars from previous ablation and low amplitude signals make diagnosis difficult. Also significant ventricular far field (VFF) can obscure AA if EGMs are measured close to the mitral valve.

Various techniques have been suggested to remove VFF artifacts during AFib, like Template Matching and Subtraction [2] or Principal Component Analysis (PCA) [3].

This is the first work known to the authors introducing the Periodic Component Analysis (πCA) as a new method for VFF removal in AF, in which it utilizes the stable dynamic pattern of cardiac excitation for optimized signal filtering.

2. Available data and methods

Simulated electrograms
In total 1200 signals s_{comp} of length 5s were simulated, containing both AA and VFF (compare Fig. 1 (a-c)). Flutter cycle length (FCL) was chosen to be 280 ms and 200 ms for 2:1 and 3:1 conduction rate, respectively [1]. RR intervals were varied within the signals to mimic variability in atrioventricular conduction time. A time shift between VFF and AA was introduced to simulate recordings at 6 different phases of the flutter circuit, including both simultaneously (S, as in Fig. 1 (c)) and non-simultaneously (NS) occurring VFF and AA.

Clinical signals

A clinical signal recorded during stable atrial flutter (FCL 330 ms, rate 2:1) was selected for demonstration. Data was acquired during activation time mapping using a 10 pole circular mapping catheter (Optima, St. Jude Medical, St. Paul, MN, USA), in connection with the EnSite Velocity electroanatomical mapping system (St. Jude Medical). It was filtered by the mapping system (30-250 Hz) and exported for a continuous segment of 7.9 s (sampling rate 2034.5 Hz) with stable catheter position close to the inferior mitral valve annulus.

Principal Component Analysis

PCA was used in previous works to remove VFF in both AFib and AF [3]. It was applied on a matrix of segmented VFF to identify eigenvectors accounting for at least 90 % of the total variance. These were expected to primarily contain VFF and subsequently neglected when reconstructing the signal s_{PCA}, resulting in pure AA without VFF. Since this approach relies on the statistical independence of atrial and ventricular depolarization, its applicability during stable AF is questioned as atrial and ventricular activities are temporarily coupled in this case.

Periodic Component Analysis

The general concept behind πCA is to find an optimal mixing vector **w** for the linear combination $s(t)=\mathbf{w}^T\mathbf{x}(t)$ of input signals **x**(t), which maximizes the periodicity of the output signal s(t) for a given period of τ. This can be formulated as minimizing the measure

$$\epsilon(\mathbf{w},\tau)=\frac{\sum_t |s(t+\tau)-s(t)|^2}{\sum_t |s(t)|^2}=2\left(1-\frac{\mathbf{w}^T C_{xx}(\tau)\mathbf{w}}{\mathbf{w}^T C_{xx}(0)\mathbf{w}}\right) \quad \text{with} \quad C_{xx}(\tau)=E_t\left\{\mathbf{x}(t+\tau)\mathbf{x}(t)^T\right\}$$

and solved using the Rayleigh-Ritz theorem [4]. The mixing vector **w** corresponds to the eigenvector of the largest generalized eigenvalue of the matrix pair $\{C_{xx}(\tau),C_{xx}(0)\}$.

In the context of VFF removal, the desired output signal $s\pi_{CA}=s(t)$ is given by pure AA, repeated periodically with FCL. Since VFF is caused by ventricular depolarization, all samples recorded during the QS time t_{QS} might be compromised by VFF. Therefore the compromised EGM channel s_{comp} is combined with a set of N additional channels to form the input signal matrix **x**(t), where N corresponds to the number of samples recorded during t_{QS}. Single Dirac pulses are placed synchronously to the ventricular depolarization in each new channel, see Fig. 1 (e). No Dirac pulses are placed outside t_{QS}, so that pure AA cannot be altered by the linear combination. Consequently, πCA is supposed to determine the optimal vector **w,** which enables us to uncover the periodic component of AA by weighting the additional channels to form an inverse VFF template.

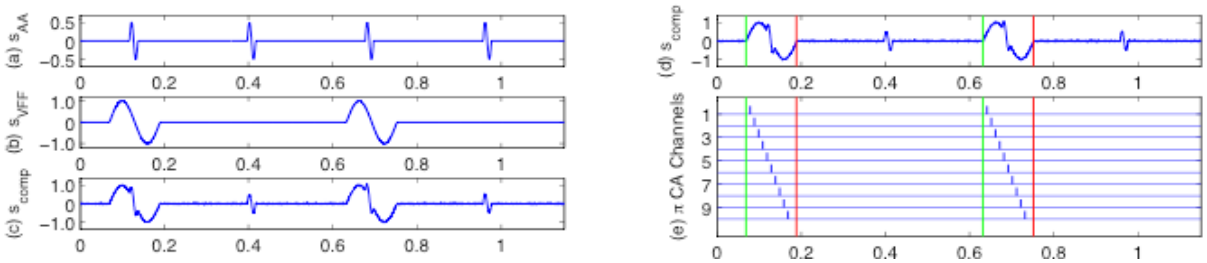

Fig. 1. Composition of simulated signals and additional channels for application of πCA. Simulated signals s_{comp} (c) are composed of pure AA s_{AA}(a), ventricular far field s_{VFF} (b) and noise. AA and VFF can superpose (S) or occur non-simultaneously (NS). For πCA application, additional channels (e) are added to form the πCA input matrix **x**. Each channel contains Dirac pulses placed synchronously to the ventricular depolarization only during t_{QS} (indicated by vertical lines). Amplitudes in mV, time in s.

Performance evaluation

Correlation coefficients between s_{AA} and signals s_{comp}, s_{PCA} and $s\pi_{CA}$ were computed. Statistics were generated considering both types S and NS. White Gaussian noise (σ_n=0.02 mV) was added to each signal. Statistical values were computed as μ±SD. Statistical significance was evaluated using the one-sided paired t-test at a significance level of 0.01, after Gaussian-like distribution of the data was confirmed.

3. Results

The result of filtering compromised signals of type S using both PCA and πCA is depicted in Fig. 2 (a-c). While AA was recovered using πCA, its morphology was deformed when PCA was applied. The same result can be observed in the clinical signal in parts (d-f), where the VFF preceding the atrial component was successfully removed by πCA.

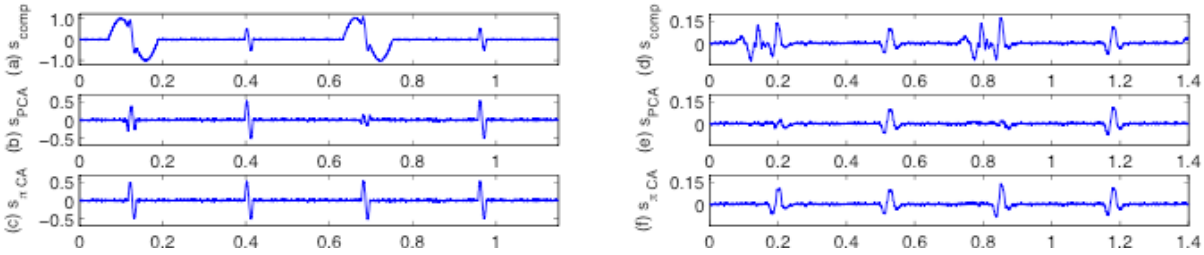

Fig. 2. Removing VFF artifacts using PCA and πCA. Each signal contains four atrial activations with the first and third compromised by VFF. Filtering the simulated signal (a) using PCA resulted in changes to AA morphology (b), while it was retained when applying πCA (c). Measured clinical signal with biphasic VFF preceding AA (d). Using PCA, every second AA complex was removed since it was synchronous to the VFF (e). Application of πCA yielded reasonable results (f). Amplitudes in mV, time in s.

Since the ground truth was known for simulated data, correlation coefficients were computed as measure of performance and are provided in Table 1. Similar results were obtained for both rates 2:1 and 3:1. Averaging over both, difference between PCA and πCA was significant for type S (0.98 vs. 0.90, $p<0.001$), but not for NS (0.98 vs. 0.98, ns).

Table 1. Statistics of correlation coefficients between s_{AA} and s_{comp}, s_{PCA} and $s_{\pi CA}$ filtered data.

Signal	Compromised Signal		Filtering using PCA		Filtering using πCA	
Type	S	NS	S	NS	S	NS
Rate 2:1	0.26±0.07	0.27±0.00	0.88±0.04	0.98±0.00	0.98±0.00	0.98±0.00
Rate 3:1	0.33±0.05	0.30±0.03	0.91±0.03	0.96±0.04	0.98±0.00	0.98±0.00

4. Discussion

Qualitative and quantitative benchmarking

Initial average correlation coefficient between s_{AA} and s_{comp} was strongly improved by both filtering methods. However, πCA performed better than PCA on global average over all types (0.98 vs. 0.93) and significantly for superimposed AA and VFF. This is in agreement with the assumption for PCA, that simultaneous AA would be considered part of VFF and thus be removed, while AA would not be affected when occurring non-simultaneous to VFF.

Impact on clinical signal processing
VFF artifacts can obscure diagnostically relevant atrial activity in uni- and bipolar EGMs. πCA seems to provide a new mean of removing VFF, requiring only the time of ventricular depolarization (which can be determined from QRS position) and the atrial activation rate (derived from coronary sinus activity). Thus no manual settings are required.

Limitations and future goals
Further work should include more realistic templates for AA and VFF, or realistic simulations using cardiac excitation models. However, impact of this aspect on benchmarking results seems limited. It is important to note that πCA relies on stability of AA and VFF morphology.

Conduction rates were set to 2:1 or 3:1, but might also be varying in clinical practice. Considered RR interval dynamics ranged 560±6.7 ms and 600±6.6 ms, respectively.

Additional channels for πCA were formed using periodic Dirac pulses. Other functions like the Gaussian bell or the Mexican hat wavelet might be applicable as well. They could potentially reduce the number of basis functions needed for VFF cancellation.

5. Conclusions

Periodic Component Analysis (πCA) was shown to be a suitable new method to remove VFF artifacts by utilizing the stable dynamics of atrial flutter. Comparison with Principal Component Analysis (PCA) on simulated data yielded statistically significant superior performance (correlation of 0.98 vs. 0.90, $p<0.001$) for superimposed activities. This was in agreement with the initial assumption that PCA might fail since it relies on the statistical independence of atrial and ventricular activity. Recovering obscured atrial activity using πCA was also demonstrated on clinical data. All parameters necessary for πCA application could be determined automatically from surface ECG and intracardiac recordings, making it a perfect filtering tool for next generation electroanatomical mapping systems.

Acknowledgements

The work of Tobias Oesterlein is funded by the German Research Foundation (DO637/14-1).

References

[1] Patel AM, d'Avila A, Neuzil P, Kim SJ, Mela T, Singh JP, Ruskin JN, Reddy VY. Atrial tachycardia after ablation of persistent atrial fibrillation: identification of the critical isthmus with a combination of multielectrode activation mapping and targeted entrainment mapping. *Circulation Arrhythmia and Electrophysiology*, 2008; 1(1): 14-22.

[2] Rieta JJ, Hornero F. Comparative study of methods for ventricular activity cancellation in atrial electrograms of atrial fibrillation. *Physiological Measurement*, 2007; 28(8): 925-936.

[3] Schilling C, Aubreville M, Luik A, Schmitt C, Dössel O. PCA-based ventricular far field cancellation in intraatrial electrograms. In proceedings of Biomedical Engineering, 2010; 5(s1): 49-52.

[4] Sameni R, Jutten C, Shamsollahi, MB. Multichannel electrocardiogram decomposition using periodic component analysis. *IEEE Transactions on Biomedical Engineering*, 2008; 55(8): 1935-1940.

An Iterative Method for Solving the Inverse Problem in Electrocardiography in Normal and Fibrillation Conditions: A Simulation Study

N. Zemzemi

Carmen team – INRIA Bordeaux Sud-Ouest, Talence, France,
Email: Nejib.zemzemi@inria.fr

Abstract. *Electrocardiographic Imaging (ECGI) is a new imaging technique that noninvasively images cardiac electrical activity on the heart surface. In ECGI, a multi-electrode vest is used to record the body surface potential maps (BSPMs). Then, using geometrical information from CT-scans and a mathematical algorithm we construct the electrical potentials on the heart surface. The reconstruction of cardiac activity from BSPMs is an ill-posed problem. Some algorithms work well in sinus rhythm, but in arrhythmic conditions the reconstruction of the heart potential becomes worse. In this work we present an iterative mathematical approach based on domain decomposition methods and test it on synthetically generated data for normal and fibrillating heart conditions using anatomical 43 years old women geometry.*

Keywords: Electrocardiographic imaging, inverse problem, domain decomposition, bidomain model, ECG modeling

1. Introduction

The inverse problem in cardiac electrophysiology also known as electrocardiographic imaging (ECGI) is a new and a powerful diagnostic technique. It allows the reconstruction of the electrical potential on the heart surface from electrical potentials measured on the body surface. The computation of the electrical potential on the heart surface giving data on the body surface is known to be ill posed in the sense that a small variation of the body surface potential could highly modify the solution on the heart surface. In the mathematical community it is known by data completion as the Cauchy problem. Since 1923, Hadamard [1] has given an example illustrating the ill posedness of this problem. In the electrocardiographic community, different methods of regularization have been used and compared in order to solve the problem. These methods include Thikhonov regularization with L-curve [2], Composite Residual and Smoothing Operator (CRESO) [3], truncated SVD regularization and other regularization techniques (see [4] and the references there). In most of the papers in the literature the used formulation of the inverse problem is based on a transfer matrix that maps the electrical potential on the heart onto the body surface. The matrix is computed using the Green formula if the torso is supposed isotropic and homogenous or by the boundary elements method if the torso is supposed to be isotropic and piecewise homogeneous or by the finite element method in a more general situation in cases where the torso can be supposed anisotropic and/or inhomogeneous.

In this work we go back to the original formulation of the problem and propose a new mathematical way to solve the problem. The method that we present in this paper is based on a domain decomposition technique. It has been recently proposed at the international Conference of Domain Decomposition by Zemzemi [5] and tested on concentric spheres representing the torso. In this work it will be tested on synthetically generated data of a real human torso.

2. Methods

Anatomical Model

The torso geometry was generated from CT images of a 43 years old woman. The DICOM images were segmented using the medical imaging software Osirix. In order to take into account the torso heterogeneity we distinguish three different volume regions (lungs, bones, and the rest). After generating the surfaces we use INRIA meshing Software MMG3D to generate the 3D volume of the computational mesh. In Fig. 1, we show a screenshot of the mesh with the different regions. We assigned isotropic conductivities of 0.389 and 0.2 mS/cm to the lung and bone elements, respectively and 2.16 mS/cm to the rest.

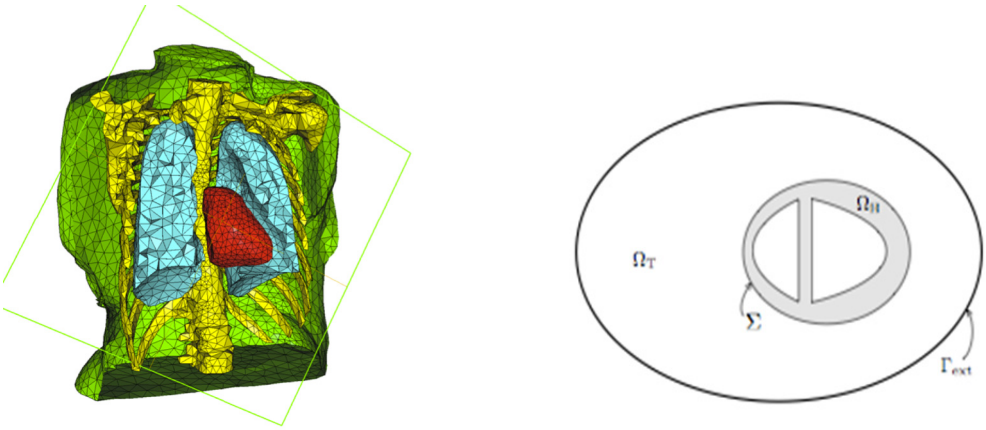

Fig. 1. Left: a cut of the torso computational domain showing the three different regions considered in the torso and the internal and external boundaries of the torso. Right: Two-dimensional schematic representation of the heart and torso domains.

Mathematical Modeling and Numerical Method

Let us suppose that Ω_T denotes the torso domain, Γ_{ext} is the external boundary, Σ is the heart torso interface and u_T is the electrical potential in the torso. The electrical potential on the torso is governed by the diffusion equation. For given electrical potential $\boldsymbol{d}$ on the external boundary, the inverse problem in electrocardiography is to find the electrical potential on the heart surface Σ satisfying both Dirichlet and Neumann boundary conditions on Γ_{ext} as shown in Eq. (1):

$$\begin{cases} \operatorname{div}(\boldsymbol{\sigma}_{\mathrm{T}} \boldsymbol{\nabla} u_{\mathrm{T}}) = 0, \text{ in } \Omega_{\mathrm{T}}, \\ u_{\mathrm{T}} = d \text{ and } \boldsymbol{\sigma}_{\mathrm{T}} \boldsymbol{\nabla} u_{\mathrm{T}}.\boldsymbol{n} = 0, \text{ on } \Gamma_{\mathrm{ext}}, \\ u_{\mathrm{T}} = ?, \text{ on } \Sigma. \end{cases} \tag{1}$$

Here σ_T denotes the conductivity parameter and depends on the three considered regions. The domain decomposition technique used for solving this inverse problem splits the ill posed problem (1) into two well posed problems:

$$\begin{cases} \operatorname{div}(\boldsymbol{\sigma}_{\mathrm{T}} \boldsymbol{\nabla} u = 0, \text{ in } \Omega_{\mathrm{T}}, \\ u = d, \text{ on } \Gamma_{\mathrm{ext}}, \\ \boldsymbol{\sigma}_{\mathrm{T}} \boldsymbol{\nabla} u.\boldsymbol{n} = -\boldsymbol{\sigma}_{\mathrm{T}} \boldsymbol{\nabla} v.\boldsymbol{n}, \text{ on } \Sigma. \end{cases} \qquad \begin{cases} \operatorname{div}(\boldsymbol{\sigma}_{\mathrm{T}} \boldsymbol{\nabla} v) = 0, \text{ in } -\Omega_{\mathrm{T}}, \\ \boldsymbol{\sigma}_{\mathrm{T}} \boldsymbol{\nabla} v.\boldsymbol{n} = 0, \text{ on } -\Gamma_{\mathrm{ext}}, \\ v = u, \text{ on } \Sigma. \end{cases} \tag{2}$$

where $(-\Omega_T)$ and $(-\Gamma_{ext})$ are respectively the symmetrical images of Ω_T and Γ_{ext} through the boundary Σ. The well-posed problem (2) could be mathematically seen as the Poincaré-Steklov formulation of a domain decomposition problem. The only non-classic part in this

problem is the fact that we have opposite fluxes at the boundary Σ. Different methods have been presented in the monograph [6] in order to solve domain decomposition problems using iterative procedures. In this paper we use the method presented in [5].

3. Results

In order to generate synthetic data by our ECG simulator based on the bidomain model we simulated two cases: In the first case the heart was stimulated at the apex and the electrical wave propagated from apex to base. We refer to this simulation as a normal case. In the second case we applied S1-S2 protocol in order to produce a re-entry wave. We refer to this case as a fibrillation case. Further information about the forward problem modelling can be found in [7]. We extract the BSP and use it as the input data ***d***. Fig. 2 shows snapshots of the electrical potential distribution in the first and second case for the exact inverse solution. We remark that the wave front is well captured but in the inverse solution it is much smoother than in the exact solution.

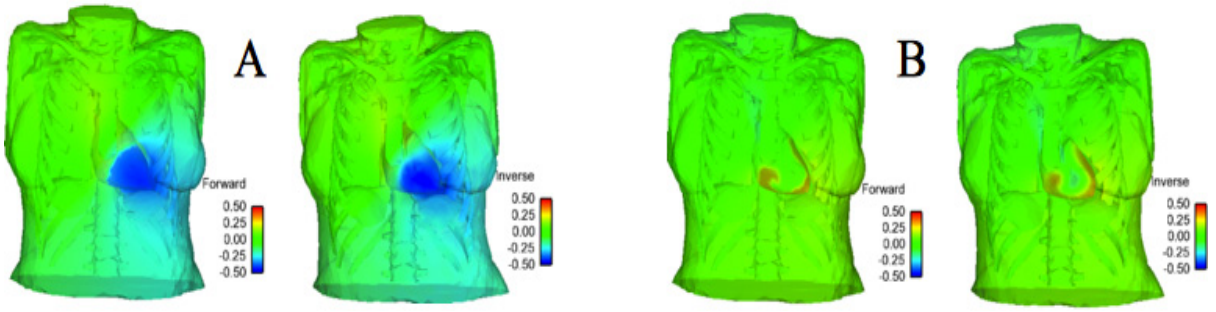

Fig. 2. A: Snapshots of potential distribution in the normal case. B: a snapshot of potential distribution for re-entry case. Forward solution (left) and Inverse solution (right).

In Fig. 3, we show a comparison of the time course of the heart potential between the inverse and the exact solutions at a point located in the right epicardium. The inverse solution is much more accurate in the normal case Fig. 3 (left). In the re-entry case the electrical potential is not accurate in terms of amplitude but looks synchronized with the exact solution. In fact in Fig.4, we show the evolution of the relative error, its mean in time is 0.45. In contrary, the correlation coefficient looks very good (Fig. 4 right) and the inverse solution looks at least 93% accurate in terms of the pattern of activation.

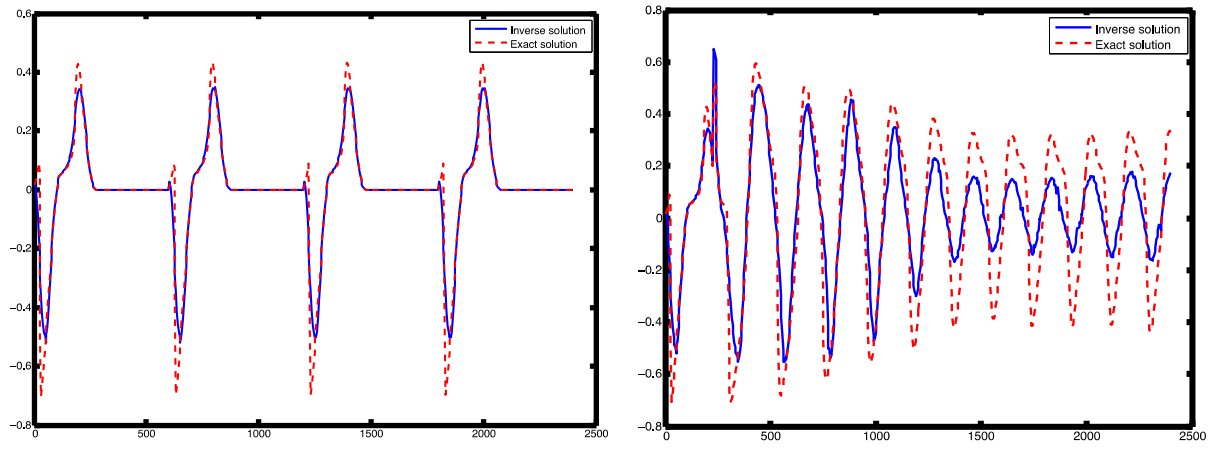

Fig. 3. Comparision of exact (red) and inverse (blue) solutions at a given point on the heart surface for normal (left) and fibrillating (right) heart conditions. X-axis: time (ms) and Y-axis: potential (mV)

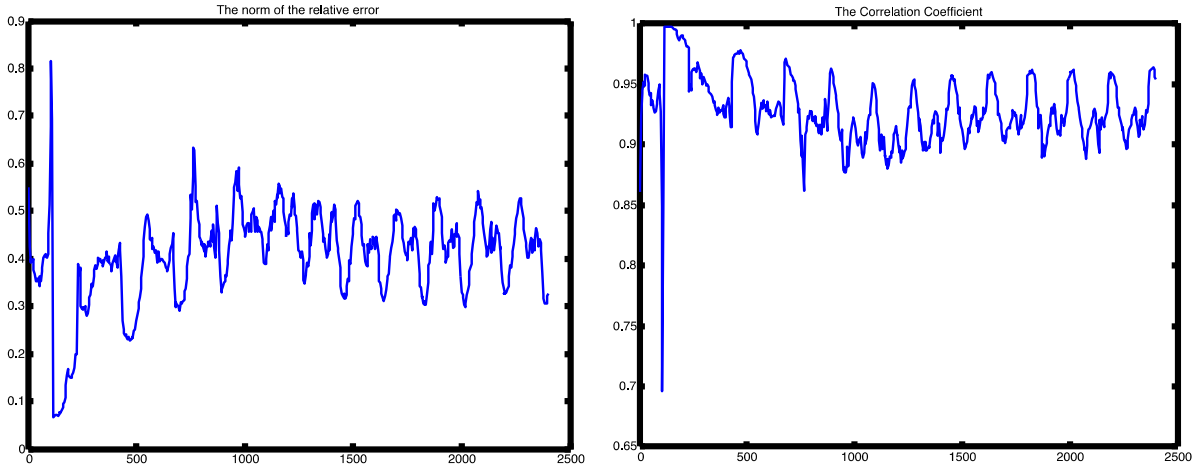

Fig. 4. Time course of the relative error (left) and correlation coefficient (right) computed using the exact and inverse solutions in case of fibrillating heart conditions. X-axis: time (ms) and Y-axis: (dimensionless).

4. Discussion and Conclusions

In this paper, we presented a new approach to solving the inverse problem in electrocardiography. The method is based on a Poincaré-Steklov operator that has solved using a domain decomposition technique. We used a segmented 3D-anatomical model of a 43 years old women torso. We generated synthetic data using the bidomain model for sinus rhythm and fibrillation conditions. In the normal case the reconstruction was very accurate; we have only seen a slight difference in terms of amplitude. In the re-entry wave case, the accuracy is very low in terms of relative error, mainly because the wave front is highly smoothened and the amplitude of the electrical potential is remarkably lower than the electrical potential of the exact solution. In contrary, the mean of the correlation coefficient over the time is 0.93. This gives an important potential for this method to be used in clinical applications.

References

[1] Hadamard J. Lectures on Cauchy's problem in linear partial differential equations, Yale University Press, New Haven, 1923.

[2] Ghosh S, Rudy Y. Application of l1-norm regularization to epicardial potential solution of the inverse electrocardiography problem. *Annals of Biomedical Engineering*, 37(5): 902--912, 2009.

[3] Franzone PC, Guerri L, Taccardi B, Viganotti C. Finite element approximation of regularized solutions of the inverse potential problem of electrocardiography and applications to experimental data. *Calcolo* 22(1): 91-186. 1985.

[4] Pullan A, Cheng L, Nash M, Ghodrati A, Macleod R, Brooks D. The inverse problem of electrocardiography. In Comprehensive Electrocardiology. Vol. 1, ch. 8, pp. 299–344, Springer, 2011.

[5] Zemzemi N. A Domain Decomposition Approach in the Electrocardiography Inverse Problem. LNCS, In proceedings of the 22nd Domain Decomposition International Conference. To appear.

[6] A. Quarteroni, A. Valli, Domain decomposition methods for partial differential equations, Numerical Mathematics and Scientific Computation, The Clarendon Press, Oxford University Press, 1999, Oxford Science Publications.

[7] Zemzemi N. A Steklov-Poincaré approach to solve the inverse problem in electrocardiography. *IEEE Computing in Cardiology Conference* (CinC), 2013, 703-706.

Respiratory Rate Simultaneous Estimation from Two ECG-derived Respiratory Waveforms Using an Adaptive Frequency Tracking Algorithm

L. Mirmohamadsadeghi, J.-M. Vesin

Swiss Federal Institute of Technology Lausanne (EPFL), Lausanne, Switzerland,
Email: leila.mirmohamadsadeghi@epfl.ch

Abstract. *Monitoring the respiratory rate (RR) in a fast, inexpensive and continuous manner is of great interest as its direct measurement requires bulky, expensive and inconvenient equipment. In this study, the RR is estimated in an instantaneous manner from the electrocardiogram (ECG) using two ECG-derived respiratory waveforms: the respiratory sinus arrhythmia (RSA) and the modulation of R-peak amplitudes (RPA). An adaptive weighted oscillator-based (W-OSC) frequency tracking algorithm is used to estimate their common frequency. The algorithm is evaluated on a public data set and it is shown that combining RSA and RPA is beneficial to using either alone.*

Keywords: Respiratory rate, adaptive frequency tracking, respiratory sinus arrhythmia.

1. Introduction

Respiration influences cardiac activity and thus the electrocardiogram (ECG) in several ways. The heart rate increases during inspiration due to physiological processes and the autonomic control of the cardiorespiratory system [1]. On the ECG, this modulation of the R-peak intervals by respiration is referred to as respiratory sinus arrhythmia (RSA). Furthermore, the mechanical aspects of respiration alter the electric dipole of the heart and the impedance of the thorax, which yield a respiratory modulation of the R-peak amplitudes in the ECG, referred to as the R-peak amplitudes (RPA) waveform [1].

Several methods exist to estimate the respiratory rate (RR) from either the RSA or the RPA waveforms [1]. In a pioneering work, Orphanidou *et al.* fused spectral information from both the RSA and RPA waveforms in order to derive the RR [2]. The most dominant peak from the autoregressive estimated spectra of the RSA and RPA was taken as representing the RR. However, this method does not provide a robust, real-time and automatic estimate of the RR in a continuous manner. Motivated by this concept of information fusion, the purpose of the present study was to estimate the instantaneous real-time RR by using the weighted multi-signal oscillator based band-pass filtering (W-OSC) algorithm [3] to track the common frequency component present in the RSA and RPA waveforms. This multi-signal frequency tracking method operates recursively on several signals simultaneously to track a common frequency component. It is instantaneous and provides an automatic approach to RR estimation from the RSA and RPA, in contrast to the ad hoc processing proposed in [2].

2. Materials and Methods

Data Set

The publicly available Physionet Fantasia data set [4][5] was used to evaluate the proposed algorithm. This data set contains 2-hour long records of simultaneously acquired ECG and respiratory (pneumography) waveforms from 20 young (21-34 years) and 20 elderly (68-85 years) subjects. The recordings were digitized at 250 Hz.

Extracting the Respiratory Waveforms from the ECG

The RSA is the modulation of the interbeat interval time series by the respiratory activity. The ECG R-peaks were extracted using a classic maxima detection algorithm. The time differences between consecutive peaks were computed and resampled uniformly using cubic splines at 2 Hz. This waveform was then band-pass filtered at respiratory frequencies, i.e., 0.1-0.5 Hz. The R-peak amplitudes were also resampled and filtered similarly to the RSA [1, 2].

Estimating the RR from the RSA and RPA waveforms

The W-OSC frequency tracking algorithm is based on a band-pass filter (BPF), the central frequency of which is adaptively updated to correspond to the common frequency of the inputs [3]. The inputs, i.e., the RSA and RPA waveforms, were filtered with the same BPF. At each new sample, the central frequency of the BPF was updated using a linear combination of the optimal updates for each input based on the difference between each output and a discrete oscillator model. The weights were computed in a recursive manner and were proportional to the inverse of the variance of the estimates of each input, in order to maximize the effect of inputs with high signal-to-noise ratio outcomes.

At each new sample, the overall central frequency coefficient $\propto$ was a weighted sum of coefficients obtained for each of the m = 1,…M inputs, i.e.,

$$\propto [n] = \sum_{m=1}^{M} W_m[n] \propto_m [n] \quad (1)$$

where W_m is the weight of the mth input and $\propto_m$ is the central frequency coefficient corresponding to the input. The instantaneous frequency f was computed as

$$f[n] = \arccos(\propto [n]) / 2\pi. \quad (2)$$

In order to assess the benefit of using RSA and RPA simultaneously, as opposed to either separately, the RR is also estimated by using the OSC algorithm, which is the single-signal version of the W-OSC algorithm, on the RSA and RPA waveforms separately.

This tracking algorithm is adaptive and has an inherent adaptation delay, which should be taken into account. This delay is estimated by using the cross-correlation between the estimate RR and the reference RR. An average delay is computed and used in all evaluations. The average delay was 25 ± 12 samples (which corresponds to 12.5 ± 6 s) over the data set.

Reference RR

The reference RRs were estimated from the data set respiratory waveform, which were resampled at 2 Hz. A combination of eight different estimates was used: a short time Fourier transform maximum frequency estimate, an estimate using the empirical mode decomposition followed by the Hilbert transform [6], an estimate based on respiration peak intervals, an estimate based on the number of peaks per window, an estimate based on the Teager-Kaiser energy tracking operator [7], an estimate based on the modified covariance method [8], an estimate based on autoregressive modelling [2] and an estimate based on Prony's method [9]. At each sample, the median of the eight estimates was computed, and the three closest estimates to it were averaged to produce a robust RR reference. The reference RR was filtered using a low-pass filter with a normalized cut-off frequency of 0.2 to smooth sudden changes due to the imperfect fulfilment of the assumptions regarding the different methods.

Experimental Setup

The W-OSC and OSC tracking algorithms were applied to RSA and RPA waveforms. Errors with respect to the reference RR were computed in 60 s sliding windows. The mean absolute error (MAE) was computed in breaths-per-minute (bpm) as

$$MAE = \frac{1}{N}\sum_{i=1}^{N}\left|bpm_{estim} - bpm_{ref}\right| \quad (3)$$

And the error percentage (EP) was computed as

$$EP = \frac{100}{N}\sum_{i=1}^{N}\frac{\left|bpm_{estim} - bpm_{ref}\right|}{bpm_{ref}} \quad (4)$$

where N is the length of the window, bpm_{estim} is the estimate RR and bpm_{ref} is the reference RR.

3. Results

An example RR estimate from the W-OSC is presented in Figure 1. The reference RR and the respiratory signal are shown as well. The estimate is truthful to the real RR in this example.

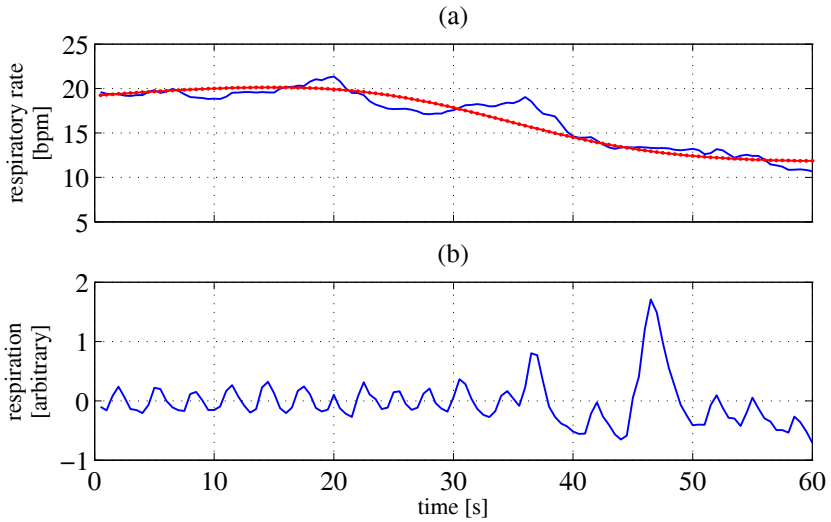

Fig. 1. RR estimate from the W-OSC method. (a) W-OSC RR estimate (solid blue) and the reference RR (dotted red); (b) respiratory waveform. Signals from minutes 33 to 34 of the Fantasia f1y08 record.

The estimates from the W-OSC tracking method with the RSA and RPA simultaneously and the estimates from the OSC tracking method with the RSA and RPA separately are compared to the reference RR in terms of MAE and EP in Table 1. It can be seen that the W-OSC estimate using both RSA and RPA results in higher accuracy than the OSC estimates using either the RSA or the RPA. Furthermore, the errors are smaller for the young population than for the elderly population using either both, or the RSA alone. However, the RPA yields more accurate estimates for the elderly population than for the young population.

Table 1. Errors of the W-OSC and the OSC tracking estimates over the Fantasia data set.

	young		elderly	
	MAE [bpm]	EP	MAE [bpm]	EP
W-OSC(RSA, RPA)	1.1	8.70%	1.39	9.25%
OSC(RSA)	1.72	12.12%	2.06	13.16%
OSC(RPA)	2.63	22.14%	2.01	14.49%

4. Discussion

Tracking the common respiratory frequency component of the RSA and RPA simultaneously yields a better RR estimate than tracking the respiratory frequency in either alone. Even

though estimation errors regarding the elderly population are slightly higher than those of the young population, the difference is smaller than those of either the RSA or the RPA alone. Thus, this scheme compensates for the decreasing RSA in the elderly.

The W-OSC tracking algorithm yields estimates comparable to the state of the art [2]. However, direct comparison is impossible, as the W-OSC is an instantaneous method in contrast to [2]. Also, in this reference, the ground-truth RRs were computed differently and parts of the records were discarded.

The W-OSC tracking is an adaptive method, however, it has an inherent adaptation delay of around 12 s. This is better than the state-of-the-art, where at best, estimates are produced for 60 s windows [2].

The W-OSC tracking is an automatic method and does not require any identification of abnormal beats, as it can rectify their effect within a few iterations.

5. Conclusions

This paper presented the instantaneous RR estimation from the RSA and the RPA using the W-OSC frequency tracking method. This RR estimate is comparable in accuracy to the state-of-the-art and is computed with a smaller delay. The method is automatic and does not require special subject-dependent adjustments. It has the potential to be used in real applications, where an RR estimate is needed and a single-lead ECG is available.

Acknowledgements

This work was funded thanks to the NanoTera ObeSense initiative.

References

[1] Bailon R, Sornmo L, Laguna P. Ch 8: ECG- Derived Respiratory Frequency Estimation. Advanced Methods and Tools for ECG Data Analysis. Artech House, Norwood, MA, USA, 1 edition, 2006.

[2] Orphanidou C, Fleming S, Shah SA, Tarassenko L. Data fusion for estimating respiratory rate from a single-lead ECG. *Biomed. Sig. Process. Control*, 8(1):98–105, 2013.

[3] Prudat Y, Vesin JM. Multi-signal extension of adaptive frequency tracking algorithms. *Sig. Process.*, 89(6):963–973, 2009.

[4] Iyengar N, Peng CK, Morin R, Goldberger A, Lipsitz LA. Age-related alterations in the fractal scaling of cardiac interbeat interval dynamics. *Am. J. Physiol.*, 271(4):1078–1084, 1996.

[5] Goldberger AL, Amaral LA, Glass L, Hausdorff JM, Ivanov PC, Mark RG, Mietus JE, Moody GB, Peng CK, Stanley HE. PhysioBank, PhysioToolkit, and PhysioNet: components of a new research resource for complex physiologic signals. *Circ.*, 101(23):215–220, 2000.

[6] Huang NE, Shen Z, Long SR, Wu MC, Shih HH, Zheng Q, Yen NC, Tung CC, Liu HH. The empirical mode decomposition and the Hilbert spectrum for nonlinear and non-stationary time series analysis. *Proc. Roy. Soc. London.*, 454(1971):903–995, 1998.

[7] Potamianos A, Maragos P. A comparison of the energy operator and the hilbert transform approach to signal and speech demodulation. *Sig. Process.*, 37(1):95–120, 1994.

[8] So HC. A comparative study of three recursive least-squares algorithms for single-tone frequency tracking. *Sig. Process.*, 83(9):2059–2062, 2003.

[9] Fertig LB, McClellan JH. Instantaneous frequency estimation using linear prediction with comparisons to the DESAs. *IEEE Sig. Process. Let.*, 3:54–56, Feb. 1996.

Novel Method for Deriving Vectorcardiographic Leads Based on Artificial Neural Networks

M. Vozda, T. Peterek, M. Cerny

FEECS, Department of Cybernetics and Biomedical Engineering, VSB – Technical University of Ostrava, Ostrava – Poruba, Czech Republic
Email: michal.vozda@vsb.cz

Abstract. *Many methods for deriving vectorcardiographic (VCG) leads from 12-lead electrocardiogram (ECG) were published. All of them are based on a linear transformation. Differences are only in coefficients of transformation matrixes which are designed based on a model or on linear regression methods. This paper presents and assesses a new nonlinear transformation method based on artificial neural networks (ANNs) which offer better accuracy of the transformation. Derived VCG leads were compared with directly measured Frank leads for a group of 283 records from the PTB database. Methods based on ANNs achieve significantly lower MSE in all leads and significantly higher correlation coefficient in Z lead compared with both Kors and inverse Dower method.*

Keywords: vectorcardiography, artificial neural network, Frank leads

1. Introduction

The vectorcardiogram is the spatial representation of electromotive forces generated during cardiac activity and is analysed in three spatial planes (horizontal, frontal and sagittal). Although there are several VCG lead systems, in clinical practice they are not measured directly but usually derived from the 12-led ECG using some transformation method like inverse Dower [4] or Kors [5] method. Many methods for deriving VCG leads were developed. Modern methods try to minimalize the error of the transformation between lead systems. Most methods are based on linear transformation and the differences between them are in coefficients of transformation matrices. No nonlinear methods have been tested yet. There are some methods that can be used for solving nonlinear regression problems. The most popular methods are based on artificial neural network or support vector machine.

The purpose of this study is to present the nonlinear regression method based on ANNs for deriving VCG leads from the 12-lead ECG.

2. Subject and Methods

Study Population
We used the PTB diagnostic database that has been recorded on healthy volunteers and patients with different heart diseases at the Department of Cardiology of University Clinic Benjamin Franklin in Berlin, Germany. The database contains 549 records from 286 subjects (aged 17 to 87, mean 57.2; 209 men, mean age 55.5, and 81 women, mean age 61.6). Each subject is represented by one to five records. Each record includes 15 simultaneously measured signals: the conventional 12 leads (I, II, III, aVR, aVL, aVF, V1, V2, V3, V4, V5, V6) together with the 3 Frank VCG leads (X, Y, Z). Each signal is digitized at 1000 samples per second, with 16-bit resolution over a range of ±16.384 mV [3].

Only the first records that excluded patients with pacemaker were taken into account. The records were band-passed by a FIR filter with linear phase response in band from 0.25 to 150 Hz (-3dB). From the filtered records representative beats were chosen; PVCs and artefacts

were excluded. The beginning of the beat was defined as the distance from the R wave: $T_R - 0.4 \cdot T_{\min(RR)}$ and the end of the beat was defined as $T_R + 0.6 \cdot T_{\min(RR)}$, where T_R is the time instant of an R wave and $T_{\min(RR)}$ is a minimal heart cycle in the record. Individual representative beats were averaged in each of the 15 leads. Averaging should improve the signal-noise ratio. In this way we obtained 283 representative beats in 15 leads.

Design of Neural Network Architecture

To synthetize VCG leads from the 12-lead ECG we use a multilayer feed-forward ANN trained by means of the supervised back-propagation algorithm. The architecture includes input layer, hidden and output layers. Each layer includes neurons with specific activation function.

ANNs with 1, 2, 3 and 4 hidden layers and different numbers of neurons in hidden layers were tested. ANN with 2 hidden layers and 4 neurons in each hidden layer achieved the best accuracy of transformation. With increasing number of layers and/or neurons increased the training time of ANN with insignificant impact on the accuracy of the transformation. The input layer contains 8 neurons. Input and hidden layers contain neurons with hyperbolic tangent sigmoid activation function. The output layer contains 3 neurons with linear activation function.

Committee machine method is popular in processing with neural networks. This method uses a divide and conquer strategy in which the responses of multiple ANNs are averaged into a single response. This method was used in similar application for deriving chest leads from quasi-orthogonal leads I, II and V2 in work [1]. We decided to compare the impact of this method on the accuracy of the transformation, too.

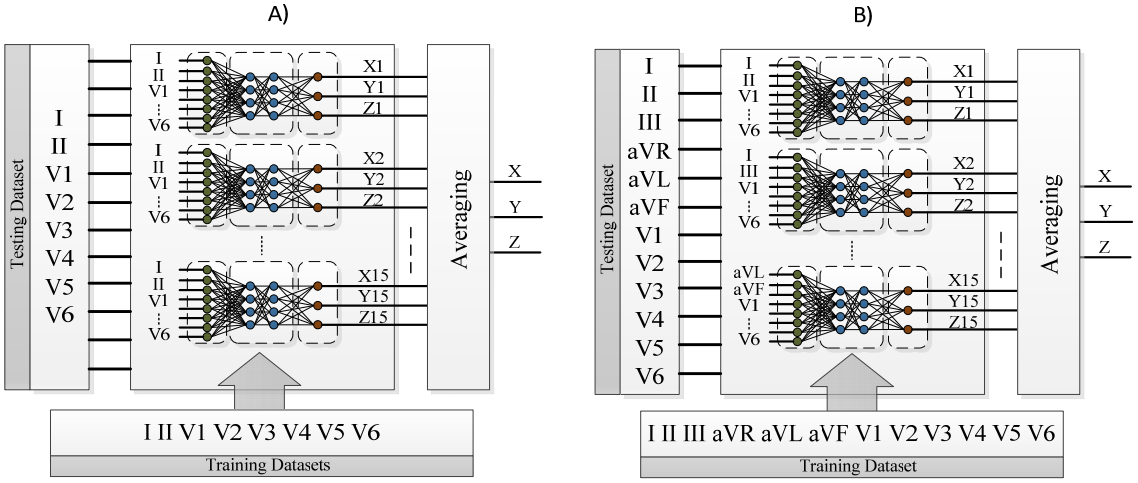

Fig. 1. Committee of ANNs for different training datasets A) and different ECG leads B).

Tested Methods

Four new and two commonly used methods were tested. ANN1 represents a method based on one ANN which is described above. The ANN is trained on all records from the training dataset. Its inputs are independent ECG leads which are usually used for transformations (I, II and V1…V6). ANN2 represents a method based on committee of 15 ANNs. Each ANN has 8 inputs represented by 8 independent ECG leads. Six of them are leads V1…V6 and the last two leads are some of the 15 combinations of limb leads pairs (I, II; I, III; I, aVL; … aVR, aVF). Each ANN has different combination of independent ECG leads what is shown in Fig.2B. ANN3 represents a committee of 15 ANNs. Each ANN is trained on slightly different training dataset in sense of cross validation (Fig. 2A). ANN4 represents a combination of methods ANN2 and ANN3. The committee includes altogether 75 ANNs. Fifteen different

combinations of independent ECG leads were used for group of 5 ANNs which are trained on slightly different training datasets. All described methods were compared with the inverse Dower and the regression based Kors transformations which are commonly used in clinical and research practice [2].

Verification and Validation

All methods were tested under the same conditions, with the same testing datasets and with 10-folds cross validation. This approach is usually used for testing the performance of supervised learning-based methods. Records were randomly divided into 10 groups, 9 of them (255 records) served for training the ANNs as the training dataset. One remaining group (28 records) served for testing of all methods as the testing dataset. In the next step other 9 groups were chosen and 1 remaining group was again used as the testing dataset. We continued in this way 10 times. This is the most efficient way how to test the supervised learning-based methods with maximum usage of the training data.

Performance of all methods was evaluated by the two most often used parameters: Pearson correlation coefficient and Mean Squared Error (MSE) [1], [2]. Pearson correlation coefficient indicates the degree of similarity between two signals and is independent from the differences in their amplitudes. The MSE is a measure of differences in amplitudes between two signals. Each method was tested for all VCG leads. MSEs and correlations between leads computed by the tested methods and directly measured Frank leads were evaluated.

3. Results

One sample t-test was used for testing the normality of MSE and correlation coefficients for all methods and in all leads. Whereas that data are not from a normal distribution, the nonparametric Mann-Whitney U-test was used for testing the differences between the methods. The null hypothesis was tested that the data obtained from two compared methods are samples with equal medians. Rejecting the null hypothesis we prove statistical difference between the two methods at the 5% significance level ($\alpha = 0.05$).

The statistical tests prove that the differences between the methods based on ANNs are not significant. For all of them the MSE is for all leads significantly lower than for Kors and inverse Dower transformation. The correlation coefficient for methods with ANNs is significantly higher only for lead Z when compared with the Kors transform. Differences in correlations for X and Y leads are not significant. For the Kors method, the MSE is significantly lower for all leads and correlation coefficient is higher for leads X and Z when compared with the inverse Dower transformation.

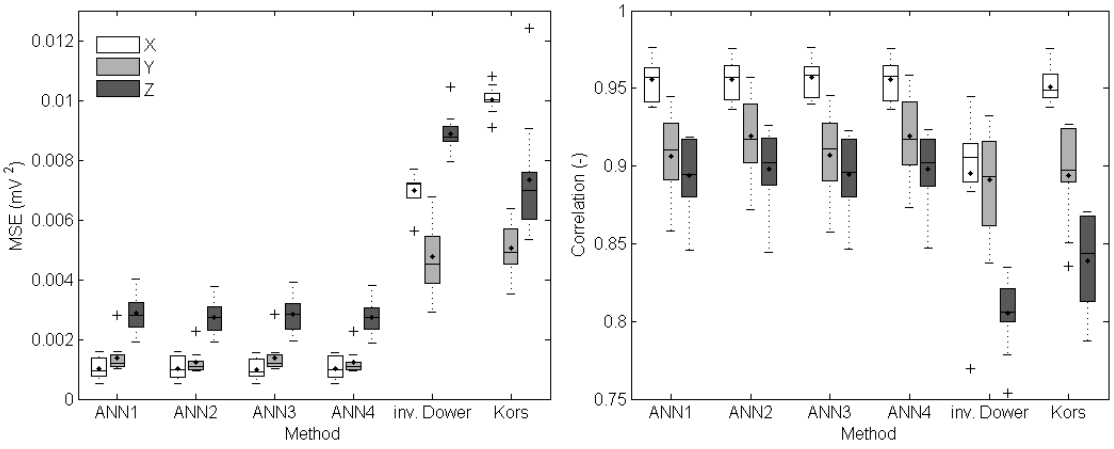

Fig. 2. Box-Whisker diagram of the MSE and correlation for individual methods in leads X, Y and Z.

4. Discussion

In this study, six transformation methods were tested and compared under the same conditions. Differences between methods based on ANN are insignificant and all of them are more accurate than both Kors and inverse Dower method that are commonly used. We validated that the Kors method achieves better accuracy when compared with the inverse Dower method what was shown also in other publications [2], [5]. Our results suggest that nonlinear regression method could improve the accuracy of transformation for the 12-lead vectorcardiography but for practical application its testing on a larger dataset is needed. In addition to the PTB database, it is possible to use CSE databases that include many 15-lead records.

Evaluation of a new method based on MSE and correlation is often used but it cannot replace the experience of a skilled cardiologist who can evaluate differences in diagnostic information which is the most important parameter. For future work we would like to test nonlinear regression methods on larger datasets measured in cooperation with cardiologists at different workplaces. Further, we would like to test the performance of transformation methods based on features that are commonly used in vectorcardiography, like QRST or planar angle.

5. Conclusions

The 12-lead vectorcardiography is based on transformations of the 12-lead ECG to VCG leads. Each transformation introduces certain error of amplitude and shape of the derived VCG leads. In this article we proposed a new method based on ANNs that provides significantly higher accuracy of transformation when compared with conventional commonly used methods. Methods based on ANNs can improve the state of the art in transformations between lead systems.

Acknowledgements

The work and the contributions were supported by the project SV SP2014/194 “Biomedical engineering systems X” and the project Opportunity for young researchers, reg. no. CZ.1.07/2.3.00/30.0016, supported by Operational Programme Education for Competitiveness and co-financed by the European Social Fund and the state budget of the Czech Republic.

References

[1] Atoui H, Fayn J, Rubel P. A Novel Neural-Network Model for Deriving Standard 12-Lead ECGs From Serial Three-Lead ECGs: Application to Self-Care," Information Technology in Biomedicine*, IEEE Transactions on* , vol.14, no.3, pp.883-890, May 2010.

[2] Rubel P, Fayn J. Quantitative assessment of eight different methods for synthesizing frank VCGs from simultaneously recorded standard ECG leads. *Journal of Electrocardiology*. 1991, vol. 24, s. 197-202.

[3] Bousseljot R, Kreiseler D, Schnabel, A. Nutzung der EKG-Signaldatenbank CARDIODAT der PTB über das Internet. Biomedizinische Technik, Band 40, Ergänzungsband 1 (1995) S 317.

[4] Edenbrandt L, Pahlm O. Vectorcardiogram synthesized from a 12-lead ECG: Superiority of the inverse Dower matrix. *Journal of Electrocardiology*. 1988, vol. 21, issue 4, s. 361-367. DOI: 10.1016/0022-0736(88)90113-6.

[5] Kors JA, Van Herpen G, Sittig AG, Van Bemmel JH. Reconstruction of the Frank vectorcardiogram from standard electrocardiographic leads: diagnostic comparison of different methods *Eur Heart J* (1990) 11 (12): 1083-1092.

Modified Lewis ECG Lead System for Ambulatory Monitoring of Atrial Arrhythmias

[1]A. Petrėnas, [1]V. Marozas, [2]L. Sörnmo, [3]G. Jaruševičius, [1]D. Gogolinskaitė

[1]Biomedical Engineering Institute, Kaunas University of Technology, Kaunas, Lithuania
[2]Department of Biomedical Engineering, Lund University, Lund, Sweden
[3]Institute of Cardiology, Lithuanian University of Health Sciences, Kaunas, Lithuania
Email: andrius.petrenas@ktu.lt

Abstract. *The analysis of atrial activity (AA) during atrial arrhythmias can be problematic when a reduced lead system is used due to low amplitude and noise. Although leads for AA enhancement were proposed many years ago by Sir Thomas Lewis, two electrodes need to be placed directly on the chest, and therefore arm movement artefacts are likely to occur. In this study, we propose a modified Lewis lead system better suited for ambulatory applications where the electrodes are placed in areas with less muscle. The proposed modification was compared to the Lewis leads as well as to the ES lead of the EASI system. Forty-one healthy volunteers and 8 patients with atrial fibrillation participated in the study. The results show that the proposed lead exhibits the best atrial-to-electromyographic activity ratio, with twice as large AA amplitude as the original leads. Furthermore, the atrial-to-ventricular activity ratio is 50% better than that of the ES lead. The results suggest that the proposed modification of the Lewis lead system has a potential to improve ambulatory monitoring of atrial arrhythmias.*

Keywords: Atrial activity enhancement; atrial fibrillation; Lewis ECG lead system

1. Introduction

While it is well-known that atrial fibrillation (AF) is a progressive disease, with brief episodes evolving into longer and eventually persistent, a recent debate has arisen whether brief episodes of AF are related to cryptogenic ischemic stroke [1], [2]. The hypothesis that brief AF episodes (< 30 s) can contribute to thrombus formation has yet to be proven, and thus automatic detection of very short episodes could accelerate more accurate diagnosis. The problem of false alarms due to electromyographic (EMG) noise, motion artefacts, and ectopic beats of commercial equipment for AF detection [3] forces cardiologists to review software-defined arrhythmia episodes manually, especially if AF events are brief [1], [2]. Since manual revision is exceedingly time-consuming and sometimes unreliable [4], increased accuracy of AF detection devices is required to ensure that brief AF events are detected in long-term ECG recordings.

Since most algorithms for AF detection are based solely on the analysis of RR interval irregularity, the many false positives still represent an unsolved problem. While attempts have been made to reduce the number of false positives by involving information on atrial activity (AA) in the AF detection process, the performance of such algorithms has turned out to not be better than those based on RR interval information [3]. The main reason for this outcome is that the conventional 12-lead ECG system, as well as reduced-lead modifications, are focused on ventricular activity (VA), and thus the electrode placement is not optimal for analysing AA. Due to the fact that AA amplitude is small compared to VA, an ECG lead with increased AA amplitude is beneficial to better discriminate between various arrhythmias of atrial origin (atrial tachycardia / flutter / fibrillation), as well other arrhythmias such as wide QRS complex tachycardia [5].

An ECG lead system for AA enhancement was proposed by Sir Thomas Lewis many years ago [6]. Unfortunately, this system requires that two electrodes are placed directly on the chest where arm movement artefacts may occur. In order to avoid leads on the chest muscles, the lead *ES* of the EASI lead system can be employed since it is potentially more immune to noise and offers a good projection of AA. However, there is so far a lack of studies which examine these properties for different leads.

In the present study, we propose a modified Lewis lead system where electrodes have been moved to a thorax area with less muscle. The purpose of the present study is to quantitatively evaluate different leads with respect to AA enhancement, including our proposed modified Lewis system in terms of AA amplitude, atrial-to-ventricular activity ratio, immunity to EMG noise, and motion artefacts. We anticipate that better understanding of the aforementioned properties will help to establish a lead well-suited for atrial arrhythmia monitoring.

2. Methods

The modified Lewis lead, denoted by L_{M1}, was obtained by removing electrode 2 and moving electrode 3 one intercostal space downwards (from 4th to 5th) in order to increase the immunity to arm movements (Fig. 1A). The modified lead system includes two additional leads L_{M2} and L_3. The proposed ECG lead system was compared to the original Lewis leads (L_1, L_2 and L_3) and the lead *ES*.

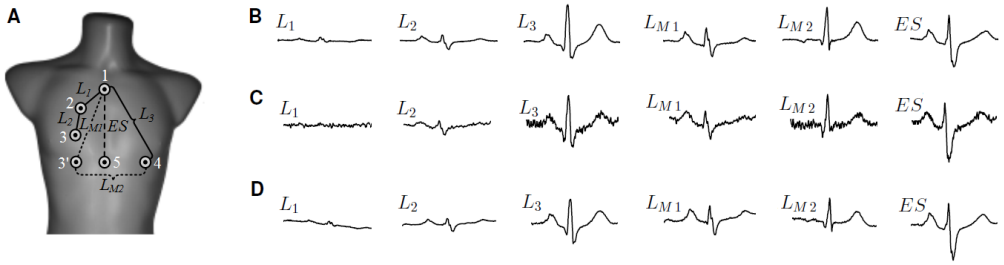

Fig. 1. ECG electrodes placement and ECG signal examples: ECG leads selected for investigation (each line type indicates leads of separate lead system) (A); ECG beats recorded during rest (B), weight holding (C), and exercising on elliptical trainer (D). Note that weight holding increases EMG activity, while exercising on elliptical trainer increases baseline wander.

Two groups of participants were enrolled in the study. The first group was 41 healthy volunteers (16 women), 25.0 ± 5.9 years old, with body mass index (BMI) of 22.2 ± 3.2 kg/m^2. The second group was 8 patients (3 women) with AF, 64.8 ± 9.6 years old, with BMI of 28.7 ± 4.3 kg/m^2. The healthy volunteers were included for the purpose of evaluating artefact related properties, e.g., EMG noise and baseline wander, induced by physical exercise. In order to investigate the peak-to-peak amplitude of AA, the healthy volunteers were asked to sit at rest for one minute. Then, they were instructed to perform two consecutive standardized physical activities which stimulate EMG noise and baseline wander. EMG noise was induced by holding a 1 kg weight with each straight arm horizontally when standing, while workout was performed on an elliptical trainer in order to increase baseline wander. The ECG was recorded simultaneously for each type of activity using the Quark T12x Telemetry Stress Testing ECG recording device (Cosmed, Rome, Italy).

The amplitudes of AA and VA was determined for each healthy volunteer by finding the mean peak-to-peak amplitude in consecutive beats of 1-min ECG segments recorded at rest. EMG noise was extracted by high-pass filtering the ECG signal recorded during weight holding according to the procedure described in [7]. Then, the root-mean-square (RMS) value (γ_{EMG}) of the high-pass filtered signal was computed. Baseline wander was acquired by low-pass filtering (cut-off frequency at 0.5 Hz) 1-min ECG segment recorded during workout on

the elliptical trainer. Baseline wander was quantified by the RMS value (γ_{BW}) of the low-pass filtered signal.

The AA amplitude (A_{AA}), the VA amplitude (A_{VA}) and the ratios A_{AA}/A_{VA}, A_{AA}/γ_{EMG}, A_{AA}/γ_{BW} were estimated for each of the studied leads. For AF patients, only amplitude-related properties were computed excluding physical activities. Since relatively large-amplitude f-waves are usually observed in the bipolar limb lead *II* [8], this lead was included for comparison. The mean peak-to-peak amplitude of AA was computed in individual f-waves appearing in the TQ interval so that the influence of VA would be minimal. The overall results are expressed as mean and two-sided confidence interval (95%). The statistical significance of the differences was determined using 2-sample *t*-test.

3. Results

Figure 2A shows that the AA (P wave) amplitudes in L_{M1} and *ES* are nearly 3 times higher than in the original Lewis leads L_1 and L_2. However, due to the markedly suppressed amplitude of VA, the Lewis leads produce the highest A_{AA}/A_{VA} ratio of 0.24 ± 0.04 and 0.23 ± 0.04 for L_1 and L_2, respectively (Fig. 2B). The modified lead L_{M1} has a ratio A_{AA}/A_{VA} (0.23 ± 0.04) similar to that of the original Lewis leads, however, the ratio A_{AA}/A_{VA} of *ES* is significantly lower (0.15 ± 0.02, $p < 0.001$). Moreover, L_{M1} gives the highest AA amplitude comparing to the level of EMG noise and provides statistically significantly higher A_{AA}/γ_{EMG} ratio (5.12 ± 0.72) than the Lewis leads and *ES* (see Fig. 2C). Despite the highest ratio A_{AA}/A_{VA}, the low amplitude of AA in L_1 gives 2.9 times lower A_{AA}/γ_{EMG} ratio than in L_{M1}. Figure 2D demonstrates that the level of baseline wander does not change significantly for any of the AA enhancing leads.

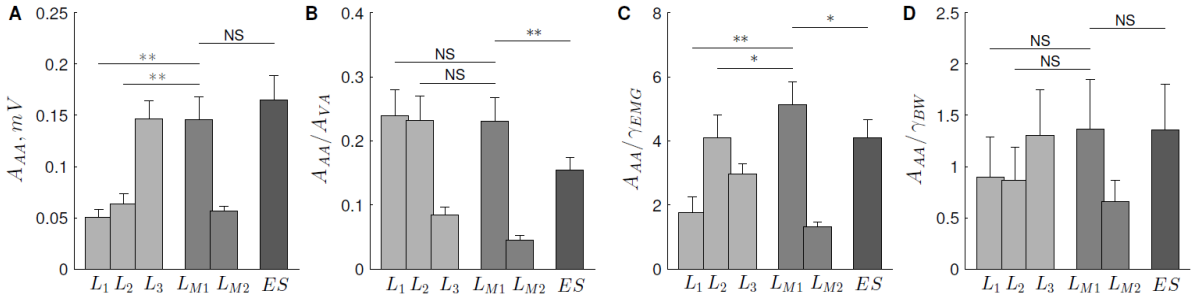

Fig. 2. Healthy volunteers results: the comparison of atrial activity amplitude (A), atrial to ventricular activity ratio (B), atrial to electromyographic activity ratio (C), and atrial activity to baseline wander ratio (D) in different ECG leads. Data represent mean ± CI (95 %); $*p \leq 0.05$, $**p \leq 0.001$, NS for $p > 0.05$.

The results computed from the AF signals show similar A_{AA} and A_{AA}/A_{VA} tendencies as were observed for healthy volunteers (Table 1). The amplitude of AA (f-waves) in L_{M1} is nearly twice as large as in *II*, while A_{AA}/A_{VA} in L_{M1} is 3.5 times higher than in *II*.

Table 1. Results from AF patients: the comparison of AA amplitude in leads of the modified lead system (L_{M1}, L_{M2}, L_3) and lead *II* when AF signals are analyzed. Values shown are mean ± CI (95 %).

Lead	L_{M1}	L_{M2}	L_3	*II*
A_{AA}, mV	0.16 ± 0.09	0.04 ± 0.02	0.13 ± 0.07	0.09 ± 0.05
A_{AA}/A_{VA}	0.21 ± 0.11	0.04 ± 0.03	0.09 ± 0.06	0.06 ± 0.04

4. Discussion

The aim of the present study is to gain better understanding of the properties of ECG leads considered to be suitable for AA enhancement. The potential use of the Lewis lead configuration in clinical practice was recently promoted by Bakker et al. [5], however,

according to the findings of this study, very low AA amplitude makes the Lewis leads prone to EMG noise. For long-term monitoring, we suggest the use of the modified Lewis lead which was demonstrated to have twice as large AA amplitude, therefore offering better immunity to EMG noise. Another interesting finding is that L_{M2} is associated with 5 times lower atrial-to-ventricular activity ratio than is L_{M1}, together with a low inter-subject variability. This finding can be especially important for f-wave extraction from ECG signal using adaptive filtering approach when a lead with negligible atrial activity is required [9].

5. Conclusions

This study shows that the modified Lewis lead has the best atrial to electromyographic activity ratio and produces twice as large amplitude of atrial activity as does the original leads. The results suggest that the proposed modification of the Lewis lead system has potential to improve ambulatory monitoring of atrial arrhythmias.

Acknowledgements

This work was partially supported by the European Social Fund (Agreement No VP1-3.1-SMM-10-V-02-004).

References

[1] Seet RCS, Friedman PA, Rabinstein AA. Prolonged rhythm monitoring for the detection of occult paroxysmal atrial fibrillation in ischemic stroke of unknown cause. *Circulation*, 124: 477–486, 2011.

[2] Flint AC, Banki NM, Ren X, Rao VA, Go AS. Detection of paroxysmal atrial fibrillation by 30-day event monitoring in cryptogenic ischemic stroke: The stroke and monitoring for PAF in real time (SMART) registry. *Stroke*, 43(10): 2788–2790, 2012.

[3] Harris K, Edwards D, Mant J. How can we best detect atrial fibrillation? *Journal of the Royal College of Physicians of Edinburgh,* 42(18): 5–22, 2012.

[4] Mant J, Fitzmaurice DA, Richard Hobbs FD, Jowett S, Murray ET, Holder R, Davies M, Lip GYH. Accuracy of diagnosing atrial fibrillation on electrocardiogram by primary care practitioners and interpretative diagnostic software: analysis of data from screening for atrial fibrillation in the elderly (SAFE) trial. *BMJ*, 335: 380–382, 2007.

[5] Bakker ALM, Nijkerk G, Groenemeijer BE, Waalewijn RA, Koomen EM, Braam RL, Wellens HJJ. The Lewis lead: making recognition of P waves easy during wide QRS complex tachycardia. *Circulation*, 119: e592–e593, 2009.

[6] Lewis T. Clinical Electrocardiography. New York: Shaw & Sons. 1913.

[7] Welinder A, Sörnmo L, Feild DQ, Feldman CL, Pettersson J, Wagner GS, Pahlm O. Comparison of signal quality between EASI and standard Mason-Likar 12-lead electrocardiograms during physical activity. *American Journal of Critical Care*, 13: 228–234, 2004.

[8] Nault I, Lellouche N, Matsuo S, Knecht S, Wright M, Lim KT, Sacher F, Platonov P, Deplagne A, Bordachar P, Derval N, O'Neill MD, Klein GJ, Hocini M, Jaïs P, Clémenty J, Haïssaguerre M. Clinical value of fibrillatory wave amplitude on surface ECG in patients with persistent atrial fibrillation. *Journal of Interventional Cardiac Electrophysiology,* 26(1): 11–19, 2009.

[9] Petrėnas A, Marozas V, Sörnmo L, Lukoševičius A. An echo state neural network for QRST cancellation during atrial fibrillation. *IEEE Transactions on Biomedical Engineering*, 59(10): 2950–2957, 2012.

Body Surface Potential Mapping During Heart Hypertrophy Development in Infant Rats

A. Rasputina, I. Roshchevskaya

Laboratory of comparative cardiology, Komi Science Center, RAS, Syktyvkar, Russia
Email: nastyur@rambler.ru

Abstract. *Body surface potential mapping (BSPM) was performed in Wistar rats and in rats with inherited stress-induced arterial hypertension (ISIAH) at the age of 1, 7, 17 and 30 days. When analyzing isopotential maps of rats 3 phases of the ventricular depolarization were defined, and significant changes in durations of these phases in Wistar and ISIAH rats during early postnatal ontogenesis were determined. It was revealed that the duration of the ventricular depolarization in Wistar rats increased gradually from the 1st to the 30th day of postnatal ontogenesis and mostly on account of the middle phase. Duration of the ventricular depolarization in 1 day aged ISIAH rats was significantly larger than in Wistar rats of the same age, but it didn't change during the 1st month of postnatal ontogenesis and moreover it paradoxically decreased from the 1st to 17th day on account of the initial and terminal phases. For the first time significant changes in the durations of the ventricular depolarization and its phases between normotensive and hypertensive rats of the same ages revealed by the using BSPM may be considered as initial markers of the ventricular hypertrophy that developed in ISIAH rats during the early postnatal ontogenesis.*

Keywords: heart hypertrophy, depolarization, rats, ontogenesis

1. Introduction

Early postnatal ontogenesis is a period of powerful morphological and physiological changes of an organism. These changes are more expressed in immature born mammals, such as rats and murine rodents, and they affect all systems, including cardiovascular system.

During early postnatal ontogenesis of normotensive rats a relative prevalence of heart right ventricle disappears [1], number and sizes of cardiomyocytes increase [2], ion channel expression and function change [3]. All these factors affect an electrical heart activity of rats.

Rats with inherited stress-induced arterial hypertension (ISIAH) are characterized by the pronounced genetic predisposition to the development of arterial hypertension [4] that causes myocardial hypertrophy [5]. Previously it was shown that arterial pressure of 1-month old ISIAH rats was significantly higher in comparison with Wistar rats reaching the "hypertensive level" (> 150 mm Hg) to the age of 3 months, but this hypertension development didn't cause any ECG changes typical for myocardial hypertrophy in 3-months old ISIAH rats [4].

The goal of this work is to investigate age-specific alterations of heart ventricular depolarization in normotensive rats and in ISIAH rats to establish whether some signs of the ventricular hypertrophy caused by inherited arterial hypertension during postnatal ontogenesis are "visible" even at birth.

2. Subject and Methods

The study was conducted according to the local ethic committee of the Laboratory of comparative cardiology of the Komi Science Centre, Ural Division, Russian Academy of Sciences and to the principles of the humane relation to animals as provided by clauses of

«The European Convention for the Protection of Vertebrate Animals used for Experimental and Other Scientific Purposes» (ETS N 123 from 18.03.1986).

Body surface potential mapping (BSPM) was done in Wistar and ISIAH rats at the age of 1 (n = 29 and n = 12, respectively), 7 (n = 26 and n = 10, respectively), 17 (n = 18 and n = 10, respectively) and 30 (n = 11 and n = 9, respectively) days of postnatal ontogenesis. Animals were anaesthetized with ether (inhalation narcosis) or urethane (1.5 g/kg, im). Electrophysiological data were obtained from the anaesthetized rats lying on the back.

Cardioelectric potentials were recorded from 32 subcutaneous needle electrodes uniformly distributed on an animal chest from the neck base to the last costa in 4 vertical lines. Electrocardiograms (ECGs) from limb leads were recorded synchronously with ECGs from the body surface. All time values were represented relatively to the RII-peak. Electrical heart activity was analyzed during heart ventricular depolarization by the spatial and temporal parameters of body surface isopotential maps. Data were given as mean ± standard deviation.

3. Results

It was shown that electrical heart field during ventricular depolarization was formed on the body surface of Wistar and ISIAH rats aged from 1 to 30 days on 7-10 ms before the RII-peak. The zones of positive and negative cardiopotentials changed their locations twice during ventricular depolarization in all rats, and three phases of depolarization were detected by the beginning and ending of these two inversions [6]. After the first inversion of mutual cardiopotentials' distribution the zone of negative cardioelectric potentials was situated on the cranial, the area of positive one – on the caudal part of the chest. This distribution of cardiopotentials was retained during the middle phase of ventricular depolarization. During the terminal phase of depolarization the area of electronegativity was situated on the caudal, the zone electropositivity – on the cranial surface of the chest. This localization of cardioelectric potentials on the body surface didn't change till the end of ventricular depolarization.

When analyzing body surface potential maps of Wistar and ISIAH rats significant changes in durations of ventricular depolarization phases were determined (Fig. 1). Duration of the initial phase of depolarization didn't change with age in Wistar rats (Fig. 1a), but in ISIAH rats (Fig. 1b) it slightly increased with the age from 1 to 7 days from 6.83 ± 1.62 ms to 7.3 ± 1.92 ms, then it significantly decreased to the age of 17 days to 4.8 ± 0.93 ms ($p < 0.05$), and then increased to the age of 30 days to 6.83 ± 2.02 ms ($p < 0.05$). Duration of the middle phase in Wistar rats significantly increased with the age from 1 to 30 days from 5.67 ± 1.47 ms to 10.36 ± 1.06 ms ($p < 0.05$), but in ISIAH rats it didn't change with age. Duration of the terminal phase in Wistar rats slightly increased with the age from 1 to 30 days from 1.86 ± 0.81 ms to 2.77 ± 1.36 ms, while in ISIAH rats it decreased with age from 1 to 17 days from 6.15 ± 2.1 ms to 3.68 ± 1.07 ms and then it increased to the age of 30 days to 5.72 ± 1.51 ms ($p < 0.05$).

It was revealed that the duration of the ventricular depolarization in Wistar rats increased gradually from the 1st to the 30th day of postnatal ontogenesis and mostly on account of the middle phase. Duration of the ventricular depolarization in 1 day aged ISIAH rats was significantly larger than in Wistar rats of the same age, but it didn't change during the 1st month of postnatal ontogenesis and moreover it paradoxically decreased from the 1st to 17th day on account of the initial and terminal phases.

4. Discussion

It was revealed that the spatial dynamics of body surface cardioelectric field of ISIAH rats during ventricular depolarization and repolarization didn't change with age and was similar to that of newborn Wistar rats [7]. When analyzing the temporal dynamics of body surface cardioelectric field it was shown that durations of depolarization phases changed with age in different ways. The decreasing of the initial and terminal phases of depolarization with age from 1 to 17 days in ISIAH rats might be the evidence of a gradual disappearance of the relative heart hypertrophy that caused after the birth till 10-17 days of postnatal ontogenesis [1]. The increasing of these parameters to the age of 30 days might be the evidence of the beginning of the left ventricular hypertrophy development. This hypertrophy is typical for ISIAH rats [4]. In normotensive Wistar rats changes in durations of depolarization phases during early postnatal ontogenesis differed from those in ISIAH rats – the significant increase of duration of the middle phase was detected, and this increase was resulted in the increase of duration of the whole depolarization.

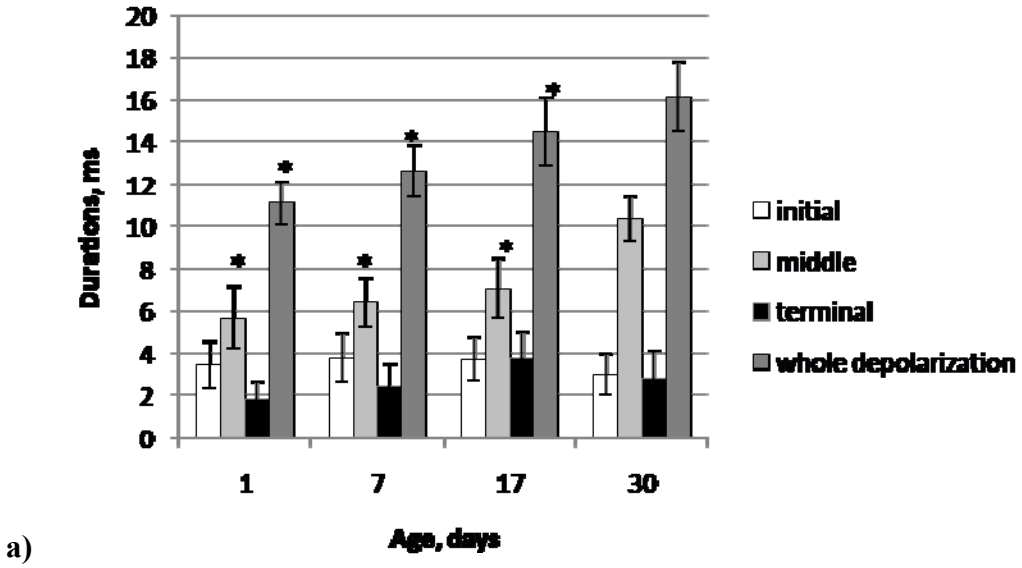

a)

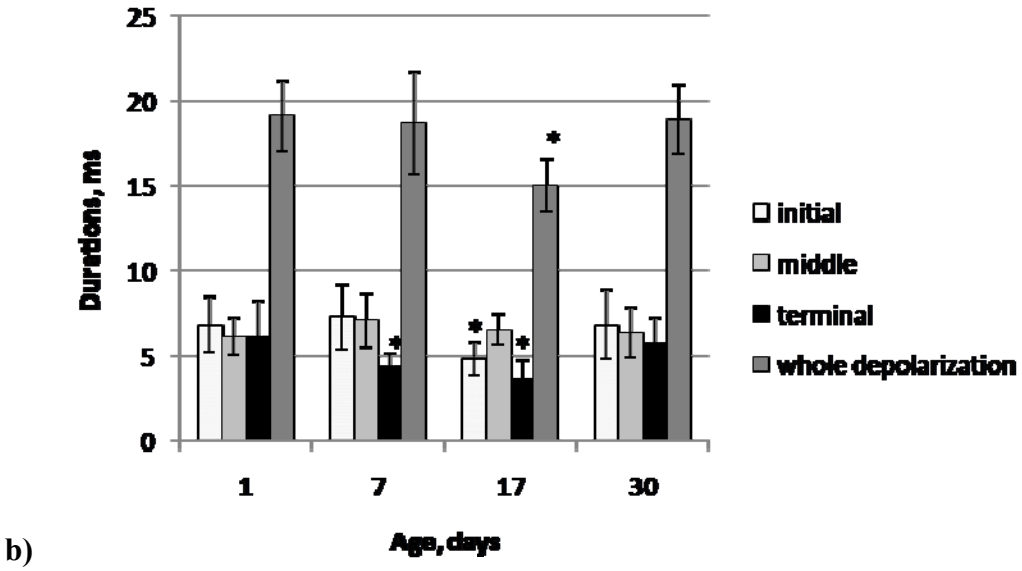

b)

Fig. 1. Durations of ventricular depolarization phases detected by BSPM in Wistar (a) and ISIAH (b) rats of different ages. * - $p<0.05$ in comparison with rats at the age of 30 days.

For the first time significant changes in the durations of the ventricular depolarization and its phases between normotensive and hypertensive rats of the same ages revealed by the using BSPM may be considered as initial markers of the ventricular hypertrophy that developed in ISIAH rats during the early postnatal ontogenesis.

Acknowledgements

The work is supported by the program of the basis investigations between UD and SD RAS № 12-C-4-1037.

References

[1] Anversa P., Olivetti G., Loud A. Morfometric study of early postnatal development in the left and right ventricular myocardium of the rat. *Circulation Research*, 46 (4): 495-502, 1980.

[2] Guo W., Kamiya K., Cheng J., Toyama J. Changes in action potentials and ion currents in long-term cultured neonatal rat ventricular cells. *American Journal of Physiology*, 271: C93-C102, 1996.

[3] Ferron L., Capuano V., Deroubaix E., Coulombe A., Renaud J-F. Functional and molecular characterization of a T-type Ca2+ channel during fetal and postnatal rat heart development. *Journal of Molecular and Cellular Cardiology*, 34: 533-546, 2002.

[4] Makhanova N.A., Antonov A.R., Markel' A.L., Yakobson G.S. Ontogenetic dynamics of arterial pressure and ECG in NISAG rats. *Bulletin of Experimental Biology and Medicine*, 6: 614-618, 1997.

[5] Suslonova O.V., Smirnova S.L., Roshchevskaya I.M. Ventricular myocardial layers and propagation of excitation in rat with stress-induced arterial hypertension. In Abstracts of the XXXVth International Congress on Electrocardiology, 2008, 108.

[6] Rasputina A.A., Roshchevskaya I.M. Electrical heart field during ventricular depolarization on the body surface of rats in the early postnatal ontogenesis. *Izvestia of the Komi Science Centre Ural Division RAS*, 1: 20-24, 2014 (in Russian).

[7] Roshchevsky M.P., Yurkova (Rasputina) A.A., Roshchevskaya I.M. Dynamics of the body surface cardioelectric field of one-day old rat. *Doclady Biological Sciences*. 410 (4): 571-573, 2006.

Effect of the Repeated Global Ischemia and Reperfusion on the RR and QT Interval in Isolated Rabbit Heart

[1,3]P. Veselý, [1,2]J. Halámek, [1,3]M. Ronzhina, [1,3]O. Janoušek, [1,3]J. Kolářová, [1,4]M. Nováková

[1]International Clinical Research Center, St. Anne's University Hospital, Brno, Czech Republic,
[2]Institute of Scientific Instruments, Academy of Sciences, Brno, Czech Republic,
[3]Department of Biomedical Engineering, Brno University of Technology, Brno, Czech Republic
[4]Department of Physiology, Faculty of Medicine, Masaryk University, Brno, Czech Republic
Email: p.vesely@fnusa.cz

Abstract. *This study was focused on determination of the QT/RR coupling during the repeated global ischemia and reperfusion in isolated rabbit hearts perfused according to Langendorff. In addition, the effects of these alternating states on heart function were compared between groups with and without administrated voltage-sensitive dye di-4-ANEPPS. The results showed the reverse relationship between RR and QT during ischemia as compared to reperfusion. Moreover, the heart response on the global ischemia in form of the RR prolongation was more pronounced in experiments without voltage-sensitive dye.*

Keywords: isolated rabbit heart, global ischemia, QT/RR coupling.

1. Introduction

The global ischemia effect of which was studied in this work is complete stop of coronary perfusion and therefore cannot be studied in human heart. On the other hand, the knowledge of the heart response to this pathophysiologic state may be of high importance since it might serve for early prediction of the life-threatening situations. Therefore, the animal models are used for such experiments. There is a positive coupling between QT and RR in humans under physiological conditions [1]. A trace of the reverse QT/RR coupling was studied during the stress measurement [2], [3] and during the coronary flow arrest. The aim of this study was to follow the effect of alternating phases of coronary flow arrest and full coronary flow on the heart function.

2. Subject and Methods

Eleven rabbits divided into group A (with voltage-sensitive dye di-4-ANEPPS; n = 8) and N (without di-4-ANEPPS; n = 3) were included in this study; all experiments followed the guidelines for animal treatment approved by local authorities and conformed to EU law. The isolated hearts were placed onto the Langendorff perfusion system and appended to the perfusion cannula via aorta. The Krebs-Henseleit (K-H) solution was bubbled by gas mixture (95%O_2 and 5%CO_2) during the whole experiment and used for heart perfusion. In this method of perfusion the solution flows only through the coronary system and no through the heart chambers. The measuring protocol lasted 120 minutes and consisted of two stages: preparatory stage (lasting 60 minutes) and experiment itself. In group A, the heart stabilization and voltage sensitive dye loading followed by washout was done during preparatory stage. In group N, the heart was stabilized by the K-H solution only. The experiments in both groups were divided into seven sections: control (constant perfusion with

K-H), ischemia I (I1; no perfusion), reperfusion I (R1; constant perfusion), ischemia II (I2; no perfusion), reperfusion II (R2; constant perfusion), ischemia III (I3; no perfusion), and reperfusion III (R3; constant perfusion). While the duration of ischemia and reperfusion was set strictly (10 minutes), the length of control section (at the end of preparatory stage) was about 2 minutes. Three Ag-AgCl electrodes were used for measurement of ECG in three orthogonal directions x, y, and z. Along with the ECG the action potential was measured. For the action potential measurement the optic method using the voltage sensitive dye was employed in group A. All signals were recorded by acquisition card (National Instruments) with frequency rate of 2000 Hz and 12 bit resolutions. The channels were filtered by the low-pass filter with the cut-off frequency 250 Hz. The R detection was based on wavelet transform and was performed in all available leads. For detection of the end of T wave the channels were filtered in the pass band from 0.3 to 35 Hz and the isoline regression method was consequently used for exact detection. The QR interval was considered constant and was given as mean level from manually detected QR intervals from all parts of experiment. RT intervals were detected in the one ECG channel per experiment only - the channel with the best shape of T wave was used. An example of RR and QT interval courses for one experiment from group A is shown in Fig. 1. The mean levels of RR and QT intervals were computed from the window of 40 beats at the end of all phases. The absolute values of RR and QT intervals were normalized to values in the resting state (nRR, nQT). The differences ΔnRR (ΔRR) and ΔnQT (ΔQT) between the ends of main sections (I1, R1, I2, R2, I3, R3) and the end of stabilization were computed over all experiments and both groups.

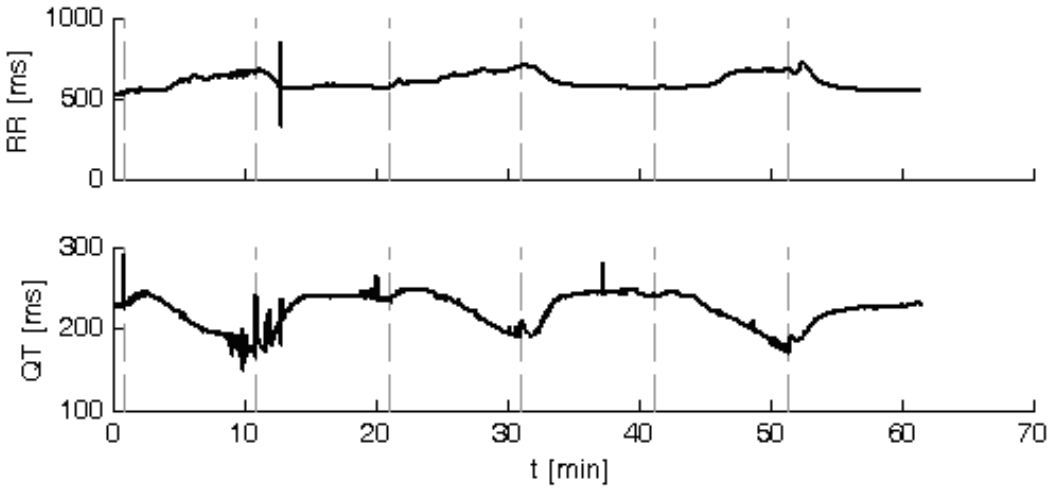

Fig. 1. An example of the RR and QT interval courses for experiment number 4 from group A. The gray dashed lines represent the beginnings of the sections.

3. Results

The mean ± STD values [ms] of RR and QT intervals at the ends of individual sections together with the differences between the values in main sections and the resting state in stabilization section computed over all experiments in each group are summarized in Table 1. The differences are supplemented by the statistical significance computed using the T-test and the ratio ΔQT/ΔRR. For clarity, the normalized differences were used for boxplots shown in Fig. 2. The values of ΔnRR and ΔnQT separately for sections ischemia and reperfusion were consequently fitted by lines over individual experiments and the mean ± STD of their slopes were for following comparison listed in Table 2.

Table 1. Mean ± STD of RR and QT interval at the ends of individual sections and their difference to the value in stabilization over all experiments and both groups. The marks in column ΔRR and ΔQT indicate the statistical significance: NS – non significant, * 0.05 >= p , ** 0.01 >= p, *** 0.001 > p.

Section (group)	RR [ms] Mean ± STD	ΔRR [ms] Mean ± STD	QT [ms] Mean ± STD	ΔQT [ms] Mean ± STD	ΔQT/ΔRR Mean ± STD
S (A)	514 ± 82	-	207 ± 19	-	-
I1 (A)	821 ± 118	307 ± 161 **	184 ± 29	-23 ± 22 *	-0.15 ± 0.15
R1 (A)	529 ± 76	15 ± 106 NS	208 ± 23	0.51 ± 8.49 NS	0.11 ± 0.13
I2 (A)	793 ± 120	279 ± 151 **	181 ± 29	-26 ± 23 *	-0.21 ± 0.25
R2 (A)	529 ± 86	16 ± 71 NS	207 ± 30	-0.59 ± 13.71 NS	0.23 ± 0.18
I3 (A)	745 ± 117	231 ± 132 **	177 ± 18	-30 ± 16 **	-0.21 ± 0.19
R3 (A)	558 ± 100	44 ± 80 NS	207 ± 29	-0.40 ± 14.43 NS	0.41 ± 0.45
S (N)	345 ± 23	-	162.2 ± 5.0	-	-
I1 (N)	617 ± 68	273 ± 91 NS	140 ± 12	-22 ± 7 *	-0.09 ± 0.02
R1 (N)	345 ± 24	0.46 ± 3.11 NS	158.2 ± 3.3	-4.0 ± 2.1 NS	-1.05 ± 1.69
I2 (N)	610 ± 67	265 ± 90 NS	123.0 ± 4.7	-39 ±5 **	-0.17 ± 0.07
R2 (N)	354 ± 13	9.0 ± 16.9 NS	166 ± 13	3.9 ± 12.4 NS	0.51 ± 0.34
I3 (N)	708 ± 32	363 ± 9 ***	101 ± 16	-62 ± 16 *	-0.17 ± 0.05
R3 (N)	341 ± 11	-3.3 ± 14.9 NS	159.4 ± 6.6	-2.7 ± 6.2 NS	0.29 ± 0.46

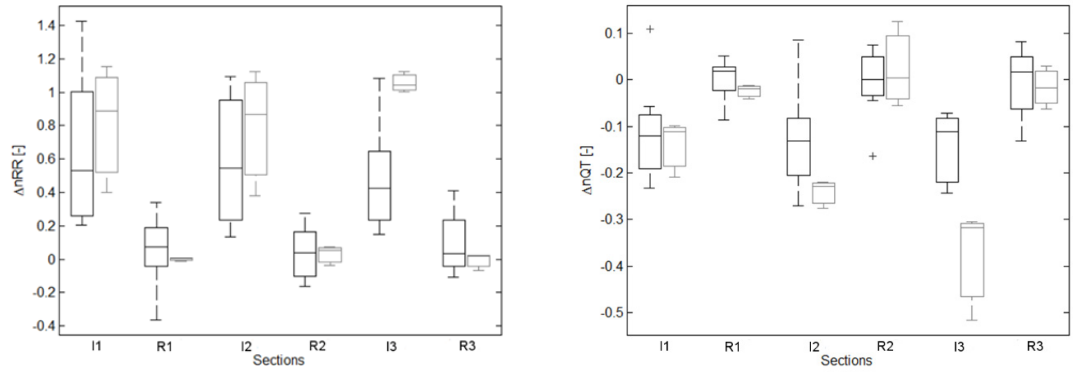

Fig. 2. The differences ΔnRR and ΔnQT between the ends of main sections and the end of stabilization over all experiments in each group. The black boxplots for group A and the gray boxplots for group N.

Table 2. The slope of the line fitted through the values of ΔnRR and ΔnQT separately for section of ischemia and reperfusion over individual experiments.

			Group A		Group N	
			Ischemia	Reperfusion	Ischemia	Reperfusion
Slope	ΔnRR	Mean±STD	-0.086 ± 0.123	0.021 ± 0.108	0.122 ± 0.134	-0.004 ± 0.022
	ΔnQT	Mean±STD	-0.015 ± 0.032	-0.003 ± 0.031	-0.120 ± 0.062	0.004 ± 0.015

4. Discussion

The standard QT/RR coupling, i.e. QT interval prolongation with increasing RR interval duration, is violated by the sections of the global ischemia. As shown in Fig. 1, QT interval shortened with elongating RR during these sections. The following reperfusion, during which the flow of perfusion solution was restored, caused the gradual return to the standard QT/RR coupling. The alternating sections of ischemia and reperfusion caused analogous changes of

RR and QT in both tested groups, but the rate of RR and QT reaction on the section transitions differed. There was a difference in the mean values of RR and QT at the end of the stabilization section between both groups, too. The mean values of RR and QT were greater for group A, meaning that the administration of voltage sensitive dye caused significant prolongation of both intervals. Therefore, only the changes computed from the normalized values (ΔnRR and ΔnQT) could be compared over the groups. The absolute values of ΔnRR and ΔnQT in group N were greater than in group A. This implied to stronger reaction of nRR and nQT on section transitions in group N. In addition, the slopes summarized in Table 2 showed almost opposite trend of ΔnRR and ΔnQT for both groups, especially the slopes computed for repeated ischemia. While in group A the impact of repeated ischemia on ΔnRR and ΔnQT is similar (ΔnQT) or even decreased (ΔnRR), in group N the impact is increased.

5. Conclusions

The standard QT/RR coupling, i.e. QT prolongation with increasing RR, was violated by the perfusion arrest in both tested groups. The differences between groups A and N were observed in the mean values of RR and QT at the end of stabilization section and in the rate of reaction of ΔnRR and ΔnQT on the perfusion arrest. The administration of voltage sensitive dye di-4-ANEPPS caused prolongation of RR and QT together with the heart function attenuation expressed as smaller reaction of ΔnRR and ΔnQT on the perfusion arrest. These results are in concordance with Fialova et al [4].

Acknowledgements

This work was partially supported by grant No. P102/12/2034 of the Grant Agency of the Czech Republic, by project MUNI/A/0957/2013, and by European Regional Development Fund – Project FNUSA-ICRC No. CZ.1.05/1.1.00/02.0123.

References

[1] J. Bazett, “An analysis of time relations of electrocardio - grams,” *Heart*, vol. 7, pp. 353 – 370, 1920.

[2] G. Roukema, J. P. Singh, M. Meijs, C. Carvalho, and G. Hart, “Effect of exercise-induced ischemia on QT interval dispersion,” *Am. Heart J.*, vol. 135, no. 1, pp. 88–92, Jan. 1998.

[3] H. Swan, M. Viitasalo, K. Piippo, P. Laitinen, K. Kontula, and L. Toivonen, “Sinus node function and ventricular repolarization during exercise stress test in long QT syndrome patients with KvLQT1 and HERG potassium channel defects,” *J. Am. Coll. Cardiol.*, vol. 34, no. 3, pp. 823–829, Sep. 1999.

[4] K. Fialova, J. Kolarova, I. Provaznik, and M. Novakova, “Comparison of Voltage-Sensitive Dye di-4-ANNEPS Effects in Isolated Hearts of Rat, Guinea Pig, and Rabbit,” *Comput. Cardiol. 2010*, vol. 37, pp. 565–568.

Vectorcardiographic Predictors of Ventricular Arrhythmia Inducibility in Patients with Tetralogy of Fallot

[1]D. Cortez, [1,2]E. Ruckdeschel, [1]A. C. McCanta,[1]K. Collins,[2]W. Sauer,[1,2]J. Kay, [2]D. Nguyen

[1]Children's Hospital of Colorado, Aurora, USA
[2]University of Colorado, Aurora, USA
Email:dr.danielcortez@gmail.com

Abstract: *Vectorcardiographic (VCG) parameters may have predictive value in Tetralogy of Fallot (TOF) patients undergoing electrophysiology studies (EPs) for ventricular arrhythmia (VA) inducibility. Methods: Blinded, retrospective analyses of 35 adult TOF patients undergoing EP studies prior to pulmonary valve replacements were performed (19 female patients, median age 37 years). VA inducibility was evaluated from EPs and resting 12-lead electrocardiograms (ECG's), respectively using heart rate adjusted Q-T interval(QTc), QRS duration, spatial QRS-T angle (peaks), principal T wave and principal QRS-complex (QRSwavev) component vectors (vector component root mean squares).Student t-tests, Mann Whitney U-tests and Analysis of Variance were used to assess differences between those with and without sustained inducible VA and the different VA morphologies. Odds ratios and relative risk were calculated. Results: 15 patients had inducible VA (5 monomorphic, 10 polymorphic VA) and 20 patients were not inducible. Only the QRSwavev showed significant differences between those with and without VA inducibility, 1.04±0.31mV vs. 1.45±0.48mV respectively ($p<0.003$), with an odds ratio of 37.53 and relative risk of 2.14. Conclusion: VCG evidence of depolarization differences was significant between TOF patients with and without inducible VA. VCG may have a role in risk stratification for arrhythmias in TOF patients.*

Keywords: vectorcardiography, tetralogy of Fallot, ventricular tachycardia

1. Introduction

Tetralogy of fallot (TOF) patients have significant arrhythmia burden post-operatively, reported to be as high as 43.3% [1]. Programmed ventricular stimulation in TOF patients has been showed to have diagnostic and prognostic value in risk stratisfying TOF patients [2].Vectorcardiographic (VCG) principles provide additional clinical information to the 12-lead electrocardiogram (ECG) and have provided further diagnostic [3,4] and prognostic [5-9] uses of the ECG in the traditional 12-lead set-up. We hypothesize that some of these parameters and their vector components may have predictive value in Tetralogy of Fallot (TOF) patients undergoing electrophysiology (EP) studies for ventricular arrhythmia (VA) inducibility.

2. Subject and Methods

A blinded retrospective analysis of 35 adult TOF patients undergoing EP studies prior to pulmonary valve replacements (PVR) was performed (19 female patients, median age 37 years). VA inducibility and vectorcardiography were evaluated from electrophysiology studies and resting 12-lead electrocardiograms, respectively using right ventricular (RV) inducibility studies as described Khairy et al. [2]. Specifically, measurements of Q-T interval adjusted for heart rate (QTc), QRS duration (QRSd), spatial peaks QRS-T angles (SPQRS-T angle), principal T wave and principal QRS-complex component vectors (Twave v and QRSwave v) (root mean square of the T–wave and QRS-complex vector components,

respectively) were used to compare those with inducible VA versus those without inducible VA. QRSwave v, Twave v and SPQRS-T angles were calculated by the visual estimation method (utilizing the Kors' et al regression-related analysis) as described by our group [10]. Figure 1 demonstrates the vectorcardiographic components of a patient with and a patient without VA inducibility. Student t-tests and the Mann-Whitney U test were used as appropriate in comparing those with and those without ventricular inducibility. Analysis of Variance were also used to assess differences between those with and without sustained inducible VA and between the three groups, respectively (non-inducible versus monomorphic versus polymorphic VA patients). An odds ratio (OR) and relative risk (RR) were calculated for inducible VA.

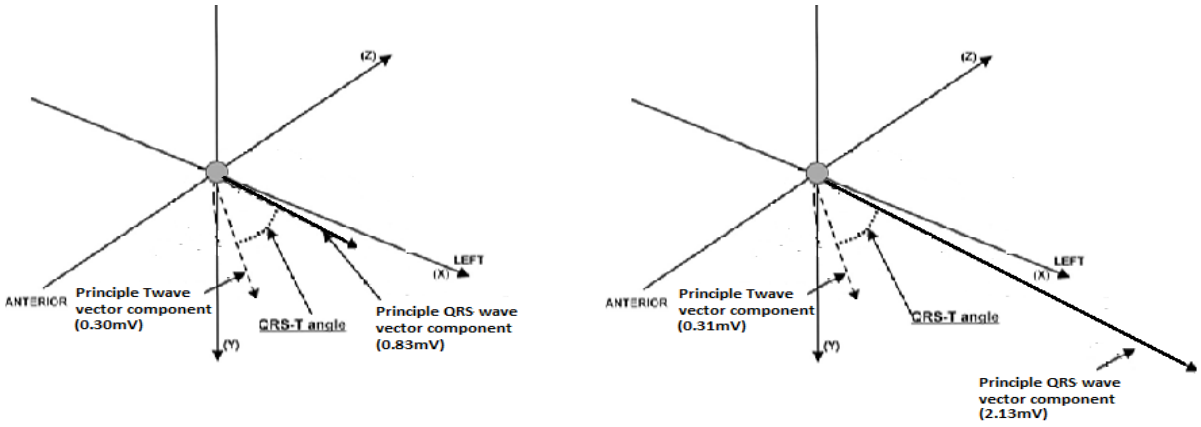

Fig. 1. Example of parameters used in TOF patients with and without ventricular inducibility

3. Results

Of the 35 patients analyzed, 15 had inducible VA (>5 beat ventricular tachycardia) with 5 having monomorphic VA and 10 having polymorphic VA. 20 patients were not inducible. Only the principal QRS-complex vector component showed significant differences between those with and those without VA inducibility, 1.04±0.31mV vs. 1.45±0.48mV respectively ($p<0.003$). Table 1 depicts all other parameters tested with associated p-values. The principle QRS-wave vector component had positive and negative predictive values of 63% and 100% respectively with an odds ratio (OR) of 37.53 (95% confidence interval (CI) 1.98 to 712.97) and relative risk (RR) of 2.14 (95% CI 1.33 to 3.46) at a cut-off of 1 standard deviation above the mean for those with VA inducibility (1.35mV) as noted in table 2. No other parameters including the QTc, QRSd or T wave vector No inter-group variability existed between those with inducible monomorphic VT, as compared to those with inducible polymorphous VT.

Table 1. Parameters used for prediction of ventricular arrhythmia inducibility (VAI)

	QTc[ms]	QRSd[ms]	SPQRS-T angle[°]	QRSwave v[mV]	Twave v[mV]
VAI(n=15)	484.0±39.7	157.5±27.9	103.6±38.4	1.04±0.31	0.46±0.15
No VAI(n=20)	486.0±37.9	162.1±34.9	98.2±45.3	1.45±0.48	0.49±0.22
p-value	0.29	0.72	0.58	0.003	0.90

Table 2. QRS wave vector component (QRS wv) positive and negative predictive values (PPV and NPV), Odds ratio and relative risk with 95% confidence intervals (95% CI).

	PPV	NPV	Odds Ratio	Relative Risk
QRSwv	0.63 (0.41-0.81)	1.00 (0.71-1.00)	37.53(1.98-712.97)	2.14 (1.33-3.46)

4. Discussion

These findings showed the root mean square of the depolarization vector components was more predictive of inducibility then any other parameter tested in our cohort. Surprisingly the QRSd and QTc were not predictive of inducible arrhythmogenicity as suggested by studies including a recent literature review by Bassareo and Mercuro[11]. This study also suggests TOF patients with increased QRSd should undergo electrophysiology studies to assess arrhythmogenicity. And since this has already proven to be predictive of ventricular tachycardia risk [2], one might confer that our small study suggests the QRSwave v should be assessed before EP study performed regardless of QRSd given the inducible average was far less then 180ms as suggested to be predictive of arrhythmogenicity [11]. Furthermore, since increased ventricular stretch and mass to volume ratio may increase arrhythmogenicity as suggested by the above author as well as by Menon et al [12] and Velente et al. [13], respectively, one could rationalize that with this increased stretch and RVH mass, there would also be differences in depolarization sub-component vector orientation. This could cause an overall sum magnitude to be smaller than those with less right ventricular stretch as the increased components in the thickened walls could disperse the magnitude of the overall vector. This fits our cohort as they are all undergoing PVR and thus have RV pressure and volume overload. Also, the association between ventricular arrhythmia inducibility and the root mean square of the QRSwave has been demonstrated in the past by el-Sherif et al [14] as well as others as part of a signal averaged ECG analysis, thus it is not surprising that derived QRSwave v is also predictive. The relative risk cut-off was chosen based on the non-normalization of TOF patient values thus having more noted to have lower values proportionally, thus served as a good cut-off to include most of these patients while not including many of the non-inducible VA patients. Of course limitations of this study include mainly the size of the study. Also, since this was a retrospective study and signal averaged ECG's were not assessed, we were unable to include those values in our risk stratification as have been suggested to be associated with arrhythmogenicity [11].

5. Conclusion

In this retrospective analysis of TOF patients undergoing EP studies, VCG evidence of depolarization differences was present between those TOF patients with and without inducible VA, while the QRS duration as well as all other parameters tested did not. This suggests that VCG, especially the QRSwave v, may have a role in risk stratification for arrhythmias in TOF patients. Larger, prospective studies are needed to validate this method.

References

[1] Khairy P, Aboulhosn J, Gurvitz M, et al., Arrhythmia burden in adults with surgically repaired tetralogy of Fallot,Circulation, 122:868-875, 2010.

[2] Khairy P, LandzbergM, Gatzoulis M et al., Value of programmed ventricular stimulation after tetralogy of fallot repair,Circulation, 109:1994-2000, 2004.

[3] Triola B, Olson MB, Reis SE, et al., Electrocardiographic predictors of cardiovascular outcome in women: the National Heart, Lung, and Blood Institute-sponsored women's ischemia syndrome evaluation (WISE) study,Journal of American College of Cardiology,46:51-56, 2005.

[4] Voulgari C, Tentolouris N, Moyssakis I, et al., Spatial QRS-T angle: association with diabetes and left ventricular performance,European Journal of Clinical Investigation, 36:608-613, 2006.

[5] Borleffs CJ, Scherptong RW, Man SC, et al., Predicting ventricular arrhythmias in patients with ischemic heart disease: clinical application of the ECG-derived QRS-T angle,Circculation Arrhythmia Electrophysiology, 2:548-554, 2009.

[6] de TorbalA, Kors JA, van Herpen G, et al., The electrical T-axis and the spatial QRS-T angle are independent predictors of long-term mortality in patients admitted with acute ischemic chest pain,Cardiology,101:199-207, 2004.

[7] Kardys I, Kors JA, van der Meer IM, HofmanA, van der Kuip DA, Witteman JC, Spatial QRS-T angle predicts cardiac death in a general population,European Heart Journal,24:1357-1364, 2003.

[8] Rautaharju PM, Ge S, Nelson JC, et al, Comparison of mortality risk for electrocardiographic abnormalities in men and women with and without coronary heart disease (from the cardiovascular health study),American Journal of Cardiology, 97:309-315, 2006.

[9] Yamazaki T, Froelicher VF, Myers J, Chun S, Wang P, Spatial QRS-T angle predicts cardiac death in a clinical population,Heart Rhythm, 2:73-78, 2005

[10] Cortez D, Sharma N, Devers C, Devers E, Schlegel TT, Visual transform applications forestimating the spatial QRS-T angle from the conventional 12-lead ECG: kors is still most frank,Journal of Electrocardiology, 47:12-19, 2014.

[11] Bassareo PP, Mercuro G, QRS complex enlargement as a predictor of ventricular arrhythmia in tetralogy of fallot: a comprehensive literature review and historical review,International Scholarly Research Notices Cardiology, 2013:7825 08, 2013

[12] Menon SC, Kaza AK, Puchalski MD, Effect of ventricular size and function on exercise performance and the electrocardiogram in repaired tetralogy of fallot with pure pulmonary regurgitation,Annals of Pediatric Cardiology, 5:151–155, 2012.

[13] Velente AM, Gauvreau K, Assenza GE et al.,Contemporary predictors of death and sustained ventricular tachycardia in patients with repaired tetralogy of fallot enrolled in the INDICATOR cohort,Heart, 100:247-253, 2014.

[14] el-Sherif N, Turitto G, Fontaine JM, Risk stratification of patients with complex arrhythmias. Value of ambulatory electrocardiographic recording, programmed electrical stimulation and the signal-averaged electrocardiogram, American Journal of Cardiology, 42: 602-612, 1978.

Advanced Interatrial Block Predicts Atrial Fibrillation Post Cavotricuspid Isthmus Ablation for Typical Atrial Flutter

[1]A. Enriquez, [1]J. Caldwell, [1]F. Sadiq Ali, [1]D. Conde, [1]W. Hopman, [1]D. P. Redfearn, [1]K. Michael, [1]H. Abdollah, [1]Ch. Simpson, [2]A. Bayés de Luna, [1]A. Baranchuk

[1]Queen's University, Kingston, Canada
[2]Hospital de la Santa Creu i Sant Pau, Barcelona, Spain
Email: andresaep@gmail.com

Abstract. Introduction*: A significant proportion of patients develop atrial fibrillation (AF) following cavo-tricuspid isthmus (CTI) ablation for typical atrial flutter (AFl). The aim of this study was to assess whether advanced interatrial block (aIAB) is associated with new AF after CTI ablation in patients with typical AFl and no prior history of AF.* ***Methods:*** *Patients with typical AFl and no prior history of AF referred for CTI ablation were included. A post-ablation ECG in sinus rhythm was evaluated for the presence of aIAB: p-wave ≥ 120 ms and biphasic morphology in inferior leads. New-onset AF was identified from 12-lead ECGs, Holter monitoring and device interrogations.* ***Results:*** *The cohort consisted of 122 patients; age 67±10.6 years, 79.5% male, left atrial diameter 42.8±6 mm, ejection fraction 55.8±11.2%. aIAB was detected in 23% of the patients. Over a mean follow-up was 30.5±15.3 months, 57 patients developed new-onset AF (46.7%). The incidence of AF was greater in patients with aIAB (71.4%) compared to those without aIAB (39.4%, p=0.003). After multivariate analysis, aIAB remained statistically significant (OR 2.9, 95% CI 1.02-8.6; p<0.04).****Conclusion:*** *Advanced IAB is a predictor of new-onset AF after successful CTI ablation in patients with typical AFl and no prior history of AF.*

Keywords: Interatrial block; atrial flutter; atrial fibrillation

1. Introduction

Catheter ablation of the cavo-tricuspid isthmus (CTI) is an established and curative first-line therapy for patients with typical atrial flutter (AFl) with success rates exceeding 90%. However, a significant proportion of successfully ablated patients will develop atrial fibrillation (AF) during follow-up (1,2).

Interatrial block (IAB), a delay of conduction over the Bachmann bundle, is manifested in the 12-lead electrocardiogram (ECG) by a P-wave duration > 120 ms either with biphasic [±] morphology in the inferior leads (advanced IAB) or without it (partial IAB) (3). Advanced IAB (aIAB) is frequently associated with atrial tachyarrhythmias and has been found to be a predictor of AF in many different clinical scenarios (4).

2. Methods

The retrospective cohort was selected from all patients admitted to Kingston General Hospital for catheter ablation of typical AFl from 2008 to 2011. Inclusion criteria were: (i) paroxysmal or persistent typical AFl and no prior history of AF, (ii) post-ablation 12-lead ECG available and (iii) successful catheter ablation defined by the demonstration of bidirectional conduction block over the isthmus.

A post ablation 12-lead electrocardiogram (ECG) in sinus rhythm was evaluated for the presence of IAB. P-wave duration was measured using semi-automatic calipers. Partial IAB

(pIAB) was defined as a p-wave ≥ 120 ms and aIAB was defined as a p-wave ≥ 120 ms accompanied by a biphasic morphology (±) in the inferior leads (Figure 1).

Catheter ablation was performed using a maximum voltage guided approach. An 8-mm large tip or a 4-mm irrigated catheter was used.

Episodes of new-onset AF were identified from 12-lead ECGs, Holter monitoring and device interrogations. In addition, any extra ECGs, Holter monitoring or event recorders driven by patient's symptoms were also considered.

Data were expressed as means and standard deviations for continuous variables, and frequencies and percentages for categorical variables. Following univariate comparisons, a multivariate logistic regression analysis was performed to identity predictors of AF. P values < 0.05 were considered statistically significant

3. Results

A total of 122 patients were included. Baseline characteristics are summarized in Table 1. The mean follow-up was 30.5 ± 15.3 months.

Table 1. Baseline characteristics. LA = left atrium; LVEF = left ventricular ejection fraction; IAB = interatrial block

Variable	Mean ± SD or %
Age, years	67 ± 10.6
Male sex	79.5
Hypertension	55.7
Diabetes	25.4
Prior stroke	4.9
Ischemic heart disease	32.0
Sleep apnea	23.0
CHADS2 score	1.3 ± 1.1
LA dimension, mm	42.8 ± 6
LVEF, % ± SD	55.8 ± 11.2
P-wave duration, ms	138.9 ± 20.3
IAB	
- Advanced	22.9
- Partial	58.2

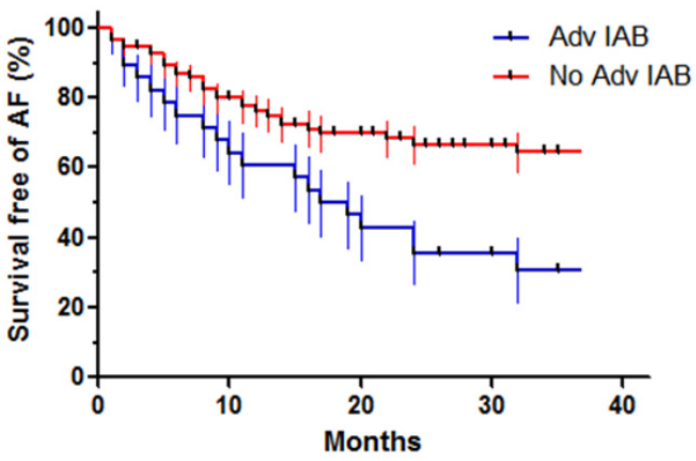

Fig. 1. Survival free of AF in patients with and without aIAB

At the moment of the electrophysiology study, 68 patients were in atrial flutter (55.7%) whereas 54 were in sinus rhythm (44.3%) and thus received an empiric CTI ablation. aIAB was detected in 28 patients (22.9%), pIAB in 71 (58.2%), and p-wave duration was normal in 23 patients (18.9%). The mean p-wave duration was 138.9 ± 20.3 ms.

At the end of the follow-up, 57 patients had displayed at least one episode of AF (46.7%). Of these, 16% (n = 9) presented early after the procedure (within 3 months)

and 56% (n = 32) occurred within the first 12 months. In patients with aIAB the incidence of AF was 71.4% compared to 39.4% in those without aIAB (p=0.003) (Figure 1). Table 2 shows the clinical characteristics of patients who developed AF compared with those who did not. aIAB was a powerful predictor of AF development after a successful AFl ablation (OR 2.9, 95% CI 1.02-8.6; p<0.04) (Table 3) after controlling for ischemic heart disease, LA dimension and LVEF, none of which were significant in the final model.

4. Discussion

AF is commonly observed after ablation of typical AFl and thus the optimal duration of anticoagulation in successfully ablated flutter patients is unknown. Previous history of AF is the strongest predictor of post-ablation AF (2) and therefore it is reasonable that patients with pre-ablation AF anticoagulation should be continued according to their estimated embolic risk. However, the approach in patients with typical AFl but no previous documented AF is less clear. In this group, clinical predictors of AF have not been consistently demonstrated and a follow-up monitoring strategy has not been well-defined.

Table 2. Clinical variables in patients with and without atrial fibrillation. AF = atrial fibrillation; LA = left atrium; LVEF = left ventricular ejection fraction; IAB = interatrial block.

Clinical variable	No AF (n = 65)	AF (n = 57)	p
Age, years ± SD	65.5 ± 11.9	68.5 ± 8.7	0.115
Male sex	80.0%	78.9%	0.886
Hypertension	53.8%	57.9%	0.653
Prior stroke	6.2%	3.5%	0.500
Ischemic heart disease	24.6%	40.4%	0.063
CHADS2 score	1.4 ± 1.2	1.2 ± 1.0	0.494
LA dimension, mm	41.7 ± 6.2	44.0 ± 5.8	0.074
LVEF, % ± SD	57.6 ± 9.8	53.8 ± 12.4	0.086
Advanced IAB	12.3%	35.1%	0.003
P-wave duration, ms	136.5 ± 21.3	141.7 ± 19.0	0.164

Table 3. Predictors of atrial fibrillation on multivariate analysis

Clinical variable	Odds ratio	95% Confidence Interval	p value
Ischemic heart disease	1.83	0.70 - 4.79	0.22
LA dimension	1.04	0.96 - 1.13	0.28
LVEF	0.99	0.95 - 1.04	0.81
Advanced IAB	**2.98**	**1.03 - 8.63**	**0.04**

In this study, almost half of the patients developed AF after a mean follow-up of 30.5 ± 15.3 months; most of them within the first post-ablation year. This observation is in keeping with previous studies which have reported the development of new-onset AF in ≥50% patients with isolated typical AFl after a follow-up period of 2-3 years (5).

The presence of aIAB was a strong predictor of new-onset AF post-ablation as the association remained significant in a multivariate analysis. Whilst there was a trend for the LA size to be an average of 2.3 mm larger in patients that developed AF this did not reach statistical significance. The association of IAB with atrial arrhythmias was first described by Bayés de Luna et al. (6), who reported a high incidence of paroxysmal supraventricular tachycardias (50% AF) in 16 patients with aIAB at 30-month follow-up (93.7% vs. 27.7% in controls; p < 0.001). IAB has also been associated with AF recurrence after electrical cardioversion (7), after pulmonary vein isolation (8) and with progression of paroxysmal AF to persistent or permanent AF (9,10). The mechanism of this association is not completely understood,

however there is some speculation on the pathophysiology. The biphasic p-wave morphology in the inferior leads reflects predominant caudo-cranial activation of the LA through the coronary sinus. Such conduction had previously been demonstrated by Puech in 1954 using a combination of surface ECG and esophageal leads (11). More recently Puech's observations were confirmed using endocardial mapping (12). This delayed and heterogeneous electrical activation of the LA results in impaired LA mechanical function, interatrial dyssynchrony and increased susceptibility to AF

5. Conclusions

In conclusion, aIAB in a surface 12-lead ECG is an independent predictor of the occurrence of AF after successful CTI ablation in patients with typical AFl and no prior history of AF. These findings may help guide decisions regarding the maintenance of anticoagulation after AFl ablation.

References

[1] Tai CT, Chen SA, Chiang CE, et al. Long-term outcome of radiofrequency catheter ablation for typical atrial flutter: risk prediction of recurrent arrhythmias. J Cardiovasc Electrophysiol 1998; 9:115–121.

[2] Chinitz JS, Gerstenfeld EP, Marchlinski FE, et al. Atrial fibrillation is common after ablation of isolated atrial flutter during long-term follow-up. Heart Rhythm. 2007; 4(8):1029-33.

[3] Bayés de Luna A, Platonov P, Cosio FG, et al. Interatrial blocks. A separate entity from left atrial enlargement: a consensus report. J Electrocardiol. 2012; 45(5):445-51.

[4] Conde D, Baranchuk A. Interatrial block as anatomical–electrical substrate for supraventricular arrhythmias: Bayes' syndrome. Arch Mex Cardiol 2013 [in press].

[5] Ellis K, Wazni O, Marrouche N, et al. Incidence of atrial fibrillation post-cavotricuspid isthmus ablation in patients with typical atrial flutter: left-atrial size as an independent predictor of atrial fibrillation recurrence. J Cardiovasc Electrophysiol. 2007; 18(8):799-802

[6] Bayes de Luna A, Cladellas M, Oter R, et al. Interatrial conduction block and retrograde activation of the left atrium and paroxysmal supraventricular tachyarrhythmia. Eur Heart J 1988; 9:1112–1118.

[7] Budeus M, Hennersdorf M, Perings C, et al. Prediction of the recurrence of atrial fibrillation after successful cardioversion with P wave signalaveraged ECG. Ann Noninv Electrocardiol 2005; 10(4): 414–419.

[8] Caldwell J, Koppikar S, Barake W, et al. Prolonged P-wave duration is associated with atrial fibrillation recurrence after successful pulmonary vein isolation for paroxysmal atrial fibrillation. J Interv Card Electrophysiol. 2013 (Epub ahead of print).

[9] Koide Y, Yotsukura M, Ando H, et al. Usefulness of P-wave dispersion in standard twelvelead electrocardiography to predict transition from paroxysmal to persistent atrial fibrillation. Am J Cardiol 2008; 102(5): 573–577.

[10] Dixen U, Vang Larsen M, Ravn L, et al. Signal-averaged P wave duration and the long-term risk of permanent atrial fibrillation. Scan Cardiovasc J 2008; 42(1): 31–37.

[11] Puech P. L'activite´ electrique auriculaire normale et pathologuique. Paris: Masson, 1956; 206.

[12] Cosío FG, Martín-Peñato A, Pastor A, et al. Atrial activation mapping in sinus rhythm in the clinical electrophysiology laboratory: observations during Bachmann's bundle block. J Cardiovasc Electrophysiol. 2004; 15(5):524-31.

Relation of Interatrial Block to New-Onset Atrial Fibrillation in Patients with Chagas Cardiomyopathy and Implantable Cardioverter-Defibrillators

A. Enriquez, D. Conde, F. Femenia, A. Bayés de Luna, A. Ribeiro, C. Muratore, M. Valentino, E. Retyk, N. Galizio, W.M. Hopman, A. Baranchuk

Queen's University, Kingston, Canada
Email: andresaep@gmail.com

Abstract. *Chagas cardiomyopathy (ChC) is an endemic disease in Latin America. A significant proportion of patients develop atrial fibrillation (AF), which may result in stroke and increased mortality. Interatrial block (IAB) has been associated with the development of AF in different clinical scenarios. The aim of our study was to determine whether IAB can predict new onset AF in patients with ChC and implantable cardioverter-defibrillators (ICDs). We conducted a retrospective study of patients with ChC and ICDs from 14 centers in Latin America. Surface ECGs were collected prior to device implantation. Partial IAB was defined as a P-wave > 120 ms and advanced IAB as a P-wave > 120 ms with biphasic morphology in inferior leads. AF events and ICD therapies were reviewed during follow-up. Eighty patients were analyzed. Mean age was 54.6±10.4 years, 52 (65%) male. Mean left ventricular ejection fraction was 40±12%. IAB was detected in 15 patients (18.8%), with 8 (10.0%) partial and 7 (8.8%) advanced. During a follow up of 33±20 months, 11 patients (13.8%) presented with new AF. IAB (partial + advanced) was strongly associated with new AF ($p<0.0001$) and inappropriate ICD therapies ($p=0.014$). In conclusion, IAB predicted new-onset AF in patients with ChC and ICDs.*

Keywords: Interatrial block, Chagas cardiomyopathy, Atrial fibrillation

1. Introduction

Chagas disease, caused by the parasite *Trypanosoma cruzi*, affects 8-10 million people in Latin America and almost 25% of them will develop chronic myocardial disease after years or decades (1). Up to one fifth of patients will develop atrial fibrillation (AF), which is associated with systemic thromboembolism and poor prognosis (2,3). Interatrial block (IAB), defined as a prolonged P-wave (> 120 ms) on a 12-lead electrocardiogram (ECG), has been associated with the development of AF in many clinical settings, probably through delayed and heterogeneous electrical activation of the left atrium (LA) (4). The aim of our study was to determine whether IAB can predict new onset AF in patients with ChC and implantable cardioverter-defibrillators (ICDs).

2. Methods

The present study was a retrospective analysis of patients with ChC and an ICD implanted for primary or secondary prevention at 14 Latin American centers.

The inclusion criteria were (i) ChC diagnosed by positive serologic tests and classic criteria including: living in endemic areas, ECG and chest X-ray criteria; (ii) ICD implanted for primary or secondary prevention of sudden cardiac death; (iii) Sinus rhythm. Patients with prior history of AF were excluded.

A standard 12-lead ECG was obtained in all patients prior to the device implantation. The P-wave duration was measured using semi-automatic calipers. Partial IAB (pIAB) was defined as a P-wave duration of > 120 ms without biphasic morphology (±) in the inferior leads, and

advanced IAB (aIAB) was defined as a P-wave > 120 ms and biphasic morphology (±) in the inferior leads (5). The ICD programming included therapy for ventricular tachycardia (VT) with antitachycardia pacing (ATP) followed by shock for ventricular fibrillation (VF).

The primary outcome was development of new onset AF. In single chamber devices AF was defined as an irregularly irregular rhythm lasting at least 30 seconds with > 80% match with the stored template. In devices with an atrial lead AF was defined as an episode of switch mode or atrial high rate lasting at least 30 seconds with electrograms compatible with fast and disorganized atrial rhythm. The secondary outcome was inappropriate ICD therapies, defined as ATP or shocks delivered by the ICD for any other rhythm rather than VT/VF. All patients attended regular follow-up visits, which were scheduled by the investigator at 3 to 6-month intervals.

Data were expressed as means and standard deviations for continuous variables and frequencies and percentages for categorical variables. Univariate comparisons and multivariate logistic regression analyses were performed to identify predictors of atrial fibrillation. P values < 0.05 were considered statistically significant.

3. Results

A total of 80 patients were analyzed. Baseline characteristics are summarized in Table 1. The indication for ICD was secondary prevention in 70%. Devices implanted were single chamber in 31%, dual chamber in 65% and resynchronization therapy in 4%.

Table 1. Baseline characteristics. LVEF = left ventricular ejection fraction; IAB = interatrial block; ARB = angotensin II receptor blockers; ACEI = angiotensin-converting-enzyme inhibitors.

Variable	Mean ± SD or %
Age (years ± SD)	54.6 ± 10.4
Male sex (%)	65
LVEF (% ± SD)	40 ± 12
Primary prevention (%)	30.0
Secondary prevention (%)	70.0
Functional capacity (%): I	45.0
II	38.8
III	16.2
P-wave duration (ms ± SD)	107.4 ± 12.6
IAB (%): Advanced	10.0
Partial	8.8
QRS duration (ms ± SD)	149.5 ± 80.5
Medical treatment (%)	
- Amiodarone	71.2%
- β-Blockers	60.0%
- ARB, ACEI	58.8%
- Spironolactone	35.0%

Mean P-wave duration was 107.4 ± 12.6 ms and IAB was detected in 15 patients (18.8%): 8 partial (10.0%; P-wave duration 126.2 ± 13.8 ms) and 7 advanced (8.8%; P-wave duration 129.7 ± 8.9 ms). Right bundle branch block (RBBB) was present in 42.5% of patients. Figure 1 shows a pattern of advanced IAB in a patient with typical ECG abnormalities of Chagas, which include RBBB and/or left anterior fascicular block (1).

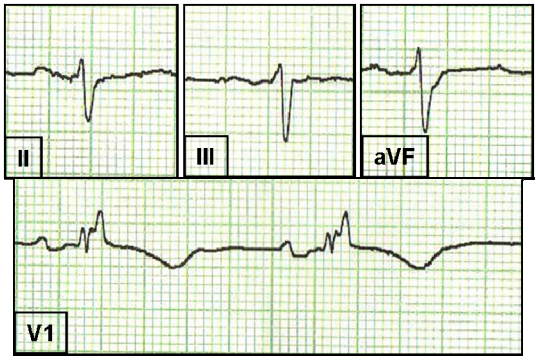

Fig. 1. Inferior + V1 leads of a patient with ChC and ICD.

During a follow up of 33 ± 20 months, 11 patients (13.8%) presented with new AF. The occurrence of AF in the group with IAB was 11/15 (73.3%) versus 0/65 (0%) in patients with normal P-wave duration ($p<0.0001$). Fourteen patients presented with inappropriate therapies during the follow-up (17.5%), all of them due to AF with rapid ventricular response. Seven patients died during the study period (8.8%).

Table 2. Comparison of patients with and without AF. AF = atrial fibrillation; LVEF = left ventricular ejection fraction; IAB = interatrial block.

Clinical variable	No AF (n = 69)	AF (n = 11)	p
Age (years ± SD)	53.7 ± 10.7	59.6 ± 6.8	0.08
Male sex (%)	63.8	72.7	0.56
LVEF (% ± SD)	40.9 ± 12.4	35.1 ± 9.2	0.14
P-wave duration (ms)	104.5 ± 10.8	125.3 ± 7.8	**< 0.0001**
IAB (%)	6.0	100.0	**< 0.0001**
QRS duration (ms ± SD)	128.8 ± 30.6	146.4 ± 23.8	0.07
Amiodarone (%)	69.6	81.8	0.40
Betablockers (%)	60.9	54.5	0.69

Table 2 shows a comparison of patients with and without AF. P-wave duration was significantly longer in patients that developed AF compared with those who did not (125.3 ± 7.8 vs 104.5 ± 10.8 ms; $p<0.0001$) and the prevalence of IAB was also significantly higher in the first group (100.0 vs 6.0%; $p<0.0001$).

In the univariate analysis IAB (partial + advanced) remained strongly associated with inappropriate therapies by the ICD (OR 4.8, 95% CI 1.3, 16.9, $p=0.014$). However, it was not possible to develop a multivariable model for AF because all 11 of the AF cases had IAB, resulting in an unstable model.

4. Discussion

The results of this study demonstrate that the presence of IAB in ChC is associated with the development of new onset AF. This is relevant considering that this arrhythmia is a major cause of stroke in this population (6) and an established predictor of poor prognosis.

The development of AF in ChC is mostly related to LA remodeling associated with progressive ventricular dysfunction. LA diameter annual variation rate, a marker of atrial remodeling, has been found to be related to the severity of heart involvement in ChC and it was associated with new onset AF (7). In addition, the inflammatory substrate of the disease may also play a pathogenic role. Parasite-dependent inflammation and immune mediated

cardiac injury result in destruction of cardiac myocites, regional fibrosis and potential substrate for reentry atrial arrhythmias.

The role of interatrial conduction disorders in the genesis of atrial arrhythmias was described long ago by Bayés de Luna et al. (8) and later confirmed by others. Intra and interatrial conduction delays lead to dispersion of refractory periods and participate in initiating and maintaining reentry circuits by promoting the occurrence of unidirectional block. Thus, a prolonged P-wave duration on 12-lead ECG or signal-averaged electrocardiography (SAECG) has been associated with new-onset AF (9), recurrence of AF after electrical or pharmacological cardioversion (10,11), AF recurrence after pulmonary vein isolation (12), and progression of paroxysmal AF to the persistent or permanent forms of the disease (13,14). Our findings are also in agreement with data reported for other cardiomyopathies such as hypertrophic or hypertensive cardiomyopathy and ischemic heart disease.

In conclusion, the presence of IAB (partial + advanced) predicted new onset AF in patients with ChC and ICDs, leading to increased risk of inappropriate therapies.

References

[1] Nunes MC, Dones W, Morillo CA, et al. Chagas disease: an overview of clinical and epidemiological aspects. *J Am Coll Cardiol* 2013;62:767-776.

[2] Rassi A Jr, Rassi A, Little WC, et al. Development and validation of a risk score for predicting death in Chagas' heart disease. *N Engl J Med* 2006;355:799-808.

[3] Espinosa RA, Pericchi LR, Carrasco HA, et al. Prognostic indicators of chronic chagasic cardiopathy. *Int J Cardiol* 1991;30:195-202.

[4] Conde D, Baranchuk A. Interatrial block as anatomical–electrical substrate for supraventricular arrhythmias: Bayes' syndrome. Arch Mex Cardiol 2013 [in press].

[5] Bayés de Luna A, Platonov P, Cosio FG, et al. Interatrial blocks. A separate entity from left atrial enlargement: a consensus report. *J Electrocardiol* 2012;45:445-451.

[6] Paixão LC, Ribeiro AL, Valacio RA, et al. Chagas disease: independent risk factor for stroke. *Stroke* 2009;40:3691-3694.

[7] Benchimol-Barbosa PR, Barbosa-Filho J. Atrial mechanical remodeling and new onset atrial fibrillation in chronic Chagas' heart disease. *Int J Cardiol* 2008;127:e113-115.

[8] Bayes de Luna A, Cladellas M, Oter R, et al. Interatrial conduction block and retrograde activation of the left atrium and paroxysmal supraventricular tachyarrhythmia. *Eur Heart J* 1988;9:1112-1118.

[9] Agarwal YK, Aronow WS, Levy JA, et al. Association of interatrial block with development of atrial fibrillation. *Am J Cardiol* 2003;91:882.

[10] Gonna H, Gallagher MM, Guo XH, et al. P-Wave Abnormality Predicts Recurrence of Atrial Fibrillation after Electrical Cardioversion: A Prospective Study. *Ann Noninvasive Electrocardiol* 2014;19(1):57-62.

[11] Enriquez A, Conde D, Hopman W, et al. Advanced interatrial block is associated with recurrence of atrial fibrillation post pharmacological cardioversion. *Cardiovasc Ther* 2014. [Epub ahead of print].

[12] Caldwell J, Koppikar S, Barake W, et al. Prolonged P-wave duration is associated with atrial fibrillation recurrence after successful pulmonary vein isolation for paroxysmal atrial fibrillation. *J Interv Card Electrophysiol* 2013. [Epub ahead of print].

[13] Koide Y, Yotsukura M, Ando H, et al. Usefulness of P-wave dispersion in standard twelve lead electrocardiography to predict transition from paroxysmal to persistent atrial fibrillation. *Am J Cardiol* 2008;102:573-577.

[14] Dixen U, Vang Larsen M, Ravn L, et al. Signal-averaged P wave duration and the long-term risk of permanent atrial fibrillation. *Scan Cardiovasc J* 2008; 42:31-37.

Dynamics of heart rate and blood pressure in hypertensive patients

[1]I. Cotet, [2]I. Kurcalte, [3]C. Rezus, [4]V.D. Moga,
[5]R. Avram, [6]A. Szekely, [7]M. Moga, [6]F. Vidu

[1]Emergency County Hospital Arad, Romania
[2]Riga Stradins University, Riga Eastern Clinical University Hospital, Latvia
[3]University of Medicine and Pharmacy "Gr.T.Popa" Iasi, Romania
[4]University of Medicine and Pharmacy "V.Babes" Cardiology Clinic Emergency County Hospital Timisoara, Romania
[5]Emergency County Hospital Timisoara
[6]IT Department of the of the Emergency County Hospital Timisoara
Email: oana_cotet@yahoo.com

Abstract. *Hypertension represents an important condition that affects the adult population worldwide; it contributes significantly to morbidity and mortality from stroke, heart failure, coronary heart disease and renal failure. Although the pathogenesis of most hypertension is unclear, imbalance of the autonomic nervous system has been implicated in its development. Heart rate variability (HRV) has emerged as a practical, non-invasive tool to quantitatively investigate cardiac autonomic imbalance in hypertension. The aim of our study was to highlight the complex heart rate modulation in hypertension and to analyze the behaviour of RR intervals dynamics compared to normotensives subjects. Beside the now consecrated well known heart rate variability parameters, it seems that new parameters like ΔHR (b/min) and ΔSBP (mmHg) can offer data related to the involvement of the circadian rhythm in hypertension.*

Keywords: Hypertension, heart rate variability, nonlinear analysis, circadian rhythm

1. Background

Hypertension represents an important condition that affects the adult population worldwide; it contributes significantly to morbidity and mortality from stroke, heart failure, coronary heart disease and renal failure [1]. There are a lot of studies and data that suggest that the autonomic nervous system plays an important role in blood pressure regulation and in the development of hypertension [3]. Early identification of individuals prone to hypertension, may allow for early interference such as: lifestyle modifications, regular exercise and weight loss, targeted at reducing the risk factors for hypertension, and reducing sympathetic nervous system activation [2].

Abnormalities of autonomic nervous system function (ANS) exist in patients with hypertension and have been considered as one of the important factors in developing of essential hypertension. Lower HRV was associated with greater risk for developing hypertension [4].

The sympatho-vagal balance is altered in the resting conditions of numerous pathophysiological processes. It is the case of essential arterial hypertension (Guzzetti *et al.* 1988), even in the presence of arterial pressure values still in the high normal range (Lucini *et al.* 2002).The ability of decreased heart rate variability to predict incident hypertension has not been well studied, and there are no studies of whether hypertension leads to changes in heart rate variability [5].

2. Method

The study was performed at the Cardiology Clinic of the Emergency County Hospital Timis, University of Medicine and Pharmacy "V. Babes "Timisoara, starting from a former study performed by one of the authors at the Riga Eastern Clinical University Hospital, Latvia. The study group (n: 47, men: 23, women: 24, mean age: 54.2 yrs) has included hypertensive patients with stage II and III of essential hypertension. A control group of twenty normotensives subjects (men: 11, women: 9, mean age: 46.7 yrs) was selected to compare the clinical data and autonomic tone parameters. ECG signal analysis and blood pressure measurements have been done using a EC-3H/ABP Combined Holter System, Labtech Ltd. The system performs simultaneously recording of the ECG signal and measurements of the blood pressure.

Twenty four hours of combined ECG and blood pressure monitoring has been performed and more than 90 % of the signals and measurements are eligible for the study. Artefacts and noise was manually removed from the signals.

All ECG analysed signals are in sinus rhythm and analysis of heart rate variability was performed in time domain, mean RR intervals (ms), standard deviation of all RR intervals (ms) and frequency domain, very low frequency (VLF, 0.01-0.05 Hz), low frequency (LF, 0.05 -0.15 Hz) and high frequency (HF, 0.15-0.50 Hz), LF/HF ratio. Kubios v. 2.1, Finland (http://kubios.uku.fi/) was used for the measurement of the nonlinear parameters of the RR series. Approximate Sample entropy, detrended fluctuation analysis and Poincare plots; have been used for the study of the behaviour of the heart rate dynamics in both groups.

Trends of heart rate (b/min) and blood pressure (mmHg) have been recorded for both groups.

Left ventricular ejection fraction (LVEF, %) has been measured echocardiography by an independent member of the team.

3. Statistical analysis

For the statistical analysis we have used Graph Pad Prism. All numeric variables were expressed as mean and the statistical analysis was performed using Student's t-test and correlation analysis by Pearson method. A p value < 0.05 was considered statistically significant.

4. Results and Discussions

In the hypertensive group the gender distribution is almost equal, suggesting a higher incidence of essential hypertension in the women population and probably that the men are much earlier hypertensive than women. In the study group, women had mean age: 57 yrs. compared to men mean age: 50.4 yrs. ($p<0.005$). Differences have been noticed also in relation to the mean heart rate. Women are more tachycardic than the men hypertensive population (mean heart rate: 87 b/min vs. 80 b/min), but the differences are not statistically significant. Considering only the gender aspects, in the hypertensive group, the left ventricular ejection fraction (LVEF %) seems to be preserved, LVEF: 60 %, mean LVEF in the men population: 58 % compared to the women mean value: 61 %. In the hypertensive group, those with events have a lower left ventricular ejection compared with the events free hypertensive population (LVEF: 48 % vs. 68 %, $p< 0.005$). All the clinical data are resumed in table 1.

Table 1. Main clinical characteristics of the study and the control group.

	Hypertension	Control	P
N	47	20	0.05
Age (yrs.)	54.2	46	0.05
Mean heart rate (b/min)	86	73	0.05
LVEF (%)	60	72	0.05
Systolic Blood Pressure (mmHg)	160	127	< 0.005
Diastolic Blood Pressure (mmHg)	105	75	< 0.005
N	47	20	0.05
Age (yrs.)	54.2	46	0.05
Mean heart rate (b/min)	86	73	0.05

Analyzing the hypertensive group, we noticed differences between the dynamics of heart rate and systolic blood pressure as a measure of the circadian rhythm. The difference between day/night heart rate and blood pressure is considered a useful parameter of the influence of the circadian rhythm (table 2).

Table 2. The influence of arrhythmic events and heart failure in the hypertensive group

	Hypertension + events	Hypertension - events	P
N	18	29	
Age (yrs)	60.5	49.7	0.05
Mean heart rate (b/min)	85	84	Ns
LVEF (%)	48	68	0.005
SBP (mmHg)	163	160	Ns
DBP (mmHg)	97	107	Ns
ΔHR (b/min)	9.65	15.62	0.005
ΔSBP (mmHg)	27.8	23.72	0.05

During the study we have not observed significant differences between the absolute values of the systolic blood pressure inside the hypertensive group. Despite this fact some parameters like the difference between day and night mean heart rate can suggest important modulations of the autonomic tone in hypertension. More of this, ΔHR (b/min) and ΔSBP (mmHg), the later as expression of the day-night differences in systolic blood pressure, seems to correlate.

The correlation between ΔHR (b/min) and ΔSBP (mmHg), opens the opportunity to analyze the influence of the autonomic tone in the modulation of heart rate and blood pressure in the hypertensive population.

The role of the autonomic tone in essential hypertension is assessed using linear and nonlinear parameters. Heart rate variability and nonlinear dynamic parameters like entropy and detrended fractal analysis was applied to the ECG signals obtained from hypertensive patients. Even in a limited and selected group of patients it is difficult to identify vulnerable

hypertensive patients. It seems adequate to perform nonlinear analysis in hypertensive patients to identify vulnerable patients. Not all parameters will have spectacular changes but approximate entropy (ApEn) and detrended fluctuation analysis parameter (DFA α1) confirm the capacity to identify risk patients even in apparently stable patients, like in essential hypertension [6, 7]. An important aspect regarding the value of these parameters is related to the coexistence of co morbidities.

5. Conclusions and limitations

The aim of the study was to offer significant data about the complex mechanisms involved in essential hypertension. The most important aspect of this study is that even in the presence of early stages of essential hypertension, the autonomic tone mechanisms are involved in the outcome and prognosis of these patients and are detectable by non-invasive methods.

Beside the now consecrated well known heart rate variability parameters, it seems that new parameters like ΔHR (b/min) and ΔSBP (mmHg) can offer data related to the involvement of the circadian rhythm in hypertension.

The study has two major limitations, one is related to the relatively small number of patients included in the study, and the other is that all the patients in the study have been under complete medical treatment.

References

[1] Marek Malik, A. John Camm – Heart Rate Variability – Futura Publishing Company, Inc, 1995.

[2] R Virtanen et al, - Reduced heart rate variability in hypertension: associations with lifestyle factors and plasma renin activity - Journal of Human Hypertension (2003) 17, 171–179.

[3] Kolasińska-Kloch W et al, - Circadian heart rate variability in patients with primary arterial hypertension – http://www.ncbi.nlm.nih.gov/pubmed

[4] Emily B. Schroeder et all. - Hypertension, Blood Pressure, and Heart Rate Variability: The Atherosclerosis Risk in Communities (ARIC) Study - *Hypertension.* 2003; 42:1106-1111;

[5] Melillo et all. - Heart rate variability and target organ damage in hypertensive patients - BMC Cardiovascular Disorders 2012, 12:105

[6] Sirkku M. Pikkujamsa, Timo H. Makikallio, K. E. Juhani Airaksinen, Heikki V. Huikuri - Determinants and interindividual variation of R-R interval dynamics in healthy middle-aged subjects - *Am J Physiol Heart Circ Physiol* 280: H1400–H1406, 2001.

[7] Darrel P. Francis et all. - Physiological basis of fractal complexity properties of heart rate variability in man - *Journal of Physiology.* 2002, 619–629.

ECG in Diagnostics of Cardiac Diseases

Computer Simulation of the Electric Activity of the Heart Using GPU. A Multi-Scale Approach

[1]A. Mena, [3]J.M. Ferrero, [1,2]J.F. Rodríguez

[1]CIBER, Zaragoza, Spain,
[2]Aragon Institute of engineering Research, Universidad de Zaragoza, Zaragoza, Spain
[3] Instituto de Investigación Interuniversitario en Bioingeniería y Tecnología Orientada al Ser Humano (I3BH), Universitat Politecnica de València, Valencia, Valencia, Spain
Email: jfrodrig@unizar.es

Abstract. *The electrophysiology problem posses a big challenge, not only because of the structural complexities inherent to the heart tissue, but also because of the complex electric behaviour of the cardiac cells. Solving the electric activity of the heart requires an enormous effort of data integration for generating a suitable model for simulation. The resulting model will be of multi-scale nature (ranging from the microscopic ionic channels to the surface ECG). The multi-scale nature of the electrophysiology problem makes difficult its numerical solution, requiring temporal and spatial resolutions of 0.1ms and 0.2mm respectively for accurate simulations, leading to models with millions degrees of freedom that need to be solved for thousand time steps. Solution of this problem requires the use of algorithms with higher level of parallelism in multi-core platforms. In this regard the newer programmable graphic processing units (GPU) has become a highly parallel, multithreaded, many-core processor with tremendous computational horsepower. This paper presents results obtained with a novel electrophysiology simulation software entirely developed in CUDA. The software implements fully explicit and semi-implicit solvers for the monodomain model, using operator splitting. Performance is compared against classical multi-core MPI based solvers operating on dedicated high-performance computer clusters. Results obtained with the GPU based solver show enormous potential for this technology not only for research but also for clinical application due to its efficiency and lower hardware cost. The versatility of in-silico simulations is demonstrated on simulating the electric activity on realist models of the human heart.*

Keywords: Electrophysiology simulation, GPU simulation, Excitable media

1. Introduction

Over the last years, mathematical modelling and computer simulations have become a useful tool in analysing electrophysiological phenomena. In this particular, one of the major contributions of computer electrophysiology has been in understanding important relations between electrophysiological parameters [1]. In addition, continuous advances on medical imaging techniques have allowed for the development of computational anatomically realistic models of the heart. These anatomically realistic models can then be integrated to multi-scale biophysical model of the heart electrophysiology to obtain reliable quantitative mechanistic models. However, despite the great increase in computer power, execution times remain still prohibitive for these computer models [2].

The multi-scale nature of the electrophysiology problem (time constants for the different kinetics ranging from 0.1 to 500ms) makes difficult its numerical solution, requiring temporal and spatial resolutions of 0.1ms and 0.2mm respectively for accurate simulations, leading to models with millions degrees of freedom that need to be solved for thousand time steps.

Solution of this problem requires the use of algorithms with higher level of parallelism in multi-core platforms. In this regard, the next generation of high-performance computing (HPC) platforms promise to deliver better performance in the PetaFLOPS range. However, achieving high performance on this platforms relies on the fact that strong scalability can be achieved, something challenging due to the performance deterioration caused by the increasing communication cost between processors as the number of cores, n, increases. That is, with increasing n, the load assigned to each processor decreases, but the communication between different processors associated with the boundaries of a given partitioned domain increases. Therefore, when communication costs domain, no further benefits are obtained from adding additional processors. An alternative to the multi-core platforms is emerging in the newer programmable graphic processing units (GPU) which in recent years has become a highly parallel, multithreaded, many-core processor with tremendous computational horsepower. GPUs outperform multi-core CPUs architectures in terms of memory band width, but underperforms in terms of double precision floating point arithmetic. However, GPUs are built to schedule a large number of threads, thus, reducing latencies in their multi-core architecture.

This paper presents results obtained using a novel electrophysiology simulation software entirely developed in CUDA. The software implements implicit and explicit solvers for the monodomain model, using operator splitting and the Finite Element Method (FEM). Performance results are compared with a multi-CPU based software [3].

2. Methods

The electric activity of the heart can be described by means of the well established monodomain equation [4]

$$\nabla \cdot (\mathbf{D}\nabla V) = C_m \frac{\partial V}{\partial t} + J_{ion}(V, \mathbf{u}) + J_{stm} \tag{1}$$

$$\frac{\partial \mathbf{u}}{dt} = \mathbf{f}(\mathbf{u}, V, t) \tag{2}$$

where V is the transmembrane potential, $\mathbf{D}$ is the second order anisotropic conductivity tensor, C_m the membrane capacitance, J_{stm} the stimulus current, J_{ion} the ionic current, and $\mathbf{u}$ is a set of state variables associated with the ionic model. The set of equations (1) is subject to the zero flux boundary conditions

$$\mathbf{n} \cdot (\mathbf{D}\nabla \mathrm{V}) = 0 \tag{3}$$

where $\mathbf{n}$ is the outward pointing unit normal to the computational domain. The monodomain model represents an important simplification of the bidomain model with important advantages for mathematical analysis and computation. Despite its simplicity, this model is adequate for studying a number of electrophysiologic problems as ventricular fibrillation or the onset of ischemia in the electric behaviour of the heart [1,5-6].

An efficient form for solving Eq. (1-3) is by applying the Strang based operator-splitting scheme in combination with a generalized trapezoidal family of method for time integrations [7,8], in conjunction with the finite element method for the spatial discretization. The basic algorithm can be summarized the following two steps:

Step 1: Using V(t) as initial condition to integrate

$$\begin{aligned} C_m \frac{\partial V}{\partial t} &= -J_{ion}(V, \mathbf{u}) - J_{stm} \\ \frac{\partial \mathbf{u}}{dt} &= \mathbf{f}(\mathbf{u}, V, t) \end{aligned} \quad \text{for} \quad t \in [t, t + \Delta t] \tag{4}$$

Step 2: Using the result in Step 1 to integrate

$$C_m \frac{\partial V}{\partial t} = \nabla \cdot (\mathbf{D}\nabla V) \quad \text{for} \quad t \in [t, t + \Delta t] \tag{5}$$

When performing Step 2, the computational domain must be discretized in space by a mesh, e.g. finite elements, to approximate the dependent variables of the problem, V and $\mathbf{u}$. Hence, after the spatial discretization, the system of partial differential equations (5) can be written in matrix notation as

$$\mathbf{M}\dot{\mathbf{V}} + \mathbf{K}\mathbf{V} = \mathbf{0} \tag{6}$$

where $\mathbf{M}$ is the mass matrix associated with $C_m \partial V/\partial t$; and $\mathbf{K}$ is the stiffness matrix associated with $\nabla \cdot (\mathbf{D}\nabla V)$. These matrices are obtained by assembling individual element matrices. Equation 7 is called a semi-discrete equation because time is left continuous.

The most well-known algorithms for integrating (6) in time are members of the generalized trapezoidal family of methods [8]. Let $\mathbf{V}^k$ and $\dot{\mathbf{V}}^{\boldsymbol{k}}$ denote vectors of the transmembrane potential and its time derivative at each nodal point of the discretized domain (mesh) at time t^k, where k is index of the time step, then at time t^{k+1} we can write

$$\mathbf{M}\dot{\mathbf{V}}^{\boldsymbol{k+1}} + \mathbf{K}\mathbf{V}^{\boldsymbol{k+1}} = \mathbf{0} \tag{7}$$

$$\boldsymbol{V}^{\boldsymbol{k+1}} = \mathbf{V}^{\boldsymbol{k}} + \Delta t \dot{\boldsymbol{V}}^{\boldsymbol{k+\theta}} \tag{8}$$

$$\dot{\boldsymbol{V}}^{\boldsymbol{k+\theta}} = (1-\theta)\dot{\mathbf{V}}^{\boldsymbol{k}} + \theta \dot{\boldsymbol{V}}^{\boldsymbol{k+1}} \tag{9}$$

where $\theta \in [0,1]$ is a scalar parameter. When using the operator-splitting, Eq. 1-3 are solved in two steps. First, the electrophysiological model, Eq. 4

$$\boldsymbol{V}^* = \boldsymbol{V}^k + \Delta t(J_{ion}(\boldsymbol{V}^k, \boldsymbol{u}) + J_{stm}) \tag{10}$$

is solved at each mesh point to obtain an intermediate transmembrane potential vector $\mathbf{V}^*$ (Step 1). With this result at hand, using Eq. 8-9 to eliminate $\dot{\mathbf{V}}^{\boldsymbol{k+1}}$ from Eq.7 and $\mathbf{M}\dot{\mathbf{V}}^{\boldsymbol{k}} = -\mathbf{K}\mathbf{V}^{\boldsymbol{k}}$ from the previous converged time increment, the transmembrane potential at time step $k+1$ (Step 2) is obtained as

$$\mathbf{M}\frac{\mathbf{V}^{\boldsymbol{k+1}} - \mathbf{V}^*}{\Delta \boldsymbol{t}} = -\mathbf{K}[\theta \mathbf{V}^{k+1} + (1-\theta)\mathbf{V}^k], \tag{11}$$

or alternatively

$$\hat{\mathbf{K}}\mathbf{V}^{k+1} = \hat{\mathbf{b}} \tag{12}$$

where $\hat{\mathbf{K}}$ is everything that multiplies onto $\mathbf{V}^{k+1}$, and $\hat{\mathbf{b}}$ contains the other terms in Eq. 11.

Hence, the basic algorithm at time t^{k+1} can be summarized, as:

Step I: Use $\mathbf{V}^k$ as initial condition to integrate Eq. 10 to obtain $\mathbf{V}^*$
Step II: Use the result obtained in Step I, $\mathbf{V}^*$, to solve Eq. 11 for $\mathbf{V}^{k+1}$

For different values of the parameter θ, different time integration schemes are obtained for integrating the discretized homogeneous parabolic equation, Eq. 5:

θ=0 Forward Euler (conditionally stable)
θ=1/2 Crank-Nicholson (unconditionally stable)
θ=2/3 Galerkin Scheme (unconditionally stable)
θ=1 Backward Euler (unconditionally stable)

Step I of the algorithm uses values of the $\mathbf{V}^k$ at each mesh point to integrate the system of ODEs (Eq. 3) corresponding to the ionic model. This step can be performed using either implicit or explicit methods. However, the use of implicit methods requires the solution of a

nonlinear system of equations at each node for each time step largely increasing the computational cost. On the contrary, explicit integration, even though computationally cheaper, imposes more stringent conditions on the size of the time step in order to avoid numerical instabilities.

Parallel implementation in GPU

In the discretized scheme, there are two main contributors to the computational cost: solving the system of ODEs at each mesh point, and solving the linear system of equations associated with the parabolic PDE. In order to maximize performance, all vectors and matrices associated with the system of equations reside on the GPU memory with the solution transferred back to the host only when the data has to be saved on disk. In addition, in order to minimize memory storage, all data is stored using sparse matrix structures.

Ionic solver in GPU: The C/C++ code of the tenTusscher and Panfilov ionic model (TP06) [9] was downloaded from the CellML model repository [10], modified by implementing the Rush-Larsen integration scheme for the gating variables [11], and then compiled for GPU. The exact same code was executed in CPU and GPU in order to validate the implementation. In addition, results were compared with the original code provided by tenTusscher and Panfilov. During execution, the vector of state variables, $\mathbf{u}$, and the current transmembrane potential, $\mathbf{V}^k$, remain in the GPU memory and use to compute $\mathbf{V}^*$ in Eq. 10. Adaptive time integration was not incorporated in the GPU implementation in order to reduce latency.

PDE solver in GPU: The linear system given in Eq. 12 was solved on GPUs using the CUSP and Thrust libraries [12] developed by Nvidia. CUSP is implemented for a single GPU and natively supports a number of sparse matrix formats providing specific subroutines for an easy passage between different sparse matrix formats. The library includes highly optimized matrix-vector multiplication algorithms and iterative solvers. In addition, a variety of preconditioners based on algebraic multigrid (AMG) and approximate inverse operators are ready available in the library. In our implementation, mass and stiffness matrices, $\mathbf{M}$ and $\mathbf{K}$ respectively, are assembled in parallel in the GPU and stored in compressed sparse row (CSR) format. These matrices are then transformed to an efficient sparse matrix format when transferred in the GPU memory for computations.

Benchmarking

Benchmarking was conducted for 1D, 2D and 3D problems. The model geometry was defined as a cable of length L, a rectangle with dimensions $L\times L$, and a cuboid with dimensions of $L\times 7\times 20$ mm^3. The dimension L was varied in order to achieve a given number of degrees of freedom in the problem. The different geometries where meshed with linear, quadrilateral and hexahedral elements of size 0.1 mm, 0.1×0.1 mm^2 and $0.1\times 0.1\times 0.1$ mm^3 respectively. For 2D and 3D problems, triangular and tetrahedral elements were also used to characterize the performance under a variable matrix bandwidth. In addition, since ventricular cardiac muscle is anisotropic, the tissue was modelled as transversally isotropic with the fibre direction oriented along the x-axis. For the benchmarking, cellular action potential was modelled using the TP06 model, which comprises 19 state variables. A propagating wave front was initiated at one of the corners of the model using a stimulation current pulse, J_{stm}, of 50 μA/cm^2 strength and 2 ms duration. The electrical activity was simulated over 100 ms, with a fixed time-step of 20 μs. The parallel performance was evaluated as the speedup, S, i.e., the execution time of the GPU implementation with respect to a single CPU core.

The efficiency of the GPU is further demonstrated on the simulation of a heart beat in a human heart and a human atria. A voxelized human heart with 1289000 elements and 1434129 nodes (DOF) has been considered. Figure 1a shows the voxel mesh (voxel size of

0.4×0.4×0.4 mm^3) along with the fiber orientation of the ventricular tissue. The TP06 model has been used to simulated the action potential model of the ventricular tissue. The efficiency of the code on non-structured meshes was demonstrated on a model of the human atria with 1378054 elements and 266450 nodes (see Figure 1b). The atrial action potential model proposed by Maleckar et al [13] was used for simulationg the electric activity of atrial tissue.

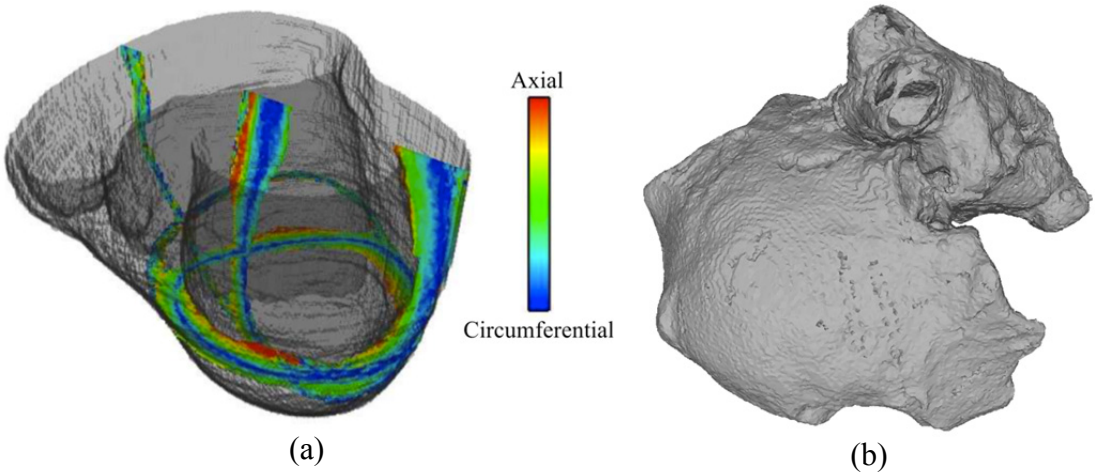

Fig. 1. Three dimensional finite element models. a) Hexahedral mesh of a biventricular human heart depicting the fibre orientation; b) Tetrahedral mesh of a human atria.

GPU simulations were run on a computer node with two Intel-Xeon Quad-Core CPUs E5620 clocked at 2.4GHz and 48GB DDR3 RAM. The node is equipped with four Nvidia Tesla M2090 GPUs, each with 6GB DDR5 RAM for a total of 24GB DDR5 RAM. All simulations were run in a single GPU. The single CPU benchmark was run on a single core of a cluster with 8 nodes with two Intel-Xeon Quad-Core E5520 clocked at 2.26GHz and 24GB DDR3 RAM connected by a high speed infiniband network.

3. Results

When solving the monodomain model, there are two critical steps in term of computation time: i) integration of the action potential model (Step I) and ii) the solution of the linear system of equations for the propagation of the electric signal (Step II). The operating splitting algorithm allows for an independent evaluation of the performance on these two steps.

Figure 2 shows the speed-up, *S*, obtained with the GPU in simulating 1 s of cellular activity (Step I) as the number of nodes in the model increases from 1 up to 6 million. The figure shows that core-to-core the GPU is much inferior to a single CPU, with a single CPU thread outperforming a single GPU thread about 480 times. However, the enormous computational horsepower of the GPU leads the GPU to overtake a single CPU as the number of nodes increases as shown in Figure 2a. This figure shows that the speedup increases linearly until reaching an asymptotic speedup of 180× for a model with more than a one million nodes.

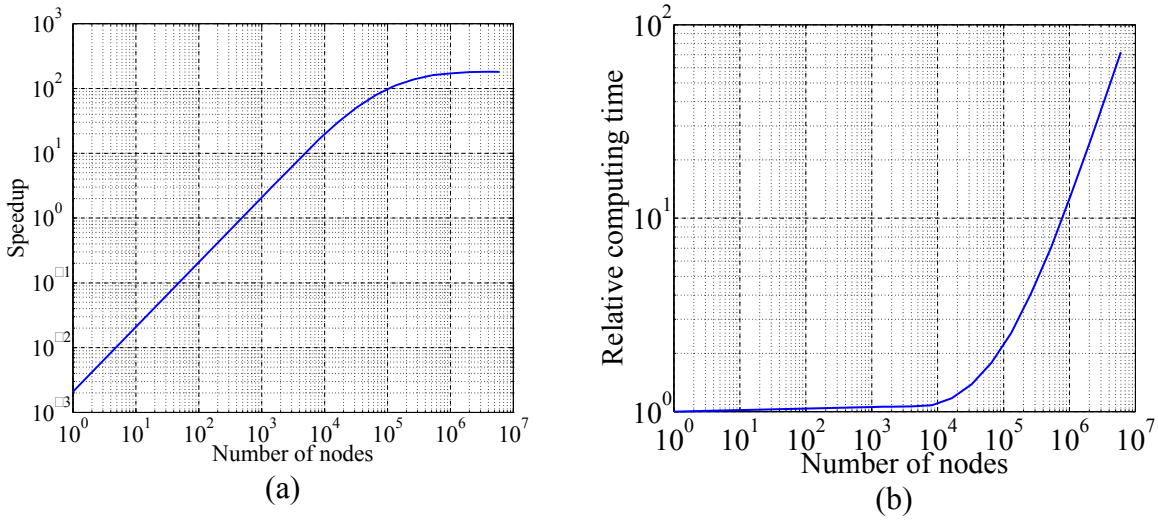

Fig. 2. Results for the integration of the ionic model for a 1s of cell activity. a) Speedup curve; b) Relative computing time for the GPU.

Regarding the relative computing time, Figure 2b shows that the C2090 GPU is able to evaluate the cell electrophysiology model in 8000 nodes simultaneously with almost no degradation in the computing time (see Figure 1b). However, for models with more than one million nodes, the computing time increases almost linearly.

The speedup, S, for the monodomain model is shown in Figure 3 for fully explicit ($\theta = 0$) and semi-implicit schemes ($\theta = 1$) for the one-, two-, and three- dimensional problems.

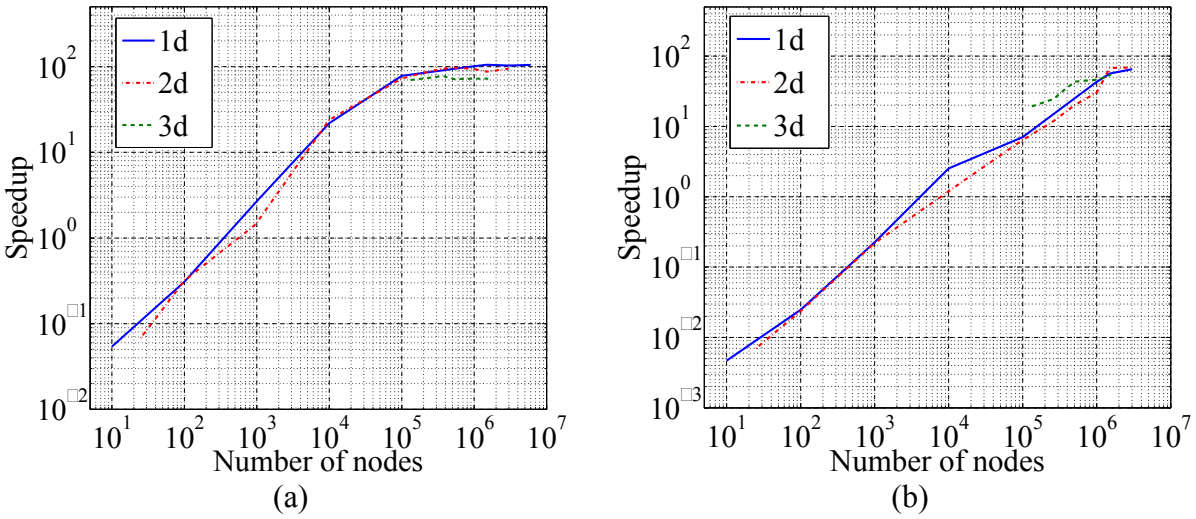

Fig. 3. Speedup curve for the solution of the monodomain model with constant time step for one-, two, and three-dimensional problems. a) Fully explicit scheme ($\theta = 0$); b) Semi-implicit scheme ($\theta = 1$).

Figure 3a shows the results for the fully explicit scheme. The same trend as in Figure 2a for the integration of the ionic model can be observed. As for the case of the integration of the ionic model, for small problems the GPU underperforms the single CPU execution due to the lower clock-speed of the single GPU with respect to the single CPU. However, as the number of degrees of freedom increases (the threshold was found close to 800 nodes) the GPU outperforms the CPU until reaching an asymptotic behaviour with a speedup of: 100× for 1d-problems, 90× for the 2d-problem, and 70× for the 3d-problem. The reduction in acceleration

is due to the additional cost implied by the matrix multiplication that takes place in Step II. For the semi-implicit scheme a similar trend as for the fully explicit scheme is observed. However, for the semi-implicit scheme the GPU does not reaches a saturation point due to the higher computational cost required for solving the system of equations (Eq. 12) on each time step. This increased computational cost is also noted by the reduction in the speed-up (65× for 1d-problem, 60× for 2d-problems, and 50× for 3d-problems), and the increased threshold up to approximately 8000 nodes as the minimum problem size for which the GPU starts to overtake the CPU.

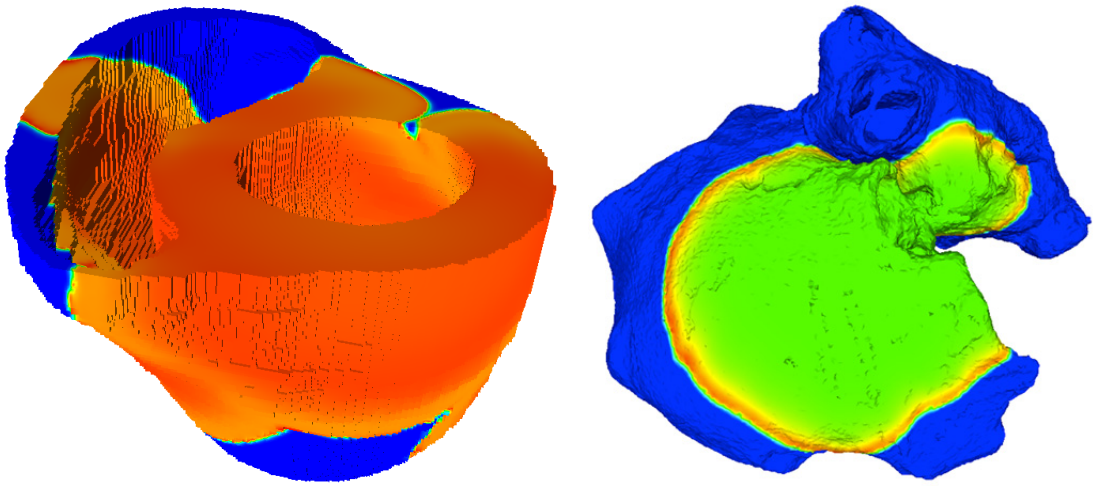

(a) (b)

Fig. 4. Depolarization fronts at 20 ms after stimulation. a) Biventricular human heart; b) Human atria.

Figure 4 shows the depolarization front for the biventricular human heart and the human atria after 20 ms of stimulation. The speed-up obtained in these cases was 50× for the human heart and 40× for the human atria with respect to a single CPU core. In addition, the GPU still performed 1.8× faster than 42 cores of the cluster described in the Methods section, demonstrating the enormous potentiality of this technology.

4. Discussion

The potential of GPU implementation for solving the monodomain equations of cardiac electrophysiology has been investigated. Scalability tests were performed for fully explicit and semi-implicit numeric schemes in 1d-, 2d-, and 3d-model problems with structured and unstructured meshes using novel software entirely developed in C++/CUDA. The performance of the method was ulteriorly demonstrated on realistic models of a biventricular human heart and human atria.

Previous studies [14] have reported speedups of 32× for the monodomain model using an explicit finite difference scheme along with the phase I Luo-Rudy ionic model [15], a much less complex model as the TP06 model used in this study (7 state variables instead the 19 state variables of the TP06 or the 28 state variables of the Maleckar et al. action potential model of atria). In their study Sato et al [14] have established the solution of the PDE equation as the bottle neck of the computation with GPU, in part because they were forced to used single precision for their computations requiring a more stringent step size when solving the Step II of the algorithm than the required for integrating the action potential model (Step I). In addition, Sato et al. were using an adaptive time stepping when integrating the system of ODEs, which introduces latencies in the computations. In our implementation, we integrate with a constant time step size that guarantees both, the stability of the ionic model (most restrictive step size) and the stability of the PDE, similarly as has been proposed in order

studies [2]. With this strategy we have been able to make full use of the GPU parallel potential by reducing latency during GPU execution leading to acceleration of up to 90× for 2d-problems similar to those considered in [14] with an explicit scheme.

Results from Figure 3 also indicate that a minimum problem size is required in order to maximize GPU performance. This is due to the slower clock speed of the GPU cores and limited double precision floating point arithmetic as compare to CPU cores. This lower core performance is, however, compensated by the capability of the GPU to schedule a vast numbers of threads and efficiently reducing latency in this many core architecture. In this regard, for the C2090 our results indicate that for the ODE solver, the GPU is able to accommodate up to 8000 nodes without degradation of computer performance. For the monodomain solver, this threshold was found to be in 800 nodes for the fully explicit scheme and in 8000 nodes for the semi-implicit scheme. After this threshold is surpassed the scalability of the GPU with the number of degrees of freedom approaches to linearity. Even though these results are dependent on the GPU card used, this threshold appeared to be independent of the problem dimensionality for the cases considered. We must remark that the bandwidth of the linear system did not change much between the structured and unstructured meshes, being 27 for the 3d-structured mesh and 31 for the 3d-unstructured mesh. This explains the similarity between the results obtained for both benchmarks, as well as the speedup found for the ventricle and atria simulations.

Another aspect worth mentioned from our studies was the influence of the sparse matrix format for storing the finite element matrices. In this regard, using the efficient Hybrid sparse matrix format offered in the CUSP-library [12] can reduce the computation time for 3-d problems up to a 10%.

5. Conclusions

This study demonstrates that significant reduction on computing time can be achieved for solving the cardiac monodomain equations. Despite the significant lower performance observed on a single GPU core with respect to a single CPU core, a single GPU card offered excellent performance with speedups of 70× for three-dimensional problems solved explicitly and near 50× for three-dimensional problems solved with a semi-implicit scheme when compared with a single CPU. These results demonstrate that personal workstation is able to perform a simulation of the electric activity of a whole heart in reasonable times that enable researchers to interact more easily with their simulations.

Working with GPUs poses additional programming challenges over traditional parallel CPU implementations. However, like parallel CPU implementations, an efficient management of threads and memory are required if maximum performance of the GPU is to be achieved.

Acknowledgments

This project was partially supported by the “VI Plan Nacional de Investigación Científica, Desarrollo e Innovación Tecnológica” from the Ministerio de Economía y Competitividad of Spain (grant numbers TIN2012-37546-C03-01 and TIN2012-37546-C03-03) and the European Commission (European Regional Development Funds – ERDF - FEDER).

References

[1] Rodríguez B, Trayanova N, Noble D, Modeling Cardiac Ischemia. *Annals of the New York Academy of Science*, 1080: 395-414, 2006.

[2] Neic A, Liebmann M, Hoetzl E, Mitchell L, Vigmond E, Haase G, Plank G. Accelerating cardiac bidomain simulations using grpahic processing units. *IEEE Transactions on Biomedical Engineering*, 59(8): 2281-90, 2012.

[3] Heidenriech E, Ferrero(Jr) JM, Doblare M, Rodriguez JF. Adaptive Macro Finite Elements for the Numerical Solution of Monodomain Equations in Cardiac Electrophysiology. Annals of Biomedical Engineering, 38(7): 2231-45, 2010.

[4] Geselowitz DB, Miller III, WT. A bidomain model for anisotropic cardiac muscle. *Annals of Biomedical Engineering*, 11: 315– 334, 1983.

[5] Trayanova N, Eason J, Aguel F. Computer simulations of cardiac defibrillation: a look inside the heart. *Computing and Visualization in Science*, 4: 259–270, 2002

[6] Ferrero JM, Trenor B, Rodriguez B, Saiz J. Electrical activity and reentry during acute regional myocardial ischemia: insights from simulations. *International Journal of Bifurcation and Chaos*, 13: 3703–3715, 2003.

[7] Sundnes J, Nielsen BF, Mardal KA, Cai X, Lines GT, Tveito A. On the computational complexity of the bidomain and the monodomain models of electrophysiology. *Annals of Biomedical Engineering*, 34: 1088–1097, 2006.

[8] Hughes TJR. The Finite Element Method: Linear Static and Dynamic Finite Element Analysis. Prentice Hall Inc., Englewwog Cliffs, NJ, 1987.

[9] ten Tusscher KHWJ, Panfilov AV. Alternants and spiral breakup in a human ventricular tissue model. *American Journal of Physiology Heart and Circulation Physiology*, 291: H1088–H1100, 2006.

[10] CellML model repository. Available: http://models.cellml. org/cellml

[11] Rush S, Larsen H. A practical algorithm for solving dynamic membrane equations. *IEEE Transactions on Biomedical Engineering*, 25(4): 389-92, 1978.

[12] Bell N, Garland M. CUSP-library: Generic Parallel Algorithms for Sparse Matrix and Graph Computations. Availablecode. google.com/p/cusp-library/, 2012.

[13] Maleckar MM, Greenstein JL, Giles WR, Trayanova N A. K+ current changes account for the rate dependence of the action potential in the human atrial myocyte. *American Journal of Physiology - Heart and Circulatory Physiology, 297*, H1398-H1410, 2009

[14] Sato D, Xie Y, Weiss JN, Qu Z, Garfinkel A, Sanderson AR. Acceleration of cardiac tissue simulation with graphic processing units. *Medical and Biological Engineering and Computing*, 47(9): 1011-15, 2009.

[15] Luo CH, Rudy Y. A model of the ventricular cardiac action potential. Depolarization, repolarization, and their interactions. *Circulation Research*, 68(6): 1501-26, 1991.

Brugada or Early Repolarization in V_1 V_2 V_3. Can VCG Aspects Differentiate the Localization of ECG Manifestations ?

C. A. Pastore, N. Samesima, H. G. Pereira Filho

Heart Institute (InCor) – Electrocardiology Clinical Unit - University of São Paulo Medical School Hospital
ecg_pastore@incor.usp.br

Abstract. *Electrocardiographic aspects in Brugada syndrome (BrS) and early repolarization (ER) may confuse the diagnosis, especially when located in the anteroseptal region of the rest-ECG (V1-V3). Vectorcardiography (VCG) is useful to differentiate the two situations, both through visual characteristics of vector loops and quantification of certain measurements. The objective of this study was to define BrS and ER characteristic and distinctive patterns, using aspects of QRS complex loops and ST segments. SÂJ-point of vectorcardiographic loops in the horizontal plane (HP) of 29 BrS patients and 30 individuals with ER were analyzed. J-point resulting vector was obtained by the non- coincidence between QRS complex onset and end. We measured and compared the angle of this resulting vector in PH between groups. Non-paired t-test and ROC curve were used, with* $P \leq 0.05$. *Men age was* 47 ± 15 *vs* 38 ± 14 *y.o.* ($p = 0.02$), *66% vs 90% male* ($p = 0.03$); *QRS duration was* 101.6 ± 10.2 *vs* 94.9 ± 12.5*ms* ($p = 0.03$); *mean SÂJ-point was* $103.4^o \pm 18.9^o$ *vs* $54.5^o \pm 16.3^o$ ($p < 0.0001$), *BrS vs ERS, respectively. SÂJ-point* $> 75^o$ *cut-off value as obtained by ROC curve better identified BrS, with 96.6 % sensitivity and 93.3 % specificity. SÂJ-point* $>75°$, *as assessed by vectorcardiography can differentiate between the Brugada syndrome and early repolarization with high sensitivity and specificity.*

Keywords. Vectorcardiography, Differential diagnosis, J-point, Early repolarization, Brugada syndrome

1. Introduction

Many experts have published scientific contributions about the relationship between early repolarization (ER) and the Brugada syndrome (BrS) [1-4]. The two electrocardiographic patterns, which are sometimes linked to sudden cardiac death, share similar features, such as patients' ages, gender, influence of parasympathetic tonus, family inheritance. Both situations show J-point and ST-segment alterations, which are critical for determining the phenotype and prognosis. ECG characteristics and electrical changes induced by drugs or heart rate can highlight the subgroup of individuals who are at greater risk. In what refers to the electrophysiological mechanisms involved, there is heated discussion over a common substrate (augmented Ito channels) in different locations of the ventricles, as an explanation for the electrical phenomena which are found and for the worse evolution.

Most cases of ER and BrS have clearly distinct ECGs. However, some of them share similar features, especially when the ECG findings are located in the anteroseptal region of the rest ECG (V1-V3). They can frequently lead to a difficult formulation of diagnosis, but an extra help could be obtained from an old method, the vectorcardiogram (VCG). Analysis of the VCG makes it possible to differentiate between these particular syndromes expressions, both from qualitative and quantitative characteristics of the QRS and J point/ST segment loops. Therefore, we conducted our study aiming to define electro/vectorcardiographic patterns of differential diagnoses.

This study sought to characterize and distinguish the changes in the QRS complex, J-point, ST-segment and T-wave, which we observed using the vectorcardiographic loops of the VCG as a tool, in individuals with electrocardiographic diagnosis of early repolarization and Brugada syndrome.

2. Material and Methods

Study subjects

All the study subjects underwent 12-lead electrocardiography and vectorcardiography examinations.

- 30 individuals with diagnosis of ERs were selected according to the ECG pattern described in the literature: presence of notch or final slowing of the QRS complex, J-point elevation, either with or without ST-segment elevation.
- 29 individuals with diagnosis of type I (n – 22) or type II (n – 7) Brugada syndrome were also selected.

Methodology

SÂJ-point of vectorcardiographic loops, obtained in the horizontal plane (HP) of BrS patients and individuals with ER were analyzed. The J-point resulting vector was obtained by the non-coincidence between the QRS complex onset point and its end (Fig. 2). We measured the angle of this resulting vector in the HP and compared its value between groups. Non-paired t-test and the ROC curve were used, with $P \leq 0.05$ significance level.

3. Results

Men age was 47 ± 15 vs 38 ± 14 y.o. ($p = 0.02$), 66% vs 90% male ($p = 0.03$); QRS duration was 101.6 ± 10.2 vs 94.9 ± 12.5ms ($p = 0.03$); mean SÂJ-point was 103.4 ± 18.9° vs 54.5 ± 16.3° ($p < 0.0001$), BrS vs ERS, respectively. SÂJ-point > 75° cut-off value as obtained by ROC curve better identified BrS, with 96.6 % sensitivity and 93.3 % specificity (Fig. 1).

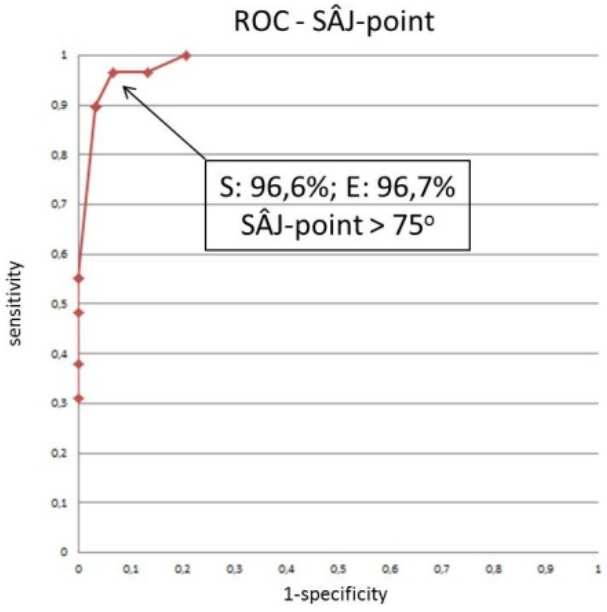

Fig. 1. SÂJ-point > 75° cut-off value obtained by ROC curve.

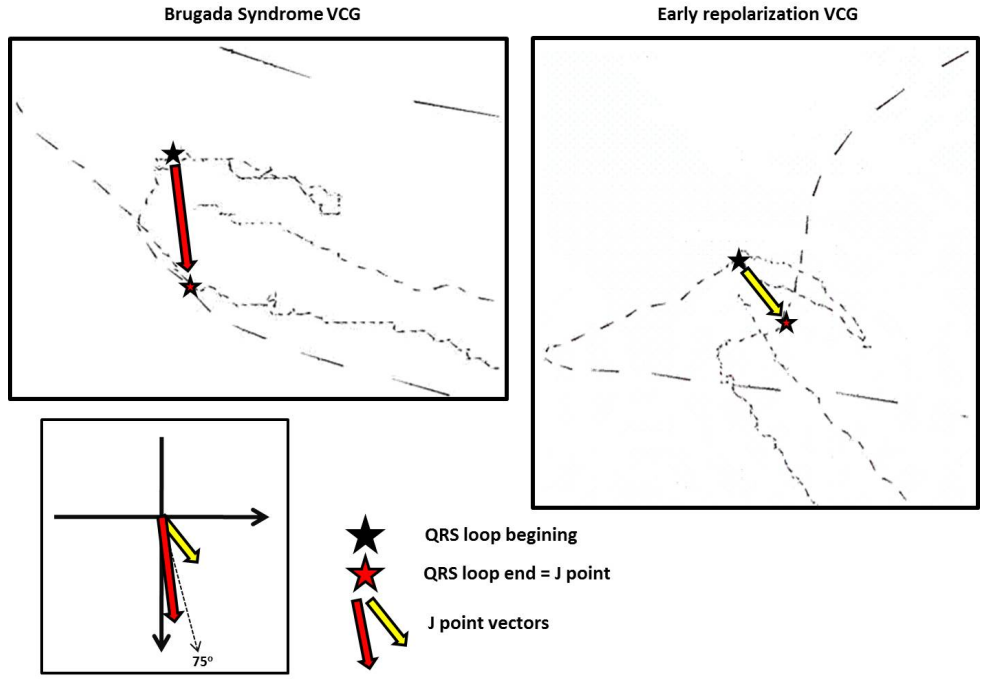

Fig. 2. Determination of the J-point resulting vector by the non-coincidence between the QRS complex onset point and its end.

4. Discussion

The electrocardiogram presents some limitations when the electrical phenomena occur concomitantly, especially if this happens in the precordial leads (V1, V2, V3). When it happens with some patterns of Brugada syndrome and a few early repolarization cases, they become differential diagnoses. It occurs frequently in some other disorders, like Wolff-Parkinson-White syndrome, anteromedial fascicular block, right bundle-branch block, right ventricular hypertrophy, lateral (formerly dorsal) myocardial infarction and dystrophies, as a result of an overlapping of ECG patterns in this region.

The spatial vectorcardiographic configuration can improve the 12-lead electrocardiogram sensitivity in order to clarify similar, but absolutely distinct, electrical phenomena. Our study was designed to compare some electrical aspects of patients with early repolarization and Brugada Syndrome using the vectorcardiogram. Initially, a qualitative J-point/ST segment analysis seemed to be a useful tool to differentiate both. A fish-hook shape of J-point/ST segment, as well as "nose" profile in Brugada, could distinguish the two syndromes. Besides, the left posterior or right anterior J-point/ST segment position could be used to determine an ER or a BrS case, respectively. In the present study, our intention was to quantify our previous findings. We measured and compared the angle of the vector generated by the non-coincidence between onset and end of the QRS loop (SÂJ-point) in the horizontal plane. The observation that such vector is oriented forward and rightward in the Brugada syndrome, with a mean value of 103.4 degrees, is in sharp contrast with the leftward and lateral orientation, and mean 54.5 degrees in the early repolarization ($p < 0.0001$). The cutpoint of SÂJ-point $> 75°$ obtained in the ROC curve plotting could identify the Brugada syndrome with 96.6 % sensitivity and 93.3 % specificity.

The differential patterns of vectorcardiographic loops, mainly displayed in the horizontal plane, between the Brugada syndrome with anterior and rightward orientation giving it the aspect of a "nose" in the presence of end-conduction delay, and the early repolarization with

its configuration as a “fishhook” and end-conduction delay oriented to the left and posteriorly, are very clearly evidenced.

Therefore, the presence of the J vector in the two contexts, although similarly generated, shows different angles in the horizontal plane, with a neat separation between the two situations as described above. The vectorcardiographic findings can make it easier to perform the ECG analysis, by creating patterns of different aspects, thus helping to make the correct diagnosis.

References

[1] Osborn JJ. Experimental hypothermia: respiratory and blood pH changes in relation to cardiac function. *American Journal of Physiology* 1953; 175: 389-398.

[2] Gussak I, Antzelevitch C. Early repolarization syndrome: clinical characteristics and possible cellular and ionic mechanisms. *Journal of Electrocardiology* 2000; 33(4): 299-309.

[3] Haissaguerre M, Derval N, Sacher F, et al. Sudden cardiac arrest associated with early repolarization. *The New England Journal of Medicine* 2008; 358(19): 2016-2023.

[4] Pérez-Riera AR, Ferreira Filho C, Abreu LC, Ferreira C, Yanowitz FG, Femenia F, et al. Do patients with electrocardiographic Brugada type 1 pattern have associated right bundle branch block? A comparative vectorcardiographic study. *Europace* 2012; 14(6): 889–897.

ECG Patterns and Genotypes in Pediatric Patients with Channelopathies - 7-year Experience in Slovakia

V. Illikova, P. Hlivak, E. Balazova, R. Hatala

Depts. of Arrhythmias and Pacing and ICU, Children's Cardiac Center, Comenius University Faculty of Medicine, and National Cardiovascular Institute, Slovak Medical University School of Medicine, Bratislava, Slovakia
Email: illikova@dkc-sr.sk

Abstract. *Primary genetic arrhythmias or channelopathies are associated with mutations of genes encoding proteins creating or interacting with the specialized ion channels in the myocardial cell membranes. The resulting increased or decreased ion channel function forms the arrhythmogenic substrate predisposing the patient with structurally normal heart to sudden cardiac death on the basis of ventricular tachycardia or fibrillation. The study focuses the clinical and ECG presentation and management of children with channelopathies in Slovakia. 18 children with suspected primary genetic arrhythmia were admitted to the Children's Cardiac Center Bratislava in the years 2007 – 2013. Results: in 10 patients the underlying channelopathy has been genetically proven: syndrome of long QT interval in 7 and catecholaminergic polymorphic ventricular tachycardia in 3 patients. The remaining patients are in the process of genetic testing, 4 of them with obvious symptoms of channelopathy. Sixteen children are treated with betablockers, 5 in combination with mexiletine or flecainide, 7 patients received implantable cardiac defibrillator and one underwent left cardiac sympathetic denervation. None of the treated patients died. Conclusion: Early diagnosis of channelopathies allows for adequate treatment and lifestyle modification. Genetic testing is important both for the optimal management of the patient and the family.*

Keywords: channelopathy, genetic testing, children

1. Introduction

Primary genetic arrhythmias or channelopathies are associated with mutations of genes encoding proteins creating or interacting with the specialized ion channels in the myocardial cell membranes. The resulting changes in the ion channel function form the arrhythmogenic substrate predisposing the patient with structurally normal heart to sudden cardiac death (SCD) on the basis of ventricular tachycardia (VT) or fibrillation [1, 2]. Channelopathies are a heterogenous group of diseases with many different causative genes. Three most commonly occurring types are long QT syndrome (LQTS), catecholaminergic polymorphic ventricular tachycardia (CPVT) and Brugada syndrome (BrS).

LQTS is characterized by QT prolongation and T wave abnormalities, specific type of arrhythmia - torsades de pointes (TdP), and predisposition for syncope, seizures and sudden cardiac death. TdP is a specific type of ventricular tachycardia (Fig. 1), often self-limiting with transient syncope, but it can also degenerate into ventricular fibrillation and cardiac arrest [3, 4]. LQTS represents a leading cause of autopsy-negative sudden death in the young [5]. Three main genes responsible for the 3 most common types of LQTS (gene KCNQ1 in LQT1, KCNH2 in LQT2 and SCN5A in LQT3), account for approximately 75% of clinically definite LQTS, minor genes contribute an additional 5% and about 20% of LQTS remain genetically elusive [2, 4, 6]. Diagnosis of LQTS is made when modified Schwartz risk score is more than 3.5 (Fig. 2) and/or pathogenic mutation of one of the LQTS genes is found or corrected QT interval of more than 500 ms is reproducibly measured on the native ECG. The

estimated yield of the genetic testing in LQTS is about 60%. Treatment options for LQTS patients include life-style modification with avoidance of specific arrhythmia triggers and QT interval prolonging drugs, beta-blockers (BB), mexiletin in LQT3, left sympathetic cervical denervation (LSCD) and implantable cardiac defibrillator (ICD) [2].

Fig. 1. Episode of torsade de pointes (in neonate with LQT3) on ECG monitor (lead II) - top part of the figure, with invasive arterial blood pressure (ABP) measurement - the bottom of the figure. Note the sudden fall of ABP to zero with the beginning of TdP and ventricular premature beats before the TdP starts.

CPVT is characterized by normal resting ECG and adrenergic-mediated VT: monomorphic premature ventricular beats (PVB) progressing to specific bidirectional and polymorphic PVB and VT with physical activity or emotional stress. Genes responsible for this disease are gene for ryanodine receptor RYR2 (60%) and calsequestrin CASQ2 (5%). The estimated yield of the genetic testing is around 40%. Treatment options include life-style modification with avoidance of physical activity, beta-blockers, ICD, LSCD, verapamil and flecainide [2].

Our study focuses the clinical and ECG presentation and management of children with channelopathies in Slovakia.

		Points
ECG findings*		
A.	QT_c†	
	≥480 msec$^{1/2}$	3
	460-470 msec$^{1/2}$	2
	450 msec$^{1/2}$ (in males)	1
B.	Torsade de pointes‡	2
C.	T-Wave alternans	1
D.	Notched T wave in three leads	1
E.	Low heart rate for age§	0.5
Clinical history		
A.	Syncope‡	
	With stress	2
	Without stress	1
B.	Congenital deafness	0.5
Family history‖		
A.	Family members with definite LQTS#	1
B.	Unexplained sudden cardiac death below age 30 among immediate family members	0.5

LQTS, long QT syndrome.
*In the absence of medications or disorders known to affect these electrocardiographic features.
†QT_c calculated by Bazett's formula, where $QT_c = QT/\sqrt{RR}$.
‡Mutually exclusive.
§Resting heart rate below the second percentile for age.[25]
‖The same family member cannot be counted in A and B.
#Definite LQTS is defined by an LQTS score ≥4.
Scoring: ≤1 point, low probability of LQTS; 2 to 3 points, intermediate probability of LQTS; ≥4 points, high probability of LQTS.

Fig.2. Modified Schwartz diagnostic criteria in LQTS

2. Subject and Methods

Eighteen children aged from neonatal to 18 years with suspected primary genetic arrhythmia were admitted to Children's Cardiac Center Bratislava in the years 2007 - 2013. Twelve patients (pts.) were symptomatic, in 8 we assumed LQTS and in 4 CPVT. 6 pts. were asymptomatic with ECG features or family history of primary genetic arrhythmia, LQTS supposed in 5 and BrS in one. Characteristics of the patients are summarized in Table 1. In 13 patients with suspected LQTS, QT interval was measured and corrected for heart rate using Bazzet's formula and risk score was measured according to modified Schwartz diagnostic criteria (Fig. 3). In 4 patients with suspected CPVT, exercise testing and 24 hours ECG Holter monitoring was made to document specific arrhythmias during exercise or emotional stress. One patient had family history of Brugada syndrome with no obvious ECG pattern and parents refused any other diagnostic testing. Genetic testing was made in the diagnostic genetic center GeneDx, US, from the sample of the isolated DNA. DNA isolation was made in a genetic laboratory in Bratislava, Slovakia. Results of the genetic testing were classified

into 4 categories: disease-causing mutation, mutation likely disease-causing, variant of unknown significance or negative testing with no mutation.

3. Results

Genetic testing has been done in 15 patients (LQTS was supposed in 11 pts., 8 of them symptomatic, and CPVT in 4, all symptomatic), with 10 results until now: LQTS was diagnosed in 7 pts.: KCNQ1 gene mutation in 3, KCNH2 in 2 and SCN5A in 4 (2 children had more than one mutation), and CPVT in 3 pts.: all three RYR2 mutations. Mutations were diagnosed as disease-causing in 5 of 7 LQTS patients and as variant of unknown significance (VUS) in 2: one in a girl whose mother was resuscitated from SCD and one in the 15-years old student athlete resuscitated from SCD, in whom a year later mutation was re-classified as very likely disease-causing. From 7 LQTS patients 4 were symptomatic: 2 were resuscitated from SCD, 2-years old girl had hundreds of TdP daily with frequent loss of consciousness and last patient had recurrent syncope. In the asymptomatic patients 2 infants had prolonged QTI found on ECG made because of sinus bradycardia and one 2-years old girl had ECG made because her mother was resuscitated from SCD. 3 CPVT patients had RYR2 mutations, twins with frequent syncope and seizures and 9-years old boy resuscitated from SCD, diagnosed and treated as epilepsy for 3 years. Genetic analysis in the remaining 5 pts. haven't been finished yet, 3 have obvious symptoms of channelopathy. 3 pts. haven't been tested yet: 1 with supposed BrS, girl resuscitated from SCD with supposed LQTS and 14 years old girl with suspected LQTS who died before therapy was started and genetic testing realized. Sixteen children are treated with betablockers, 2 of them (with SCN5A gene mutation) in combination with mexiletine and 3 (CPVT) in combination with flecainide, 7 patients (5 LQTS and 2 CPVT) received ICD, 5 pts. after resuscitated SCD, 2 with recurrent syncope on BB therapy, and 2-years old girl with LQT3 with hundreds of TdP daily underwent left cardiac sympathetic denervation. None of the treated patient died, one patient with CPVT has neurologic sequelae after cardiopulmonary resuscitation. Appropriate shock was delivered in 4, inappropriate in 3 of 7 patients with ICD. Patient characteristics are summarized in Table 1.

Table 1. Characteristics of the patients: age at presentation/diagnosis, symptoms, genetic results, treatment

Pts	Age [years]	Symptoms	Susp. dg.	Gene mutation, genetic diagnosis	Treatment
1. ZP	0	Resusc.SCD, frequent TdP	LQTS	SCN5A – LQT3	ICD + BB + mexiletin
2. MN	0,1	Asympt., bradycardia	LQTS	KCNQ1 – LQT1	BB
3. KB	1	Asympt., bradycardia	LQTS	KCNQ1 + VUS in SCN5A - LQT1 (+LQT3)	BB
4. TP	2	Syncopes, frequent TdP	LQTS	SCN5A – LQT3	ICD + BB + mexiletin
5. PM	2	Asympt., near SCD in mother	LQTS	SCN5A VUS (LQT3)	BB
6. LB	9	Syncopes, disiness	LQTS	KCNQ + KCNH2 – LQT1 + LQT2	BB
7. LF	9	Resuscitated SCD	LQTS	Not finished	ICD + BB
8. JB	9	Syncopes	LQTS	Not finished	BB
9. PJ	10	Asympt., BrS in the father	BrS	Not made	No therapy
10. MU	11	Resuscitated SCD	CPVT	RYR1 – CPVT	ICD + BB
11. MD	11	Asympt., accidental finding	LQTS	Not finished	BB
12. AD1	13	Syncopes with seizures	CPVT	RYR2 – CPVT	ICD + BB + flecainide
13. AD2	13	Syncopes with seizures	CPVT	RYR2 – CPVT	BB + flecainide
14. PB	14	Asympt., accidental finding	LQTS	Not finished	BB
15. LO	14	Palpitations, chest pain	CPVT	Not finished	BB + flecainide
16. VM	15	Syncopes, SCD	LQTS	Not made	Exitus
17. MJ	18	Resuscitated SCD	LQTS	KCNH2 – LQT2	ICD + BB
18. VS		Resuscitated SCD	LQTS	Not made	ICD + BB

4. Discussion and conclusion

Primary genetic arrhythmias are uncommon diseases presenting with syncopes, seizures or SCD. These patients are not infrequently misdiagnosed and treated as epilepsy so that correct diagnosis and treatment could be delayed with the risk of life-threatening arrhythmias (9-years old boy treated as epilepsy, CPVT diagnosed after resuscitation from SCD, neurologic sequelae). Despite the fact that life-threatening arrhythmias in LQTS occur under specific circumstances in a gene-specific manner (exercise or emotional stress in LQT1, sudden noise in LQT2 and sleep in LQT3) [7], we've observed in one patient phenotype-genotype mismatch with clinical and ECG features suggesting LQT1 (exercise or emotional stress triggered TdP with their complete disappearance during sleep, delayed onset peaked T waves) and genetic result and reaction to treatment (mexiletin proved as the only effective treatment) corresponding with LQT3. In our experience in this small series of patients, genetic testing in some cases revealed dissociation of the genetic finding and the phenotypic clinical presentation. This observation reflects the continously evolving knowledge about the relation of specific mutations to clinical presentation (mutation evaluated as the variant of uknown significance in a patient resuscitated from SCD, 1 year later re-evaluated as very likely disease-causing mutation). We conclude that both the clinical presentation and genetic testing must be considered in the diagnostic and therapeutic process. Early diagnosis of channelopathies allows for adequate treatment, lifestyle modification and avoidance of specific triggers of arrhythmic events. Genetic testing is important both for the optimal management of the patient and of the family members.

References

[1] Marban E: Cardiac channelopathies, *Nature* 2002; 415(6868): 213-218.

[2] Priori SG, Wilde AA, Horie M et al: HRS/EHRA/APHRS Expert Consensus Statement on the Diagnosis and Management of Patients with Inherited Primary Arrhythmia Syndromes, *Heart Rhythm* 2013, 12: 1932-1963.

[3] Ackerman MJ, Khositseth A, Tester DJ et al: Congenital long QT syndrome in electrical diseases of the heart; genetics, mechanisms, treatment, prevention. New York: Springer Publishing, 2008, pp. 462–482.

[4] PJ Schwartz, MJ Ackerman, AL George, AAM Wilde: Impact of genetics on the clinical management of channelopathies, *Journal of American College of Cardiology* 2013; 62: 169-180.

[5] Tester DJ, Ackerman MJ: Postmortem long QT syndrome genetic testing for sudden unexplained death in the young, *Journal of American College of Cardiology* 2007; 49: 240-246.

[6] Ackerman MJ, Priori SG, Willems S, et al.: HRS/EHRA Expert Consensus Statement on the State of Genetic Testing for the Channelopathies and Cardiomyopathies. This document was developed as a partnership between the Heart Rhythm Society (HRS) and the European Heart Rhythm Association (EHRA). *Europace* 2011;13:1077–1109.

[7] Schwartz PJ, Priori SG, Spazzolini C, et al.: Genotype-phenotype correlation in the long-QT syndrome: gene-specific triggers for life-threatening arrhythmias. *Circulation* 2001; 103: 89-95.

Brugada Phenocopy: Update 2014

A. Baranchuk, B. Gottshalk, D.D. Anselm

Division of Cardiology, Electrophysiology and Pacing, Queen's University, Kingston General Hospital, Kingston, Ontario, Canada
Email: barancha@kgh.kari.net

Abstract. *Brugada Phenocopies (BrP) continue to emerge as clinical entities that are distinct from true congenital Brugada Syndrome (BrS). BrP are characterized by type 1 and type 2 Brugada ECG patterns in leads V1-V3; however, BrP are elicited by various underlying associated conditions. A new ECG classification is proposed and a lauching of an international website is discussed. We will also review the progress made to-date regarding BrP.*

Keywords: Brugada Syndrome, Brugada Phenocopy, Genetics, Ion Channels

1. Introduction

Brugada Syndrome (BrS) is an inherited cardiac channelopathy characterized by type 1 and type 2 ECG patterns in leads V1-V3 which predispose individuals to malignant ventricular arrhythmias and sudden cardiac death (Figure 1, Panel A) (1). Brugada Phenocopies (BrP), however, are clinical entities that have ECG patterns that are identical to true congenital BrS but are elicited by various factors such as electrolyte disturbances, mechanical compression, poor ECG filters, and myocardial ischemia (Figure 1, Panel B) (2). The current BrP etiological categories are depicted in Table 1 and the diagnostic criteria in Table 2.

The term *Phenocopy* was chosen because it describes an environmental condition that imitates one produced by a gene; therefore, it served as a reasonable and succinct description for all acquired Brugada-like ECG manifestations (3). In this paper, we review the progress made to-date regarding BrP, discuss areas of ongoing controversy, and identify opportunities for further investigation.

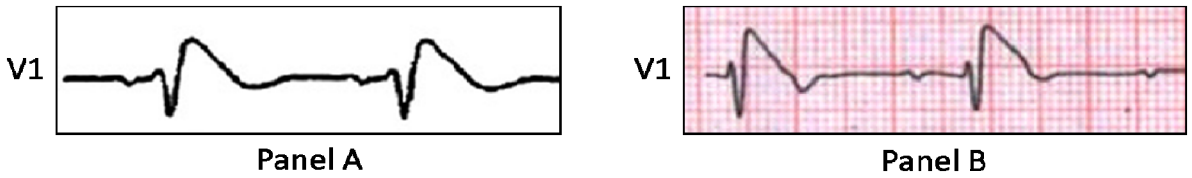

Fig. 1. Comparison of true congenital Brugada Syndrome and Brugada Phenocopy. Classical congenital type 1 "coved" Brugada ECG pattern (Panel A) (1). Brugada Phenocopy in a patient presenting with an acute inferior ST-segment elevation myocardial infarction with right ventricular involvement (Panel B) (5). Lead V1 is identical to the type 1 Brugada ECG pattern. Reproduced with permission (1,5).

Table 1. Brugada Phenocopy Etiological Categories

Etiological Category	
i.	Metabolic Conditions
ii.	Mechanical Compression
iii.	Ischemia & Pulmonary Embolism
iv.	Myocardial & Pericardial Disease
v.	ECG Modulation
vi.	Miscellaneous

Reproduced with permission (12).

Table 2. Clarification of Brugada ECG Pattern, Brugada Phenocopy, and True Congenital Brugada Syndrome

Brugada ECG Pattern
i. The ECG pattern has a type 1 or type 2 Brugada morphology as currently defined by Bayés de Luna et al (1)
Diagnostic Criteria for Brugada Phenocopy (2-12)
i. The ECG pattern has a type 1 or type 2 Brugada morphology
ii. The patient has an underlying condition that is identifiable
iii. The ECG pattern resolves after resolution of the underlying condition
iv. There is a low clinical pretest probability of true Brugada Syndrome determined by lack of symptoms, medical history, and family history
v. Negative provocative testing with sodium channel blockers such as ajmaline, flecainide, or procainamide
vi. Provocative testing not mandatory if surgical RVOT manipulation has occurred within the last 96 hours
vii. The results of genetic testing are negative (desirable but not mandatory because the SCN5A mutation is identified in only 20% to 30% of probands affected by true Brugada Syndrome)
Features that suggest true congenital Brugada Syndrome
i. The ECG pattern has a type 1 or type 2 Brugada morphology
ii. There is a high clinical pretest probability of true congenital Brugada Syndrome determined by presence of symptoms, medical history, and family history
iii. Positive provocative testing with sodium channel blockers such as ajmaline, flecainide, or procainamide. This indicates sodium channel dysfunction consistent with true Brugada Syndrome
iv. The results of genetic testing are positive (desirable but not mandatory because the SCN5A mutation is identified in only 20% to 30% of probands affected by true Brugada Syndrome)

ECG indicates electrocardiogram; RVOT, right ventricular outflow tract; and SCN5A; sodium channel voltage-gated type V alpha subunit.

2. Discussion

The diagnostic distinction between BrP and true congenital BrS focuses on a few key features. The first is that patients with BrP have a reversible underlying condition such as adrenal insufficiency, hypokalemia, or myocardial ischemia which elicits the Brugada ECG pattern. Once this underlying condition resolves, there is normalization of the ECG. Second, patients with BrP have a low clinical pretest probability of true BrS as opposed to a high pretest probability in patients with true BrS (4-9). Third, patients with BrP have a negative provocative challenge with a sodium channel blocker, while those with true BrS have a positive provocative challenge (Table 2). Additionally, while patients with high-risk true congenital BrS are candidates for ICD implantation, the clinical implications of patients with BrP remain unknown. Therefore, the only BrP treatment recommendations at this time would be to focus on resolution of the underlying condition as further intervention has not yet been investigated or validated.

Brugada Phenocopy – Genetics

The inclusion of genetic testing regarding BrP continues to be an area of discussion and will undoubtedly evolve. We have not included genetics as a mandatory diagnostic criterion since only 20-30% of probands with true congenital BrS have positive genetic tests (2, 10-12). Therefore, the vast majority of patients with BrS will have negative genetic testing at this

time. Additionally, even within families known to carry genetic mutations consistent with BrS, there is a poor correlation between genetic testing, ECG manifestations, and clinical outcomes (1). Furthermore, the presence of genetic mutations in true congenital BrS has been shown to be a poor predictor of arrhythmic events and is not a cost effective method of risk stratification in unselected patients diagnosed with BrS.

We also acknowledge that not all patients with exposure to various underlying conditions such as hypokalemia, hyperkalemia, adrenal insufficiency or myocardial ischemia will develop a Brugada ECG pattern. This suggests a possible genetic predisposition for these ECG phenomena. However, looking into the same genes that are associated with true congenital BrS may not be of diagnostic yield.

Brugada Phenocopy – Clinical Reproducibility
The chronological emergence of new ECG phenomena should include: (i) phenomenological observation; (ii) speculation on pathophysiological mechanisms; (iii) clinical reproducibility; and (iv) experimental model validation.

Speculations on the pathophysiological mechanisms of BrP were published elsewhere (2-17) and finally, clinical reproducibility was demonstrated in the context of recurrent severe hypokalemia (13). Briefly, a young patient with diarrhea was admitted to hospital due to severe hypokalemia (K 1.5 mmol/L) with acidosis. The ECG depicted a typical type 1 Brugada ECG pattern. Upon resolution the metabolic disorder, the ECG return to normal. A flecainide test did not induce a Brugada type 1 pattern. Before diarrhea completely resolved, the patient presented with a second episode of hypokalemia (K 2.6 mmol/L) without acidosis. The ECG again depicted a typical type 1 Brugada ECG pattern which resolved after correction of the metabolic abnormality. This case confirms *clinical reproducibility*, which as suggested above, is the third step in the validation model of new ECG phenomenon.

3. Future Directions

The key to completely understanding the mechanisms behind BrP is to reproduce these phenomena under strictly controlled environmental conditions (18). The development of experimental validation models will help us determine whether BrP are transient alterations of the sodium channels that are not reproducible with a sodium channel blocking test, or alternatively, a malfunction of other ion channels. Similarly, a model that induces genetic modifications to reproduce the conditions of true BrS and exposing this model to the well described conditions of BrP would help us to understand whether they are entities that belong to the same spectrum or completely different entities.

In order to learn about the natural history of BrP, we are developing an international online database at www.brugadaphenocopy.com which will allow for longitudinal follow-up. We encourage all investigators that are currently reporting on these cases to use the term *Brugada Phenocopy* in order to facilitate literature searches and to help establish this emerging concept.

Finally, we would like to comment on a morphological classification that we are about to launch. As different congenital or acquired QT prolongations can be classified based on their morphology, we propose the BrP to be classified according to:

1. **Type-1 BrP**: it is represented by a BrP that is identical to a type-1 “true” Brugada ECG pattern.

2. **Type-2 BrP**: it is represented by a BrP that is identical to a type-2 "true" Brugada ECG pattern.

Each category is divided into:

1. **Sub-type A**: all components of the definition for a BrP have been met as per Table 2
2. **Sub-type B**: not all components of the definition for a BrP have been met as per Table 2 (after completion of our website, we will submit letters-emails- to all authors that have published possible BrP that are considered to be type-1 or type-2 sub-type B; in order for them to run all tests that are necessary to become a sub-type A.
3. **Sub-type C**: not all components of the definition for a BrP have been met as per Table 2; however, no additional tests are needed (i.e. ECG modulation, see Table 1).

3. Final Remarks

The field of BrP continues to evolve as more cases are being published. The major advances in the last 18 months could be summarized as follows:

- Acceptance of the terminology by the scientific community
- Clinical reproducibility (once the "injury" is re-introduce, the ECG patterns re-appears
- New morphological classification (explained above)
- Completion of the international database that will allow for a better long-term follow-up and determination of the natural history of this condition
- Progressive utilization of the new ECG techniques to determine the presence of a Brugada pattern (19) (Beta and Alfa angles; base of the triangle). These measurements will help us to distinguish Brugada ECG patterns from other causes of r' in leads V1-V2. Once one has decided that this is not a Brugada ECG pattern, then both "true" congenital BrS and BrP have been ruled out. The systematic application of these techniques, will necessary reduced the number and categories of currently existent BrP, as in the case of Pectus Excavatum (9) and others.

References

[1] Bayés de Luna A, Brugada J, Baranchuk A, et al. Current electrocardiographic criteria for diagnosis of Brugada pattern: a consensus report. J Electrocardiol 2012;45:433.

[2] Baranchuk A, Nguyen T, Ryu MH, et al. Brugada phenocopy: new terminology and proposed classification. Ann Noninvasive Electrocardiol 2012;17:299.

[3] Arce M, Riera ARP, Femenia F, Baranchuk A. Brugada electrocardiographic phenocopy in a patient with chronic Chagasic cardiomyopathy. Cardiol J 2010;17:525.

[4] Anselm DD, Barbosa-Barros R, de Sousa Belém L, Nogueira de Macedo R, Pérez-Riera AR, Baranchuk A. Brugada Phenocopy induced by acute inferior ST-segment elevation myocardial infarction with right ventricular involvement. Inn Card Rhythm Manag 2013;4:1092.

[5] Nguyen T, Smythe J, Baranchuk A. Rhabdomyoma of the interventricular septum presenting as a Brugada phenocopy. Cardiol Young 2011;21:591.

[6] Wang JG, McIntyre WF, Kong W, Baranchuk A. Electrocution-induced Brugada phenocopy. Int J Cardiol 2012;160:e35.

[7] García-Niebla J, Serra-Autonell G, Bayés de Luna A. Brugada syndrome electrocardiographic pattern as a result of improper application of a high pass filter. Am J Cardiol 2012;110:318.

[8] Anselm DD, Pérez-Riera AR, Femenía F, Baranchuk A. Brugada Phenocopy in a patient with surgically repaired Pentalogy of Fallot. Revista Iberoamericana de Arritmologia 2012;3:20.

[9] Awad SFM, Barbosa-Barros R, de Sousa Belem L, et al. Brugada Phenocopy in a patient with Pectus Excavatum: Systematic review of the ECG manifestations associated with Pectus Excavatum. Ann Noninvasive Electrocardiol 2013; 18(5): 415-420

[10] Anselm DD, Baranchuk A. Brugada Phenocopy Emerging as a New Concept. Rev Esp Cardiol 2013;66:755.

[11] Recasens L, Meroño O, Bazan V, Ribas N. Brugada Phenocopy Emerging as a New Concept. Response. Rev Esp Cardiol 2013;66:756.

[12] Anselm DD, Baranchuk A. Brugada Phenocopy: redefinition and updated classification. Am J Cardiol 2013;111:453.

[13] Genaro NR, Anselm DD, Cervino N, et al. Brugada Phenocopy clinical reproducibility demonstrated by recurrent hypokalemia. Ann Noninvasive Electrocardiol 2013 (Epub ahead of print).

[14] Anselm DD, Baranchuk A. Brugada Phenocopy in the context of pulmonary embolism. Int J Cardiol 2013;168:560.

[15] Anselm DD, Rodriguez Genaro N, Baranchuk A. Possible Brugada Phenocopy induced by hypokalemia in a patient with congenital hypokalemic periodic paralysis. Arq Bras Cardiol 2014; 102(1): 104.

[16] Peters S. Early repolarization pattern in patients with provocable Brugada phenocopy: A marker of additional arrhythmogenic cardiomyopathy? Int J Cardiol 2013. doi: 10.1016/j.ijcard.2013.07.089. [Epub ahead of print].

[17] Anselm DD, Baranchuk A. Confirmed Brugada phenocopy in the setting of hypopituitarism. Herz 2014 (Epub ahead of print)

[18] Anselm DD, Evans JM, Baranchuk A. Brugada phenocopy: A new electrocardiogram phenomenon. World J Cardiol 2014;6(3): 81-86

[19] Serra G, Baranchuk A, Bayés-De-Luna A, Brugada J, Goldwasser D, Capulzini L, Arazo D, Boraita A, Heras ME, Garcia-Niebla J, Elosua R, Brugada R, Brugada P. New electrocardiographic criteria to differentiate the Type-2 Brugada pattern from electrocardiogram of healthy athletes with r'-wave in leads V1/V2. europace 2014 (Epub ahead of print)

Cardiac Electrophysiology

Effects of Echinochrome on Ventricular Repolarization in Acute Ischemia

[1,2]K. Sedova, [1]O. Bernikova, [1]S. Kharin, [1]D. Shmakov

[1]Laboratory of Cardiac Physiology, Institute of Physiology of the Komi Science Centre of the Ural Branch of the Russian Academy of Sciences, Syktyvkar, Russian Federation

[2]Department of Biomedical Technology, Czech Technical University in Prague, Kladno, Czech Republic

Email: sedova.ks@gmail.com

Abstract. *Ischemia-related processes, including electrophysiological alterations, are associated with the generation of reactive oxygen species. Although the cardioprotective action of antioxidants against ischemic injury has been proposed, their electrophysiological effects are not clear. The aim of this study was to investigate the effects of the antioxidant Echinochrome on ischemia-induced alterations of ventricular repolarization in a feline model of coronary occlusion. Experiments were performed on open-chest anesthetized adult cats. Activation-recovery intervals were measured from 64 ventricular epicardial unipolar electrograms recorded simultaneously before and during ligation of the left anterior descending coronary artery. Synthetic Echinochrome was infused five minutes before coronary occlusion in two different doses (1.0 mg/kg and 2.0 mg/kg, i.v.).Pre-occlusion administration of Echinochrome in a dose of 1.0 mg/kg resulted in the reduction of ischemia-induced shortening of activation-recovery intervals and the restricted increase in the repolarization dispersion during 30 minutes of ischemia. Echinochrome in a dose of 2.0 mg/kg demonstrated a more pronounced effect. Ability of the antioxidant Echinochrome to decrease ischemia-induced alterations of ventricular repolarization was demonstrated in a feline model of coronary occlusion. A dose-dependent effect was suggested.*

Keywords: Cardiac Electrophysiology, Repolarization, Ischemia, Antioxidant, Animal Model

1. Introduction

Acute cardiac ischemia causes electrophysiological alterations that may lead to fatal arrhythmias. The pathological increase in reactive oxygen species (ROS) could be a key determinant of ischemia/reperfusion-induced ventricular arrhythmias, as ROS trigger an intercellular calcium increase [1]. Antioxidants can prevent oxidative stress and, therefore, reduce the chance of cardiac arrhythmias [2].

Echinochrome (Ech) is a synthetic formulation of the sea urchin pigment echinochrome A (2,3,5,7,8-pentahydroxy-6-ethyl-1,4-naphthoquinone), which is an antioxidant agent characterized by its iron chelation and free-radical scavenging abilities [3,4]. It was shown its cardioprotective effect associated with the diminution of the infarct zone in ischemia/reperfusion models [5]. However, the electrophysiological mechanisms that underlie the cardioprotective action of the antioxidant are not well understood.

The goal of this study was to investigate the effects of theantioxidant Echinochrome (Ech) on ventricular repolarization in an open-chest feline model of 30-min ischemia.

2. Subject and Methods

The work was carried out in accordance with the Guide for the Care and Use of Laboratory Animals, 8th Edition published by the National Academies Press (US) 2011. The local institutional ethical committee approved the study protocol.

The experiments were performed on anaesthetized (zoletil 15 mg/kg; xylazine 1 mg/kg intramuscularly) adult cats in an open-chest setting under spontaneous sinus rhythm. Detailed protocol of the experiment has been described elsewhere [6].

A 64-electrode epicardial sock placed on the heart ventricles aided in recording the cardiac electrical potentials. Along with the limb lead electrocardiograms, a custom designed system (bandwidth 0.05–1000 Hz; sampling rate 4000 Hz) recorded unipolar electrograms, in reference to Wilson's central terminal.

The data was obtained at baseline state and at the 5, 15, and 30 minutes of the myocardial ischemia induced by the ligation of the left anterior descending coronary artery.

The three groups of animals were studied: the animals (n=7) received Ech in dose 2 mg/kg, the animals (n=5) with Ech application in dose 1 mg/kg, and the control group (n=5).

Synthetic Ech provided by the Pacific Institute of Bioorganic Chemistry of the Far Eastern Branch of the RAS (Vladivostok, Russia) was infused through the catheter inserted into the femoral vein as a 0.2% solution in a 0.1% sodium bicarbonate solution. Ech was administrated 5 min before to occlusion of coronary artery; the control group received a saline solution injection in equivalent volume.

The analysis of the recorded epicardial electrograms included the definition of the activation–recovery intervals (ARIs), which were corrected for heart rate by Bazett's formula and used for the evaluation of local repolarization duration. ARI was defined as the interval between the activation time (AT) and the end of the repolarization time (RT), determined as dV/dt min during the QRS complex and dV/dt max during the ST-T complex, respectively [7]. The time measurements were done with respect to the QRS onset in the I limb lead. Dispersion of repolarization was calculated as the difference between the ARI max in the non-ischemic area and ARI min at the ischemic zone.

The data are expressed as Me (25%; 75%). Statistical examination used the Friedman test, followed by the Newman–Keuls test for paired comparisons. The Mann-Whitney test aided in the comparison between groups. A chi-squared test assessed the difference in the occurrence of the ventricular arrhythmias. The differences were considered significant when $p<0.05$.

3. Results

The administration of Ech prior to the coronary occlusion did not change the local durations and distribution of the ARIs on the epicardial surface of the ventricles. There were no differences in baseline distribution of the ARIs among all groups. Acute coronary occlusion resulted in the shortening of the ARIs in the ischemic area ($p<0.05$), whereas the ARIs from non-ischemic area were invariable at ischemia during the exposure. A significant increase of dispersion of the repolarization ($p<0.05$) was demonstrated in both control and treated by Ech animals in response to acute ischemia.

The shortening of ARIs in the ischemic zone was less in animal treated by Ech (2 mg/kg) compared to control group at 15 min and 30 min of ischemia ($p<0.05$, Tabl.1). Therefore, the increase of repolarization dispersion in Ech group (2 mg/kg) was limited ($p<0.05$) in comparison with the control animals at 5 min (Δ 24 (17;34) vs Δ 53 (37;71) ms), at 15 min (Δ 37 (18;38) vs Δ 61 (59;81) ms), and at 30 min (Δ 40 (15;44) vs Δ 63 (63;65) ms). Ech in concentration of 2 mg/kg demonstrated more pronounced effect to decrease the ischemia-induced ARIs shortening (in 1.6 $p<0.05$), and the increase of repolarization dispersion at 30 min ischemia was less (in 1.7 $p<0.05$) versus the 1 mg/kg concentration of Ech.

The incidence of ischemia-induced ventricular arrhythmia did not differ between subjects treated with Ech and control animals. During ischemia, the ventricular arrhythmias, such as polymorphic and monomorphic extrasystoles as well as coupled extrasystoles, began after 10 min of coronary occlusion, and occurred under a period of exposure.

Table 1. Intensity of ischemic injury (**Δ** ARIs) during coronary occlusion (*Me* (25%;75%), ms).

ARIs shortening from baseline state (**Δ**)in ischemic area	Control(n=5)	Echinochrome 1 mg\kg(n=5)	Echinochrome 2 mg\kg (n=7)
5 min ischemia	46(38;57)	33(31;56)	17(14;35)
15 min ischemia	69(56;71)	38(19;58)	27(19;33)$^{\#}$
30 min ischemia	69(51;87)	43(36;70)	25(12;40)$^{\#*}$

$^{\#}$p<0.05 compared to control group
* p<0.05 compared to Ech 1 mg/kg

4. Discussion

The main finding of the present study is the ability of Ech to reduce ischemia-induced shortening of repolarization, and therefore to avoid the increase of repolarization dispersion which can provide the potential substrate for ventricular arrhythmias.

The role of oxidative stress in ischemic tissues has been described [8]. It has been suggested that ROS affect the ion channels [1] and contribute to the genesis of arrhythmias associated with ischemia/reperfusion.

Synthetic Echinochrome was used as an antioxidant and an iron-binding agent [3, 4], seeing that it could have a greater protective effect on oxidative stress-induced ventricular arrhythmias than the antioxidant alone [9].

Previous experimental studies pointed to the cytoprotective and anti-ischemic effects of Ech in animal model of coronary artery occlusion-reperfusion [10]. The clinical investigations confirm that treatment with Ech prevents infarct expansion induced by reperfusion [11]. These studies primarily examined other points of cardiac injury. The electrophysiological effects of Ech in feline model of coronary occlusion were demonstrated in the present study. The pre-occlusion infusion of Ech reduced the ischemia-induced shortening of ARIs. This effect could be due to the inhibition of an ionic current through the ATP-regulated potassium channels (KATP channels); however, further research is required to confirm this assumption.

All of the animal groups demonstrated ventricular arrhythmias during coronary occlusion. This was consistent with the significantly increased ARI dispersion at coronary occlusion in all the animal groups despite to the restriction in increasing repolarization dispersion in animals treated by Ech. It is possible that the restriction of the increase in the repolarization dispersion, which was induced by Ech, was insufficient to prevent the ventricular arrhythmias during ischemia. On the other hand, other key factors providing trigger activity or abnormal automaticity outside the sinoatrial node must be taken into account.

5. Conclusions

The study demonstrated the ability of the antioxidant Echinochrome to decrease ischemia-induced alterations of ventricular repolarization in a feline model of coronary occlusion. The findings suggest a dose-dependent effect of Echinochrome.

Acknowledgements

This study was supported by the Ural Branch of the Russian Academy of Sciences (project No. 12-C-4-1009 and 13-4-SP-359). Synthetic Echinochrome was provided by the G.B. Elyakov Pacific Institute of Bioorganic Chemistry of the Far Eastern Branch of the Russian Academy of Sciences (Vladivostok, Russian Federation).

References

[1] Carmeliet E. Cardiac ionic currents and acute ischemia: from channels to arrhythmias. *Physiological Reviews,* 79: 917-1017, 1999.

[2] Karahaliou A, Katsouras C, Koulouras V, Nikas D, Niokou D, Papadopoulos G, Nakos G, Sideris D, Michalis L. Ventricular arrhythmias and antioxidative medication: experimental study. *Hellenic Journal of Cardiology*, 49: 320-328, 2008.

[3] Lebedev AV, Ivanova MV, Levitsky DO. Echinochrome, a naturally occurring iron chelator and free radical scavenger in artificial and natural membrane systems. *Life Sciences*, 76: 863-875, 2005.

[4] Lebedev AV, Ivanova MV, Levitsky DO. Iron chelators and free radical scavengers in naturally occurring polyhydroxylated 1,4-naphthoquinones. *Hemoglobin*, 32: 165-179, 2008.

[5] Shvilkin AV, Serebriakov LI, Tskitishvili OV, Sadretdinov SM, Kol'tsova EA, Maksimov OB, Mishchenko NP, Novikov VL, Levitskiĭ DO, RudaMIa. Effect of echinochrom on experimental myocardial reperfusion injury. *Kardiologiia*, 31: 79-81, 1991.

[6] Sedova KA, Bernikova OG, Goshka SL, Pokhilo ND, Atopkina LN, Shmakov DN, Kharin SN. Effects of an antioxidant agent on alterations of ventricular repolarization in a coronary artery occlusion-reperfusion experimental model. *Experimental & Clinical Cardiology,* 1-6, 2013.

[7] Millar CK, Kralios FA, Lux RL. Correlation between refractory periods and activation-recovery intervals from electrograms: effects of rate and adrenergic interventions. *Circulation*, 72: 1372-1379, 1985.

[8] Xing D, Chaudhary AK, Miller FJ Jr, Martins JB. Free radical scavenger specifically prevents ischemic focal ventricular tachycardia. *Heart Rhythm*, 6: 530–536. 2009.

[9] Lebedev AV, Levitskaya EL, Tikhonova EV, Ivanova MV. Antioxidant properties, autooxidation, and mutagenic activity of echinochromea compared with its etherified derivative. *Biochemistry,* 66:885-893, 2001.

[10] Mischenko NP, Fedoreev SA, Zapara TA, Ratushnyak AS. Effects of histochrom and emoxypin on biophysical properties of electroexcitable cells. *Bulletin of Experimental Biology and Medicine,* 1479: 196-200, 2009.

[11] Buĭmov GA, Maksimov IV, Perchatkin VA, Repin AN, Afanas'ev SA, Markov VA, Karpov RS. Effect of the bioantioxidant histochrome on myocardial injury in reperfusion therapy on patients with myocardial infarction. *Terapevticheskii Arkhiv,* 74:12-16, 2002.

Can We Prevent Malignant Arrhythmias by Targeting of Cardiac Connexin-43 ?

[1]N. Tribulova, [1]B. Bacova, [1]T. Benova, [1]C. Viczenczova, [1,2]J. Radosinska, [3]V. Knezl, [1]J. Slezak

[1] Institute for Heart Research, SAS, Bratislava, Slovakia,
[2]Department of Physiology, Fac. Med., Comenius University, Bratislava, Slovakia,
[3]Institute of Experimental Pharmacology and Toxicology, SAS, Bratislava, Slovakia
Email: narcisa.tribulova@savba.sk

Abstract. *We hypothesized that cardioprotective compounds such as atorvastatin (ATO), melatonin, omega-3 FA and red palm oil (RPO) may protect from malignant arrhythmias via modulation of myocardial connexin-43 (Cx43) channels and. Experiments were conducted on male rats that were: 1/ spontaneously hypertensive (SHR) without or with intake of omega-3 FA (300mg/day/2month), melatonin (400μg/day/6 weeks) or RPO (200mg/day/6weeks); 2/ hereditary hypertriglyceridemic (HTG) without or with ATO (1.5mg/day/2mth) and omega-3 FA treatment; 3/ hyper- (TH) and hypo-thyroid (HY) without and with RPO intake, as well as age-matched Wistar rats. Results showed that compared to Wistar rats the incidence of sVF was significantly higher in SHR, HTG and TH rat hearts that exhibited abnormal distribution and down-regulation of Cx43, while sVF was not induced in HY rat hearts with up-regulation of Cx43. Treatment of SHR, HTG and TH rats with either compounds resulted in protection from sVF that was associated with attenuation of Cx43 abnormalities and improvement of integrity of cardiomyocytes. Results point out antiarrhythmic effect of atorvastatin, omega-3 FA, melatonin and red palm oil due to, at least in part, modulation of myocardial Cx43. Further studies should elucidate pathways involved in Cx43 modulation by these compounds.*

Keywords: Connexin-43, ventricular fibrillation, antiarrhythmic compounds

1. Introduction

It has been established that rapid spreading of the electrical impulse throughout the heart is essential for synchronized contraction and it is ensured by electrical coupling of cardiomyoctes at the connexin (Cx) gap junction channels. Electrical remodeling due to cardiovascular diseases, such as hypertension, dyslipidemia or altered thyroid status has been shown to involve the changes in expression, distribution and function of cell membrane ion channels, intercellular gap-junction Cx43 channels, Ca-cycling proteins, and extracellular matrix composition [1-4]. This remodeling predisposes to arrhythmogenic mechanisms such as early or delayed afterdepolarizations, resulting in premature contraction, and re-entry of excitation, thus facilitating of life-threatening ventricular tachycardias and fibrillation (VF). Re-entry arrhythmias occur predominantly due to abnormal topology and down-regulation of Cx43 that blocks of conduction [5-7]. Taking into account our previous and studies of others [8-10] we hypothesized that cardioprotective compounds such as atorvastatin (ATO), melatonin, omega-3 FA and red palm oil (RPO) may affect Cx43 and exert antiarrhythmic effects. We aimed to explore this assumption using several rat models mimicking risk factors of human cardiovascular diseases. This study is overview of our already published findings.

2. Subject and Methods

Experiments were conducted on male rats that were: 1/ spontaneously hypertensive (SHR) without or with intake of omega-3 FA (300mg/day/2month), melatonin (400μg/day/6 weeks) or RPO (200mg/day/6weeks); 2/ hereditary hypertriglyceridemic (HTG) without or with ATO

(1.5mg/day/2mth) and omega-3 FA treatment; 3/ hyper- (TH) and hypo-thyroid (HY) without and with RPO intake, as well as age-matched healthy Wistar or Lewis rats. Basic characteristics of animals were registered and left ventricular tissue was examined for myocardial ultrastructure and Cx43 analysis using immunofluorescence, immunobloting and real-time PCR. Electrically-induced sustained ventricular fibrillation (sVF) was tested in isolated perfused heart.

3. Results

Results showed that compared to healthy rats the incidence of sVF was significantly higher in SHR [11, 12, 13], HTG [14] and TH [15] rat hearts that exhibited abnormal distribution and down-regulation of Cx43, while sVF was not induced in HY rat hearts with up-regulation of Cx43. Treatment of SHR, HTG and TH rats with either compounds resulted in protection from sVF that was associated with attenuation of Cx43 abnormalities and improvement of integrity of cardiomyocytes. For details see our published studies [11-15]. Changes in myocardial Cx43 expression and the threshold to induce VF in untreated and RPO-treated hyper- and hypo-thyroid rats are demonstrated in Fig.1.

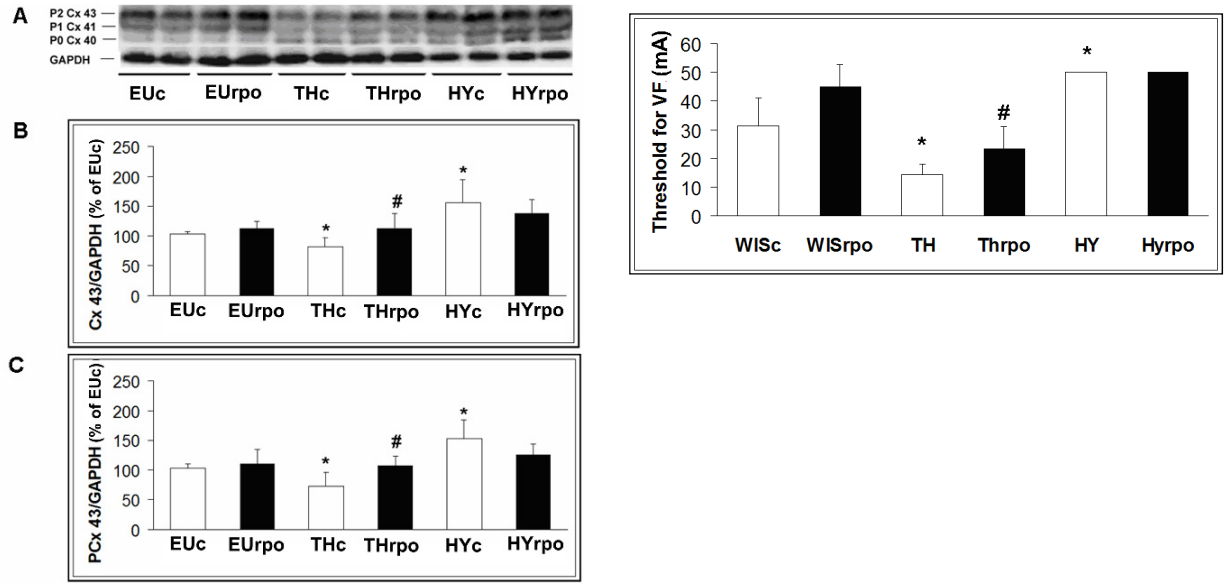

Fig. 1. Expression of myocardial total Cx43 protein (A,B) and its phosphorylated forms (A,C) normalized to GAPDH in rats with altered thyroid status (left panel), threshold to induce sVF (right panel). Abbreviations: Euthyroid control rats (Euc, n=6), EU rats treated with RPO (Eurpo, n=6), hyperthyroid rats (THc, n=6), TH rats treated with RPO (THrpo, n=6), hypothyroid rats (HYc, n=6), HY rats treated with RPO (HYrpo, n=6). Data are means ± SD, $^{*}P<0.05$ *vs*EUc, $^{\#}P<0.05$ untreated *vs* treated with RPO.

4. Discussion

We have demonstrated that the hearts of rats suffering from hypertension, hypertriglyceridemia or hyperthyroidism are more susceptible to life threatening arrhythmias, such as ventricular fibrillation (for details see references 11-15). Likewise humans exhibiting of these predisposing factors of cardiovascular diseases are in higher risk to develop malignant arrhythmias. On the other hand, some non-antiarrhythmic drugs used in treatment of cardiovascular diseases (such as statins, sartans, etc.) has been reported to exhibit pleiotropic effects and can protect from arrhythmias. Furthermore, the benefit of dietary oils intake as well as melatonin supplementation in both experimental and clinical conditions has been shown. However, the mechanisms implicated in cardioprotective and antiarrhythmic effects are still not fully elucidated. Based on our previous studies and studies of others

pointing out crucial role of intercellular Cx43 channels in myocardial synchronization we hypothesized that these compounds may modulate expression and/or phosphorylation of myocardial Cx43. The latter is crucial for Cx43 channels function. Indeed, we have demonstrated that atorvastatin, omega-3 fatty acids, red palm oil and melatonin were able to up-regulate Cx43 (i.e. increase its total expression and/or its phosphorylated forms) and hence attenuate hypertension, hypertriglyceridemia or hyperthyroidism induced abnormal distribution and expression. This was associated with protection from VF. For example, as demonstrated on Fig. 1 the down-regulation of Cx43 in hyperthyroid rats was associated with decrease while up-regulation of Cx43 in hypothyroid rats with increase of threshold for VF. The threshold was also increased after treatment of hyperthyroid rats by RPO, which increased Cx43 expression. Heart disease related deterioration of cell-to-cell communication mediated by Cx43 channels may results in unmasking of ectopic foci, enhancement of dispersion of APD and slowing of conduction[16] that promote arrhythmias. On the contrary, improvement of cell-to-cell communication by examined compounds can offer protection due to suppression of these proarrhythmic factors. Moreover, it is likely that atorvastatin, melatonin as well as omega-3 fatty acids and red palm oil might affect other ion channels functions and together with modulation of Cx43 channels to attenuate electrical instability of diseased heart and to suppress arrhythmogenesis.

5. Conclusions

In conclusion, our findings [11-15] point out antiarrhythmic effect of atorvastatin, omega-3 fatty acids, melatonin and red palm oil due to, et least in part, up-regulation of myocardial Cx43. These findings support the assumption that we can prevent malignant arrhythmias by targeting cardiac Cx43. Further studies should elucidate molecular pathways involved in Cx43 modulation by examined compounds.

Acknowledgements

This study was supported by VEGA 2/0046/12, 1/0032/14 and APVV-0348-12 grants.

References

[1] Hill JA. Electrical remodeling in cardiac hypertrophy. Trends in Cardiovasc Medicine. 13: 316–322, 2003;

[2] Kostin S, Dammer S, Hein S. Connexin 43 expression and distribution in compensated and decompensated cardiac hypetrophy in patients with aortic stenosis. Cardiovascular Research 62: 426- 436, 2004.

[3] Tribulova N, Okruhlicova L, Imanaga I, Hirosawa N, Ogawa K, Weismann P. Factors involved in the susceptibility of spontaneously hypertensive rats to low K+-induced arrhythmias. Gen Physiol Biophys 2003; 22: 369-382.

[4] Lin H, Mitasikova M, Dlugosova K, Okruhlicova L, Imanaga I, Ogawa K et al. Thyroid hormones suppress epsilon-PKC signaling, down-regulate connexin-43 and increase lethal arrhythmia susceptibility in non-diabetic and diabetic rat hearts. J Physiol Pharmacol 2008; 59: 271-285.

[5] Severs NJ. Gap junction remodelling and cardiac arrhythmogenesis: cause or coincidence? J Cell Mol Med 2001; 5: 355-366.

[6] Peters NS, Coromilas J, Severs NJ, Wit AL. Disturbed connexin 43 gap junction distribution correlates with location of reentrant circuits in the epicardial border zone of healing canine infarcts that cause ventricular tachycardia. Circulation 1997; 95: 988-996.

[7] Tribulova N, Seki S, Radosinska J, Kaplan P, Babusikova E, Knezl V, Mochizuki S. Myocardial Ca2+ handling and cell-to-cell coupling, key factors in prevention of sudden cardiac death. Can J Physiol Pharmacol 2009; 87: 1120-1129.

[8] Tribulova N, Knezl V, Okruhlicova L, Slezak J. Myocardial gap junctions: targets for novel approaches in the prevention of life-threatening cardiac arrhythmias. Physiol Res 2008; 57:1-13.

[9] Mitasikova M, Smidova S, Macsaliova A, Knezl V, Dlugosova K, Okruhlicova L et al. Aged male and female spontaneously hypertensive rats benefit from n-3 polyunsaturated fatty acids supplementation. Physiol Res. 2008;57 Suppl 2:S39-48.

[10] Fischer R, Dechend R, Qadri F, Markovic M, Feldt S, Herse F et al. Dietary n-3 Polyunsaturated Fatty Acids and Direct Renin Inhibition Improve Electrical Remodeling in a Model of High Human Renin Hypertension. Hypertension 2008; 51: 540-546.

[11] Radosinska J, Bacova B, Knezl V, Benova T, Zurmanova J, Soukup T, Arnostova P, Slezak J, Gonçalvesova E, Tribulova N. Dietary omega-3 fatty acids attenuate myocardial arrhythmogenic factors and propensity of the heart to lethal arrhythmias in a rodent model of human essential hypertension. Journal of Hypertension 31:1876-85, 2013.

[12] Benova T, Viczenczova C, Radosinska J, Bacova B, Knezl V, Dosenko V, Weismann P, Zeman M, Navarova J, Tribulova N. Melatonin attenuates hypertension-related proarrhythmic myocardial maladaptation of connexin-43 and propensity of the heart to lethal arrhythmias. Canadian Journal of Physiology and Pharmacology 91:633-9, 2013.

[13] Bacova B, Radosinska J, Viczenczova C, Knezl V, Dosenko V, Beňova T, Navarova J, Gonçalvesova E, van Rooyen J, Weismann P, Slezak J, Tribulova N. Up-regulation of myocardial connexin-43 in spontaneously hypertensive rats fed red palm oil is most likely implicated in its anti-arrhythmic effects. Canadian Journal of Physiology and Pharmacology 90:1235-45, 2012.

[14] Bacova B, Radosinska J, Knezl V, Kolenova L, Weismann P, Navarova J, Barancik M, Mitasikova M, Tribulova N. Omega-3 fatty acids and atorvastatin suppress ventricular fibrillation inducibility in hypertriglyceridemic rat hearts: implication of intracellular coupling protein, connexin-43. Journal of Physiology and Pharmacology 61:717-23, 2010.

[15] Bacova B, Viczenczova C, Zurmanova J, Kasparova D, Knezl V, Radosinska J, Benova T, Pavelka S, Soukup T, Tribulova N. Susceptibility of rats with altered thyroid status to malignant arrhythmias is related mainly to myocardial levels of connexin-43 and it can be partially ameliorated by red palm oil supplementation. Experimental and Clinical Cardiology, 18: 41A-46A, 2013.

[16] Liu F, Gustein DE. The cardiac gap junction: A potential therapeutic target in the treatment of heaert disease. Mount Sinai Journal of Medicine 69:421-4, 2002.

Modeling in Electrocardiology

The Impact of Action Potential and Conduction Velocity Distribution Changes on Markers of Repolarization Dispersion

[1]G. Kozmann, [1]G. Tuboly, [2]V. Szathmáry, [3]J. Švehlíková, [3]M. Tyšler

[1]Department of Electrical Engineering and Information Systems, Faculty of Information Technology, University of Pannonia, Veszprém, Hungary,
[2]Institute of Normal and Pathological Physiology, Slovak Academy of Sciences, Bratislava, Slovakia,
[3]Institute of Measurement Science, Slovak Academy of Sciences, Bratislava, Slovakia
Email: kozmann.gyorgy@virt.uni-pannon.hu

Abstract. *A necessary prerequisite of malignant arrhythmias is the elevated repolarisation dispersion (RD) of the ventricular myocardium. In this study, by the use of numerical heart and thorax models the RD properties were analyzed as a function of realistic action potential duration (APD) and activation propagation velocity (CV) changes taken from recent experimental studies of normal and heart failure cases. The contribution of APD and CV variability to the arrhythmogenic substrate of malignant arrhythmias was studied separately and in combination. RD was quantitatively characterized by the analysis of computer simulated QRST integral maps and non-dipolarity indices. Modelling study revealed that transmural APD variability is primarily responsible for the arrhythmogenic substrate. Depending on the transmural gradient, CV may moderate or enhance the resultant repolarization heterogeneity level.*

Keywords: Malignant Arrhythmias, Repolarization Dispersion, Numerical Heart and Thorax Models, QRST integral maps, Transmural Gradient

1. Introduction

Ventricular tachycardia and fibrillation are the most common causes of sudden cardiac death (SCD). In spite of the continuous development of risk assessment methods, still no reliable ECG based marker of arrhythmia prone status does exist according to the scientific statement of the AHA/ACCF/HRS based on hundreds of clinical trials [1]. According to theoretical expectations, parameters casually reflecting the spatial heterogeneity of the elementary myocardial volumes might be the clue of a more efficient risk assessment [2].

In this study we attempted to link the observed normal and pathological QRST integral – and non-dipolarity index (NDI) – behaviour, to mesoscopic (intramural) and even to microscopic experimental findings. To this end, numerical chest and multi-element heart models were used. In the heart model, action potential duration (APD) and activation propagation velocity (CV) values of the different myocardial layers were approximated based on the recent optical mapping results of stained subepicardial, midmyocardial and subendocardial sections taken from healthy and failing human hearts (Glukhov et al. [3]).

2. Subject and Methods

Numerical Modelling of the Heart and Thorax

A five-layer numerical heart model was used with globally or locally adjustable intramural APD and CV modulation features. In the simulations transmural gradient (TG) of epicardial and endocardial layers was defined as $APD_{epi} - APD_{endo}$. However, while keeping TG

constant, local intramural APD deviations were allowed. Similarly, different intramural CV values were allowed, expressed in modelling distance unit/modelling time unit (mdu/mtu). Finally, a piecewise realistic shape, piecewise homogeneous thoracic model was used to compute body surface potential distributions, QRST integral maps and NDIs.

Details of the simplified computer model of the human cardiac ventricles were described previously by Szathmáry and Osvald [4].

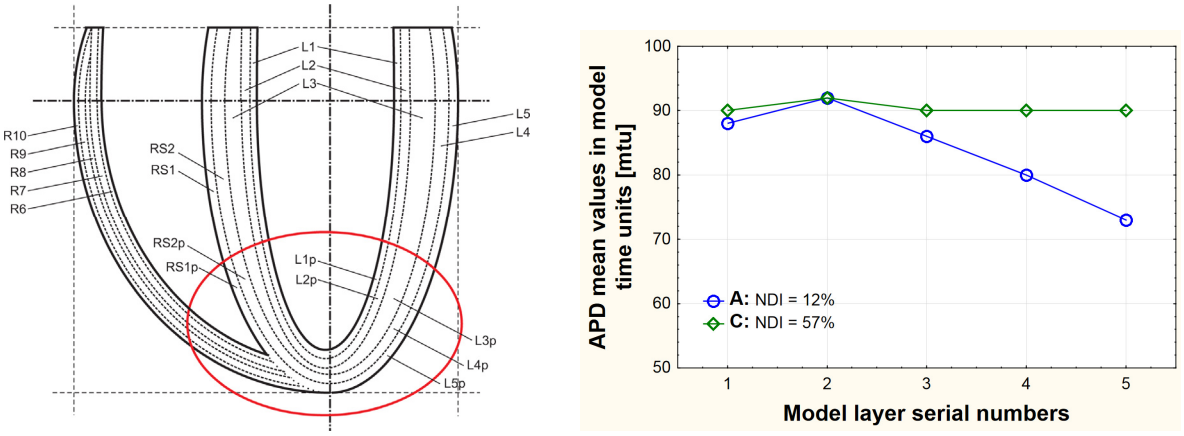

(a) (b)

Fig. 1. (a) A schematic representation of the "layered" structure and geometry of the left and right ventricles. In our study the ellipse at the apex contains the model region with pathologically modulated APD and CV. (b) Mean value of the APD profile of a healthy subject (profile 'A') and the failing heart profile of the apical region. The simplified graph is based on the experimental data of Glukhov et al. [3].

To compute the cardiac potentials as well as the QRST integral maps on the thoracic surface, the multiple-dipole cardiac generator has been inserted into the realistically shaped piecewise homogeneous torso model (Fig. 2).

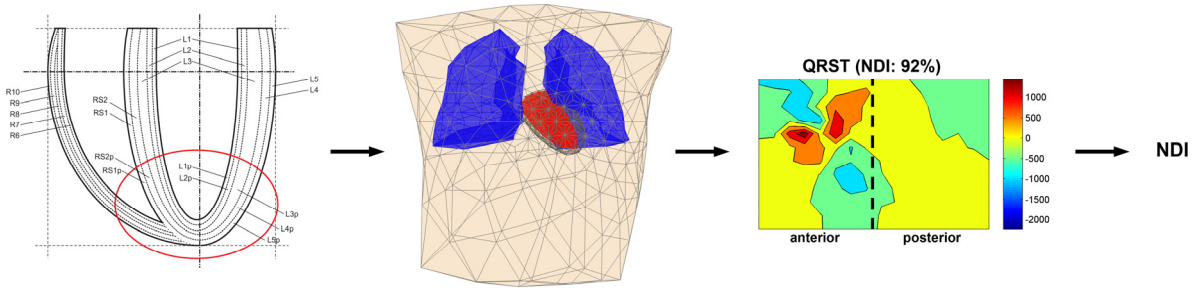

Fig. 2. Layout of the major modelling steps.

Evaluation of Repolarization Dispersion by QRST Integrals and Non-dipolarity Indices

In a concise way QRST integral maps are characterized by the beat-to-beat sequence of NDI(QRSTint), based on the c_i components of the KL expansion:

$$\mathrm{NDI(QRSTint)} = \frac{\sum_{i=4}^{12} c_i^2}{\sum_{i=1}^{12} c_i^2} = \frac{P_{\mathrm{ND}}}{P_{\mathrm{D}} + P_{\mathrm{ND}}} \cdot 100\% \qquad (1)$$

where NDI(QRSTint) non-dipolarity index of the QRST integral
c_i i. component of the KL expansion
P_{D} QRST integral map power represented by the "dipolar" KL components (i: 1-3)
P_{ND} QRST integral map power represented by the "non-dipolar" KL components (i: 4-12) according to Lux et al. [5].

3. Results

In our reference case TG was -15 mtu (modelling time unit), yielding an NDI of 16%. By the systematic change of TG in the apical part of the heart model from -15 mtu up to +14 mtu, the NDI did change from 16% up to 76%. In the reference case CV was 3 mdu/mtu in the Purkynje layer and 1 mdu/mtu in all the others. In the pathological case CV pattern was 2 mdu/mtu in the Purkynje layer, and 0.5 mdu/mtu in all the others. The NDI range due to the combined APD and CV modulations did not change, however the TG of the maximal NDI shifted slightly in the direction of positive TGs. An increase of NDIs occurred at TGs significantly positive. However the increase of APD profile slope finally caused a quick decrease of NDI. According to our modelling results uneven CV profiles between the limits shown in Fig. 3(a) resulted in NDI characteristics running between the two graphs shown in Fig. 3(b).

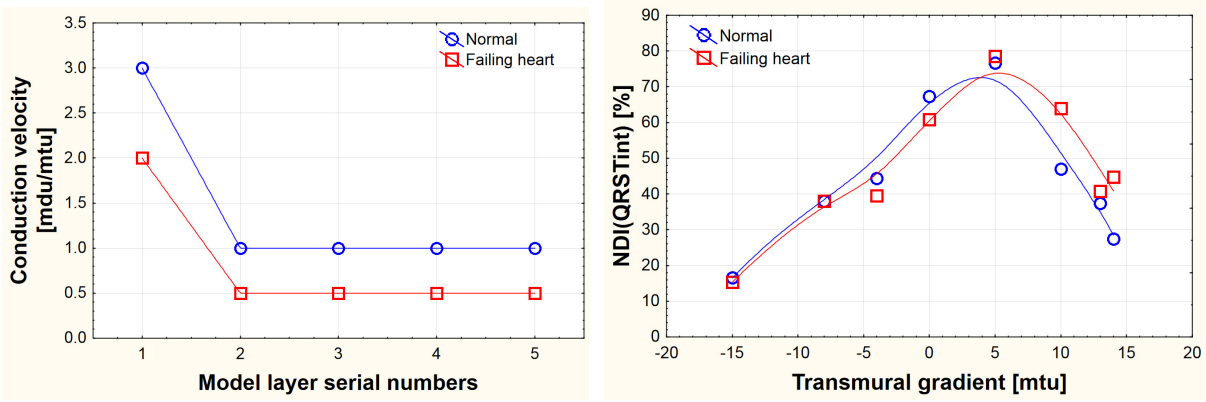

(a) (b)

Fig. 3. (a) Transmural CV and the NDI(QRSTint) vs. TG patterns. Circle markers represent the profiles in the healthy myocardium, while square markers indicate the profiles in failing heart (apical) regions. (b) NDI(QRSTint) vs. transmural gradient. Circle markers represent the relationship if CV is normal, square markers show the consequences of apical CV modulation depicted in Fig. 3(a).

A few examples of the impact of TG modulation (without CV modulation) are illustrated by the QRST integral maps shown in Fig. 4.

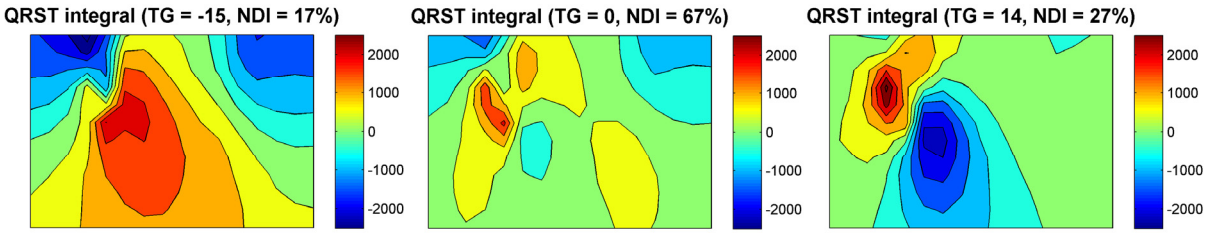

Fig. 4. Simulated QRST integral maps vs. TG. The subsequent modulation of TG results the most fragmented QRST integral pattern at the transition of TG from negative into positive value. The smallest range of amplitudes are at TG = 0.

4. Discussion

According to this model study, NDI is primarily affected by the TG value. The impact of intramural local maxima/minima on RD is negligible. The impact of decreasing CV is modest until TG is negative (i.e. close to the normal APD distribution), however at TG > 0 NDI increase is more emphasized. We should remark, that positive TG slopes > 5 mdu/mtu surpass the gradients were not found in the paper of Glukhov, possibly because physically they are not possible in failing heart myocardial tissue.

The study of QRST integral maps vs. increasing TG revealed, that after reaching the NDI maximum the map pattern turned to be more and more dipolar but with reversed polarity.

Acknowledgements

We acknowledge the financial support of the Hungarian State and the European Union under the programme TÁMOP-4.2.2.A-11/1/KONV-2012-0073 (Project title: “Telemedicine-focused research activities in the field of Mathematics, Informatics and Medical sciences”), grant APVV-0513-10 of the Slovak Research and Development Agency and grant 2/0131/13 from the VEGA Grant Agency, Slovakia.

References

[1] Goldberger JJ et al: A scientific statement from the American Heart Association Council on Cardiology Committee on Electrocardiography and Arrhythmias and Council on Epidemiology and Prevention. *Circulation*, 118: 1497-1518, 2008.

[2] Geselowitz DB. The ventricular gradient revisited: relation to the area under the action potential. *Biomedical Engineering, IEEE Transactions on*, (1): 76-77, 1983.

[3] Glukhov AV, Fedorov VV, Lou Q, Ravikumar VK, Kalish PW, Schuessler RB, Moazami N, Efimov IR. Transmural dispersion of repolarization in failing and nonfailing human ventricle. *Circulation research*, 106 (5): 981-991, 2010.

[4] Szathmáry V, Osvald R. An interactive computer model of propagated activation with analytically defined geometry of ventricles. *Computers and biomedical research*, 27 (1): 27-38, 1994.

[5] Lux RL, Evans AK, Burgess MJ, Wyatt RF, Abildskov JA. Redundancy reduction for improved display and analysis of body surface potential maps. I. Spatial compression. *Circulation Research*, 49 (1): 186-196, 1981.

Noninvasive Localization of Ectopic Activation Using BSPM and CT-Based Torso Model

[1,2]M. Tysler, [1]J. Svehlikova, [2,3]O. Punshchykova, [2]P. Kneppo, [3]V. Maksymenko

[1]Institute of Measurement Science SAS, Bratislava, Slovakia
[2]Faculty of Biomedical Engineering, CTU in Prague, Kladno, Czech Republic
[3]National Technical University of Ukraine "Kyiv Polytechnic Institute", Faculty of Biomedical Engineering, Kyiv, Ukraine
Email: tysler@savba.sk

Abstract. *In this study accuracy of the inverse localization of ectopic ventricular activity in dependence on the used heart and torso model was examined. Best agreement between the positions obtained from the inverse solution and from the electrophysiological study was achieved when the CT-based torso and heart model was used. The use of a personally adjusted general torso model with the heart model obtained from CT gave less accurate but still acceptable location of the ectopic activity. If simplified geometric heart model was used, the results depended on the fidelity of its shape and position estimation and varied from acceptable locations to locations scattered within wide range of the ventricular volume.*

Keywords: body surface potential mapping; inverse problem of electrocardiology; torso model; ectopic activation.

1. Introduction

It has been shown elsewhere [1, 2] that cardiac imaging based on multichannel surface ECG and proper torso and heart model may be useful for non-invasive assessment of electrophysiological state of the heart by solving the inverse problem of electrocardiology. The accuracy of the solution may depend on the selected model of the cardiac sources, method used for assessment of its parameters, and fidelity of the ECG data and torso model. In this study the accuracy of inverse localization of ventricular ectopic activity in dependence on the used heart and torso model was examined.

2. Subject and Methods

Two male patients (P1: 57 years old man, P2: 17 years old man) with premature ectopic activity in the ventricles causing ventricular tachycardia underwent 10 minutes of body surface potential mapping (BSPM) using the ProCardio 8 system with 62 electrodes placed according the Amsterdam lead system. Computed tomography (CT) scanning with slice thickness of 0.3 mm and a pixel size of 0.885 mm was performed on patients with attached ECG electrodes using the Toshiba Aquilion ONE™ system. Finally, intracardiac electrophysiological study (EPS) was performed using the Bard LabSystem™ PRO EP Recording System. To reveal the position of the premature ectopic activity, St. Jude EnSite NavX™ cardiac mapping and navigation system was used in the first patient and standard protocol under X-ray was used for the second patient.

For non-invasive estimation of the site of the premature ectopic activity an inverse solution based on dipole model of the cardiac electric generator and measured BSPM data was used.

Integral map over the initial time interval of the ectopic activity was used as the input for its inverse localization. The integral map values in body surface points are defined as

$$im = \int_I bm(t) = \mathbf{A} \int_I g(t) = \mathbf{A}s \qquad (1)$$

where **A** is a time independent transfer matrix that represents the properties of the inhomogeneous torso as a volume conductor (i.e. relations between potentials in individual surface points and multiple elementary dipoles within the myocardium), *g(t)* is the multiple dipole generator in particular time instant t of the heart activation and s represents an integral generator characterizing the searched pathological electrical activity within the examined time interval of the ectopic activity.

The equivalent integral generator EIG representing the original integral multiple dipole generator *s* in equation (1) can be then computed as:

$$EIG = \mathbf{A}^{+} im \qquad (2)$$

where **A+** is the pseudo-inverse of the transfer matrix **A**.

The inverse solution is an ill-posed problem that in case of local pathology (where the EIG represents only small volume of the myocardium) can be solved by approximating it by a single dipole. In the method used in this study [3, 4] the EIG is defined only by three parameters – components of the dipole moment. To avoid solving a nonlinear problem, the other three dipole parameters – its coordinates are determined so that the dipole moments are computed for many predefined possible positions within the ventricular volume that are several millimeters apart (their spacing determines the resolution of the method). The position of the pathology is then determined as the location in which the EIG best represents the input data *im* and is defined by the criterion that the root mean squared difference between the map generated by the EIG and the input integral map im is minimal. Several torso models of different fidelity were tested for the inverse solution (Fig. 1):

A - model with a common shape of torso with lungs adjusted to patient chest dimensions [5] and simplified geometrical heart model adjusted to the real heart size and position (the long heart axis was properly scaled and positioned, the short axis was properly rotated);
B - the same torso and lungs model as in A, with heart model shape and position taken from the CT scan;
C - realistic model of the torso, lungs and heart taken from the CT scan.

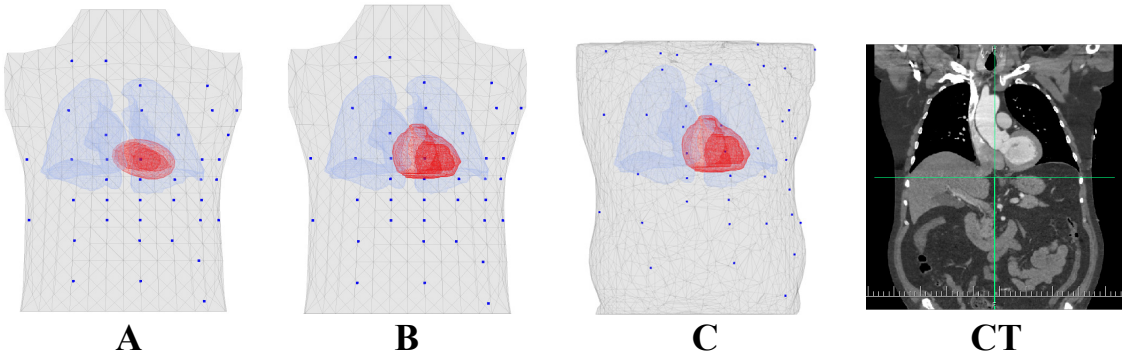

Figure 1: Torso models and CT scan of patient P1. Three models of torso, lungs and heart described in the text were used in the inverse computations. Dots mark positions of anterior electrodes.

3. Results

In patient P1, the intracardiac EPS identified the initial ectopic activation in the left ventricle in the posterior septum near heart base (Fig. 2, left), in patient P2 the focus was found in the anterior free wall of the left ventricle, near the aortic sinus (Fig. 2, right).

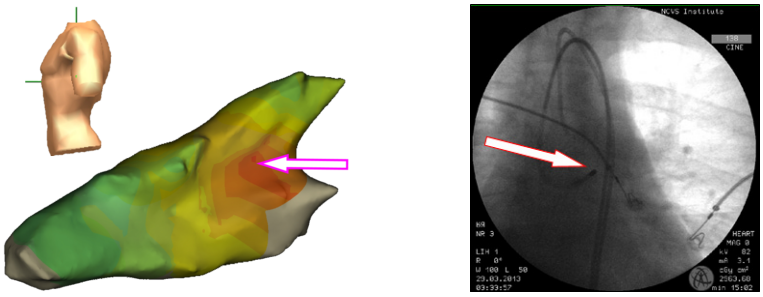

Fig. 2. Initial ectopic activation sites obtained from the EPS: from the navigation system during intracardiac mapping in patient P1 (left) and from the X-ray image as the position of the ablation electrode tip in patient P2 (right).

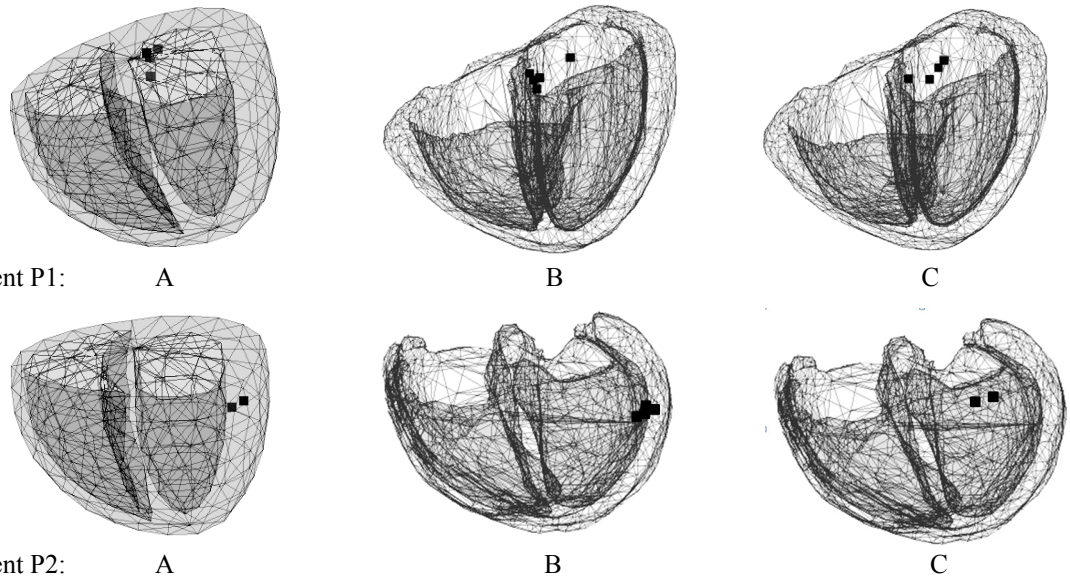

Fig. 3. Inversely found sites of initial ectopic activation (marked by little squares) in patients P1 and P2 when three different torso-heart models A, B, C described in the text were used. Five ectopic beats were used in both patients; in some cases the same site was obtained from different ectopic beats.

When torso models B or C were used, the sites of initial ectopic activity in patient P1 were located in the posterior septum near the heart base with dipole direction suggesting activation from the right to the left ventricle. The location slightly varied depending on the evaluated ectopic heart beat and was within few millimeters from that found by the EPS. When torso model C was used, the solution was more accurate and stable within the evaluated ectopic beats.

In patient P2 the ectopic beat focus was located near the aortic sinus. With torso models B and C the inversely estimated sites were positioned similarly in the anterior free wall of the left ventricle near the heart base. The dipole orientation suggested epi-to-endocardial and base-to-apex initial activation that was more pronounced when model C was used.

If the simplified torso and heart model A was used and the heart model was adjusted to approximately correspond to the real heart, in both patients the noninvasively located sites of the ectopic activity were also in concordance with the EPS as shown in Fig. 3 left.

4. Discussion

The study enabled only partial verification of the noninvasively obtained ectopic foci. In patient P1, merging of ventricle shapes obtained from CT and from the navigation system was not perfect because some differences reached more than 10 mm. Moreover, due to arteria femoralis sinistra occlusion, the EPS was terminated without ablation that could confirm the

localized focus. In patient P2 the location of the focus from the EPS study was only approximate; it was obtained from X-ray image as the location near the tip of the ablating electrode but the heart shape was not clear enough. Nevertheless, in both patients there was good correspondence between the foci estimated inversely and from the EPS if torso and heart models B or C were used.

If the simplified geometrical heart model in model A was used without any adjustment (if no information on the heart shape and position was available), the results in both patients varied in dependence on how close the heart model was to reality and the inversely estimated sites were scattered in wide range of the ventricular area, sometimes several centimeters far from the site obtained from the EPS.

The results of the inverse localization slightly depended also on the evaluated time interval. Several intervals within first 30 ms of the ectopic activity, from 10 to 30 ms long were attempted. Despite the longer and later intervals in most cases yielded more stable results, the obtained locations were sometimes shifted from the expected positions, probably due to the larger activated area that corresponded to those evaluated intervals.

5. Conclusions

Fidelity of the torso and heart model can strongly influence the inverse localization of the ectopic activity. Best results in both patients were achieved with a torso model based on the whole torso CT scan. An approximate torso shape model adjusted to patient chest dimensions with properly positioned heart model based on a CT-scan of the heart area gave less accurate but still acceptable location of the ectopic activity. However, when the real heart geometry relations were maintained in the simplified heart and torso model, the results were still able to give preliminary information about the position of the initial ectopic activity.

Acknowledgements

This study was supported by research grants 2/0131/13 from the VEGA Grant Agency and APVV-0513-10 from the Slovak Research and Development Agency in Slovakia, by project Biomedicine University Research Park Bratislava (ITMS code 26240220087) and grant 3/229/OHK4/3T/17 from the SGS CVUT in Czech Republic. The authors thank the medical team from the Institute of Cardiovascular Surgery of the Academy of Medical Sciences of Ukraine in Kyiv for cooperation in clinical measurements and kind permission to use the data.

References

[1] Rudy Y. Noninvasive Electrocardiographic Imaging of Arrhythmogenic Substrates in Humans, *Circulation Research*, 2013, 112(5), 863-874.

[2] Haissaguerre M, Hocini M, Shah AJ, et al. Noninvasive Panoramic Mapping of Human Atrial Fibrillation Mechanisms: A Feasibility Report. *Journal of Cardiovascular Electrophysiology*, 2013, 24(6), 711-717.

[3] Tysler M, Kneppo P, Turzova M, et al. Noninvasive assessment of local myocardium repolarization changes using high resolution surface ECG mapping. *Physiological Research*, 2007, 56(S1), S133-S141.

[4] Tysler M, Svehlikova J. Noninvasive finding of local repolarization changes in the heart using dipole models and simplified torso geometry. *Journal of Electrocardiology*, 2013, 46(4), 284-288.

[5] Lenkova J, Svehlikova J, Tysler M. Individualized model of torso surface for the inverse problem of electrocardiology. *Journal of Electrocardiology*, 2012, 45(3), 231-236.

Heart Rate Variability

Dynamic Beat-to-Beat Changes of the Cardiac Electric Field in Response to Situations with Increased Sympathetic Activity

[1]E. Kellerová, [1]V. Szathmáry, [2]G. Kozmann

[1]Institute of Normal and Pathological Physiology, Slovak Academy of Sciences, Bratislava, Slovak Republic
[2]Department of Electrical Engineering and Information Systems, Faculty of Information Technology, University of Pannonia, Veszprém, Hungary
Email: ekellerova@chello.sk

Abstract. *Only a few studies – evaluating body surface potential maps (BSPMs) from a selected single beat, or from an average constructed of some heart beats - have dealt with reactive changes of BSPMs in response to different physiological conditions. Our aim was to analyse the previously unexplored dynamic beat-to-beat pattern of the reactive changes in the ventricular depolarization and repolarization, induced by different physiological mechanisms – by tilt table test or by psycho-emotional stress. Continual records of body surface ECG and repetitive BP measurements were taken in supine rest, during tilting to 60°(TU,TI), back to supine and sitting (SIT), or seated during the mental arithmetic test (MA). R-R intervals and selected BSPMs parameters were evaluated for each heartbeat. With changing position from supine to TI, there was a significant gradual decrease of the QRSTampl, in the average to 73% and with SIT to 81% of the resting supine value. The MA stress induced changes began with a short latency, peaked significantly at 30-60 seconds, returning to the control values at the end of the test, or some heart beats after. The main parameter of repolarization BSPM –STampl fell to 81% of its control value. These reactions correspond to the pattern of the complex sympathergic cardiovascular responses to postural or mental tasks.*

Keywords: Integral ECG body surface maps, Beat-to-beat dynamism, Reactive changes, Head-up tilting Psycho-emotional stress.

1. Introduction

The body surface potential maps (BSPMs) are still an important source of information in the electrocardiographic research of autonomic nervous system control of cardiac function. Several papers offer basic data on the pattern of ventricular depolarization and repolarization time-integral BSPMs in clinically normal subjects at rest [1-7]. However, in subjects with no cardiovascular symptomatology, only a few studies have dealt so far with the problem of variability in the pattern of BSPMs, or with reactive changes due to different physiological conditions, involving variations in the autonomic drive of ventricles [2, 5-8]. However, there is a cogent limitation in interpreting these studies, as only a single BSPM from one selected heartbeat (technical bounds of the equipments), or averages from a short sequence of several maps were used to evaluate the significance of their changes in time or in different situations. Reliable testing of cardiovascular reactivity to somatic or psycho-emotional tasks, involves the monitoring of investigated parameters during the anticipation of, administration of, and recovery from stimuli or tasks. Computer based BSPMs recording enabled a beat-to-beat analysis of the dynamic behaviour of the cardiac electric field [9]. In our previous study we provided the first evidence of spontaneous, non-random, respiratory and low frequency oscillations of the ventricular repolarization pattern, and the first insight into the dynamics of body posture associated changes in ventricular recovery [10]. The aim of the present study was a comparative beat-to-beat description of the reactive changes of various parameters of

the BSPMs in sympathergic states, but induced by different mechanisms - changing body posture, or using mental arithmetic (MA) as a consistent test which involves increased alertness with intellectual and emotional strain.

2. Subject and Methods

In two homogeneous groups of 9 men aged 19 and 29 y., with no history of cardiovascular diseases, using 64 torso electrodes, unipolar ECGs were continuously recorded in following postural situations: i) 300 sec - supine in quiet baseline conditions ii) passive head up tilting partitioned into 30 sec – starting supine position (SU), 90 sec – gradual tilting to plus 60° (TU) and 180 - 240 sec – in the passive tilted position (TI), iii) 90 sec - gradual head down tilting to horizontal (TD) and 180 - 240 sec – supine rest (SU 2) iv) 180 sec – sitting rest (SE), recorded immediately after active sitting up from the supine position (SU). Mental stress testing involved 30 s. in seated position at rest, 120 s. during mental arithmetic test (MA) and 120 s. during the recovery after the test. From the respective integral QRS, ST and QRST BSPMs, R-R intervals and selected parameters were evaluated for each heartbeat. In individual subjects, depending on their HR, 906 – 1262 postural and/or 335-426 MA BSPMs were evaluated. The blood pressure (BP) was measured repetitively by a semi-automatic oscillometric method, in each experimental situation. For details on data recording and processing see [4, 7, 10]. The minimal level of significance was set to $P < 0.05$.

3. Results

Representative beat-to-beat recordings of RR and of selected integral BSPMs parameters characterizing the ventricular depolarization (QRSampl), changes of myocardial recovery processes (QRSTampl or STampl), respective nondipolarity indices (NDI) and the angle between the QRS and QRST or ST eigenvectors (**α**), illustrate the effect of tilted semivertical and of seated body position (Fig. 1A) or of the emotional stress (Fig. 2A), in one subject.

In spite of the substantial inter-individual variability, the highly significant body position dependent differences of the selected group-mean parameters QRSTampl and QRSampl document the dynamic pattern and proportions of the reactive postural depolarization and repolarization BSPMs changes. With head-up tilt, there was a significant gradual decrease in the QRSTampl, in the average to 73% and with sitting to 81% of the resting supine value ($p<0.001$) (Fig. 1B). Simultaneously the angle **α** significantly increased in the average by 12.3° in tilted and by 13.0° in the seated position, and the nondipolarity QRST BSPM indexes fell, to 87%, resp. to 78% of their respective supine values. All these reactive changes were significant, characterized by transition phenomena and prolonged after-effects. Tilting back to horizontal restored the resting supine values within 3 – 4 minutes, in all subjects.

The stress induced changes (Fig. 2B), began in all subjects with a short latency after initiation of the mental task, usually peaked significantly at 30-60 seconds, returning to the control values to the end of the test, or some heart beats after. The HR rose from 75 to 98 beats/min, the BP from 118/69 to 137/76 mmHg, the main parameter of the integral repolarization BSPM – the QRSTampl fell to 81% from 154 to 126 μVs,

The pattern of both responses was inter-individually conformable, however variable in magnitude and pronounced in about 2/3 of subjects. The effects of both situations on depolarization were individually more variable and in the average caused only minimal QRSampl increases.

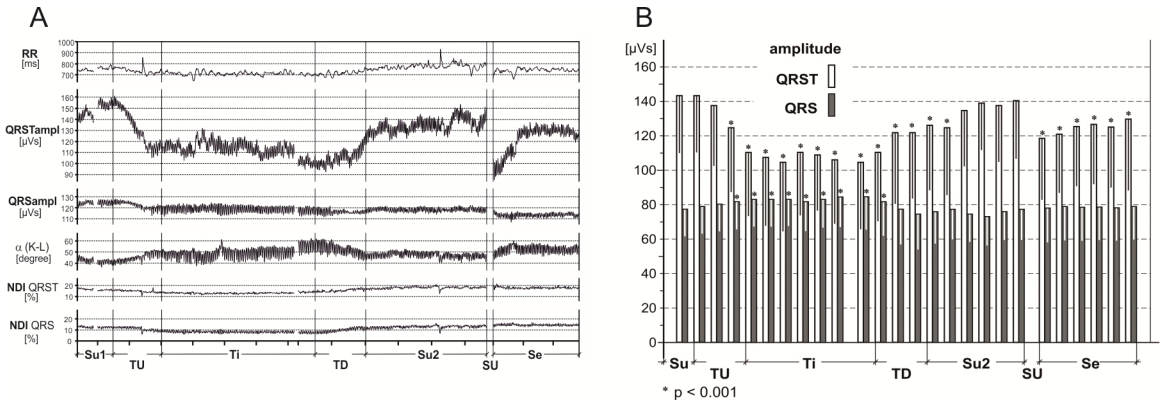

Fig. 1 **A)** Representative continual body posture dependent beat-to-beat recording of **RR** and of selected QRST and QRS BSPMs parameters from one subject. **Su1** - baseline, supine; **TU** - gradual tilting up to +60°; **Ti** - tilted; **TD** - gradual tilting down to horizontal; **Su2** - supine; **SU** - active sitting up; **Se** - seated..
B) Mean group values ±SD of **QRSTampl** and **QRSampl,** averaged in 30 s intervals during consecutive body position changes.
Time scale unit – 1 min

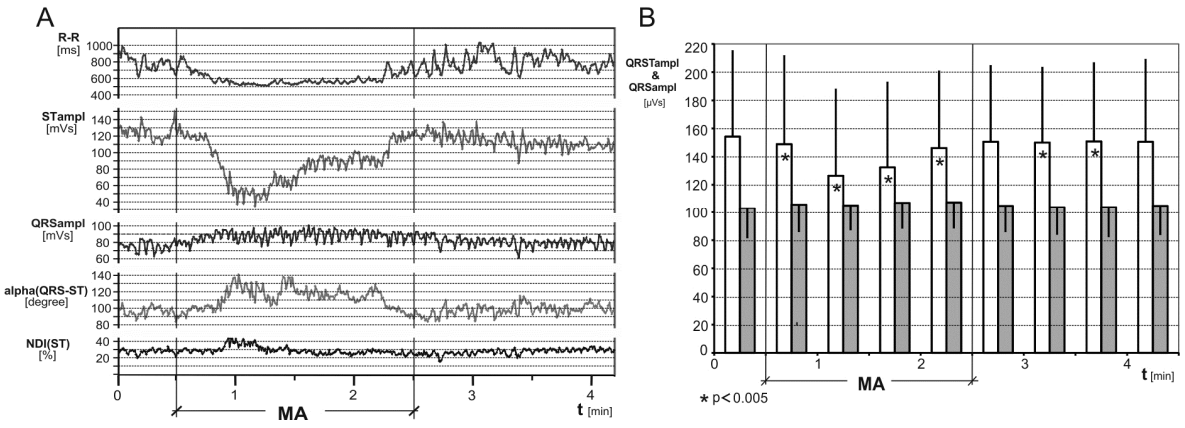

Fig. 2 **A)** Representative continual beat-to-beat recording of **RR** and of selected ST and QRS BSPMs parameters from one subject, before, during and after the mental arithmetic test (MA) .
B) Mean group values ± SD of **ST ampl** and **QRS ampl,** averaged in 30 s intervals during the test
Time scale unit - 1 minute
* significantly different in relation to respective baseline supine values.

4. Discussion

The presented qualitative and quantitative characteristics of depolarization and repolarization time-integral BSPMs at rest are concordant with previous reports for clinically normal males [1-7]. Circulatory adaptations, involving autonomic control, constitute an essential part of the "spontaneous" intra-individual variability of these electrophysiological functions. Results of this study call attention to the body position and emotional stress dependent beat-to-beat variations of the investigated cardiac electric field. These stimuli of different physiological meaning, deviate substantially, in particular the repolarization BSPM parameters from their respective means, in a dynamic way, with evident transition periods in reaching new levels, or with several minutes lasting after-effects.

They are in agreement with previous studies reviewed by Ruttkay-Nedecky [11], documenting on selected small samples or single heart beats, the responsiveness of ventricular repolarization to a variety of sympathergic situations – as upright posture, hand grip test, psycho-emotional load, smoking, adrenergic agonists or specific changes in subjects

with high normal blood pressure at rest [12]. It is concluded, that these findings are explained by stimulus specific pattern of the sympathetic response, which involves selective activation of the ventricular myocardium in reaction to different physiological situations.

Detailed analysis of the beat to beat BSPMs variability allows a more accurate definition of the autonomic modulation of the ventricular activation with a promising possibility to discover subjects with abundant sympathetic activity and higher risk of ventricular dysfunction.

We point to the importance of including these aspects of dynamic intraindividual variability of the cardiac electric field influenced by the manifest or latent stimuli, into the ECG assessment both for interpreting current cardiac state, for ambulatory monitoring, laboratory testing etc.

Acknowledgement

The authors acknowledge the financial support of the Slovak Research and Development Agency, project APVV–0513-10 and of the Hungarian State and the European Union, project TÁMOP - 4.2.2.A-11/1KONV-2012-0073.

References

[1] Montague TJ, Smith ER, Cameron DA, Rautaharju PM, Klassen GA, Flemington CS, Horacek BM: Isointegral analysis of body surface maps: Surface distribution and temporal variability in normal subjects. *Circulation* (63**)**: 1166-1172, 1981.

[2] Sutherland DJ, McPherson DD, Spencer CA, Armstrong CS, Horacek BM, Montague TJ: Effects of posture and respiration on body surface electrocardiogram. *Am J Cardiol* (52): 595- 600, 1983.

[3] Green LS, Lux RL, Haws CW, Williams RL, Hunt SC, Burgess MJ: Effects of age, sex and body habitus on QRS and ST-T potential maps of 1100 normal subjects. *Circulation* (71): 244-253, 1985

[4] Kozmann G, Farkas N, Sandor G, Szakolczai K, Szathmary V, Tysler M, Turzova M: QRST integral maps of normal subjects. Statistical analysis and simulation study. *Comput Cardiol* (25): 521-524, 1998.

[5] Slavíček J, Kittnar O, Trefný Z, Horáček Bm: ECG body surface isointegral and isoarea maps (BSM) in 30- and 60-year-old healthy humans. *Sbor lék* (102): 369-374, 2001.

[6] Ruttkay-Nedecký I, Regecová: Normal variability of the peak-to through amplitude of isointegral QRST body surface maps. *J Electrocardiol* (35): 327-332, 2002.

[7] Kellerová E, Regecová V, Katina S, Titomir Li, Aidu Eai, Trunov Vg, Szathmáry V: The effect of psychoemotional load on ventricular repolarization reflected in integral body surface potential maps. *Physiol Res* (55) (Suppl1): 99-105, 2006.

[8] Schusterman V, Aysin B, Shah I, Flanigan S, Anderson KP: Autonomic nervous system effects on ventricular repolarization and RR interval variability during head-up tilt. *Comput Cardiol* (25): 717-720, 1998.

[9] Kozmann Gy, Haraszti K: Importance of body surface potential field representation fidelity: analysis of beat-to-beat repolarization measurements. *Anadolu Kardiyol Der* [7](Supl.1):5-7 2007

[10] Kellerová E, Szathmáry V, Kozmann G, Haraszti K, Tarjányi Z: Spontaneous variability and reactive postural beat-to-beat changes of integral ECG body surface potential maps. *Physiol Res,* (59): 887-896, 2010.

[11] Ruttkay-Nedecký I: The effect of the autonomic nervous system on the heart. Electrocardiographic evaluation: Problems and concerns. Cardiol. (10): 42-48, 2001.

[12] Kellerová E, Regecová V Repolarization pattern indicates enhanced sympathetic drive of the ventricular myocardium already at normal and high-normal blood pressure. *Kidney & Blood Pressure Research*, (32): 310-331 , 2009.

Body Surface Potential Mapping

Body Surface Potential Mapping in Rats with Experimental Pulmonary Hypertension

O. Suslonova, I. Roshchevskaya

Laboratory of Comparative Cardiology, Komi Science Centre, UD, RAS, Syktyvkar, Russia
Email: compcard@mail.ru

Abstract. *Body surface potential mapping (BSPM) was performed in female rats with pulmonary arterial hypertension (PAH) induced by a single subcutaneous injection monocrotaline (60 mg/kg body wt). Analysis of data was produced by equipotential momentous maps during ventricle depolarization. In rats with monocrotaline-induced PAH was confirmed hypertrophy of the right ventricle. It is reflected on equipotential momentous maps by a significant change of amplitudes of positive and negative extrema and increase of the duration of the first and second inversions during ventricular depolarization.*

Keywards: body surface potential mapping, pulmonary hypertension, monocrotaline

1. Introduction

Pulmonary arterial hypertension (PAH) is a clinical condition characterized by a progressive increase in pulmonary artery pressure, elevation of the pulmonary vascular resistance and overloading of the right side of the heart [1]. The increase in pulmonary resistance is caused by remodelling of pulmonary vessels, a vasoconstriction, an inflammation and thrombosis [2]. Animal models of pulmonary hypertension have contributed to our understanding of the underlying mechanisms of development this pathology [3]. The most widely used is monocrotaline-induced rat models of pulmonary arterial hypertension [4]. Monocrotaline (MCT) is a pyrrolizidine alkaloid derived from *Crotalaria spectabilis*, causes a pulmonary vascular syndrome in rats characterized by proliferative pulmonary vasculitis, PAH, and cor pulmonale [5]. In rats with MCT-induced PAH changes in heart structure were observed: considerable dilatation of the right ventricle, subendocardial fibrosis and increase in diameter of right ventricle cardiomyocytes [6]. Signs of essential hypertrophy of the right ventricle in rats with MCT-induced PAH develop on the 30^{th} -35^{th} day [7].

Diagnosis of PAH is often delayed. The routine electrocardiogram (ECG) is an inadequate screening tool of pulmonary hypertension. ECG in PAH has sensitivity (55 %) and 70 % specificity [8]. Bogy surface potential mapping (BSPM) offers considerable promise as a method that allows more comprehensive analysis of electrocardiographic information than is possible with standard ECG method [9 - 11]. A study of the development of pulmonary arterial hypertension by simulation on experimental animals will diagnose this disease at early stages.

The aim of this work was to analyze the change of amplitude-temporal characteristics of body surface potential maps in rats with experimental pulmonary hypertension during ventricular depolarization.

2. Subject and Methods

The investigation conformed to the National Institutes of Health *Guide for the Care and Use of Laboratory Animals* (National Institutes of Health, volume 25, no 28, revised 1996).

The experiments were carried out in female Wistar rats (n = 17) weighing 200–250 g. Pulmonary hypertension was caused by a single subcutaneous injection of MCT (60 mg/kg body wt). MCT was dissolved in 1 N HCl, and the pH was adjusted to 7.4 with 1 N NaOH. Before and four weeks after an injection of the drug cardioelectrical potentials were recorded by a method of cardioelectrotopography from 64 subcutaneous needle electrodes uniformly distributed around the animal chest. During registration, the animals were anesthetized with zoletil (3.5 mg / 100 g body weight) intramuscularly. ECG signals from 64 torso and three limb electrode sites are sampled simultaneously and the data are recorded in digital format with Wilson's central terminal as reference. Analysis of data was produced by equipotential momentous maps during ventricle depolarization.

The heart ventricles were transversally sectioned by cryostat Leica CM 1510S (Germany). The right ventricle wall thickness was assessed under light microscopy.

Values given are means ± SE. Data analysis was performed with the computer-based statistical package (Statistica 6.0). Validity was defined by the Wilcoxon criterion for two dependent samples. P value < 0.05 was considered to indicate statistical significance.

3. Results

In hypertensive rats, at the initial moments of the QRS complex in the ECG in the limb leads the zone of positive cardiopotentials is situated cranially, whereas the zone of negative potentials is located caudally. During the ascending phase of the QRS complex, a shift of positive and negative zones takes place that leads to a change of their mutual location – the first inversion of cardiopotentials, as a result, the negative zone is located cranially, while the positive zone - caudally. The first inversion finishes on -3.18 ± 0.79 ms from the RII - peak that is significantly later than in the initial state (-3.65 ± 0.47 ms). In the period of time between the first and the second inversions the spatial location of the areas of positive and negative cardiopotentials doesn't change. The second inversion of cardiopotential areas finishes in the ascending phase of the SII-wave (6.08 ± 1.25 ms relative to the RII-peak) that is significantly later than in the initial state (5.33 ± 0.50 ms). As a result of the second inversion, the distribution of cardiopotentials with the area of the positive potential situated in the cranial zone, and the area of the negative potential located in the caudal zone is formed.

In rats with experimentally induced pulmonary hypertension during the depolarization, the maximum amplitude of positive and negative extrema of cardiopotentials significantly increases, the positive extremum makes 1.39 ± 0.37 mV, the negative extremum makes - 0.87 ± 0.41 mV in comparison with a control group (1.05 ± 0.38 mV; -0.61 ± 0.19 mV, respectively). The time of achievement of positive and negative extrema of their maximum values doesn't significantly differ. In hypertensive rats, the positive extremum reaches its maximum value on 0.32 ± 0.73 ms that corresponds to the moment of the R–peak in the ECG, the negative extremum on the 4.57 ± 0.62 ms after the R–peak, in the initial state it was (0.57 ± 0.40 ms; 4.11 ± 0.79 ms), respectively (Fig. 1.).

It is shown, that the thickness of right ventricle wall increased in MCT-induced rat. The maximal thickening was observed in area of pulmonary cone. The thickness of right ventricle was 1.83 ± 0.20 mm in hypertensive rats and 0.95 ± 0.11 mm in controls on the ventricle base level. It is shown, that thickening of right ventricle is due to the fibres of middle layer, that absent in control rats.

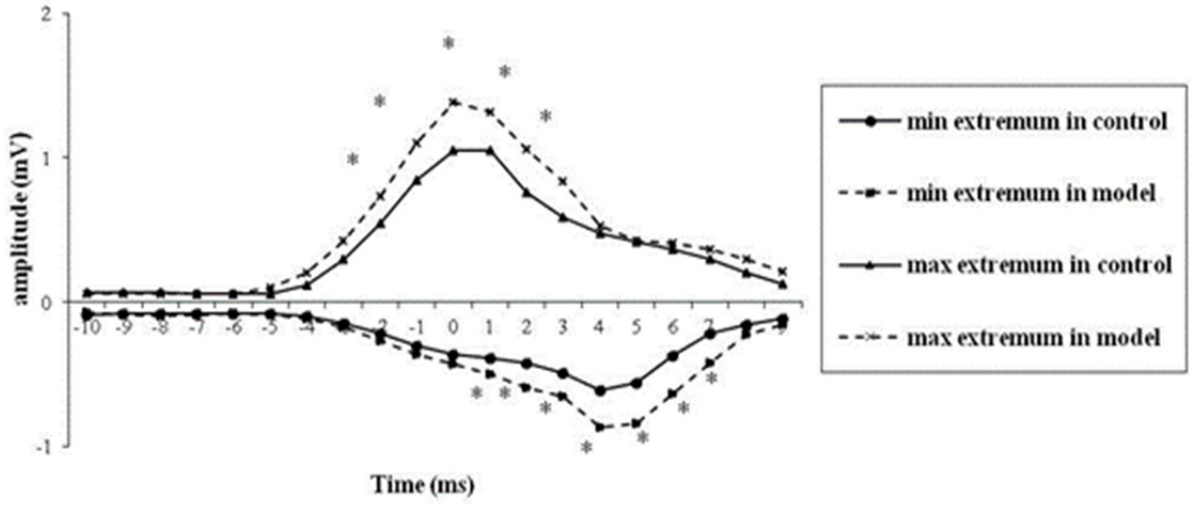

Fig.1. Amplitudes of extrema of cardioelectric field on the body surface during depolarization in rat
*- differences significant relatively to the control

4. Discussion

In rats with MCT-induced pulmonary hypertension, hypertrophy of the right ventricle was observed. The thickening of the right ventricle is due to the fibres of middle layer that absent in control rats [12]. It is reflected on body surface potential maps by a significant change of amplitudes of extrema and increase of the duration of the first and second inversions during ventricular depolarization. The increased duration of ventricular depolarization is associated with right ventricular hypertrophy. The increase of the duration could be accounted for by a decline in longitudinal conduction velocity in hypertrophied myocardium [13]. It was shown, that conduction velocity of hypertrophied ventricular myocardium decreases progressively as cell diameter increases [14]. Recently, increase duration of depolarization in rat with left ventricle hypertrophy of different genesis was shown. It was connected with hypertrophy of myocardial fibres and with an increase of connective tissue volume compared to normotensive animals [15].

5. Conclusion

Right ventricular hypertrophy of the heart in monocrotaline-induced rat models of pulmonary arterial hypertension results in changes of temporal and amplitude characteristics of the body surface cardioelectric potential distribution during ventricular depolarization.

Acknowledgement

The work is supported by the grant 09-0498814-a Russian Science Support Foundation, grant 12-P-4-1069.

References

[1] Simonneau G, Galiè N, Rubin LJ, Langleben D, Seeger W, Domenighetti G, Gibbs S, Lebrec D, Speich R, Beghetti M, Rich S, Fishman A. Clinical classification of pulmonary hypertension. *Journal of the American College of Cardiology*. 43 (12 Suppl. S): 5S-12S, 2004.

[2] Nicod LP. The endothelium and genetics in pulmonary arterial hypertension. *Swiss Medical Weekly*. 137(31-32): 437-442, 2007.

[3] Tanino Y. Monocrotaline-induced pulmonary hypertension in animals. *Nippon Rinsho*. 59(6): 1076-1080, 2001.
[4] Morimatsu Y, Sakashita N, Komohara Y, Ohnishi K, Masuda H, Dahan D, Takeya M, Guibert C, Marthan R. Development and characterization of an animal model of severe pulmonary arterial hypertension. *Journal of vascular research*. 49(1): 33-42, 2012.
[5] Benoist D, Stones R, Drinkhill M, Bernus O, White E. Arrhythmogenic substrate in hearts of rats with monocrotaline-induced pulmonary hypertension and right ventricular hypertrophy. *American Journal of Physiology, Heart and Circulatory Physiology*. 300(6): H2230-H2237, 2011.
[6] Tatebe S, Miyamura H, Sugawara M, Watanabe H, Eguchi S. Induction of right ventricular hypertrophy in neonatal guinea pigs by monocrotoline. *Japanese Circulation Journal*. 60(8): 604-608, 1996.
[7] Meyrick B, Gamble W, Reid L. Development of Crotalaria pulmonary hypertension: hemodynamic and structural study. *American Journal of Physiology*. 239(5): H692-H702, 1980.
[8] Ahearn GS, Tapson VF, Rebeiz A, Greenfield JC. Electrocardiography to define clinical status in primary pulmonary hypertension and pulmonary arterial hypertension secondary to collagen vascular disease. *Chest.* 122(2): 524-527, 2002.
[9] Van der Graaf AW, Bhagirath P, Ramanna H, van Driel VJ, de Hooge J, de Groot NM, Götte MJ. Noninvasive imaging of cardiac excitation: current status and future perspective. *Annals of Noninvasive Electrocardiology.* 19(2): 105-113, 2014.
[10] Roshchevsky MP, Arteeva NV, Kolomeyets NL, Antonova NA, Kambolov MU, Shmakov DN, Roshchevskaya IM. The system «CARDIOINFORM» for visualization and analysis of the heart electric field. *Medical academic journal*. 5(3): 74-79, 2005.
[11] Roshchevskaya IM. Cardioelectric field of warm-blooded animals and man. Saint-Petersburg. Science. 2008.
[12] Suslonova OV, Roshchevskaya IM. Architecture of the rat ventricular myocardium. *Morfologiia*. 128(5): 45-47, 2005.
[13] Carey PA, Turner M, Fry CH, Sheridan DJ. Reduced anisotropy of action potential conduction in left ventricular hypertrophy. *Journal Cardiovascular Electrophysiology*. 12(7): 830–835, 2001.
[14] Tritthart H, Luedcke H, Bayer R, Stierle H, Kaufmann R. Right ventricular hypertrophy in the cat – an electrophysiological and anatomical study. *Journal of Molecular and Cellular Cardiology*. 7(3): 163-174, 1975.
[15] Roshchevskaya IM, Suslonova OV, Roshchevsky MP. The sequence of depolarization and structural organization of the myocardium in rats with hypertrophy of different genesis. *Journal of Electrocardiology*. 46(4): e33, 2012.

The Time Course of the Extrema of Isopotential P Wave Maps in Young Adult Men and Women

K. Kozlíková, M. Trnka, M. Šrajerová

Institute of Medical Physics, Biophysics, Informatics and Telemedicine,
Faculty of Medicine in Bratislava, Comenius University in Bratislava, Bratislava,
Slovak Republic
Email: katarina.kozlikova@fmed.uniba.sk

Abstract. *The electrical activity of the heart atria is represented by the P wave that can be recorded and analysed using different procedures. The aim of this retrospective study was to analyse the sequence of isopotential maps in young adults when using time standardisation of the P wave. We constructed 21 isopotential maps from 24-lead system after Barr in 88 young adult subjects without cardiovascular diseases (40 men). We analysed values and the time course of extrema. The mean P wave duration was (84 ± 10) ms. The potential values varied from – 187 μV to 193 μV in individual maps. We always found lower mean values of extrema (flatter maps) in women than in men. The mean absolute maximum appeared in the middle of the P wave and preceded the absolute minimum in average by 1 or 2 maps. The time courses of extrema were fitted by polynomial curves against the sequential map number x = 1, 2,....21. We have shown that a limited lead system can offer reasonable information comparable to full lead systems.*

Keywords: Body surface potential mapping; P wave; Time standardisation

1. Introduction

The electrical activity of the heart atria is represented by the P wave. This can be recorded and analysed using different procedures. As the research on body surface potential mapping concerned predominantly the ventricular excitation process, there is still only limited data available documenting body surface potential distribution during atrial electric events and is mainly devoted to maps recorded using full lead systems.

The aim of this retrospective study was to establish the distributions and selected quantitative parameters of the atrial isopotential maps recorded using a limited 24-lead system in the young adult subjects based on the P wave time standardisation.

2. Subject and Methods

Subjects

We studied 88 young adults, 48 women, 40 men, mean age (18.6 ± 0.4) years. None of the subjects had signs of cardiovascular diseases or cardiovascular risk. All subjects had normal 12-lead standard electrocardiographic and echocardiographic findings as well as blood pressure values.

Body Surface Potential Mapping

Unipolar electrocardiograms for body surface potential mapping were registered using the limited 24-lead system after Barr and processed using the mapping system ProCardio [1, 2]. All data were registered in supine position during normal expiration. Linear baselines were taken through TP segments in each electrocardiogram. The onset and offset of the P wave were established manually from the root mean square signal. The limiting points were set at

the end of a sequence of decreasing values when starting from the middle of the P wave. For better comparison, each P wave was divided into 20 equidistant intervals and 21 isopotential maps per each wave were constructed. The first map corresponded to the P wave beginning, the last map to its end (see Fig. 1). We analysed the values and the time course of extrema: maximum, minimum and peak-to-peak value (maximum minus minimum) [3].

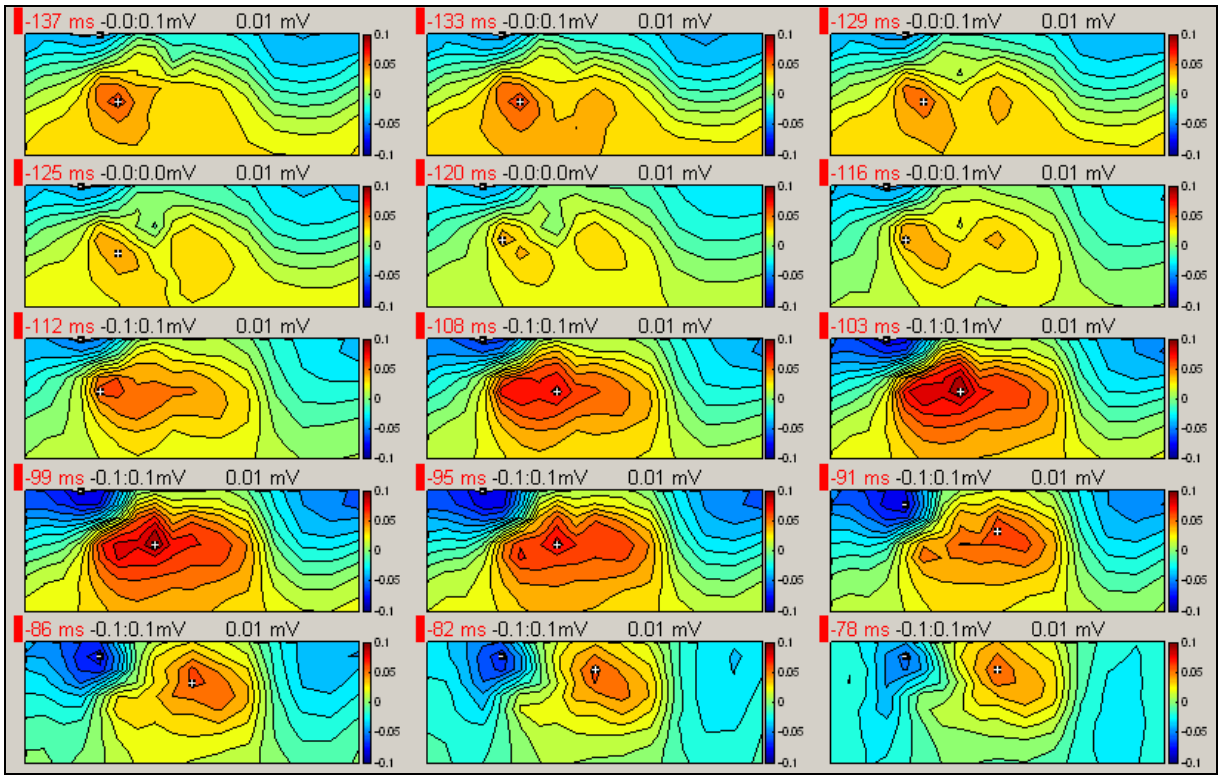

Fig. 1. Example of a sequence of P wave isopotential maps in a young man. Maps 4 to 18 are displayed. The left half of each rectangle corresponds to the anterior chest, the right half to the back. Step between isopotential lines is 0.01 mV.

Statistical Evaluation

Statistical evaluation was done using unpaired two-tailed Student's t-test for means of normally distributed data or the chi-square test with Yates´ correction for frequencies [4]. The value of $p < 0.05$ was considered as statistically significant.

3. Results

The mean P wave duration measured in the root mean square signal was (84 ± 10) ms, significantly longer in men ((86 ± 9) ms versus (82 ± 10) ms, $p < 0.05$). The potential values varied from – 187 µV to 193 µV in individual maps. We always found lower mean values of extrema (flatter maps) in women than in men (see Fig. 2). Statistically significant differences between men and women were found in 19/21 comparisons of maxima, in 19/21 of minima comparisons, and in all peak-to-peak value comparisons ($p < 0.05$). The time courses of mean extrema of all subjects (expressed in µV) were very good fitted by polynomial curves against the sequential map number $x = 1, 2, ..., 21$:

Table 1. Polynomial curves for map extrema

Regression curve	Correlation coefficient r
Maximum $= -0.7 \cdot x^2 + 15.2 \cdot x + 3.3$	0.992
Minimum $= -0.006 \cdot x^4 + 0.3 \cdot x^3 - 4.0 \cdot x^2 + 10.7 \cdot x - 22.8$	0.991
Peak-to-peak value $= 0.008 \cdot x^4 + 0.4 \cdot x^3 + 4.2 \cdot x^2 + x - 28.7$	0.999

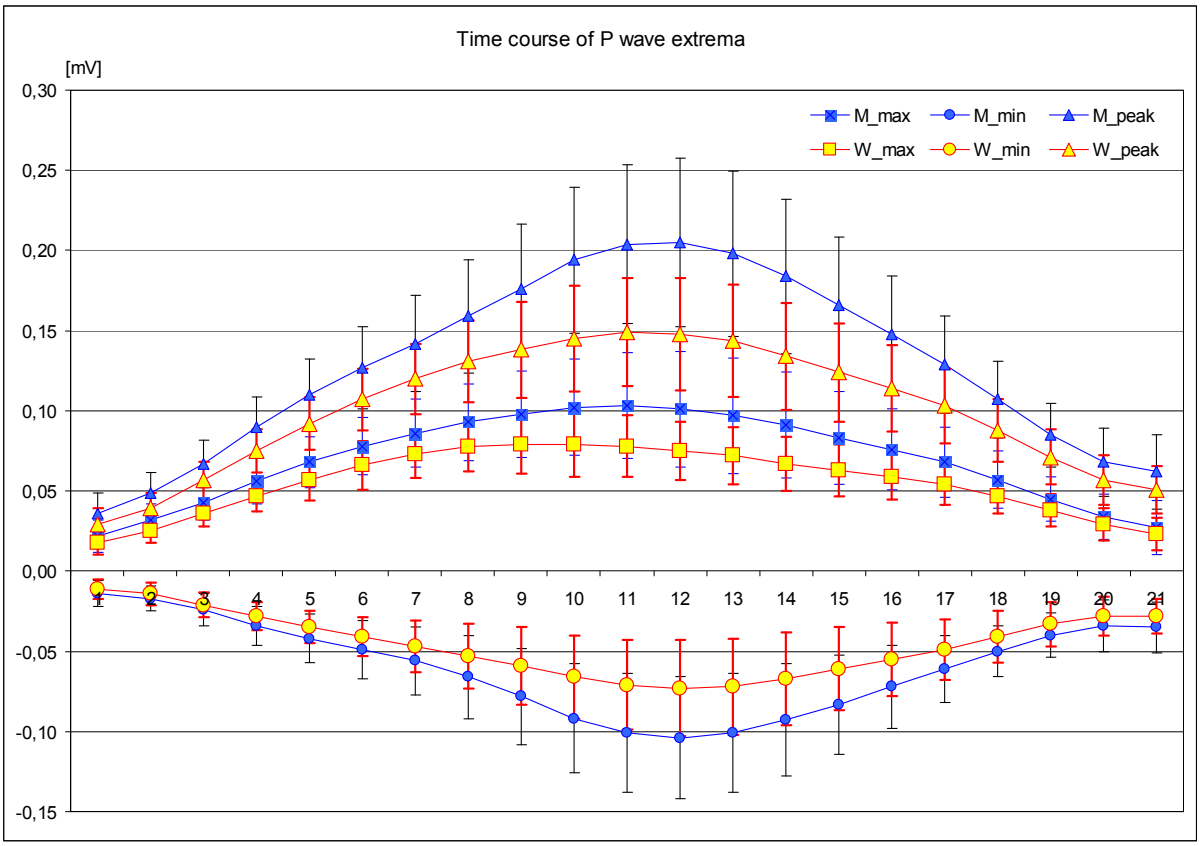

Fig. 2. Time courses of mean extrema values and standard deviations during the P wave in men and women.

During the time course of map maxima and/or minima in individual subjects, two or three maxima appeared in maps of 19/48 women and of 7/40 men ($p < 0.05$) and two or three minima appeared in maps of 14/48 women and of 3/40 men ($p < 0.05$). The absolute (highest) maximum appeared mainly in the middle of the P wave (women: map number 10 ± 2, mean value (79 ± 20) µV; men: map number 11 ± 2, value (103 ± 33) µV ($p < 0.05$); all subjects: map number 10 ± 2, mean value (89 ± 29) µV) and preceded the absolute (deepest) minimum that appeared in average map number 12 ± 2 in both men and women (mean values women: $(- 73 \pm 30)$ µV; men: $(- 104 \pm 33)$ µV ($p < 0.05$); all subjects: $(- 87 \pm 37)$ µV).

4. Discussion and Conclusions

The distributions of potentials on the chest surface during atrial activation were in accordance with published results although obtained with different lead systems [5 – 9]. The position of maxima and minima corresponded to the previously published data for isointegral P wave maps [10]. The values of absolute maxima in our study corresponded to the published data in [6, 9], but were significantly higher compared to the data from [8]. The values of absolute minima are more positive than those published in [8, 9]. These differences could be caused by

divers age of the examined subjects in the studies as the potential amplitudes change with the age [11].
The time standardisation allowed to compare various durations of the P wave in separate subjects. We have shown that a limited lead system can offer reasonable information comparable to full lead systems. We provided a quantitative evaluation of isopotential map extrema that can be useful for diagnostic purposes.

Acknowledgements

This work was partially supported by the VEGA project 1/0727/14 from the Ministry of Education, Science, Research and Sport of the Slovak Republic.

References

[1] Barr RC, Spach MS, Herman-Giddens GS. Selection of the number and positions of measuring locations for electrocardiography. *IEEE Transactions on Biomedical Engineering,* 18 (1): 125 – 138, 1971.

[2] Rosík V, Tyšler M, Turzová M. Portable device of for ECG mapping. In Proceedings of International Conference of Measurement. Frollo I and Plačková A, (Eds.), SAV, Bratislava, 1997, 367 – 370.

[3] Kozlíková K. Surface integral maps, their characteristics and methods of quantitative analysis. *Bratislavské lekárske Listy*, 91 (11): 815 – 823, 1990 (Slovak).

[4] Kozlíková K, Martinka J. *The Essentials of Biomedical Measurement Processing II*. Asklepios, Bratislava, 2009 (Slovak).

[5] Mirvis DM. Body surface distribution of electrical potential during atrial depolarization and repolarization. *Circulation,* 62 (1): 167 – 173, 1980.

[6] Kawano S, Sawanobori T, Hiraoka M. Human body surface mapping during atrial depolarization in normal and diseased subjects. *Journal of Electrocardiology,* 16 (2): 151 – 159, 1983.

[7] Popperová E, Sabolová K, Maco M et al. Two types of atrial activation in children during puberty. *Bratislavské lekárske Listy*, 89 (10): 766 – 769, 1988 (Slovak).

[8] Stilli D, Musso E, Barone P et al. Newer data on the configuration and variability ranges of body surface maps in a sample of normal subjects. *Journal of Electrocardiology,* 21 (1): 1 – 14, 1988.

[9] Jagielski J, Kałka D, Sobiesczańska M. Estimation of the chosen parameters of the body surface maps recorded during atrial excitation in normal subjects. In Electrocardiology 96. Liebman J. (Eds.), World Scientific, Singapore, 1997, 511 – 514.

[10] Kozlíková K. P-Wave body surface isointegral maps in children and in young adults. *Physiological Research*, 56 (Suppl. 1): S123 – S128, 2007.

[11] Appendix 1: Adult Normal Limits, in Comprehensive Electrocardiology. Macfarlane P et al. (Eds.), Springer, London, 2011, 2058 – 2083.

Impact of the Heart Rate on Normal STT Integral Body Surface Potential Maps

[1]J. Svehlikova, [2]M.Kania, [2]R. Maniewski, [1]M. Tysler

[1]Institute of Measurement Science SAS, Bratislava, Slovakia,
[2]Nalecz Institute of Biocybernetics and Biomedical Engineering PAS, Warsaw, Poland
Email: jana.svehlikova@savba.sk

Abstract. *We suggested a method for localization of ischemic lesions from difference integral body surface potential maps (IBSPMs) computed by subtraction of IBSPM without manifestation of ischemia from the IBSPM during ischemia that can be obtained at rest and during the stress test. In this work the possible changes in IBSPMs of healthy subjects with increasing HR were studied. BSPMs were measured during the stress test in 12 subjects (age 30-53). During the test, the HR of each subject increased from the rest value up to the value higher than 85% of the value (220-age) at the top of the load. The IBSPMs were computed for 5 HR values up to the highest one. Correlation and power of IBSPMs at subsequent values of the HR were evaluated. The correlation coefficient between the IBSPM at rest and IBSPM at the top HR was higher than 70%. The root-mean-square value of the IBSPM at the top HR varied from 43% to 128% of the root-mean-square value of the IBSPM at rest. The existence of remarkable differences in STT IBSPMs at rest and at stress in healthy subjects should be considered when the IBSPMs during the stress test are evaluated for ischemic patients.*

Keywords: STT integral body surface potential maps, stress test, heart rate, local repolarization changes

1. Introduction

Local repolarization changes (e.g. during ischemia) are reflected in integral body surface potential maps (IBSPMs) of the STT interval [1]. In previous simulation study we suggested a method for identification and localization of local ischemic lesions from difference IBSPMs using the inhomogeneous torso model and the geometrical model of heart ventricles [2], [3]. The activation propagation was simulated by cellular automaton and ischemic lesions were modelled by shortening the action potential duration by 20% in selected areas of the ventricles. The difference IBSPM was computed by subtraction of IBSPM without manifestation of ischemia from the IBSPM during ischemia. It was supposed that for real patients such data can be obtained from ECG measurements performed before and during the stress test. However, in the simulation study all changes in IBSPMs were considered as the effect of repolarization changes. During a real stress test the HR considerably increases, so the question is how to compute the difference IBSPM correctly if each member of the subtraction is computed for significantly different HRs, thus for a different time interval.

The aim of this work was to study the behavior of IBSPMs in dependence on the HR for subjects with no heart disease history, whether we can suppose, that the changes in IBSPM during the stress test reflect only pathological repolarization changes or there are some changes that can be considered physiological.

2. Subject and Methods

Multichannel ECG recordings with 64 leads were performed during the stress test on 12 volunteers (age 30-53) with no heart disease history in Medical University Warsaw as it is described also in [4]. BSPMs from 64 measured leads were computed. Simultaneously, the 12-lead ECG was measured to evaluate the measured data in a standard way. During the test,

the HR of each subject increased from the basal value at rest up to the value higher than 85% of the value 220-age at the top of the load.

The IBSPMs from STT time interval were computed for each subject at the basal and at the highest HR as well as for three HR values in between (together in 5 levels of HR). The IBSPMs at each HR level were computed from signals averaged over intervals of 10 seconds [4]. The fiducial points Q, J and the end of T wave were set manually. To compensate for the changes in STT interval duration with increasing HR, the IBSPMs were normalized by dividing them by the length of the corresponding STT time interval. Then at each level of the HR the root-mean-square (RMS) signal of the normalized IBSPM was computed according the Eq. 1 as well as its correlation with the normalized IBSPM measured at rest (at the beginning of the exercise). The differences between normalized IBSPMs at observed levels of the HR were evaluated for each subject.

$$RMS = \sqrt{\frac{\sum_{i=1}^{n} x_i^2}{n}} \qquad (1)$$

Where x_i STT integral of the measured ECG signal in the lead i
n number of measured leads

Although the multichannel measurements of ECG are usually interpolated and visualized in regular rectangular grid (Fig. 2), in this work the evaluated parameters of IBSPMs were computed only from the measured signals (not from interpolated map values). IBSPM was handled as a multidimensional vector.

3. Results

The increasing HR shortened the QRST interval significantly from 100% to 66.3 ± 4.6%. The shortening of the STT interval was more dramatic – from 100% to 58.4 ± 5.9%, while the QRS interval shortened slightly from 100% to 92.7 ± 7.4%. All next parameters were computed for the normalized IBSPMs.

The mean value of the correlation coefficient between the IBSPM at rest and IBSPM at the top of HR was 88.1 ± 9.5% (70% – 98%) (Fig. 1).

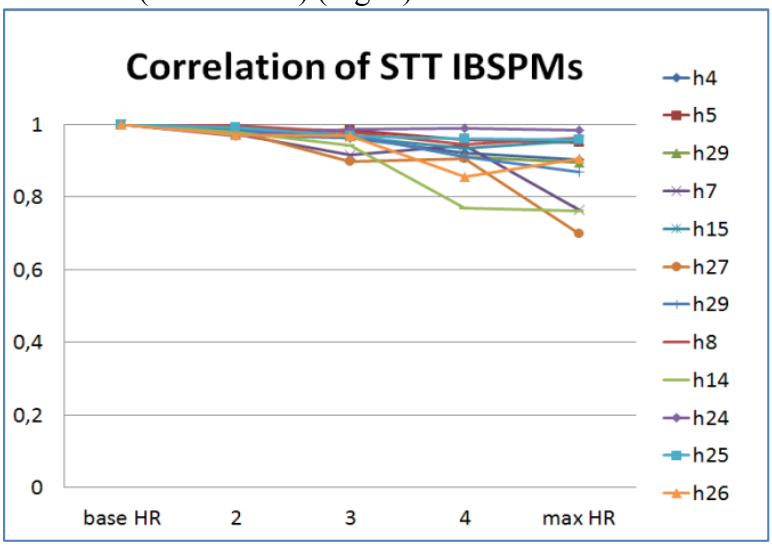

Fig. 1. Correlation coefficient between the IBSPM at rest and IBSPMs computed at 4 values of HR up to the maximal reached value of HR at the top of the load for 12 measured subjects.

The RMS value of the IBSPM at the top HR varied more significantly for different subjects from 43% to 128 % (mean 79.7 ± 36.4%) of the RMS value of the IBSPM at rest (Fig. 2).

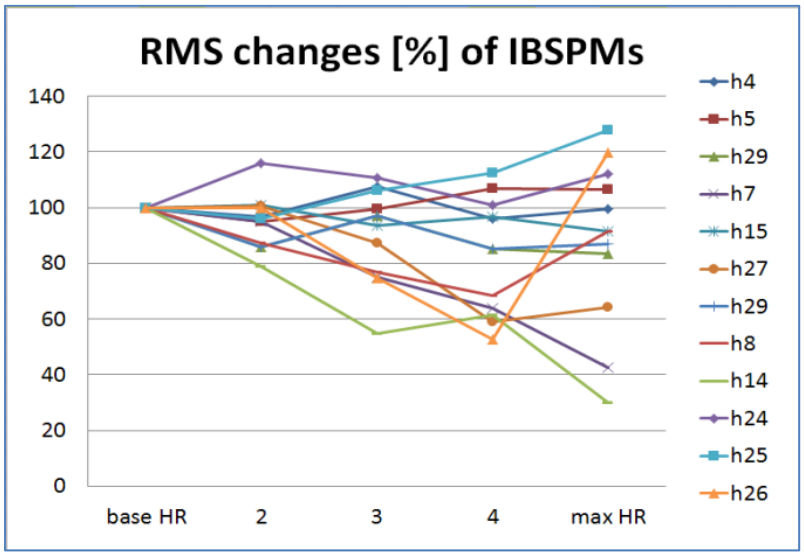

Fig. 2. Percentage of RMS values of IBSPMs for 4 values of HR in comparison to the RMS value of IBSPM at the beginning of the exercise.

In Fig. 3 the examples of changes in IBSPMs during the stress test are depicted.

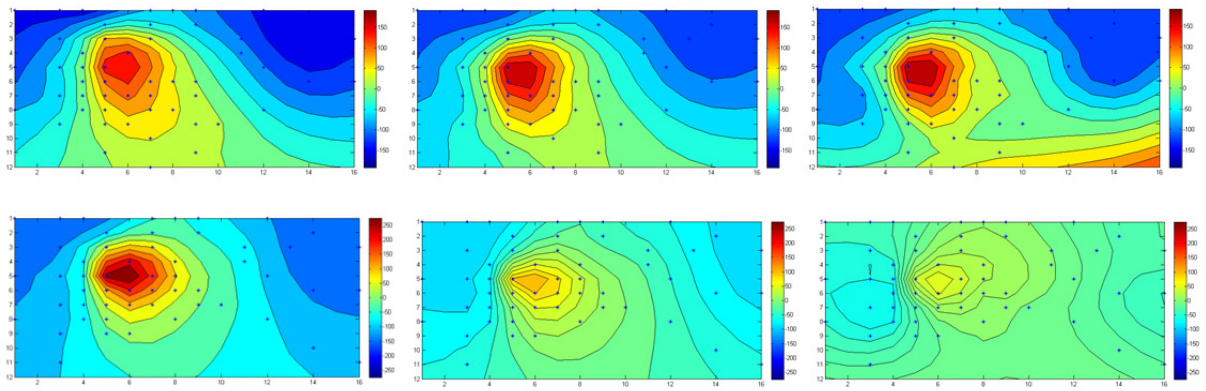

Fig. 3. IBSPMs at the beginning of the exercise (left), at the 3rd level of HR (middle) and at maximal value of HR (right) for the subject h15 with minimal changes of observed parameters (top) and for the subject h14 with maximal changes of observed parameters (bottom). Asterisks mark the measured points.

4. Discussion and Conclusions

Remarkable differences in STT IBSPMs at rest and during the stress test were observed in healthy subjects, so the hypothesis that all changes in STT integral BSPMs during the stress test can be considered pathological was not confirmed.

We can suppose that there are additional physiological factors influencing the ECG signal during increasing the HR that reflected in RMS signal of BSPMs.

The measured signals for higher HR were very noisy because of the presence of myopotentials and moving artefacts. In some cases the signal was completely damaged and was excluded from evaluation. If the number of "bad" electrodes varied in different levels of HR for one particular subject, the final evaluation and comparison of observed parameters was made only for leads that had produced acceptable signal in all HR levels. Better quality of signals could be obtained if the stress is evoked by pharmacological or mental load [6].

The limitation of the study was small number of measured subjects and also the age of subjects (30 – 50 years). The results from younger population would be desirable.

For ischemic patients, similar changes in IBSPMs that were observed in healthy subjects during the stress test can be associated with repolarization changes. From the obtained results it implies that for ischemic patients we cannot assign all changes in IBSPM during the stress test to the pathological repolarization changes and it is questionable whether the simple difference IBSPM computed from the IBSPM at rest and at the top of the load can be used as input data for inverse localization of possible ischemic lesions. Additional properties of IBSPMs should be searched for distinguishing between normal physiological changes and pathological repolarization changes during the stress test.

Acknowledgements

The study was supported by grant 2/0131/13 from the VEGA Grant Agency, Slovakia, by grant APVV-0513-10 from the Slovak Research and Development Agency and by project Biomedicine University Research Park Bratislava (ITMS code 26240220087).

References

[1] Trudel MC, Dube B, Potse M, Gulrajani RM, Leon LJ. "Simulation of QRST integral maps with a membrane-based computer heart model employing parallel processing," *Ieee Trans. Biomed. Eng.*, vol. 51, no. 8, pp. 1319–1329, 2004.

[2] Tysler M, Kneppo P, Turzova M, Svehlikova J, Karas S, Heblakova E, Hana K, Filipova S. "Noninvasive assessment of local myocardium repolarization changes using high resolution surface ECG mapping," *Physiol. Res.*, vol. 56, pp. S133–S141, 2007.

[3] Tysler M, Svehlikova J. "Noninvasive finding of local repolarization changes in the heart using dipole models and simplified torso geometry.," *J. Electrocardiol.*, vol. 46, no. 4, pp. 284–8, 2013.

[4] Kania MR, Zaczek M, Zavala-Fernandez R, Janusek D, Kobylecka M, Krolicki L, Opolski G, "ST-segment changes in high-resolution BSPM measured during exercise to assess myocardial ischemia : a pilot study," *Arch. Med. Sci.*, DOI:10.5114/aoms.2013.39938, p. in press, 2014.

[5] Barr RC, Ramsey 3rd M, Spach MS. "Relating epicardial to body surface potential distributions by means of transfer coefficients based on geometry measurements," *IEEE Trans. Biomed. Eng.*, vol. 24, no. 1, pp. 1–11, 1977.

[6] Bossimini E, Galli M, Guagliumi G, Giubbini R, Tavazzi L. "Electrocardiographic Markers of Ischemia During Mental Stress Testing in Postinfarction Patients," *Circ. Suppl. II*, vol. 83, no. 4, pp. 115–127, 1991.

Atrial Fibrillation

Circadian Heart Rate Variability in Permanent Atrial Fibrillation Patients

I. Kurcalte, O. Kalejs, R. Erts, I. Konrade, A. Lejnieks

Riga Stradins University, Riga, Latvia
Email: irenakurcalte@gmail.com

Abstract. *Atrial fibrillation (AF) is the most common sustained cardiac arrhythmia occurring in 1-2% of general population, and approximately 13% of AF patients suffer from diabetes. Cardiovascular autonomic control impairment is associated with total mortality, but current practical use of ECG-based risk predictors is limited in permanent AF (PAF) patients due to absolute irregularity of ventricular contractions. We assume that it is possible to use measurements of circadian heart rate (HR) changes for mortality risk and cardiac autonomic control assessment in PAF patients. In 327 symptomatic PAF patients (259 non-diabetic, 68 diabetic), exposed to Holter monitoring in 2007-2010, circadian HR variability and standard Heart Rate Variability (HRV) Time domain indices were calculated and compared in patients who died or survived, and non-diabetic and diabetic patients. Patients were followed for a median period of 39 months (1-60). It was found that circadian HR indices were significantly lower in the dead as compared with alive patients ($p < 0.001$); in diabetic patients as compared with those without diabetes ($p < 0.01$), and in diabetic patients with approved diabetic neuropathy diagnosis ($p < 0.05$). Measured HRV indices didn't show significant differences in studied patients groups. Circadian HR variability showed promising predictive value for risk assessment in PAF patients.*

Keywords: circadian heart rate variability; average day night heart rate ratio; average day night heart rate difference.

1. Introduction

Current practical use of heart rate variability (HRV) is limited in permanent atrial fibrillation (PAF) patients as there is a consensus of opinion as to which parameters of HRV to record and which method of assessing HRV is required [1]. Although autonomic dysfunction is likely to pose the same risks for death or electrical instability in patients with AF as in sinus rhythm, the relevance or significance of "traditional" time domain or spectral HRV parameters to assess autonomic function in PAF is uncertain. It may be possible to assess autonomic function in AF by measuring the circadian changes in electrophysiological parameters over a 24 h period [1].

Different measurements of HRV, in addition to traditional ones based on different calculation techniques, were studied and reported for different SR and PAF patient groups for risk assessment, such as delta HR [2], circadian rhythm of atrioventricular nodal functional refractory period [1], HRV Fraction [3], and so on.

The "National Russian Guidelines on Clinical Application of the method of Holter Monitoring in Clinical Practice", being a valuable tool for patients risk assessment, recommend the "circadian index" with an optimal cut off point 1.32 (range 1.24 – 1.44) with no reference to heart rhythm.

2. Subject and Methods

The aim of this study is to analyze circadian HR changes in PAF patients and to come up with working parameters to be further applied for non-invasive mortality risk assessment and cardiac autonomic control evaluation. Study cohort: 327 symptomatic PAF patients (mean age

74.6 (9.7), 148 (45.3%) male), exposed to Holter monitoring in 2007-2010, 259 non-diabetics (mean age 74.4 (10), 121 male (46.4%)) and 68 diabetic patients (mean age 75.7 (8.5), 28 male (40%)). Primary end-point: death for any reason.

Table 1. Clinical characteristics of study patients

	N [%]
CHF NYHA class II/IV	277 [85]
Hypertension	219 [67]
Stroke/embolism	136 [42]
Diabetes	68 [21]
Cancer	45 [14]
COPD	65 [20]
CAD	114 [35]
CKD	90 [28]
Wide QRS >120ms	48 [15]
CHADS-VAS	5.04

Schiller MT200 Microvit and Seer Light Extend GE 3-channel Holter recorders with standard lead configurations were used for registration of recordings. Recordings were analysed by using accordingly Schiller MT200 and Mars Version 7.2 software with manual post processing of ventricular ectopic complexes, longest and shortest RR intervals and extreme heart rates.

Characteristics of 24 hour HR changes: average day and night HR ratio (AveDNHRratio) and difference (AveDNHRdif), with the day time from 9 a.m. to 21 p.m. , and night time – from midnight to 6 a.m., were compared between the groups and within the groups of patients who died before, or survived after 1.1.2011, as well as in patients with or without DM.

Statistical analysis: IBM SPSS v.18.program was used. Data were presented as mean (M) (SD) or median (Me) ([IQR]) for continuous variables, and patient (%) for categorical variables. Comparisons were made using t-test, Mann-Whitney test in case of non-normality and chi-square test. All tests were two-sided and considered significant at $p < 0.05$. Receiver operating characteristic (ROC) curves were used for measurement of diagnostic effectiveness of circadian HR indices and for detection of diagnostic thresholds distinguishing between patients with high mortality risk and those without it. The Kaplan - Meijer method was used to test validity of the cut off points found for survival analysis.

3. Results

During the follow-up 103 (31.5%) patients (50 male (48.5%) died. The dead patients were older than the alive ones (77.9 y.o (7.9) vs. 73.1 y.o. (10.1)). Measured circadian HR changes were lower (the difference being statistically significant) in dead patient group, but standard HRV Time domain indices didn't show any significant differences in studied PAF cohort (Table 2). ROC curves used for detecting cut off points discriminating high risk patients from non- high risk ones showed fair diagnostic effectiveness of calculated circadian HR indices (Fig. 1).

Table 2 Comparison of standard Time domain and circadian HRV indices between dead and alive patient groups.

Variable	Dead [n=103]	Alive [n=224]	P value †	AUC	Cut off point
AveDNHRratio [M (SD)]	1.13 [0.14]	1.24 [0.16]	< 0.001	0.702 (0.642;0.761)***	1.14
AveDNHRdif [bpm][Me[IQR]]	8 [11]	15 [13]	< 0.001	0.711 (0.652;0.770)***	9
SDNN [ms] [Me [IQR]]	223 [89]	222 [68]	n.s.	0.522 (0.452;0.591)	-
SDANN [ms] [Me [IQR]]	86 [54]	89 [46]	n.s.	0.532 (0.462;0.599)	-
rMSSD [ms] [Me [IQR]]	212 [149]	227 [113]	n.s.	0.553 (0.485; 0.620)	-

† t-test or M-W test; *** p-value for area under the curve [AUC] < 0.001.

Decrease of circadian HRV indices under the estimated thresholds is acociated with higher death probability in studied patients. Cut off points for circadian HRV characteristics obtained from ROC curves showed an acceptable prognostic properties (Table 3).

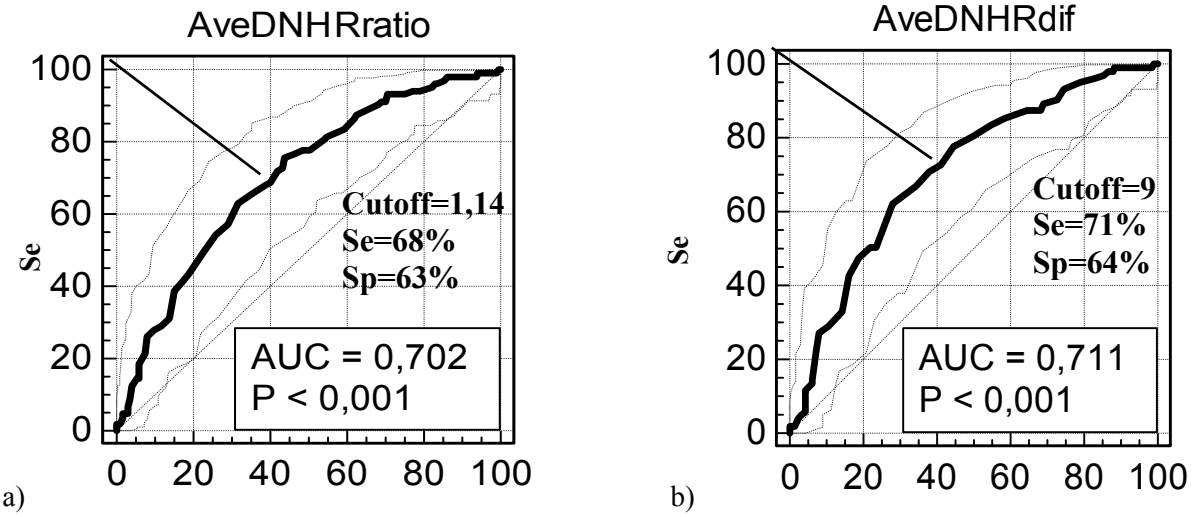

Fig. 1 ROC curves for AveDNHRratio (a) and AveDNHRdif (b) diagnostic effectiveness evaluation and optimal cut off points detection.

Table 3 Diagnostic characteristics for circadian HRV cut off points estimated from ROC curves

Variable	Dead [n=103]	Alive [n=224]	p-value	OR [95% CI]	Sensitivity [%]	Specificity [%]
AveDNHRratio < 1,14 [patients [%]]	65 [63.1]	71 [31.7]	< 0.001	3.69 [2.26; 6.01]	68	63
AveDNHRdif < 9 bpm [patients [%]]	63 [61.2]	56 [25%]	< 0.001	4.73 [2.87; 7.79]	71	64

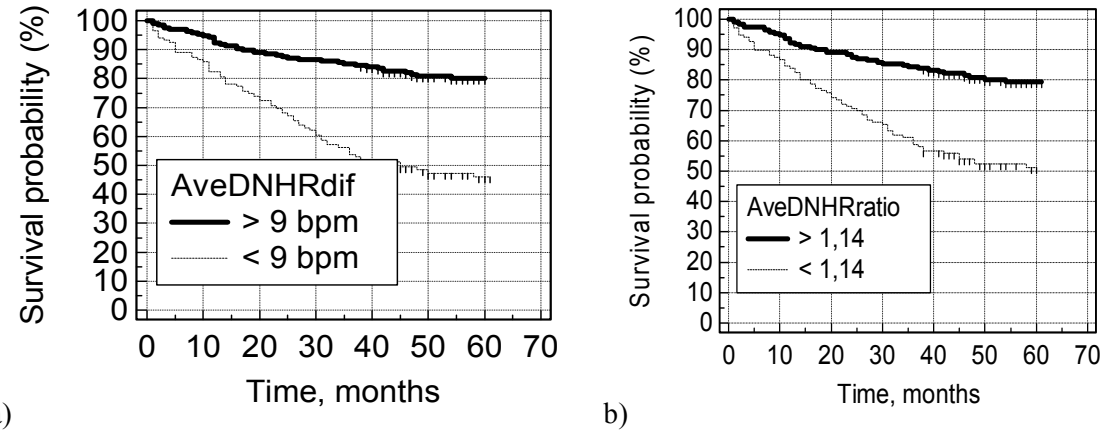

Fig. 2 Circadian HR parameters cut-off thresholds AveDNHRdif (a) and AveDNHRratio (b) tried for survival analysis showed promising prognostic value for survival prediction in studied cohort

Circadian HRV in Diabetic Patient Group

Community studies showed prevalence of DM in 13% of patients with AF [5]. Prevalence of DM in studied cohort was higher - 21%. During the follow-up, 65 (25%) patients in the non-diabetic group and 38 (54.3%) diabetic ones died (OR – 2.97 (1.73; 5.09 95% CI)).

Cardiac autonomic neuropathy is significantly associated with total mortality [6]. In study cohort the measurements of circadian HR changes were significantly lower in diabetic patient group as compared with the non-diabetics (Table 4). Measurements of circadian HRV compared between dead and alive diabetic patients were low in both groups and didn't show any statistically significant differences (1.15 [0.15] vs. 1.19 [0.19] for AveDNHRratio and 9 [15] vs. 12 [20] for AveDNHRdif), which may be due to the underlying diabetic autonomic neuropathy and cardiomyopathy.

Table 4. Circadian HRV indices are significantly lower in the diabetic patient group

Variable	Non-diabetic [n=259]	Diabetic [n=68]	p-value
AveDNHRratio [M (SD)]	1.22 [0.16]	1.16 [0.16]	< 0.01
AveDNHRdif [Me[IQR]]	13 [14]	9 [14]	< 0.01

In the studied diabetic patient cohort AveDNHRratio was significantly lower in patient group (n = 12) with recognised diabetic neuropathy diagnosis (1.08 [0.13] vs. 1.16 [0.17], p – .036).

4. Conclusions and discussion

Circadian HR variability showed promising properties to be a relevant ECG-based diagnostic and predictive tool for patient risk assessment irrespectively of AF presence. Indices of circadian HR variability could be easily measured and analysed for every patient exposed to long-term (24 hours and more) ECG monitoring. In the studied aging patient group including patients with mostly more than one dichotomous high risk predictor, application of additional dynamic risk parameters could help to distinguish between two patients with equally high dichotomous risk the one with higher immediate risk. The important question still remaining open, especially for clinicians, is validity period of the dynamic risk stratification parameters and optimal time interval for high risk patients follow-up. The challenge would be to identify a parameter with a certain threshold value, which could be informative enough for a certain patient group within a certain (validity) time period. And of course, the impact of antiarrhythmic drug on dynamic parameters derived from heart rate measurements can't be underestimated. Additional prospective studies with more patients included in dynamic evaluation are required to find answers to at least part of clinical questions.

References

[1] Aleem U. Khand, A. C. Rankin. The assessment of autonomic function in chronic atrial fibrillation: description of a non-invasive technique based on circadian rhythm of atrioventricular nodal functional refractory periods. *Europace* 8 (11):927-934, 2006.

[2] Madsen BK, Rasmussen V, Hansen JF. Predictors of sudden death and death from pump failure in congestive heart failure are different. Analysis of 24 h Holter monitoring, clinical variables, blood chemistry, exercise test and radionuclide angiography. *International Journal of Cardiology*, 58: 151–162, 1997.

[3] Sosnowski M, Macfarlane PW, Parma R, Skrzypek-Wanha J, Tendera M. Prognostic Value of Heart Rate Variability Analysis in Patients with Depressed Left Ventricular Function Irrespective of Cardiac Rhythm. *Computers in Cardiology,* 33:81-84, 2006.

[4] Комолятова и др. "Национальные российские рекомендации по применению методики холтеровского мониторирования в клинической практике", Москва, 2013

[5] Lars Ryden, Peter J. Grant et al. ESC Guidelines on diabetes, pre-diabetes, and cardiovascular diseases in collaboration with the EASD. *European Heart Journal;* doi: 10. 1093/eurheartj/eht108. 2013.

[6] Rodica Pop-Busul, Cardiac Autonomic Neuropathy in Diabetes. *Diabetes care*, volume 33 number 2, February, 2010.

Posters:
Experimental and Clinical Electrocardiology

Alterations in Cardiac Cell-to-Cell Coupling Can Facilitate AF in Old Guinea Pig.

[1]N. Tribulova, [2]V. Nagibin, [1]T. Benova, [1]C. Viczenczova, [1,3]J. Radosinska, [4]V. Knezl, [5]I. Dovinova, [1]M. Barancik

[1]Institute for Heart Research, SAS, Bratislava, Slovakia,
[2]Bogomoletz Institute of Physiology, Kyiv, Ukraine,
[3]Institute of Physiology, Fac. of Medicine, Comenius University, Bratislava, Slovakia,
[4]Institute of Experimental Pharmacology & Toxicology, SAS, Bratislava, Slovakia,
[5]Institute of Normal and Pathological Physiology, SAS, Bratislava, Slovakia
Email: narcisa.tribulova@savba.sk

Abstract. *We hypothesize that in addition to atrial structural remodeling the alterations in cardiac cell-to-cell coupling due to the ageing may facilitate induction and persistence of AF. Experiments were conducted on male and female 4-weeks-old and 24-weeks-old guinea pigs (GP). Heart atrial tissue was processed for ultrastructure examination using electron microscopy. Gap junction connexin-43 distribution was detected by in situ immunostaining while the level of Cx43 mRNA and expression of Cx43 protein were determined by real time PCR and western blotting. Expression of mRNA of extracellular matrix metalloproteinase-2 (MMP2) that is involved in myocardial remodeling was also analyzed. Subcellular examination revealed interstitial fibrosis, flattened adhesive junctions with widened extracellular spaces and lower number of gap junctions in old versus young GP heart atria. The density of Cx43-positive gap junctions was lower in atria of old comparing to young GPs. In parallel, the atrial tissue levels of Cx43 mRNA and Cx43 protein were decreased in old versus young GP. In contrast, mRNA expression of MMP2 was significantly higher in old versus young GP. The changes were more pronounced in old males comparing to females GP. Findings indicate that age-related down-regulation of atrial Cx43, dehiscence of adhesive junctions and up-regulation of MMP-2 can facilitate development of AF in old heart.*

Key words: cardiac connexin-43; MMP2, atrial fibrillation, old guinea pig

1. Introduction

Atrial fibrillation (AF) affects approximately 1 % of the general population and up to 8 % of subjects over the age of 80 [1]. AF is associated with decreased quality of life, increased morbidity and a 30 % higher risk of death [2], and thus is a major contributor to cardiovascular mortality. Indeed, AF has long been recognized as a powerful risk factor for stroke (up to 15 % of all strokes are attributable to this disorder), heart failure and mortality. Advancing age amplifies the risk of all of these sequels of AF. The prevalence of this arrhythmia rises sharply with aging [3, 4, 5]. High incidence of AF creates a huge burden on the health care system, both in terms of morbidity, mortality, and cost. Despite recent advances in AF therapy, including the broader use of anticoagulant therapy, adequate rate control, and newer, safer techniques to maintain sinus rhythm, which may prospectively help to prevent adverse outcomes in AF patients, mortality and morbidity in AF patients remains unacceptably high [5]. Because of demographic changes, the prevalence of AF will increase in the next decades, requiring better primary prevention strategies and better treatment options. Despite the progress in pathophysiology of atrial fibrillation (AF) the molecular mechanisms of this most common cardiac arrhythmia in aged population are still not fully elucidated. We have previously shown that unlike to young the aged guinea pig heart is much prone to develop AF upon repetitive burst stimulation. We hypothesize that in addition to

atrial structural remodeling the alterations in cardiac cell-to-cell coupling due to the ageing may facilitate induction and persistence of AF.

2. Subject and Methods

Experiments were conducted on male and female 4-weeks-old and 24-weeks-old guinea pigs (GP). Heart atrial tissue was processed for ultrastructure examination using electron microscopy. Gap junction connexin-43 distribution was detected by in situ immunostaining while the level of Cx43 mRNA and expression of Cx43 protein were determined by real time PCR and western blotting. Expression of mRNA of extracellular matrix metalloproteinase-2 (MMP2) that is involved in myocardial structural remodeling was also analyzed.

3. Results

Burst pacing induced only very brief (1 to 6 s) posstimulus arrhythmias in young while prolonged (5 to 15 minutes) atrial fibrilloflutter in old guinea pig heart (Fig. 1). Subcellular examination revealed interstitial fibrosis, flattened adhesive junctions with widened extracellular spaces and lower number of gap junctions in old versus young GP heart atria (Fig. 2). The density of Cx43-positive gap junctions was lower in atria of old comparing to young GPs. In parallel, the atrial tissue levels of Cx43 mRNA and Cx43 protein were decreased in old versus young GP. In contrast, mRNA expression of MMP2 was significantly higher in old versus young GP. The changes were more pronounced in old males comparing to females GP.

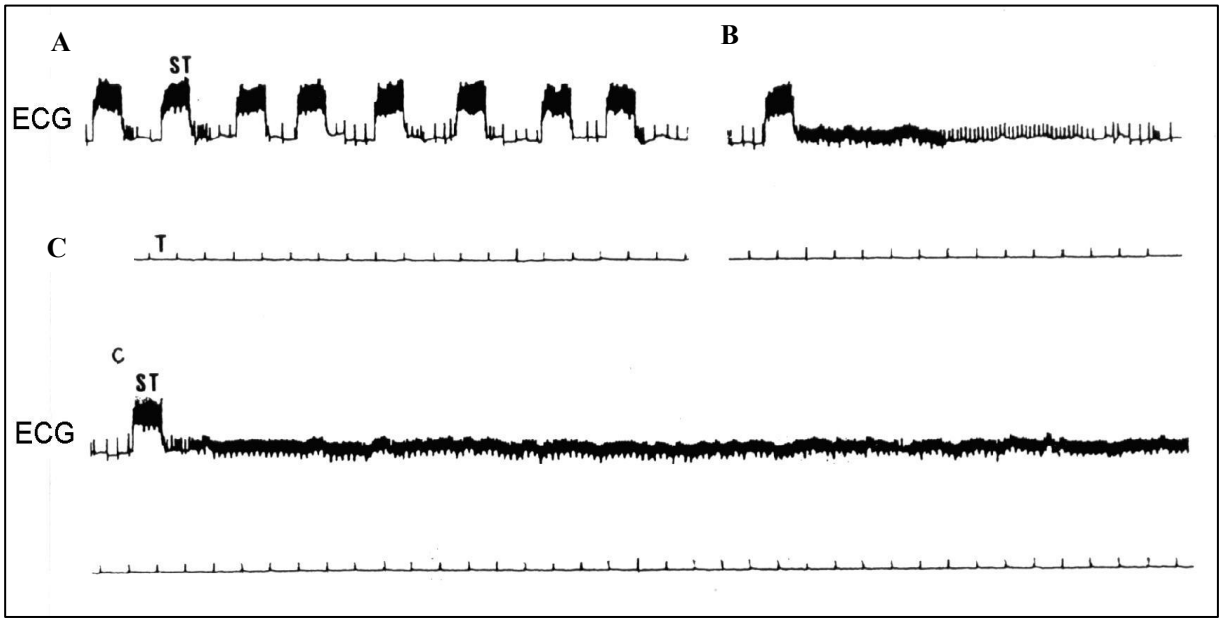

Fig.1. ECG of the atria during burst stimulation (A) and post-stimuli arrhythmias in young (B) and old (C) guinea pig heart.

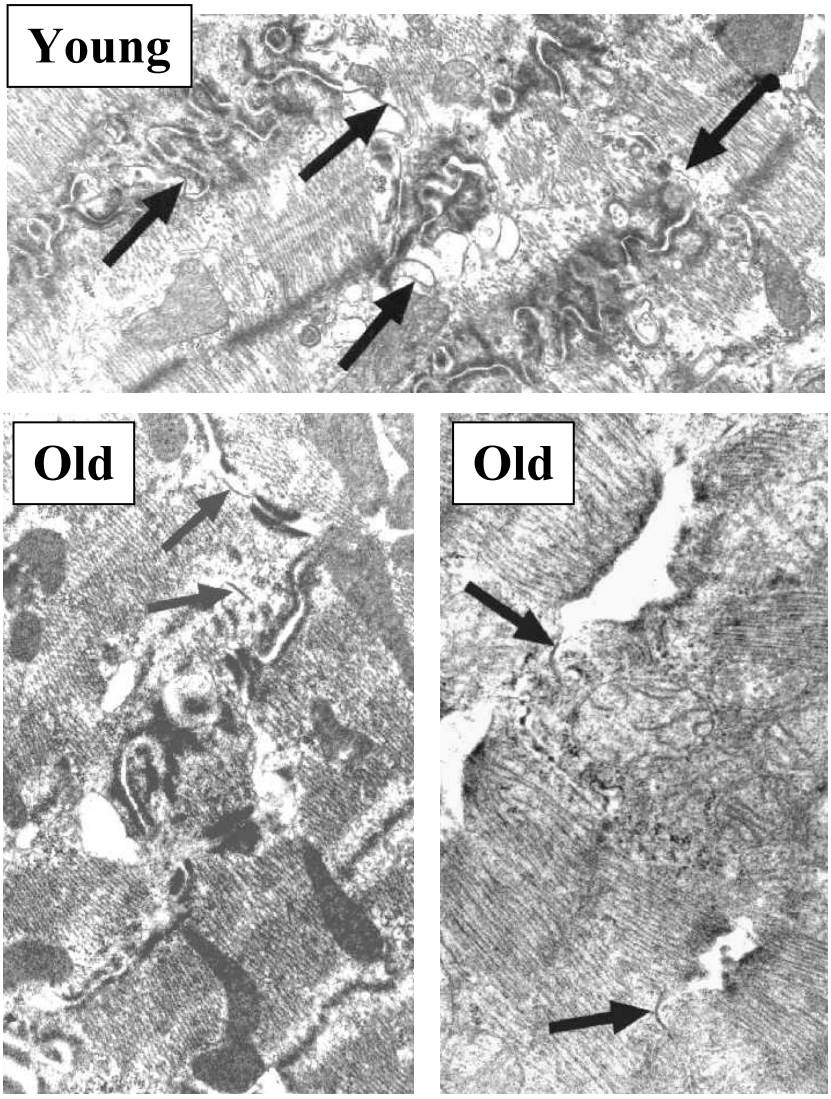

Fig. 2. Representative electron microscopic pictures showing numerous gap junctions (arrows) in young guinea pig atria. While lower number of gap junctions and dehiscence of adhesive junctions is seen in atrial tissue of old guinea pig heart. Magnification 25 000x.

4. Discussion

Atrial fibrillation (AF) is the most common cardiac arrhythmia in clinical practice. However, precise mechanisms that lead to the onset and persistence of AF have not completely been elucidated. Numerous risk factors have been established for incident AF and its progression, such as cardiovascular diseases (hypertension, diabetes, coronary artery disease, valvular heart disease, failing heart), subclinical hyperthyroidism, genetic components as well as obesity and aging. These pathophysiological conditions are associated with acute and/or chronic inflammation and oxidative stress. Consequently, it results in activation of endogenous mechanisms of adaptation to preserve cardiovascular function. However, the process of adaptation is paradoxically linked with mal-adaptation. Its adverse effects contribute, besides others, to the in increased propensity of the heart to life-threatening arrhythmias including AF that increases a risk of stroke. Our findings revealed pronounced extracellular matrix remodelling, i.e. fibrosis and increased expression of MMP2 in old guinea pig atria compared to atrial tissue of young guinea pig heart. It was accompanied by alterations in size and number of gap junctions as well as by down-regulation of gap junction protein, Cx43. Impairment of cell-to-cell communication has been established to contribute to

arrhythmogenesis and occurrence of re-entry atrrhythmias, such as AF or VT/VF [7]. Thus, age-related alterations in Cx43-mediated electrical coupling may promote development of AF.

5. Conclusions

Our findings indicate that age-related down-regulation of atrial Cx43, dehiscence of adhesive junctions and up-regulation of MMP-2 can facilitate development of AF in old heart.

Acknowledgement

This study was supported by VEGA 2/0046/12, 1/0032/14 and APVV-0348-12 grants.

References

[1] Fuster V, Rydén LE, Cannom DS, Crijns HJ, Curtis AB, Ellenbogen KA, Halperin JL, Le Heuzey JY, Kay GN, Lowe JE, Olsson SB, Prystowsky EN, Tamargo JL, Wann S: ACC/AHA/ESC 2006 guidelines for the management of patients with atrial fibrillation-executive summary. *European Heart Journal* 27: 1979-2030, 2006.

[2] Benjamin EJ, Wolf PA, D'Agostino RB, Silbershatz H, Kannel WB, Levy D: Impact of atrial fibrillation on the risk of death: the Framingham Heart Study. *Circulation* 98: 946-952, 1998.

[3] Bhave P, Passman R: Age as a Risk factor for Atrial Fibrillation and Flutter after Coronary Artery Bypass Grafting. *Journal of Atrial Fibrillation* 2, 2012.

[4] Tribulova N, Varon D, Polack-Charcon S, Buscemi P, Slezak J, Manoach M: Aged heart as a model for prolonged atrial fibrilloflutter. *Experimental&Clinical Cardiology*, 4: 64-72, 1999

[5] Aldhoon B, Melenovský V, Peichl P, Kautzner J: New insights into mechanisms of atrial fibrillation. *Physiological Research* 59: 1-12, 2010.

[6] Kirchhof P and Camm AJ. Comprehensive risk reduction in patients with atrial fibrillation: emerging diagnostic and therapeutic options – a report from the 3rd atrial fibrillation competence NETwork/European heart rhythm, association consensus conference. *Europace* 14: 18-27, 2012

[7] Severs NJ. Gap junction remodelling and cardiac arrhythmogenesis: cause or coincidence? *Journal of Cellular and Molecular Medicine* 2001; 5: 355-366.

Hyper- and Hypothyroidism Affect Myocardial Connexin-43 Expression and Susceptibility of the Rat Heart to Malignant Arrhythmias

[1]B. Bacova, [1]C. Viczenczova, [1]T. Benova, [2]J. Zurmanova, [3]S. Pavelka, [3]T. Soukup, [1]N. Tribulova

[1]Institute for Heart Research, SAS, Bratislava, Slovakia,
[2]Faculty of Science, Charles University in Prague, Prague, Czech Republic,
[3]Institute of Physiology, v.v.i., AS CR, Prague, Czech Republic,
Email: barbara.bacova@savba.sk

Abstract. *We aimed to explore relationship between myocardial electrical coupling protein connexin-43 (Cx43) and susceptibility of rats with altered thyroid status to malignant arrhythmias and to examine possible beneficial effect of red palm oil (RPO). We used as experimental model euthyroid (EU), hypothyroid (HY) and hyperthyroid (TH) rats, which were fed RPO (100μl/100g b.w./day) for 6 weeks. Left ventricular tissue was taken for determination of mRNA and protein expression of Cx43 and PKCε. Sustained ventricular fibrillation (sVF) induction was estimated using isolated perfused heart. Results showed that the threshold for sVF was significantly decreased in the TH, in which Cx43 and PKCε expression was down-regulated in comparison with the EU. On the contrary, sustained VF was not induced even by the highest stimulus strength in the HY, in which Cx43 and PKCε expression was up-regulated. RPO intake partly, although significantly, increased VF threshold in TH as well as Cx43 and PKCε proteins expression. We conclude that there is an inverse relationship between myocardial Cx43 expression and heart susceptibility of rats with altered thyroid status to VF.*

Keywords: thyroid hormones, cardiac arrhythmias, connexin-43

1. Introduction

Mammalian heart is a major target organ for thyroid hormone (triiodo-L-thyronine, T_3) action. T_3 plays an important role in cardiac electrophysiology and Ca^{2+} handling through both genomic and nongenomic mechanisms [1, 2]. Thyroid dysfunction is classified as hyperthyroidism and hypothyroidism. Chronic changes in the amount of plasma concentration of thyroid hormones result in structural, electrophysiological and Ca^{2+} handling remodeling of the heart, while acute changes may influence basal metabolic activity of cardiomyocytes [3]. Consequently, these alterations may affect heart function as well as its susceptibility to arrhythmias [1]. We have previously shown that increased propensity to arrhythmias was associated with T_3-induced down-regulation of atrial and ventricular connexin-43 (Cx43) [4, 5]. Defects in expression and/or distribution of Cx43 have been established to impair Cx43 channels mediated cell-to-cell communication and electrical coupling that is highly arrhythmogenic [6, 7]. Because the fundamental role of Cx43 in intercellular communication and action potential propagation, it seems likely that it might be a molecular target for novel approaches to prevent life-threatening cardiac arrhythmias.

We aimed to explore our hypothesis that different propensity to malignant arrhythmias in rats with altered thyroid status is most likely inversely associated with up- or down-regulation of myocardial Cx43 (in relation to PKCε expression).

2. Subject and Methods

The experiments were carried out on 3-month-old male Wistar rats. Rats were randomly divided into 3 groups: 1) euthyroid (EU), 2) hypothyroid (HY) and 3) hyperthyroid (TH). HY status was induced and maintained with a 0.05 % solution of methimazole in drinking water and TH status by intraperitoneal injection of T_3 (0.15 mg/kg body weight) three times a week. Red palm oil (RPO) was administered orally daily to half of animals a week before and during six week thyroid hormone alteration period (100 µl/100g BW/day). At the end of experiment body weight (BW), blood glucose (BG) as well as the levels of T_3 and T_4 were registered. The heart was excised into ice-cold saline and both heart (HW) and left ventricular weight (LVW) were quickly registered. Snap frozen left ventricular (LV) tissue was taken for Cx43, PKCε protein analysis using western blots [8] and for mRNA determination by Real Time PCR. Threshold to induce VF in fibrillating heart were estimated using isolated heart preparation as described elsewhere [8]. Statistical evaluations was performed using ANOVA and Bonferroni's Multiple Comparison Test. Data were expressed as mean ± SD to analyze the statistical significance determined at $P < 0.05$.

3. Results

As shown in Table 1 the administration of T_3/T_4 or methimazole caused TH or HY status of experimental rats. RPO significantly increased T_3 level in the HY rats, even above the level of the EU rats. Compared to EU, TH status was characterized by significant increase of HW, LVW, while HY status led to a decrease of LVW. BG was increased in the TH group and it was further enhanced by RPO. Compared to EU rats the threshold to induce sustained VF was significantly lower in TH group and this decrease was partly compensated by RPO intake. In contrast to TH rats, it was not possible to induce VF in the HY and HY+RPO rats even by the highest stimulus strengths (50 mA). There was no significant difference in myocardial mRNA levels for Cx43 in the TH versus EU rats unlike the HY and HY+RPO rats, in which Cx43 gene transcription was markedly increased (Fig. 1). RPO intake did not affect Cx43 mRNA expression in either group. As shown by WB (Fig. 2A), expression of total Cx43 protein (Fig. 2A, B) as well as its phosphorylated forms (Fig. 2A, C) were significantly decreased in TH and increased in the HY compared to the EU rats. Intake of RPO enhanced levels of both total and phosphorylated forms of Cx43 in TH compared to EU status and suppressed, although not significantly, elevation of Cx43 in the HY rats. Comparing to EU rats, mRNA (Fig. 3A) as well as protein expression for PKCε (Fig.3B,C) were significantly increased in the HY unlike TH rats, in which both parameters were significantly decreased. RPO intake had no effect on Cx43 mRNA levels, but it partly normalized changes in rats with altered thyroid status.

Table. 1 Main characteristics of rats with altered thyroid status without and with RPO intake

	EUc	EUrpo	THc	THrpo	HYc	HYrpo
T3 (nmol/l)	1.2 ± 0.3	1.4 ± 0.2	3.1 ± 1.3*	3.1 ± 1.8	0.85 ± 0.07*	1.9 ± 0.2#
T4 (nmol/l)	49 ± 18	71 ± 10	122 ± 40*	107 ± 22	14 ± 2*	14 ± 1,5
BG(mmol/l)	3.33 ± 1.05	4.43 ± 0.38	5.23 ± 0.06*	6.18 ± 0.22#	3.87 ± 0.40	4.03 ± 0.49
BW (g)	379 ± 88	411 ± 7	419 ± 50	414 ± 52	406 ± 14	346 ± 49#
HW (g)	1.04 ± 0.18	1.15 ± 0.08	1.35 ± 0.1*	1.18 ± 0.12#	0.84 ± 0.08	0.81 ± 0.03
LVW (g)	0.75 ± 0.14	0.82 ± 0.01	0.97 ± 0.04*	0.84 ± 0,13#	0.59 ± 0.04*	0.57 ± 0.02
Threshold for sVF	31.2 ± 9.7	45.1 ± 7.8	14.2 ± 3.7*	23.3 ± 7.6#	50 ± 0*	50 ± 0

Abbreviations: Euthyroid control rats (Euc, n = 6), EU rats treated with RPO (Eurpo, n = 6), hyperthyroid rats (THc, n = 6), TH rats treated with RPO (THrpo, n = 6), hypothyroid rats (HYc, n = 6), HY rats treated with RPO (HYrpo, n = 6), BG-blood glucose, BW-body weight, HW-heart weight, LVW- left ventricular weight, sVF - sustained ventricular fibrillation. Data are means ± SD, $^{*}P < 0.05$ *vs* EUc, $^{\#}P < 0.05$ untreated *vs* treated

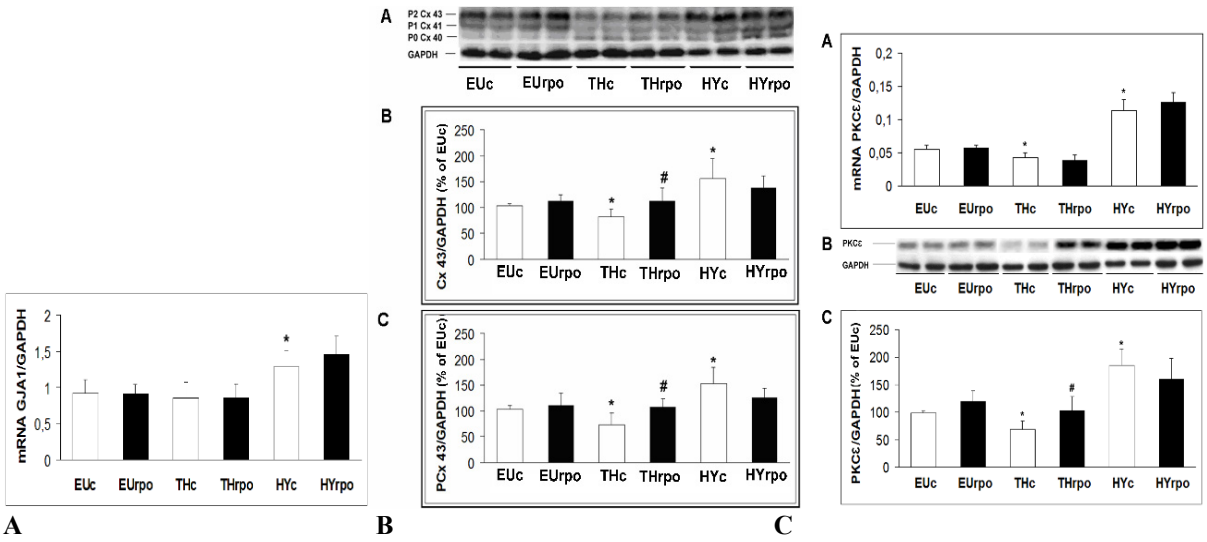

Fig. 1: A. Myocardial expression of mRNA CXA1 normalized to GAPDH in rats with altered thyroid status, B. Expression of myocardial total Cx43 protein (A, B) and its phosphorylated forms (A, C) normalized to GAPDH in rats with altered thyroid status. C. Myocardial expression of PKCε mRNA (A) and protein (B, C) normalized to GAPDH in rats with altered thyroid status. Abbreviations: Euthyroid control rats (Euc, n = 6), EU rats treated with RPO (Eurpo, n = 6), hyperthyroid rats (THc, n = 6), TH rats treated with RPO (THrpo, n = 6), hypothyroid rats (HYc, n = 6), HY rats treated with RPO (HYrpo, n = 6). Data are means ± SD, $^{*}P < 0.05$ *vs* EUc, $^{\#}P < 0.05$ untreated *vs* treated with RPO.

4. Discussion

According to the general classification of cardiac arrhythmias all disturbances of rhythm result from one of two primary abnormalities in electrical activity. The first is an abnormality in impulse initiation and the second, an abnormality in impulse propagation, whereby both may co-exist [9]. The former abnormality is associated particularly with triggered activity and/or abnormal automaticity, whereas the latter with block of conduction and re-entry. In this context it should be noted that down-regulation of Cx43 in TH rats is most likely crucial in the process of arrhythmogenesis due to promoting of re-entry mechanism and hence VF [6], while an increase of K^{+}, Ca^{2+} and RyR currents in TH rats [10] can contribute to development of transient arrhythmias by promoting triggered activity [1]. In contrast, suppression of these channels activity in HY status can decrease this risk. Transient arrhythmias in the setting of impaired Cx43-mediated cell-to-cell coupling often lead to VF. We have further demonstrated that RPO intake resulted in increase of threshold to induce VF and shortening the time to sinus rhythm restoration in the TH rats. Antiarrhythmic effect of RPO was associated predominantly with up-regulation of Cx43 protein together with an increase of its functional phosphorylated forms. This fact points out the implication of Cx43 in prevention of malignant arrhythmias. PKCε has been shown to be involved in Cx43 phosphorylation and to be implicated in influence of conductivity and permeability of Cx43 channels [11]. Noteworthy, the protein as well as mRNA levels for PKCε were up-regulated in HY but down-regulated in TH status. It appears that thyroid hormones affect PKC signaling pathway in the heart by modulation of PKC gene transcription. Positive correlation between myocardial expression of PKCε and phosphorylated forms of Cx43 suggests its implication in Cx43 phosphorylation. RPO intake resulted in up-regulation of both PKCε and Cx43 protein expression in the TH rats that can explain its antiarrhythmic effects. Besides, antioxidant-rich RPO can via inhibition of oxidative stress prevent Cx43 degradation [12]. However, it is not clear yet how the enhancement and suppression of Cx43 phosphorylation by PKCε in rats with altered thyroid status would affect Cx43 channel function. Data dealing with direct Cx43 channel

related conductivity in the TH or HY rat heart are missing. Nevertheless, we have shown previously that down-regulation of PKCε and Cx43 proteins was associated with faster myocardial conduction velocity (CV) in the the TH comparing to EU rats [4]. Taken together, we can speculate that partial slowing of Cx43 channels conduction (in case of the diabetic and the HY rats as well as the RPO-treated TH rats) can make the heart more electrically stable likewise slowing of voltage-dependent Na^+ channels (involved in conduction of electrical signals) by antiarrhythmic agents. In conclusion, our findings indicate that there is an inverse relationship between myocardial Cx43 expression and susceptibility of the heart of rats with altered thyroid status to VF. RPO intake increased threshold for induction of VF in hyperthyroid rats apparently expressed due to up-regulation of Cx43.

References

[1] Tribulova N, Knezl V, Shainberg A, et al. Thyroid hormones and cardiac arrhythmias. *Vascular Pharmacology* 2010;52:102-12.

[2] Soukup T. Effects of long-term thyroid hormone level alteration, n-3 poly-unsaturated fatty acid supplementation and statin administration in rats. *Physiological Research* Suppl, 2014.

[3] Dilmann WH. Cellular action of thyroid hormone on the heart. *Thyroid* 2002;447-466.

[4] Lin H, Mitasikova M, Dlugosova K, et al. Thyroid hormones suppress epsilon-PKC signalling, down-regulate connexin-43 and increase lethal arrhythmia susceptibility in non-diabetic and diabetic rat hearts. *Journal of Physiology and Pharmacology* 2008;59:271-85.

[5] Mitasíková M, Smidová S, Macsaliová A, et al. Aged male and female spontaneously hypertensive rats benefit from n-3 polyunsaturated fatty acids supplementation. *Physiol Res* 2008;57:39-48.

[6] Saffitz JE, Laing JG, Yamada KA. Connexin expression and turnover : implications for cardiac excitability. *Circulation Research* 2000;86:723-8.

[7] Tribulová N, Knezl V, Okruhlicová L, et al. Myocardial gap junctions: targets for novel approaches in the prevention of life-threatening cardiac arrhythmias. *Physiological Research* 2008;57:1-13.

[8] Benova T, Viczenczova C, Radosinska J, et al. Melatonin attenuates hypertension-related proarrhythmic myocardial maladaptation of connexin-43 and propensity of the heart to lethal arrhythmias. *Canadian Journal of Physiology and Pharmacology* 2013;91:633-9.

[9] Hoffman BF, Rosen MR. Cellular mechanisms for cardiac arrhythmias. *Circulation Research* 1981;49:1-15.

[10] Nishiyama A, Kambe F, Kamiya K, et al. Effects of thyroid status on expression of voltage-gated potassium channels in rat left ventricle. *Cardiovascular Research* 1998;40:343-51.

[11] Salameh A, Dhein S. Pharmacology of gap junctions. New pharmacological targets for treatment of arrhythmia, seizure and cancer? *Biochimica et Biophysica Acta* 2005;1719:36-58.

[12] Smyth JW, Hong TT, Gao D, et al. Limited forward trafficking of connexin 43 reduces cell-cell coupling in stressed human and mouse myocardium. *The Journal of Clinical Investigation* 2010;120:266-79.

Evaluation of Repeated Global Ischemia in Isolated Rabbit Heart

[1,2]M. Ronzhina, [3]V. Olejníčková, [3]T. Stračina, [1]T. Potočňák, [1,2]O. Janoušek, [1,2]P. Veselý, [1,2]J. Kolářová, [2,4]M. Nováková, [1,2]I. Provazník

[1]Brno University of Technology, Brno, Czech Republic,
[2]International Clinical Research Center – Center of Biomedical Engineering, St. Anne´s University Hospital Brno, Brno, Czech Republic,
[3]Masaryk University, Brno, Czech Republic,
[2]International Clinical Research Center – Animal Center, St. Anne´s University Hospital Brno, Brno, Czech Republic
Email: ronzhina@feec.vutbr.cz

Abstract. *The paper is focused on evaluation of morphology changes of electrograms recorded from isolated rabbit hearts during experiments with short repeated global ischemia with and without prior loading of the heart with voltage-sensitive dye di-4-ANEPPS. It is shown that degree and time course of certain morphology changes in these two cases are quite different and must be taken into account.*

Keywords: Isolated rabbit heart, repeated global ischemia, electrogram, voltage-sensitive dye

1. Introduction

Animal models are often used to study the changes of heart electrical activity caused by myocardial ischemia. Rabbit biomodel is quite useful tool because of the similarity of rabbit cardiac physiology to that of human. Conventional ECG technique and optical recording of action potential using voltage-sensitive dye (VSD) can be successfully employed simultaneously in such studies. However, it is known that some VSDs, such as frequently used di-4-ANEPPS, may affect cardiac tissue of various species [1]. Consequently, results of analysis of ECG data recorded during experiment with VSD application must be carefully interpreted taking into account possible signal changes related to VSD side effects.

In this study, the time course of changes caused by global repeated ischemia has been investigated in EGs recorded from isolated rabbit hearts without chemical intervention and undergoing loading with di-4-ANEPPS. Four morphological indexes calculated from EGs have been evaluated using the ischemic changes sensor to describe their capacity to detect the ischemic changes in both cases.

2. Methods

The animal experiments were performed in accordance with the guidelines for animal treatment approved by local authorities and conformed to the EU law. The isolated hearts of twelve New Zealand rabbits perfused with Krebs-Henseleit solution (1.25mM Ca^{2+}, 37°C) according to Langendorff in the mode of constant perfusion pressure were used [2].

The electrograms (EGs) were recorded simultaneously by touch-less method using the orthogonal system which includes three pairs of Ag-AgCl disc electrodes (see Fig. 1a) placed in the bath wall. The sampling frequency of 2 kHz was used for the correct detection of QRS complexes.

EGs were recorded according to two protocols. In the first one (see Fig. 1b), VSD di-4-ANEPPS was added to the perfusate to record left ventricular action potential by optical method simultaneously with EG (optical part of recording system is not shown in Fig. 1a).

After stabilization period (20 min), heart was loaded with di-4-ANEPPS for 20 minutes. After washout (15 min) and control (5 min), three consecutive periods of ischemia and reperfusion (10 min each) were carried out. More detailed information about experimental setup and data recording according to this protocol can be found in [2]. In the second type of experiments, only EGs were recorded in isolated hearts. Thus, dye loading and washout periods were excluded from the second experimental protocol (see Fig. 1c). Control and three ischemia-reperfusion repetitions (of the same duration as in the first experimental setup) were followed by 30 minutes long stabilization period.

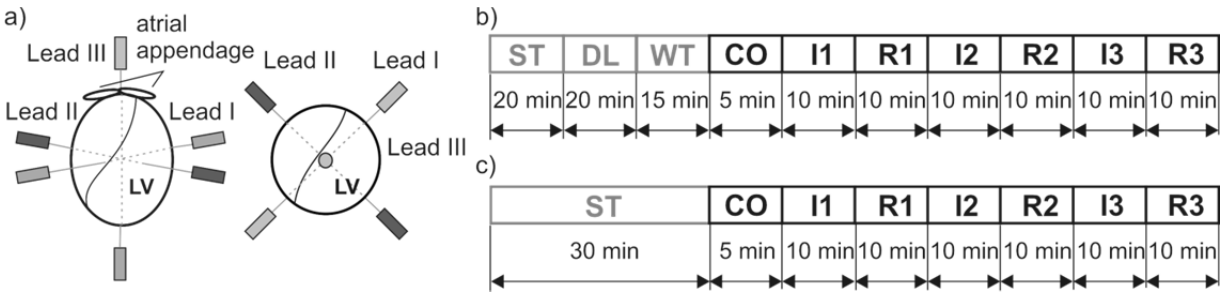

Fig. 1. Electrograms recording: a) orthogonal system of electrodes, b) protocol of experiments with voltage-sensitive dye di-4-ANEPPS application, c) protocol of experiments without di-4-ANEPPS application. LV – left ventricle, ST – stabilization, DL – loading with di-4-ANEPPS, WT – washout, CO – control, I1, I2, I3 – ischemia, R1, R2, R3 - reperfusion.

EGs recorded using lead II (depicted with dark grey colour in Fig. 1a) during control and ischemia-reperfusion periods (depicted with black in Fig. 1b and Fig. 1c) were used for further analysis. The low-frequency baseline wander was suppressed using Lynn's filter with cut-off frequency of 0.5 Hz. QRS complexes were then detected automatically with the wavelet based detector and verified manually. The beginning of QRS, J point, and the end of T wave were manually detected to calculate four *indexes*: duration of QJ interval (QJ width), position of maximum deviation of JT interval with respect to the J point (J-Tmax width), level of JT interval at J+10ms (JT10 level), and maximum deviation of JT interval (J-Tmax).

The ischemic changes sensor (ICS) previously introduced by García et al. [3] was then used to describe the indexes changes caused by repeated short-term global ischemia. The ICS describes the changes in EG indexes during ischemic (or reperfusion) period in relation with background noise represented with the standard deviation of a certain index in control period. The ICS was estimated for all indexes for every 10 seconds from the beginning of the first ischemic period to the end of the third reperfusion period.

3. Results

The example of typical time courses of indexes calculated from EG recorded during control period and first ischemia-reperfusion repetition and corresponding EGs are shown in Fig. 2. Progress of morphological changes in lead II EG during global ischemia can be divided into following parts: 1) widening of QJ interval from the 1st second of ischemia and often inversion of T wave (B in Fig. 2), 2) shifting of the T wave to the QRS complex (is associated with QT shortening) (B-C in Fig. 2), 3) changes in JT (elevation) and inverting of T wave back to the positive values at the 5th minute of ischemia (C in Fig. 2), 4) overlapping of depolarization and repolarization phases of EG after 5-7 minutes of ischemia (D in Fig. 2). In reperfusion, the backward changes occur (E-F in Fig 2). These changes are carried out more quickly than in ischemia and thus EG morphology at the 3rd minute of reperfusion is almost the same as in control period (A in Fig. 2).

Time courses of mean ICS calculated from their absolute values among six experiments (for experiments with and without VSD application individually) during repeated ischemia are presented in Fig. 3.

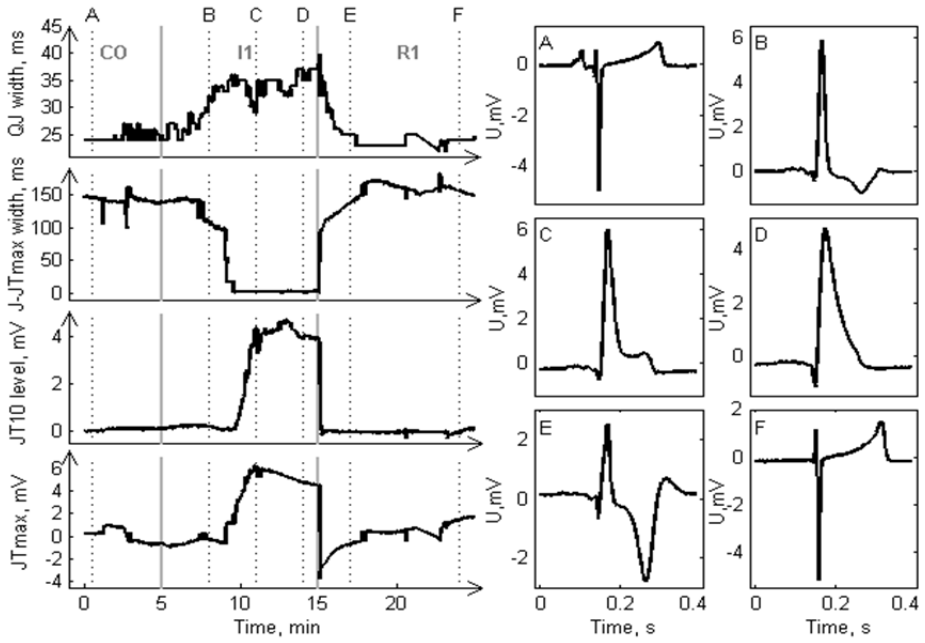

Fig. 2. EG morphology changes (lead II) caused by global ischemia (experiment without application of di-4-ANEPPS): time courses of EG indexes calculated from control to the end of the first reperfusion period (left), corresponding EG courses (right). CO – control, I1, R1- first ischemic and reperfusion period, respectively.

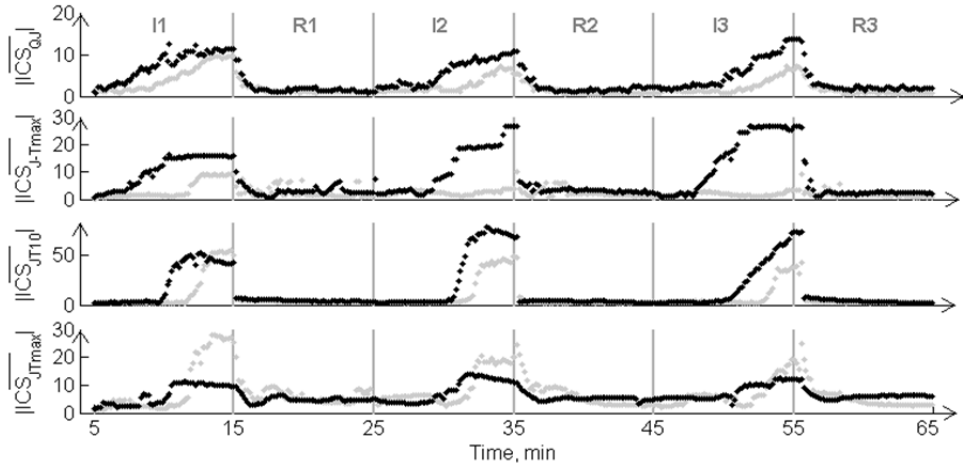

Fig. 3. Mean of absolute values of ICS indexes among six experiments with (light-grey) and without (black) application of di-4-ANEPPS during three ischemia-reperfusion repetitions. I1, I2, I3 – ischemic periods, R1 ,R2 ,R3 – reperfusion periods.

It is obvious that indexes calculated from data recorded according to the first protocol except for J-Tmax show larger values of mean ICS, indicating that these indexes have larger capacity to detect ischemic changes in such data. For both data sets, mean ICS values of all indexes calculated for different ischemia-reperfusion repetitions are quite similar. QJ and J-Tmax calculated from the first data set have the highest ICS value during the 1st ischemia, whereas J-Tmax and JT10 calculated from the second data set have the highest ICS during 2nd and 3rd ischemia. Moreover, J-Tmax of the data recorded with SVD application does not show marked changes in its mean value during the 2nd and 3rd ischemia.

Mean ICS calculated for different indexes during the 1st ischemia-reperfusion repetition are presented together in Fig. 4 to further evaluation. During the first half of ischemia, the larger ICS values are characteristic for QJ and J-Tmax and for QJ and J-Tmax calculated from the first and second data set, respectively. It implies a faster response of these indexes to ischemia. Moreover, the changes occur earlier in the second case. In both cases, JT10 has the largest ICS value than other indexes from the 5th minute of ischemia. Moreover, ICS for J-Tmax is much more noticeable and ICS for J-Tmax is slightly higher than other ICS. It is obvious from Fig. 3 and Fig. 4 that the changes in indexes during ischemic periods are slower than the return of indexes to their control values at the beginning of reperfusion.

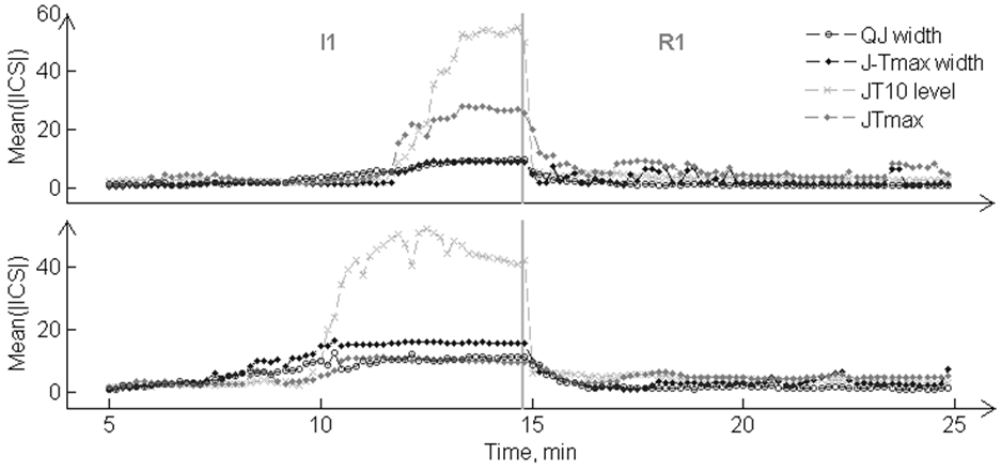

Fig. 4. Time course of mean ICS indexes (absolute values among six experiments) during the first ischemia-reperfusion repetition for experiments with (top) and without (bottom) application of di-4-ANEPPS. I1, R1 – first ischemic and reperfusion period, respectively.

4. Conclusions

The degree and time course of ischemic changes of some indexes calculated from EG recorded in experiments with and without di-4-ANEPPS application are quite different. These differences are probably due to effect of VSD on myocardial tissue and must be taken into account. In both cases, the changes in JT part of EG are delayed with respect to changes in QJ part for approx. 2 minutes. All ischemic changes are fully reversible in both cases.

Acknowledgements

The work was supported by European Regional Development Fund - Project FNUSA-ICRC (No. CZ.1.05/1.1.00/02.0123), grant projects of the Grant Agency GACR 102/12/2034, and MUNI/A/0957/2013.

References

[1] Fialova K, Kolarova J, Provaznik I, Novakova M. Comparison of voltage-sensitive dye di-4-ANEPPS effects in isolated hearts of rat, guinea pig, and rabbit. In proceedings of Computing in Cardiology 2010, 2010, 1-4.

[2] Kolářová J, Fialová K, Janoušek O, Nováková M, Provazník I. Experimental methods for simultaneous measurement of action potentials and electrograms in isolated heart. *Physiological Research,* 59(S1): 71-80, 2010.

[3] García J, Wagner G, Sörnmo L, Olmos S, Lander P, Laguna P. Temporal evaluation of traditional versus transformed ECG-based indexes in patients with induced myocardial ischemia. *Journal of Electrocardiology*, 33: 37-47, 2000.

Electrocardiographic Predictors of Response to Vasoreactivity Testing in Patients with Pulmonary Arterial Hypertension

[1]E. Blinova, [1]T. Sakhnova, [1]O. Arkhipova, [1]N. Danilov, [1]T. Martynyuk,

[1]I. Chazova, [2]V. Trunov, [2]E. Aidu

[1]Cardiology Research Complex, Moscow, Russia,
[2]Institute for Information Transmission Problems RAS, Moscow, Russia
Email: blinova2009.73@gmail.com

Abstract. *The aim: to assess the possibilities of electrocardiography for prediction of response to vasoreactivity testing (VT) in patients with pulmonary arterial hypertension (PAH). 65 PAH patients who underwent right-heart catheterization and VT were evaluated. We analyzed P wave amplitude in lead II, QRS axis, QRS duration, R and S wave amplitudes in leads V1 and V5, spatial QRS-T angle, magnitude G and spatial components Gx, Gy, Gz of the "recovery acceleration" vector. 23 responders to VT had lower mean pulmonary artery pressure (46.6±11.0 mm Hg versus 61.3±19.0 mm Hg, p <0.01), PII (1.70±0.79 mm versus 2.34±0.97 mm, p <0.01), QRS-T angle (61.3±27.3 dgr versus 104.5±39.9 dgr, p <0.01), RV1+SV5 (8.98±5.04 mm versus 15.7±8.0 mm, p <0.01) and higher values of Gx (22.6±15.1 ms versus 5.3±17.9 ms, p <0.001) and Gy (22.6±11.2 ms versus 8.8±8.4 ms, p <0.001) as compared with non-responders. The most informative variables were Gx (the area under the ROC curve 0.77, SE 0.07), Gy (0.84±0.06) and QRS-T angle (0.81±0.05). On multivariate logistic regression analysis Gy emerged as an independent predictor of response (OR 1.17; 95% CI 1.06-1.30; p = 0.01). Decartographic parameters of repolarization may be helpful for predicting the results of VT in patients with PAH.*

Keywords: pulmonary arterial hypertension, electrocardiography, acute pulmonary vasodilator testing

1. Introduction

Vasoreactivity testing (VT) in patients with pulmonary arterial hypertension (PAH) is important for the optimization of the treatment and evaluation of prognosis [1], [2]. The commonly used test with inhaled nitric oxide (iNO) is well tolerated, has minimal side effects, but time-consuming and needs special equipment [3]. The use of simple noninvasive techniques for predicting the VT results may be of interest, but the available data about the predictors of response are small. The aim of the study was to assess the possibilities of electrocardiographic parameters for prediction of response to VT in patients with PAH.

2. Subject and Methods

Patients

65 patients (mean age 41.4±12.4 years; 81% women) with PAH who underwent right-heart catheterization and VT were evaluated. The diagnosis of PAH was made according to the current guidelines definition [4]. The presence of PAH was verified with clinical and instrumental methods. There were 10 patients with chronic thromboembolic disease, 4 patients with systemic sclerosis, 3 patients with septal defects, 2 patients with portal hypertension, in 46 patients after comprehensive clinical and instrumental examination PAH was considered to be idiopathic. All patients underwent echocardiographic examination using

a high-quality ultrasound machine (Vivid 7; GE, USA). The estimated systolic pulmonary artery pressure (SPAP) was defined as the right ventricular to right atrial pressure gradient added to the right atrial pressure. Right atrial pressure was estimated 5 to 15 mm Hg, according to the diameter and inspiratory collapse of the inferior caval vein.

Electrocardiography

Conventional 10-s digital electrocardiograms were recorded by certified ECG technicians using the standard 12-lead electrode configuration on commercially available digital electrocardiograph and averaged into 1 single beat. ECG parameters under investigation were: P wave amplitude in lead II (PII), QRS axis, QRS duration, R and S wave amplitudes in leads V1 and V5. The averaged beat was also converted into a derived orthogonal-lead beat and processed by means of software developed in Cardiology Research Complex and Institute for Information Transmission Problems. We studied spatial QRS-T angle and magnitude G (in ms) and spatial components Gx, Gy, Gz of the "recovery acceleration" vector (directed to the left, inferior, and anterior). Decartographic "recovery acceleration" map shows the distribution of the dipole component of the depolarized state duration over the heart surface, projected onto the image sphere which encloses the heart ventricles. The image sphere radius is taken equal to the maximum magnitude of the heart vector in the QRS period. The use of the maximal QRS vector as a scale helps to understand more clearly internal interrelationships between different parts of QRST complex. Concerning the electrophysiological meaning, "recovery acceleration" vector is close to the ventricular gradient vector.

Right Heart Catheterization with VT

All PAH patients underwent right heart catheterization, during which pulmonary artery pressure (PAP), right atrial and right ventricular pressure, pulmonary capillary wedge pressure were measured using Swan-Ganz catheter("Edwards", USA). Cardiac output was calculated using Fick's method. Pulmonary vascular resistance (PVR) was calculated by dividing the transpulmonary gradient (pressure difference between mean PAP and pulmonary capillary wedge pressure) by cardiac output. Following the measurement of baseline hemodynamic parameters, acute vasodilators (iNO or/and PGE1) were administered sequentially. iNO was administered via face mask at start concentration 10 ppm, with increase to 20 and 40 ppm every 5 minutes. After 15 minutes of administration hemodynamic parameters were measured. After 30 minutes of a washout phase PGE1 was administered intravenously at start dosage 0.4 mg/ml/kg which every 10 minutes was redoubled up to maximal dosage 1.6 mg/ml/kg. Responders were defined as patients who showed a decrease in mean pulmonary artery pressure of at least 10 mmHg to an absolute level below 40 mmHg with preserved or increased cardiac output at least with one vasodilator.

Statistical Analysis

Data were analyzed using MedCalc Statistical Software version 12.7.8 (MedCalc Software bvba, Ostend, Belgium). Results are presented as mean ± standard deviation. To evaluate the differences between two independent samples unpaired t-test was used. A value of $p<0.05$ was considered to be statistically significant.

3. Results

There were 23 (35%) responders to VT. Baseline clinical characteristics and hemodynamic findings in responders and non-responders are presented in Table 1. Statistically significant ($p<0.05$) differences are marked with *.

Table 1. Baseline clinical characteristics and hemodynamic findings in responders and non-responders to VT.

Parameter	Responders	Non-responders
Age, years	39.6±10.6	42.7±13.3
% females	96	74*
Functional class	2.13±0.55	2.67±0.68*
Heart rate, bpm	69.5±10.8	81.3±13.7*
SPAP, mm Hg	71,5±17.3	99.5±26.6*
Mean PAP, mm Hg	46.6±11.0	61.3±19.0*
PVR, dyn•s/cm5	837±447	1386±741

Baseline electrocardiographic characteristics in responders and non-responders are presented in Table 2. Statistically significant ($p<0.05$) differences are marked with *.

Table 2. Baseline electrocardiographic characteristics in responders and non-responders to VT.

Parameter	Responders	Non-responders
PII, mm	1.70±0.79	2.34±0.97*
QRS axis, degrees	89.7±42.2	105.6±51.8
QRS duration, ms	101.0±7.6	106.3±15.6
RV1+SV5, mm	8.97±5.04	15.72±8.01*
spatial QRS-T angle, degrees	61.3±27.3	104.4±39.9*
Gx, ms	22.56±15.08	5.31±17.87*
Gy, ms	22.57±11.24	8.76±8.43*
Gz, ms	6.87±19.64	4.55±18.43

At receiver operating characteristic curve analysis the most informative variables were Gx (the area under the ROC curve 0.77, SE 0.07), Gy (0.84±0.06), QRS-T angle (0.81±0.05) and RV1+SV5 (0.76±0.06). On multivariate logistic regression analysis after correction for age, sex, heart rate, WHO class, and echocardiographic systolic pulmonary artery pressure, Gy emerged as an independent predictor of response (odds ratio, 1.17; 95% confidence interval 1.06-1.30; $p = 0.01$).

4. Discussion

Predicting of the VT results in PAH patients by simple noninvasive techniques may be useful in clinical practice. Some attempts were made to do it by means of echocardiography [5]. Results of 6-minute walking test also may have predictive value. In our study non-responders

as compared with responders were characterized with the more pronounced changes of electrocardiographic parameters, which corresponded to the more deteriorated hemodynamic state. It is interesting to note that parameters which describe cardiac repolarization in its relation to the preceding depolarization, namely spatial QRT-angle and components of the "recovery acceleration" vector were the most informative. Ventricular gradient, which is close to "recovery acceleration" vector, and especially spatial QRT-angle were shown to be important for mortality prediction in different clinical populations [6], [7], [8]. From theoretical point of view, these parameters may reflect the changes in myocardial electrophysiological properties, namely, the alteration in action potential duration heterogeneity in the ventricles. Further research of the mechanisms of ECG changes in right ventricular hypertrophy may contribute to the more accurate evaluation of the heart state in PAH patients.

5. Conclusions

The use of repolarization process mapping by DECARTO technique may be helpful for predicting the results of VT in patients with PAH.

References

[1] Galie N, Hoeper MM, Humbert M, et al. Guidelines for the diagnosis and treatment of pulmonary hypertension. *Eur Respir J,* 34:1219-1263, 2009.

[2] Malhotra R, Hess D, Lewis GD, et al. Vasoreactivity to inhaled nitric oxide with oxygen predicts long-term survival in pulmonary arterial hypertension. *Pulm Circ*, 1:250-258, 2011.

[3] Ricciardi M.J., Knight B.P., Martinez F.J., Rubenfire M. Inhaled nitric oxide in primary pulmonary hypertension: a safe and effective agent for predicting response to nifedipine. *J Am Coll Cardiol*, 32(4): 1068-1073, 1998.

[4] McLaughlin V.V., Archer S., Badesch D.B. et al. ACCF/AHA 2009 Expert Consensus Document on Pulmonary Hypertension: A Report of the American College of Cardiology Foundation Task Force of Expert Consensus Documents and the American Heart Association Developed in Collaboration With the American College of Chest Physicians; American Thoracic Society and the Pulmonary Hypertension Association. *J Am Coll Cardiol*, 53; 1573-1619, 2009.

[5] Liu YT, Li MT, Fang Q, et al. Right-heart function related to the results of acute pulmonary vasodilator testing in patients with pulmonary arterial hypertension caused by connective tissue disease. *J Am Soc Echocardiogr*, 25(3):274-279, 2012.

[6] Scherptong RW, Henkens IR, Kapel GF, et al. Diagnosis and mortality prediction in pulmonary hypertension: the value of the electrocardiogram-derived ventricular gradient. *J Electrocardiol,* 45(3):312-318, 2012.

[7] Kardys I, Kors JA, van der Meer IM, et al. Spatial QRS-T angle predicts cardiac death in a general population. *Eur Heart J*, 24(14):1357-1364, 2003.

[8] Yamazaki T, Froelicher VF, Myers J, Chun S, Wang P. Spatial QRS-T angle predicts cardiac death in a clinical population. *Heart Rhythm*, 2(1):73-78, 2005.

QRS Complex Changes after Pulmonary Endarterectomy in Patients with Chronic Thromboembolic Pulmonary Hypertension

[1]M. Boháčeková, [1]T. Valkovičová, [2]M. Kaldarárová, [1]I. Šimková, [3]L. Bachárová

[1]National Institute of Cardiovascular Diseases, Bratislava, Slovak Republic
[2]National Institute of Cardiovascular Diseases – Children's Cardiac Center, Bratislava, Slovak Republic
[3]International Laser Center, Bratislava, Slovak Republic
Email: marcela.bohacekova@gmail.com

Abstract. *Chronic thromboembolic pulmonary hypertension (CTEPH) is a progressive disease with persistent thrombotic occlusion of pulmonary artery bed with consequent right ventricular dilation and hypertrophy affecting ECG findings. The aim of the study was to analyze QRS complex changes after pulmonary endarterectomy in patients with CTEPH.* ***Material and Methods:*** *The study population consisted of 33 patients with CTEPH divided in two groups: Group (1): 21 operable patients (6F/15M, average age 64.1 years) undergoing endarterectomy; and Group (2): 12 non-operable patients (9F/3M, average age 68.9 years). The following ECG parameters were analyzed: maximum QRS spatial vector magnitude (QRSmax), Butler-Leggett formula for RVH (BL), Sokolow-Lyon criterion for RVH (SL-RVH). The right ventricular diameter (RVD) was measured by echocardiography.* ***Results:*** *A significant differences in SL-RVH (12.9±6.2mm vs 8.9±4.5mm) as well as in RVD (57±6.8mm vs 38.5±4.3mm) were found between the groups at the beginning of study. After endarterectomy the values of BL and SL-RVH decreased significantly (13.7±7.6mm vs 7.4±5.4mm and 12.9±6.2mm vs 6.4±3.3mm) as well as the RVD values (57±6.8mm vs 32.7±3.3mm). However, the changes in QRS and RVD did not correlate significantly.* ***Conclusion:*** *The lack of correlation in changes of QRS complex and RVD indicates that the decrease in RVD was not the main factor influencing the QRS complex voltage.*

Keywords: CTEPH, ECG, right ventricular hypertrophy, pulmonary endarterectomy

1. Introduction

Chronic thromboembolic pulmonary hypertension (CTEPH) is a progressive disease, defined as the mean pulmonary artery pressure ≥ 25 mm Hg following an episode of pulmonary thromboembolism. CTEPH is characterized by persistent thrombotic occlusion of pulmonary artery bed due to non-resolved and organized thrombus leading to vascular remodeling and resulting in pulmonary hypertension. The combination of persistent macrovascular obstruction, small vessel arteriopathy, and vasoconstriction results in pulmonary hypertension and right ventricular pressure overload. Presumed gradual progression of pulmonary hypertension occurs in the absence of documented recurrent pulmonary embolic events and is thought to reflect progressive remodelling of the unobstructed pulmonary vasculature, stimulated by increased blood flow through these vessels. If left untreated, the condition is fatal due to increased right ventricular afterload and right heart failure. Pulmonary endarterectomy (PEA) is the surgical procedure which removes the obstructing thromboembolic material, resulting in significant improvements of right ventricular hemodynamics and function.

The aim of the study was to study the ECG signs of right ventricular hypertrophy (RVH) in patients with CTEPH and their changes after pulmonary endarterectomy.

2. Material and Methods

The study population consisted of 33 patients with CTEPH (15 women/18 men, average age 66.5 years, ranged 42 to 81 years). The diagnosis of CTEPH was confirmed by right heart catheterization (RHC), with a mean pulmonary arterial pressure (PAP) equal or over 25 mmHg and a pulmonary wedge pressure (PCWP) equal or under 15 mmHg in accordance with ESC/ERS guidelines for the diagnosis and treatment of pulmonary hypertension [1].

The patients were divided in two groups:

Group 1: 21 operable patients (6 women/ 15 men, average age 64.1 years, ranged 42 to 74 years) who underwent pulmonary endarterectomy;

Group 2: 12 non-operable patients (9 women/ 3 men, average age 68.9 years, ranged 52 to 81 years) treated conservatively (anticoagulant therapy: warfarin/ low molecular weight heparin).

The 12 leads ECG was recorded and the following parameters were analyzed:

- the maximum spatial QRS vector magnitude (QRS max), calculated as:

  $$\text{QRS max} = \sqrt{[V_5^2 + aVF^2 + V_2^2]} \quad (1)$$

- Butler Leggett (BL) formula for RVH [2], calculated as:

  $$BL = [\text{tallest R or R' in } V_1 \text{ or } V_2 \text{ lead}] + [\text{deepest S in 1 or } V_6 \text{ lead}] + [\text{S in } V_1 \text{ lead}] \quad (2)$$

- Sokolow - Lyon (SL-RVH) criteria for RVH [3], calculated as :

  $$SL = [\text{R in } V_1 \text{ lead}] + [\text{S in } V_5 \text{ or } V_6 \text{ lead}] \quad (3)$$

The ECGs were examined by one trained person; the QRS amplitudes were measured manually. The right ventricular diameter (RVD) was measured echocardiographically.

All results are expressed as the mean ± standard deviation. The differences between groups were tested using Student's t-test, values of $p < 0.05$ were considered to be significant. Statistical analysis was performed using Windows Microsoft Excel 2007.

3. Results

The values of parameters under study are presented in Table 1.

Table 1. Values of parameters under study. SL-RVH: Sokolow-Lyon criterion for right ventricular hypertrophy; BL: Butler-Leggett formula; QRSmax: maximum QRS spatial vector magnitude; RVD: right ventricular diameter. ***: $p < 0.001$. Group 1: patients undergoing endarterectomy, Group 2: inoperable patients, treated conservatively.

		BL [mm] average (SD)	**SL - RVH [mm] average (SD)**	**QRS max [mm] average (SD)**	**RVD [mm] average (SD)**
Group 1	before PEA	13.7 (7.6)	12.9 (6.2)	16.4 (4.8)	57.0 (6.8)
	after PEA	7.4 (5.4)***	6.4 (3.3)***	15.1 (5.2)	32.7 (3.3)***
Group 2	before th	9.2 (7.1)	8.9 (4.5)	17.0 (4.6)	38.5 (4.3)
	after th	11.7 (10.2)	8.9 (4.6)	17.5 (5.2)	39.4 (7.8)

At the beginning of the study, there was a significant difference between the groups in SL-RVH (12.88 mm ± 6.15 mm vs 8.89 mm ± 4.48 mm), as well as in RVD (57 mm ±6.76 mm vs 38.5 mm ±4.30 mm).

In patients who underwent PEA, the values of SL-RVH and BL decreased significantly after the endarterectomy (12.88 mm ± 6.15 mm vs 6.37 mm ± 3.26 mm; and 13.65 mm ± 7.55 mm vs 7.35 mm ± 5.40 mm). No significant changes were observed in QRSmax. The echocardiographically measured RVD decreased significantly after the endarterectomy (57 mm ± 6.76 mm vs 32.67 mm ±3.26 mm)

The changes in QRS complex and RVD in patients after endarterectomy did not correlate significantly (Figure 1).

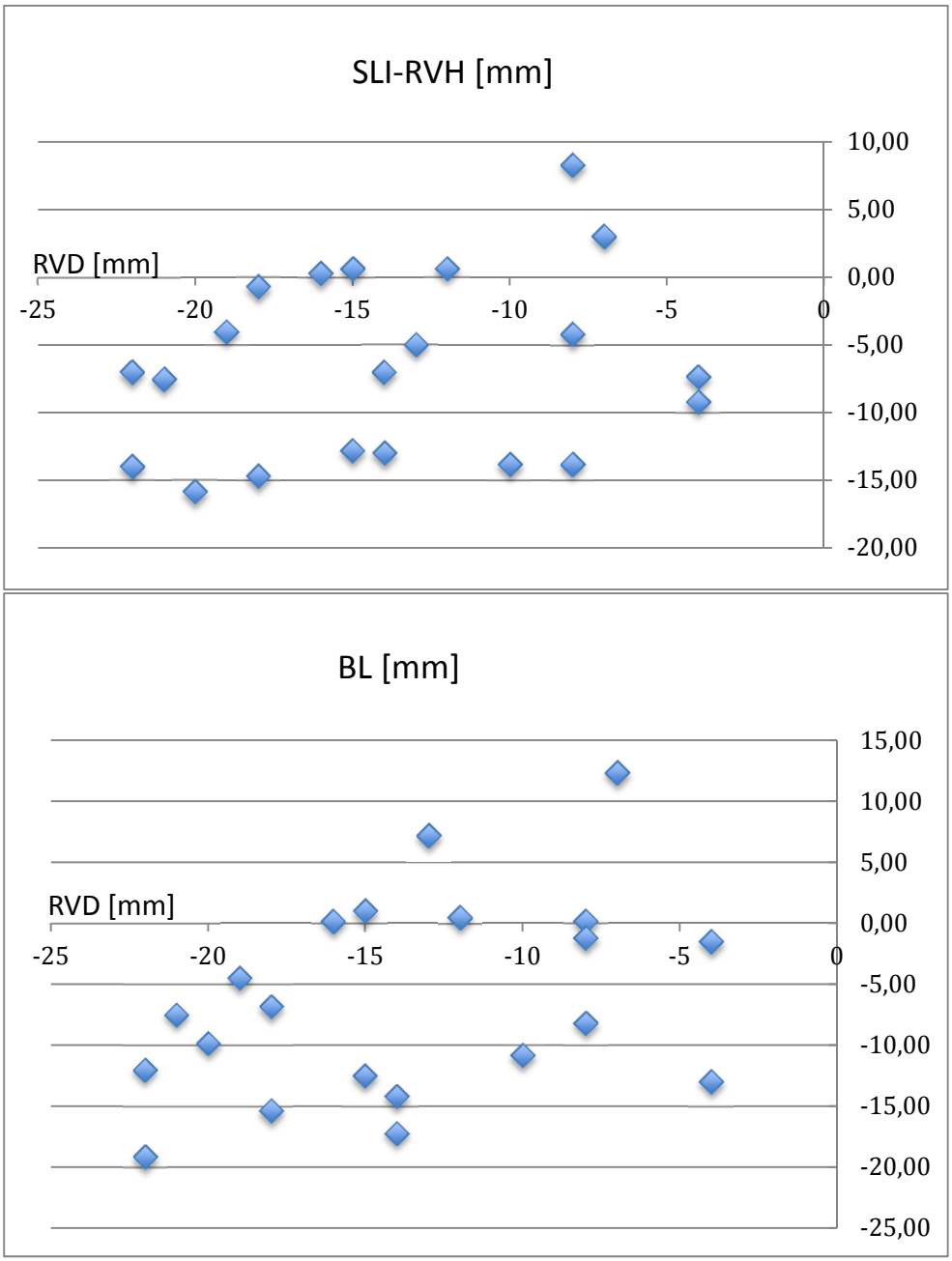

Fig. 1. The relation between the right ventricular diameter and Sokolow-Lyon criterion for RVH (top) and Buttler-Leggett criterion (bottom).

In contrary, no significant differences in SL-RVH and BL, as well as in RVD were observed in patients treated conservatively.

4. Discussion

There was a significant difference between groups at the beginning of the study. The Group 2 consisted of patients that were not indicated for endarterectomy because of the more severe clinical status and/or co-morbidities.

After endarterectomy the values of RVH-ECG indicators as well as RVD decreased significantly, on the other hand, in the patients treated conservatively this effect was not observed. It can be therefore suggested that these changes can be attributed to the improvement of the hemodynamic overload of the right ventricle. However the QRS changes and the decrease in the dimension of the right ventricular diameter did not correlate significantly, indicating that the reduction in the right ventricular diameter due to decreased volume overload did not affect the QRS amplitude as could be theoretically expected.

5. .Conclusions

The study results showed that patients with CTEPH after endarterectomy have significantly decreased ECG indices for RVH as well as decreased RVD. However these changes did not correlate, suggesting that the decrease in RVD was not the main factor influencing the QRS complex voltage.

References

[1] Galie N et al.: The Task Force for the Diagnosis and Treatment of Pulmonary Hypertension of the European Society of Cardiology (ESC) and the European Respiratory Society (ERS), endorsed by the International Society of Heart and Lung Transplantation (ISHLT). *Europ Heart J* 30: 2493-2537, 2009.

[2] Buttler PM, Leggett SI, Howe CM et al.: Identification of electrocardiographic criteria for diagnosis of right ventricular hypertrophy due to mitral stenosis. *Am J Cardiol* 57: 639-643, 1986.

[3] Sokolow M, Lyon TP: The ventricular complex in left ventricular hypertrophy as obtained by unipolar and limb leads. *Am Heart J* 37: 161–186, 1949.

Application of SFHAM Model for Diagnosis of Ischemic Heart Disease

[1]J. S. Janicki, [2]A. Teresińska, [3]W. Leoński, [1]M. Chąpiński, [4]M. Sobieszczańska, [5]R. Piotrowicz

1Physico-Medical Research Institute, Puszczykowo, Poland
2Department of Nuclear Medicine, Institute of Cardiology in Warsaw, Poland
3Institute of Physics, University of Zielona Góra, Zielona Góra, Poland
4Department of Pathophysiology, Wrocław Medical University, Wrocław, Poland
5Department and Clinic of Cardiac Rehabilitation, Institute of Cardiology, Warsaw, Poland
Email: prezes@ibf.com.pl

Abstract. Introduction. *The ECG examination allows to obtain information about the electrical processes occurring in the heart, the course of which may be disturbed by a number of pathological changes occurring in it. However, the both, currently used criteria and issues in interpretation of the results, lead to limited diagnostic value of this method. Any improvement in ECG examination requires considerable extension of currently applied electric signals analysis. To achieve this, we have used proposed in [1] model of the electrical activity of the heart – SFHAM. This model describes the morphology of the QRS complex, and was implemented in the SATRO ECG system. Our main aim was to assess the effectiveness of SATRO ECG system in CHD diagnosis, and compare its results with those of myocardial perfusion scintigraphy Tc99m SPECT.*

Methods and Materials. *For a group of 243 subjects (75 females and 168 males, average age: 58±10 years) supposed to have CHD, standard resting and stress ECG (ECG (R) and ECG (S), respectively), and examinations of myocardial perfusion disturbances using perfusion scintigraphy method SPECT were performed. Then, with use of SATRO ECG system, parameters describing electric activity of various segments of the left ventricle were calculated on basis of ECG (R) results.*

Results. *Sensitivity of SATRO ECG in CHD diagnosing was equal to 100% and specificity 70%, whereas predictive values of the positive and negative results were equal to 98% and 100%, respectively. Moreover, statistical kappa Cohen test showed that statistical correlation between SATRO ECG and SPECT methods ($k=0.817$, $p<0.001$) exists. Such correlations are not detected when SPECT was compared to ECG (R) ($k = 0.055$, $p = 0.031$) and ECG (S) ($k = 0.018$, $p = 0.294$).*

Conclusions. *SATRO ECG examination method seems to be more useful in detecting perfusion defects recognized with use of SPECT method, as compared with resting and stress ECG. The results of the comparative assessment revealed a high correlation between test results of SATRO ECG and SPECT in diagnosis of the both: CHD and location of the blood supply to the heart muscle disorders.*

Keywords: ECG; QRS complex; SATRO ECG; SFHAM; CHD

1. Introduction

The existing ECG diagnosis methods of myocardial ischemia, based on the analysis of ECG signals most often concern the evaluation of parameters related to the shape of the ST-segment and QRS complex. However, the mentioned features of ECG are relatively insensitive and less specific symptom of ischemia, particularly if the analysed electrocardiogram was performed during the period when patients did not suffered from pain,

and for persons with a low probability of coronary artery disease (CAD) [2,3]. Moreover, QRS vectorcardiogram analysis based on a standard method of convolution and deconvolution and described in [4, 5], not lived to see the independent tests that would confirm its effectiveness in the assessment of CHD.

A low diagnostic value of ECG components related to ventricular muscle repolarisation mechanism, encourages for drawing attention to the potential application of observations of ventricular depolarization abnormalities in the diagnosis of CHD. However, the evaluation of parameters of the electrical activity of individual segments of the left ventricle of heart requires a significant exceeding the limits established by methods of analysis used so far. At this point, newly defined and applied models of electrical heart activity could be helpful.

Thus, discussed here, *single fibres heart activity model* (SFHAM) proposed in [1], could be potentially exploited for our purposes. This model was implemented in diagnostic system SATRO ECG. For recollection, within the frame of SFHAM, electrical activity of the heart is presented as the effect of propagation of electric charge waves along a "effective" myocardial fibres. Each fibre represents a particular segment of the left ventricle, and this representation is related to the both: anatomy of ventricle and structure of the hearth's electrical conduction system. For each of the fibres, based on the dynamics of charges flow through the cell membrane, propagation of the depolarization wave was determined. Decrease in conduction velocity inside the fibres caused by ischemia reduces the density of the resultant electric charge. This reduction, influences the ECG signal measured on the surface of the chest.

The main objective of this study is objective verification of SATRO ECG method, in particular, the evaluation of SATRO ECG system in the both: diagnosis of CHD and location of the disorders in blood supply to the heart muscle. Such verification can be done with use of the results obtained from perfusion scintigraphy Tc99m SPECT examination.

2. Methods and Materials

In this study 243 people over 30 years of age (75 women and 168 men, mean age 58±10 years), with a diagnosis of ischemic heart disease or its suspicion, were included. All individuals were subjected to ECG (R), ECG (S) and resting-stress perfusion scintigraphy SPECT examination. The patients with implanted defibrillators, left bundle branch block, the diagnosis of hypertrophic and dilated cardiomyopathy, and treated with digitalis or antiarrhythmic drugs of group I and III were excluded from the study. The research program was carried out with the consent of patients and approval by the Ethics Committee (the approval No. 740/2003) to conduct clinical research at the Institute of Cardiology in Warsaw.

Parameters of the electrical activity of individual segments of the left ventricle were calculated using the SATRO ECG system on the basis of ECG (R) signals. According to the model SFHAM [1], the total potential, which forms a QRS complex, consists mostly of potentials generated during the sequential depolarization of five anatomical segments of the left ventricle. These are: *interventricular septum* (*IS), anterior wall (AW), inferior wall (IW)*, *lateral wall (LW)* and *posterior wall (PW)*. This model does not take into account the potentials that occur during depolarization of the right ventricle, what generally should not affect the results of the calculations, since their values are much smaller and duration is longer, compared to the parameters of the partial potentials of the left ventricle [6, 7].

It was therefore assumed that each of the partial potentials forming QRS complex is generated by charge waves flowing through some effective fibers representing particular segments of the left ventricle. Practical implementation of this model was implemented in the SATRO ECG system, where, based on measurements of the standard ECG, the parameters of the partial potentials were calculated. The values of these potentials are compared with the certain

standards, defined by us. As a result, it was possible to select segments of reduced electrical activity in an automatic way.

In order to confirm validity of our assumptions concerning applicability of discussed method for the evaluation of myocardial perfusion disturbances, the perfusion scintigraphy method combined with registration of Tc99m SPECT (SPECT) was chosen. The latter method allows a precise location of perfusion abnormalities in several parts of each segment of the left ventricle. In order to compare the results of the both methods, a reduction of the quantities of these areas to five major segments was made. It was assumed that the perfusion disturbances in any part of the segment of the left ventricle, e.g. anterior wall, concern the entire anterior wall. However, perfusion disturbances in such area as inferior-lateral segment were treated as a disturbance in the inferior and lateral walls. This allowed for a comparison of the observed location of ischemia with use of both methods.

3. Results and Statistical Analysis

Positive results of CHD were observed: for SATRO ECG in 229 subjects, which accounted for 97% of the study group, for SPECT in 233 (96%), and for ECG (S) in 73 (30%), while for ECG (R) in 142 (61%). The number of nondiagnostic patients was: for SATRO ECG – 7 (3%), and for ECG(S) – 87 (36%). These results are shown in Table 1.

Table 1. Confirmation (+) or exclusion (-) of ischemia and nondiagnostic patients (0) in methods: SATRO ECG, SPECT, ECG (R), ECG (S)

	Result (+) (number of patients)	Result (–) (number of patients)	Result (0) (number of patients)
SATRO ECG	229	7	7
SPECT	233	10	0
ECG (R)	142	101	0
ECG (S)	73	83	87

For SATRO ECG and SPECT methods perfusion was also evaluated in the individual segments of the left ventricle of myocardium, as shown in Table 2.

Table 2. Number of patients with perfusion disturbances in individual segments of the left ventricle on basis of the results of SATRO ECG and SPECT.

	IS	AW	IW	LW
SPECT	131	190	198	161
SATRO ECG	131	181	203	173

Table 3. The effectiveness of the SATRO ECG, ECG (R), ECG (S) methods relative to SPECT in CHD diagnosis and location of perfusion disturbances in individual segments of the left ventricle.

	SATRO ECG					ECG (R)	ECG (S)
	IS	AW	IW	LW	Total		
sensitivity [%]	87	89	95	94	100	59	47
specificity [%]	83	76	63	72	70	70	62
positive predictive value [%]	87	93	93	87	98	97	95
negative predictive value [%]	83	63	72	85	100	6	6

For the group of diagnostic patients: sensitivity, specificity and predictive positive and negative values were calculated for each of the methods: SATRO ECG, ECG (R), ECG (S), relative to the reference method SPECT. The results are shown in Table 3.

Sensitivity of the SATRO ECG system in CHD diagnosis was 100%, specificity 70%, positive predictive value 98%, and negative 100%. For comparison, the results of ECG (R) and ECG (S) in CHD diagnosis were: sensitivity: ECG (R) - 59%, ECG (S) - 47%, specificity:

ECG (R) - 70%, ECG (S) - 62%, positive predictive value: ECG (R) - 97%, ECG (S) - 95%, and negative: ECG (R) - 6%, ECG (S) - 6%.

The statistical kappa Cohen's test results showed that diagnosis results of CHD in SATRO ECG method has statistically significant correlation with the results of SPECT method - ($k = 0.817$, $p < 0.001$), as shown in Table 4. What is important, results corresponding to ECG (R) and ECG (S) methods did not show such correlation. For ECG (R) we had $k = 0.055$, $p = 0.031$, whereas for ECG (S) we obtained $k = 0.018$, $p = 0.294$.

Table 4. The results of kappa Cohen's test for the results of SATRO ECG, ECG (R) and ECG (S) relative to SPECT and the levels of significance (p).

	SATRO ECG					ECG (R)	ECG (S)
	IS	AW	IW	LW	Total		
Cohen's kappa	0.708	0.610	0.619	0.694	0.817	0.055	0.018
p-value	<0.001	<0.001	<0.001	<0.001	<0.001	0.031	0.294

4. Conclusions

The results of the comparative assessment revealed a high correlation between the test results of SATRO ECG and SPECT, both in the diagnosis of CHD and location of the disorders in blood supply to the heart muscle.

Only SATRO ECG examination had statistically significant ($p < 0.001$) discriminative value in predicting a positive result of SPECT.

Applying the SATRO ECG system analysis of the parameters to determine the activity of individual segments of the myocardium during depolarization process, indicates the potential possibility to expand the range of non-invasive methods of CHD.

References

[1] Janicki JS, Leoński W, Jagielski J, Partial potentials of selected cardiac muscle regions and heart activity model based on single fibres. *Medical Engineering & Physics*, 31, 1276-1282, 2009

[2] Mieres JH, Makaryus AN, Redberg RF, Shaw LJ. Noninvasive cardiac imaging. *American Family Physician,* 2007;75:1219.

[3] Michaelides A., Ryan J.M., VanFossen D., Pozderac R., Boudoulas H.: Exercise-induced QRS prolongation in patients with coronary artery disease: a marker of myocardial ischemia. *American. Heart Journal*, 1993, 126, 1320.

[4] Krzyminiewski R.: Computer enhancement of complex spectroscopic spectra resolution. *Molecular Physics Reports*, 1994, 6,174.

[5] Krzyminiewski R, Panek G. Stępień A, Stępień R, Piszczek I.: High-resolution Vectorcardiograms in the Diagnosis of Myocardial Ischaemia. *Polish Journal of Medical Physics and Engineering* 1999, Vol. 5, No.1 (15), 1-9.

[6] Scherlag BJ, Lau SH, Helfant RH. Catheter technique for recording His bundle activity in man. *Circulation* 1969;39:13–8.

[7] Horowitz LN, Josephson ME, Harken AJ. Epicardial and endocardial activation during sustained ventricular tachycardia in man. *Circulation* 1980;61:1227–38.

Does Synthesized Lead V9 Reflect Left Atrial Activity During Atrial Fibrillation ?

[1]X. Zhu, [1]Y. Yoshida, [2]D. Wei, [2]K. Fukusha and [2]H. Shimokawa

[1]Biomedical Information Technology Lab, Aizu-Wakamatsu, Japan,
[2]School of Medicine, Tohoku University, Sendai, Japan
Email: zhuxin@u-aizu.ac.jp

Abstract. *Previous studies have demonstrated right-sided precordial leads could reflect mostly right atrial (RA) activity, while posterior lead V9 could reflect mostly left atrial (LA) activity. 18 synthesized lead ECG enables us to extrapolate posterior leads V7-9 and right-sided precordial leads (V3R-V5R). Therefore, we conducted a preliminary study on whether synthesized leads are able to evaluate both atrial activities during atrial fibrillation. We recorded the standard 12-lead ECG, posterior leads V7–V9, right-sided precordial leads V3R–V5R and intracardiac electrograms (EGM) in the RA, LA and coronary sinus (CS) simultaneously from 1 male subject with paroxysmal AF before pulmonary vein isolation. The corresponding dominant frequency (DF) was estimated from the peak frequency of each lead's fibrillatory wave or EGM's FFT. The DFs in LA from EGMs in CS and LA (5.1 and 5.1 Hz) were consistent with that in lead V9 (5.1 Hz). Furthermore, that in synthesized lead V9 showed a close value (5.0 Hz). Furthermore, the DF in intracardiac RA (4.8 Hz) was close to that in V1 (4.8 Hz) and V3R-V5R. Synthesize lead V9 may evaluate the LA activity, and help in monitoring AF and identifying ablation sites through combining with the standard 12-lead ECG.*

Keywords: Atrial fibrillation, dominant frequency, frequency analysis, intracardiac electrogram, posterior lead

1. Introduction

Atrial fibrillation (AF) is the most popular cardiac arrhythmia, occurring in 1~2% of residents in Europe and United States [1]-[2], and in 0.56% in Japan [3]. Furthermore, the prevalence and incidence of AF increase with age, and reach about 10% in Europe and US and about 4.4% in Japan at 80 years' old.[1]-[3] AF is also an independent mortality predictor with a doubled death rate among AF subjects, and AF is the cause of 20% stroke.[2] The mechanism of AF is not completely confirmed but is usually attributed to focal mechanisms and multiple wavelets.[2] The main AF therapeutic methods are antiarrhythmic drug therapies including rate control and rhythm control [2], and cathode ablation.[2][4] Recent publications have also reported that significantly more atrial fibrillation (AF) patients after cathode ablations were free from any AF and symptomatic AF compared with AF patients underneath antiarrhythmic drug therapies. Furthermore, AF patients after cathode ablations have significantly better life quality at 12 and 24 months.[2] Therefore, catheter ablation is recommended as the first line therapy for atrial fibrillation (AF) patients with paroxysmal AF, with low CHA_2DS_2-VASc values, and without marked structural heart diseases.

Researches on frequency analysis of surface ECG and intracardiac electrograms have been conducted to discover the mechanism of AF and predict the resurrection of AF after cathode ablation.[5]-[7] Sanders et al. found that localized sites of high-frequency activity during AF may play roles in the maintenance of AF because ablation at these sites results in the prolongation of atrial fibrillation cycle length and termination of paroxysmal AF.[5] Mansour et al. concluded that left-to-right gradient of atrial frequencies supports the hypothesis that AF is the result of high-frequency periodic sources in the left atria.[6] Atienza et al. reported that

cathode ablation leading to elimination of left-to-right frequency predicts long-term SR maintenance in AF patients.[7]

Petutiu et al. found a strong correlation between V1 and right atrial EGM and between V9 and left atrial EGM, and therefore recording additional posterior ECG leads may noninvasively monitor right and left atrial events and interatrial frequency gradients.[8] Guillem et al. discovered that spectral analysis of body surface recordings during AF allows a noninvasive characterization of the global distribution of the atrial dominant frequency, and the identification of the atrium with the highest frequency noninvasively.[9]

Additional ECG leads such as posterior and right-sided precordial leads are not routine clinical tools for the diagnosis of AF, and the measurement of posterior leads is inconvenient and impractical in most situations. Wei has proposed an information redundancy method to derive posterior leads V7-9 from the standard 12 leads [10] and proved their usefulness in the diagnosis of right ventricular or posterior wall ischemia. In this paper, based on Wei's method, we conducted a preliminary study on whether synthesized posterior leads can also reflect left atrial activities during atrial fibrillation. Surface ECG and atrial electrograms were simultaneously recorded from an AF patient and the synthesized posterior and right precordial leads were synthesized from standard 12 leads. The f waves of surface leads were estimated by employing a QT-based method developed by our research team.[11] Then frequency analysis was conducted to get the dominant frequencies (DF) of f waves & atrial electrograms and their spatial distributions. Finally, the DFs obtained from the standard 12 leads, posterior leads, right-sided precordial leads, synthesized leads, and EGM were compared to unmask.

2. Subject and Methods

The surface ECG and intracardiac electrograms were recorded from a 49-year-old male paroxysmal AF subject before the performance of radiofrequency ablation. The 12 standard ECG and additional leads were simultaneously recorded together with His bundle, coronary sinus (CS), right atrial (RA), superior vena cava (SVC) electrograms. LA electrograms was measured by an ablation catheter. The body surface ECG was previously processed by a 0.05-100 Hz filter, and atrial electrograms were processed by a 30-150 Hz filter in the EP device. Powerline noise was removed by using a 50-60 Hz notch filter.

This research has been permitted by the medical ethics committee of Tohoku University, Japan and was conducted based on the rules of the same committee.

We employed a QT-based method to extract f waves from surface ECG instead of the traditional average beat subtraction method. The details of the QT-based method were reported in our previous publication [11].

The surface ECG during AF can be expressed as a combination of ventricular activity atrial activity, and noise as follows,

$$x(t) = v(t) + a(t) + n(t), \quad (1)$$

where x, v, a, n, and t are ECG, ventricular activity, atrial activity (f wave), noise, and time, respectively.

Frequency analysis of f wave is conducted in a traditional way [11], where Fourier transform, a Hamming window (16.384 s) were used in this research. Furthermore, the value of FFT's amplitude is normalized to 0-1 in this research. DF is determined by the peak in the frequency bandwidth 4~9 Hz.

As atrial electrograms were previously processed by a bandpass filter, they were rectified in order to get the dominant frequency in 4-9 Hz. Then FFT with the same parameters as those

in the frequency analysis on f waves, was conducted to get dominant frequencies in the rectified atrial electrograms [11].

3. Results

Fig. 1 illustrates the locations of standard 12 lead ECG and additional leads including V7-9 and V3-5R. The derivation of right precordial and posterior leads is based on an information redundancy method proposed by Wei.[10] Fig. 2 illustrates frequency spectra of f waves extracted from V1 (blue curve) and V9 (red curve) leads. Table 1 shows the dominant frequencies estimated from surface ECG and atrial electrograms.

It is observed that there is a left-to-right atrial frequency difference as the DFs of RA distal and LA distal EGMs are 4.8 and 5.1 Hz, respectively. Furthermore, the DFs of additional leads were closer to those of synthesized additional leads. The DF of V1, 4.8 Hz was also lower than those of posterior leads and synthesized posterior leads (5.0~5.1 Hz).

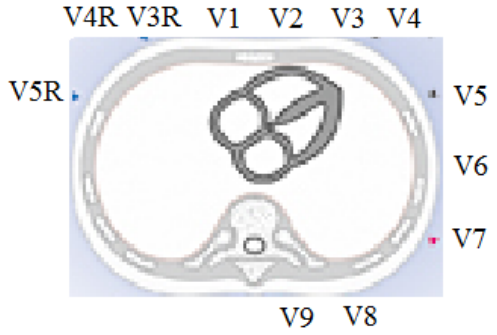

Fig. 1. Locations of standard 12 leads, right precordial leads, and posterior leads.

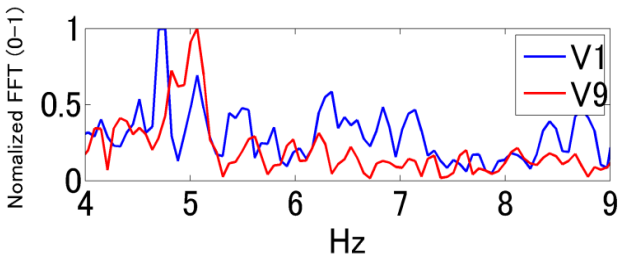

Fig. 2. Frequency spectra of f waves extracted from V1 (blue curve) and V9 (red curve) leads.

Table 1. Dominant frequencies estimated from surface ECG and atrial electrograms

Lead	DF (Hz)	Lead	DF (Hz)	Lead	DF (Hz)	Lead	DF (Hz)
I	5.2	V3R	4.8	synthesized V3R	4.9	RA dist.	5.5
II	5.0	V4R	4.8	synthesized V4R	4.8	RA prox.	4.8
III	5.0	V5R	4.8	synthesized V5R	4.8	CS dist.	5.0
aVL	5.0	V7	5.0	synthesized V7	5.0	CS prox.	5.1
aVF	5.0	V8	5.0	synthesized V8	5.0	LA dist.	5.1
V1	4.8	V9	5.1	synthesized V9	5.0	LA prox.	5.0

4. Discussion

Guillem et al. [9] have reported that it might be possible to localize the atrial fibrillation occurrence using surface ECG. Petrutiu et al.'s researches showed that a strong correlation between V1 and right atria and between V9 and left atria, and therefore recording additional posterior ECG leads may noninvasively monitor right and left atria events and interatrial frequency gradients [8]. As the measurement of posterior leads is inconvenient, we synthesized posterior leads from standard 12 lead to confirm whether synthesized posterior leads may reflect the electric activities of left atria. In this case, we observed that V9 and synthesized V9 leads had a similar DF to that of the left atrial EGMs, and V1 lead had a similar DF to that of the right atrial EGM. And there was a left-to-right atrial frequency difference, which was confirmed using the frequency analysis of left and right atrial EGMs. Therefore, synthesized V9 lead may be useful for noninvasively unmasking interatrial frequency difference. Of course, this should be further validated using more clinical data.

5. Conclusion

The result of the preliminary study demonstrated that DFs obtained from V1 & posterior and synthesized posterior leads may serve as non-invasive indexes to reflect the right and left atrial activities during AF, respectively. This may lead to a convenient noninvasive detecting for the responsible atrial chamber of AF maintenance before cathode ablation.

Acknowledgements

This study was sponsored in part by Japan Society for the Promotion of Science under Grants-In-Aid for Scientific Research (No. 24500369).

References

[1] Go AS, Hylek EM, Phillips KA, Chang YC, Henault LE, Selby JV. Prevalence of diagnosed atrial fibrillation in adults. National implications for rhythm management and stroke prevention: the Anticoagulation and risk factors inatrial fibrillation (ATRIA) study, JAMA, 285:2370-2375, 2001.

[2] The task force for the management of atrial fibrillation of the European Society of Cardiology, Guidelines for the management of atrial fibrillation, European Heart Journal, 31:2369-2429, 2010.

[3] Inoue H, Fujiki A, Origasa H, Ogawa S, Okumura K, Kubota I. Prevalence of atrial fibrillation in the general population of Japan: An analysis based on periodic health examination, Int J Cardiol, 137(2):102-107, 2009.

[4] Jais P, Haissaguerre M, Shah DC, Chouairi S, Gencel L, Hocini M, Clementy J. A focal source of atrial fibrillation treated by discrete radiofrequency ablation, Circulation, 95:572-576, 1997.

[5] Sanders P, Berenfeld O, Hocini M, et al. Spectral analysis identifies sites of high-frequency activity maintaining atrial fibrillation in humans. Circulation, 112:789–797, 2005.

[6] Mansour M, Mandapati R, Berenfeld O, Chen J, Samie FH, and Jalife J, Left-to-right gradient of atrial frequencies during acute atrial fibrillation in the isolated sheep heart, Circulation, 103:2631-2636, 2001.

[7] Atienza F, Almendral J, Jalife J, Zlochiver S, Ploutz-Snyder R, Arenal A, Kalif J, Fernandez-Aviles F, Berenfeld O. Real-time dominant frequency mapping and ablation of dominant frequency sites in atrial fibrillation with left-to-right frequency gradients predicts long-term maintenance of sinus rhythm, Heart Rhythm, 6:33-40,2009.

[8] Petrutiu S, Sahakian AV, Fisher W, Swiryn S, Manifestation of left atrial and interatrial frequency gradients in the surface electrocardiogram during atrial fibrillation: contributions from posterior leads, J Cardiovsc Electrophysiol, 20:1231-1236,2009.

[9] Guillem MS, Climent AM, Millet J, Arenal Á, Fernández-Avilés F, Jalife J, Atienza F, Berenfeld O., Noninvasive localization of maximal frequency sites of atrial fibrillation by body surface potential mapping, Circ Arrhythm Electrophysiol, 6, 294-301, 2013.

[10] Wei D. Derived electrocardiograms on the posterior leads from 12-lead system: method and evaluation, Proc. Of the 25th Annual International Conference of the IEEE EMBS, 2003, 74-77.

[11] Zhu X, Wei D, Fukuda K, Shimokawa H. A simple atrial fibrillatory wave reconstruction method for frequency analysis of atrial fibrillation using single-lead ECG, Proc. of IASTED Biomed 2013, 791-016.

QRS Complex Patterns in Patients with Obstructive Sleep Apnea

[1,2]L. Bacharova, [2]E. Triantafyllou, [2]C. Vazaios, [3]R. Tisko, [3]I. Paranicova, [3,4]R. Tkacova

[1] International Laser Center, Bratislava, Slovakia
[2] Institute of Pathological Physiology, Medical Faculty, Comenius University, Bratislava, Slovakia
[3]Dept. Respiratory Medicine, Faculty of Medicine, P.J. Safarik University, Kosice, Slovakia
[4]L. Pasteur University Hospital, Kosice, Slovakia
Email: bacharova@ilc.sk

Abstract. *We evaluated QRS complex morphology in patients with obstructive sleep apnea (OSA) that could be potentially linked to arrhythmias. The study population consisted of 199 consecutive patients examined in the sleep laboratory, divided into quartiles according to the apnea/hypopnea index (AHI):Group Q1: AHI 0.7-10.9 #/h; Group Q2: AHI 11.0-32.3 #/h; Group Q3: AHI 32.3-63.0 #/h; Group Q4: AHI 65.1-133 #/h. Resting 12-lead ECG was recorded, the QRS parameters analyzed included QRS amplitude in individual leads, QRS spatial vector magnitude (QRSmax), electrical axis (EA), ECG criteria for left ventricular hypertrophy (ECG-LVH) and right ventricular hypertrophy (ECG-RVH). There were no significant differences in QRSmax values between the groups. The occurrence of ECG-LVH was low (total 7%), on the other hand 96 % of patients showed signs of ECG-RVH. The values of EA were significantly shifted gradually to the left (Q1: 40.1±19.8°; Q2: 34.5±18.0°; Q3: 27.6±15.3°; Q4: 31.6±16.2°). Additionally, QRS morphology showed a variety of intraventricular conduction defects, including QRS notching, non-specific conduction defects and patterns of left/ or right bundle branch blocks. Conclusions: The OSA patients displayed significant changes in QRS complex morphology suggestive of depolarization sequence deterioration indicative of considerable electrical remodeling that could be potentially linked to occurrence of arrhythmias.*

Keywords: sleep apnea, QRS complex, right ventricular hypertrophy, left ventricular hypertrophy, right bundle branch block

1. Introduction

Obstructive sleep apnea (OSA) is a clinical condition characterized by repeated disruptions of breathing during sleep, leading to repetitive episodes of hypoxia and reoxygenation. OSA is associated with multiple disorders and co-morbidities, such as obesity, hypertension, insulin resistance/ metabolic syndrome, chronic obstructive pulmonary disease [1]. These clinical conditions themselves result in a complex impairment of myocardium that is reflected in the QRS morphology changes as a result of altered sequence of depolarization. The increased occurrence of arrhythmias and the prolongation of QRS complex have been described previously [2, 3].

In this study we analyzed the morphology of the QRS complex in relation to the degree of apnea/ hypopnea index (AHI) as a measure of intermittently reduced oxygen supply. We were interested if hypoxia has additional effect on the sequence of depolarization observed in the given cardiac pathology.

2. Subject and Methods

Study population
The study subjects were recruited within the Project APVV- 0134 -11 Effects of Hypoxia on Molecular Pathways related to Increased Cardiovascular Risk in Patients with Sleep Apnea and their Reversal by Therapy (HICART).

The total number of 199 OSA patients was divided into quartiles according to the apnea/hypopnea index:

- Group Q1 (n = 50): AHI 0.7-10.9 #/h, aged 24 to 80 years, mean 50.9 years;
- Group Q2 (n = 50): AHI 11.0-32.3 #/h; aged 23 to 80 years, mean 51.3 years;
- Group Q3 (n = 50): AHI 32.3-63.0 #/h, aged 29 to 78 years, mean 57.9 years;
- Group Q4 (n = 49): AHI 65.1-133.8 #/h, aged 31 to 70 years, mean 54.8 years.

The basic characteristics of the study population are presented in Table 1.

Table 1. Baseline characteristics of the study population.

	n	Age yrs mean SD	Gender M/F (%)	sBP mmHg mean SD	dBP mmHg mean SD	Hypertension n (%)	BMI kg/m^2 mean SD
Q1	50	50.9 11.9	22/28 (44/56)	121.9 16.1	79.5 9.6	26 (52)	28.7 4.8
Q2	50	51.3 12.3	34/17 (66/34)	126.2 16.6	82.5 10.6	26 (52)	30.3 5.0
Q3	50	57.9 9.8	40/10 (80/20)	137.3 16.5	86.7 9.2	37 (74)	32.8 4.1
Q4	49	54.8 12.8	43/6 (87/13)	139.6 24.2	88.2 14.8	42 (84)	38.8 6.1

All participants underwent diagnostic overnight polysomnography (Alice 4, Respironics Inc., Murrysville, Pennsylvania, USA). All records were scored manually following the AASM 2007 rules [4]. Apnea was identified as a drop in airflow of >90% from the baseline excursion for ≥10 seconds; hypopnea was defined as a reduction in airflow of at least 50% of baseline for ≥10 seconds accompanied either by a decrease in hemoglobin saturation for ≥3%, an EEG-recorded arousal, or both. The apnea-hypopnea index (AHI) was defined as the number of apnea and hypopnea episodes per hour of sleep.

The standard 12-lead ECG was recorded using a Marquette Centra electrocardiograph. The amplitudes of the QRS waves in individual leads were measured manually.

The following ECG parameters were analyzed:

- The maximum spatial vector magnitude (QRSmax) estimated as:

$$QRS_{max} = \sqrt{V2^2 + aVF^2 + V5^2} \quad (1)$$

where V2 the maximum QRS deflection in lead V2
aVF the maximum QRS deflection in lead aVF
V5 the maximum QRS deflection in lead V5.

- The electrical QRS axis (EA) was calculated using the formula:

$$EA = arc\tan\left(\frac{2*aVF}{I+\sqrt{3}}\right) \quad (2)$$

where aVF the maximum QRS deflection in lead aVF
I the maximum QRS deflection in lead I.

ECG-LVH criteria:

- The Sokolow-Lyon index calculated as a sum of V1 and RV5 or V6;
- The Cornell voltage calculated as a sum of RaVL and SV3;
- The Gubner criterion, calculated as a sum of RI and SIII;

ECG-RVH criteria:

- The Sokolow-Lyon criterion for right ventricular hypertrophy, calculated as a sum of RV1 and SV5(or V6);
- Butler-Leggett formula, calculated as sum of R (or R') V1 (or V2) and S I (or V6) minus SV1.

The occurrence of complete or incomplete RBBB with and without LAD was also evaluated.

3. Results

The values of QRSmax were low, and there were no significant differences in QRSmax values between the groups. The values of EA were significantly shifted gradually to the left with increasing values of AHI (Figure 1).

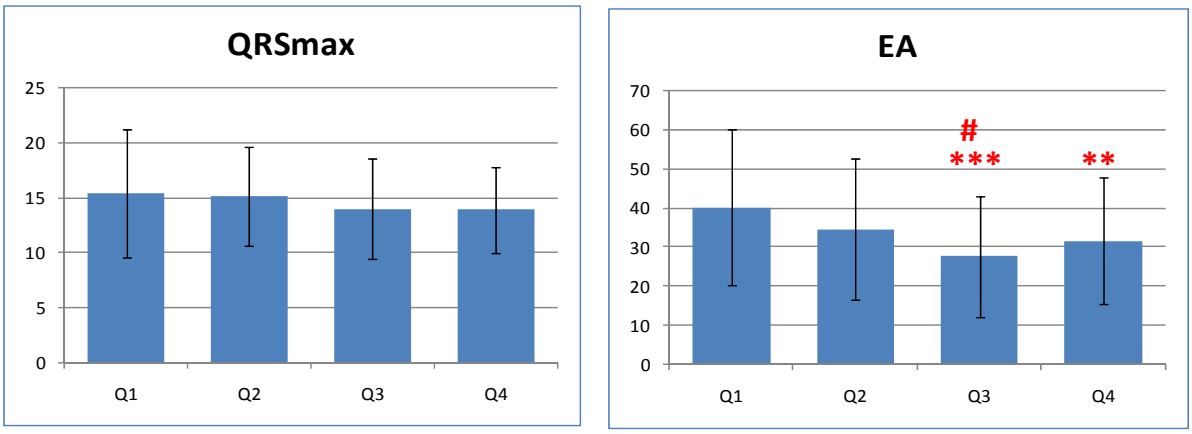

Figure 1. **Values of maximum** QRS spatial vector magnitude and electrical axis. Values presented as means, the error bars represent standard deviations. **: p<0.01 with respect to Q1, ***: p<0.001 with respect to Q1. #: p<0.05 between Q2 and Q3.

The occurrence of ECG-LVH was low (total 7%). On the other hand, nearly all patients (96%) showed signs of ECG-RVH by BL criteria and total 17% by SLI-RVH criteria with maximum (7%) in the Q4 group. The values of ECG criteria for right ventricular hypertrophy are presented in Table 2.

Table 2. Values of ECG criteria for right ventricular hypertrophy. SL-RVH: Sokolow-Lyon criterion for right ventricular hypertrophy, BL: Butler-Leggett formula. *Significant as compared to Q1 and Q3.

	SL [mm] mean (SD)	**BL [mm] mean (SD)**
Q1	7.3 (3.8)	13.4 (4.0)
Q2	8.0 (3.9)	14.2 (4.9)
Q3	7.5 (3.7)	13.3 (4.3)
Q4	9.2 (3.9)*	14.0 (5.2)

The QRS patterns of complete or incomplete RBBB occurred in 12.5% of patients (in combination with left axis deviation 10.5%), there were no significant differences among the groups.

4. Discussion

Regarding the QRS patterns, we observed low QRSmax values in all quartiles, the ECG-LVH criteria did not exceed partition values. On the other hand, the ECG-RVH signs and a slight but significant shift of electrical axis to the left were present, pronounced in quartiles with increasing AHI.

The low QRS values are traditionally attributed to the effect of obesity; however there were no differences between the groups in spite of significantly increased BMI values in higher quartiles. Although a great proportion of patients were hypertensive (in Q4 group 84%), none of the patients had ECG-LVH signs. As mentioned above, the absence of increased QRS voltage is attributed to the effect of obesity. However, the effect of obesity did not affect the ECG-RVH criteria – it cannot be assumed that the effect of obesity works selectively for ECG-LVH criteria.

ECG-RVH signs were present in almost all patients. Theoretically it could be attributed to pulmonary hypertension and/or concomitant chronic obstructive pulmonary disease. However, we observed a gradual shift of the electrical axis to the left and not to the right as it would be expected in RVH.

5. Conclusions

Obstructive sleep apnea represents a clinical condition with a variety of comorbidities, such as systemic and pulmonary hypertension, obesity, metabolic syndrome, chronic obstructive pulmonary disease, etc., each of them with possible considerable impairment of myocardium and an additional effect of intermittent hypoxia. We observed non-typical QRS changes that are suspected of intraventricular conduction defects. This assumption is consistent with the published evidence of cardiac arrhythmias and conduction disturbances documented in OSA patients.

Acknowledgements

Supported by the grant APVV- 0134 -11: Effects of Hypoxia on Molecular Pathways related to Increased Cardiovascular Risk in Patients with Sleep Apnea and their Reversal by Therapy (HICART), Slovak Republic.

References

[1] Zamarrón C1, Valdés Cuadrado L, Alvarez-Sala R, Pathophysiologic mechanisms of cardiovascular disease in obstructive sleep apnea syndrome, *Pulmonary Medicine*, 2013: 1-16, 2013.

[2] Baranchuk A, Sleep apnea, cardiac arrhythmias, and conduction disorders, *Journal of Electrocardiology*, 45: 508-512, 2012.

[3] Gupta S1, Cepeda-Valery B, Romero-Corral A, Shamsuzzaman A, Somers VK, Pressman GS, Association between QRS duration and obstructive sleep apnea, *Journal of Clinical Sleep Medicine*, 8: 649-654, 2012.

[4] Berry RB, Budhiraja R, Gottlieb DJ, et al.: Rules for scoring respiratory events in sleep: update of the 2007 AASM Manual for the Scoring of Sleep and Associated Events. Deliberations of the Sleep Apnea Definitions Task Force of the American Academy of Sleep Medicine. *J Clin Sleep Med* 15: 597-619, 2012.

QRS Complex Characteristics in Patients with Eisenmenger Syndrome with Pre- and Post-Tricuspid Defects

[1,2]T. Valkovičová, [3]M. Kaldararová, [1,2]M. Boháčeková, [4]L. Bachárová, [1,2]I. Šimková

[1] Department of Cardiology and Angiology, Slovak Medical University, Bratislava, Slovak Republic
[2] National Institute of Cardiovascular Diseases, Bratislava, Slovak Republic
[3] National Institute of Cardiovascular Diseases – Children's Cardiac Center, Bratislava, Slovak Republic
[4] International Laser Center, Bratislava, Slovak Republic
Email: valkovicova.tatiana@gmail.com

Abstract. *Eisenmenger syndrome (extreme pulmonary arterial hypertension due to congenital shunt lesion) results in severe right ventricular (RV) pressure overload. Patients´ prognosis depends on RV morphology and function and differs according to the shunt location. The aim of this study was to compare the echocardiographic and ECG signs of right ventricular hypertrophy (RVH) in patients with different location of the defect. The study population consisted of 43 patients (30F/13M, median age 41 years). The ECG and echocardiographic (ECHO) parameters as well as the serum N-terminal brain natriuretic peptide concentration (NTpBNP) were analyzed in a group of patients with pre-tricuspid (pre-TD) and post-tricuspid (post-TD) locations of defects. Sokolow-Lyon index for RVH and Butler-Leggett index exceeded the upper normal limits, however there were no significant differences between groups. Significant difference was found in QRSmax (16.6±6.8 vs 25.2±8.9mm). The RV wall thickness showed severe hypertrophy in both groups, significantly more prominent in the post-TD group (8.7±2.1 vs 10.4±2.9mm). The RV diameter showed significant dilatation in the pre-TD group (42.9±10.05 vs 28.5±6.9mm). ECG indexes correlated significantly ($p<0.0001$) with ECHO RV wall thickness. The NTpBNP concentrations exceeded the upper normal limits considerably in both groups, without significant difference between the groups. Despite significant difference in morphological RV configuration (hypertrophy and dilatation) between groups according to defect location and significant correlation of ECG and ECHO parameters, ECG criteria for RV hypertrophy did not differ between the groups, suggesting that the morphological configuration of RV was not the main factor influencing the QRS patterns.*

Keywords: Eisenmenger syndrome, pulmonary arterial hypertension, location of the defect, right ventricular hypertrophy, brain natriuretic peptide

1. Introduction

Eisenmenger syndrome is characterized by severe pulmonary arterial hypertension (PAH) associated with congenital heart disease [1,2]. Depending on the size and location of the underlying cardiac defect, severe PAH invariably results in severe right ventricular (RV) due to the pressure overload [3,4]. The most important factor for prognosis is considered the specific RV morphology and preserved good RV function, dominantly influenced by the presence of a shunt [7]. Additionally, the defect location enables a more-less effective utilization of RV own compensatory mechanisms [8]. Post-tricuspid defects (post-TD) are typically associated with severe RV hypertrophy (RVH) and only mild dilatation and good systolic RV function. On the contrary, the pre-tricuspid defects (pre-TD) tend to more prominent RV dilatation and less preserved RV systolic function [4,7]. Serum N-

terminal brain natriuretic peptide (NTpBNP) concentration is considered a good marker of RV dysfunction and is often used as a prognostic parameter in patients with PAH [5,8].

The aim of the study was to compare ECG, echocardiographic parameters (ECHO) and plasma neurohormone levels (serum NTpBNP) in patients with the pre-TD and post-TD locations of the defects.

2. Subject and Methods

The study population consisted of 43 patients with ES divided in two groups:

- Group Pre-TD: 19 patients (14 women/ 5 men, age ranged 33-78 years, median 57 years);
- Group Post-TD: 24 patients (16 women/ 8 men, age ranged 24-69 years, median 41 years).

The following parameters were measured:

12-leads ECG: Butler-Leggett formula (BL), Sokolow-Lyon index for RV hypertrophy (SL-RVH) and maximum spatial QRS vector magnitude (QRSmax)

Echocardiography: RV diameter (RVD), RV wall thickness (WT), RV function by the tricuspid annular plane systolic excursion (TAPSE) and RV ventricular fractional area change (FAC).

NTpBNP (ng/l) concentrations were determined by an electrochemiluminescence method.

3. Results

The values of parameters under study are presented in Table 1.

Table 1. The values of ECG and echocardiographic parameters under study in patients with pre-tricuspid and post-tricuspid location of defects. Pre-TD - Pre-tricuspid defect, Post-TD - Post-tricuspid defect, SD – standard deviation, QRSmax- maximum QRS spatial vector magnitude, RV WT - right ventricular wall thickness, RVd - right ventricular diameter, TAPSE - tricuspid annular plane systolic excursion, FAC - right ventricular fractional area change, NTpBNP-N - N-terminal brain natriuretic peptide, NS - not significant.

	Pre-TD average (SD)	**Post-TD average (SD)**	**T test p**
Sokolow-Lyon (mm)	14.76 (10.17)	18.67 (10.71)	NS
Butler-Legget (mm)	13.45 (10.25)	17.83 (12.49)	NS
QRS max (mV)	16.57 (6.76)	25.2 (8.85)	0.0004
RV WT (mm)	8.71 (2.09)	10.35 (2.91)	0.037
RVd (mm)	42.94 (10.05)	28.5 (6.85)	0.001
TAPSE (mm)	20.79 (5.49)	22.83 (4.14)	NS
FAC (%)	48.26 (12.38)	53.13 (11.67)	NS
NTpBNP (ng/l)	2140 (2962)	1679 (2847)	NS

The ECG parameters exceeded the upper normal limits in both groups (Sokolow-Lyon index for RVH 14.76 mm ±10.17 mm / 18.67 mm ±10.71 mm; Butler-Leggett formula 13.45 mm ±10.25 mm/ 17.83 mm ±12.49 mm), however there was no significant difference between the groups. Significant difference between groups was found in QRSmax values (16.57 mm ±6.75 mm/ 25.20 mm ±8.85 mm, P=0004).

The ECHO parameters showed signs of RVH: RV wall thickness 8.71mm ±2.09 mm /10.35 mm ± 2.91 mm (p=0,037); and RV diameter 42.94 mm ± 10.05 mm / 28.5 mm ± 6.85 mm

(P<0.001). The values of TAPSE and FAC were within normal limits, no significant difference was observed between the groups.

NTpBNP levels exceeded the upper normal limits in both groups, without significant differences between the groups.

Significant correlation of both ECG indexes for RV hypertrophy (Sokolow-Lyon criterion for RVH, Butler-Leggett formula) with ECHO RV wall thickness (p<0.0001) was observed (Figure 1 and 2).

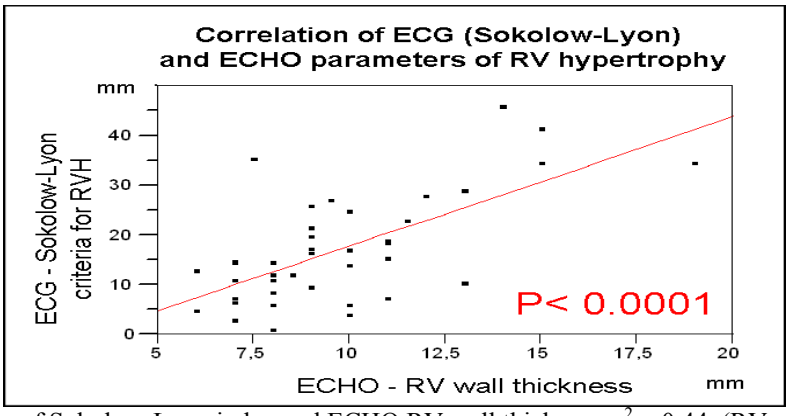

Figure 1. Correlation of Sokolow-Lyon index and ECHO RV wall thickness. $r^2 = 0.44$. (RV: right ventricle, RVH: right ventricular hypertrophy).

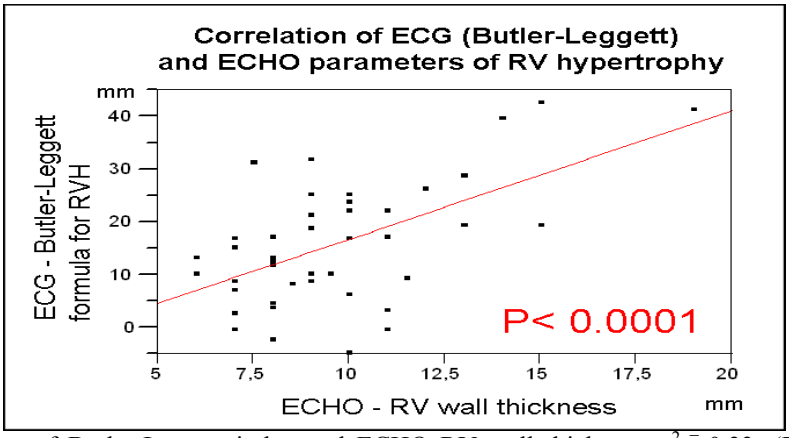

Figure 2. Correlation of Butler-Leggett index and ECHO RV wall thickness. $r^2 = 0.33$. (RV: right ventricle, RVH: right ventricular hypertrophy).

4. Discussion

Eisenmenger syndrome with severe pulmonary hypertension leads to compensatory RV hypertrophy and in some degree to RV dilatation. Due to different hemodynamic situation it is important to distinguish defects according to the shunt location (pre-TD versus post-TD). In our study the ECG as well as ECHO parameters confirmed the presence of severe RV hypertrophy in both group of patients and significant correlation between ECG signs of RVH and ECHO parameters. However, despite significant difference in morphological RV configuration in different defect locations (with significantly more prominent hypertrophy in post-TD and RV dilatation in pre-TD), ECG criteria for hypertrophy did not differ between the groups, except the spatial QRS vector magnitude, reflecting RV hypertrophy and dilatation. RV function according to ECHO was well preserved in both groups. However, positive NTpBNP levels (although without significant difference between groups) reflect severe RV overload in these patients. It can be concluded that that the morphological configuration of RV was not the main factor influencing the QRS patterns.

References

[1] Eisenmenger V. Die angeborenen Defekte der Kammerscheidewände des Herzens. *Zeitschrift fürKlinische Medizin,* 32: 1–28, 1897.

[2] Wood P. The Eisenmenger syndrome or pulmonary hypertension with reversed central shunt. *British Medical Journal,* 46: 755–762, 1958.

[3] Diller GP, Gatzoulis MA. Pulmonary vascular disease in adults with congenital heart disease. *Circulation,* 115: 1039–1050, 2007.

[4] Diller GP, Dimopoulos K, Kafka H. Model of chronic adaptation: right ventricular function in Eisenmenger syndrom. *European Heart Journal,* 9(Suppl H): 54–60, 2007.

[5] Hopkins WE. The remarkable right ventricle of patients with Eisenmenger syndrome. *Coronary Artery Disease*,16: 19–25, 2005.

[6] Fijalkowska A, Kurzyna M, Torbicki A et. al. Serum N-terminal brain natriuretic peptide as a prognostic parameter in patients with pulmonary hypertension. *Chest,* 129: 1313–1321, 2006.

Holter ECG Findings in Patients with Medial Arterial Calcinosis

[1]L. Gaspar, [2]I. Gasparova, [1]M. Makovnik, [1]P. Gavornik, [1]A. Dukat

[1]2nd Department of Internal Medicine, Comenius University, Bratislava, Slovakia
[2]Institute of Medical Biology, Genetics and Clinical Genetics, Comenius University, Bratislava, Slovakia
Email: ludovitgaspar@gmail.com

Abstract. *Introduction: Medial arterial calcinosis is an independent risk factor for cardiovascular and all-cause mortality.Aim of the study: To determine the incidence of cardiac arrhythmia and ischemia with the use of Holter ECG monitoring in a group of patients with medial calcinosis. Patients and Methods: 22 individuals (10 men and 12 women) with the mean age of 59 years were examined. Holter ECG monitoring with an average duration of 22.16 hours was carried out using Marquette-Hellige General Electric (USA) devices. Medial calcinosis was defined as ankle-brachial pressure index (ABI) with a value of 1.3 and more. Results: Only 2 patients (9 %) from our group had normal Holter ECG records, without arrhythmia or ischemia. Complex form of arrhythmia (Myerburg 4B or 4C) was in 11 patients (50 %), atrial fibrillation in 6 (27 %), 2nd degree A-V block Mobitz type I in 1 patient (4.5 %) and myocardial ischemia in 6 persons (27 %). Conclusions: In our study we found significant cardiac arrhythmia and/or ischemia in 91 % of investigated patients with medial arterial calcinosis. Our results confirm the importance of Holter ECG monitoring in this patients, because of increased cardiovascular risk, including sudden cardiac death.*

Keywords: medial calcinosis; Holter ECG; cardiac arrhythmia; ischemia

1. Introduction

The ankle-brachial pressure index (ABI) is a reliable warning sign of increased cardiovascular risk (1). In addition to peripheral artery disease, the ABI is an indicator of generalized atherosclerosis. According to recent studies low ABI levels are associated with higher incidence of coronary artery diseases as well as stroke.

Medial calcinosis (Mönckeberg's sclerosis) is a degenerative and apparently non-inflammatory disease in which the media of small and medium-sized muscular arteries becomes calcified independently of atherosclerosis. The disease is frequently related to diabetes mellitus, aging, male gender, autonomic neuropathy, osteoporosis, chronic kidney disease, hyperparathyroidism, smoking and hyperuricaemia.

Decreased ankle-brachial pressure index (ABI) is a well-known cardiovascular risk marker. ABI >1.3 in the presence of medial calcinosis is associated with increased cardiovascular morbidity and mortality.

2. Subject and Methods

We examined 22 individuals (10 men and 12 women) with the mean age of 59 year. The age range was 50-85 years. Diabetes mellitus was defined as current use of dietary interventions (2 patients), use of diabetes medications – oral hypoglycemic agents (6 patients) and insulin (8 patients). 9 patients had signs of chronic renal disease of which five were in the 4th stage according to K/DOQI classification. The median BMI (body mass index) was 32; the waist circumference median was 104 cm in men and 95 cm in women. 7 members of the group had

a history of previous myocardial infarction and 4 members had an ischemic stroke. During 1 year follow-up 3 patients died at home. An autopsy was not performed.

Holter ECG monitoring with an average duration of 22.16 hours was carried out using Marquette-Hellige General Electric (USA) devices with three channel electrodes system and MARS analyzing software. Artifacts were eliminated by visual inspection of each record.

Medial calcinosis was defined using the handheld Doppler probe as ankle-brachial index with a value of 1.3 and more. ABI measurement is noninvasive, simple and reproducible examination method, in which the Doppler probe measures the value of blood pressure in the arm and ankle.

3. Results

ABI values in the group of our patients ranged from 1.3 to 1.7 (median 1.5). Only 2 patients (9%) from group had no signs of arrhythmia and ischemia during ECG monitoring. All other members of the group (91%) had cardiac dysrhythmia and/or ischemia. Complex form of cardiac dysrhythmia – Myerburg 4B and 4C was found in 11 records. Results of all Holter ECG examinations are summarized in Table 1.

Table 1. Results of the Holter ECG monitoring (n=22).

Findings	Occurrence
Normal record – without ischemia or dysrhythmia	n = 2 (9%)
Atrial fibrillation	n = 6 (27%)
Complex form of dysrhythmia - Myerburg 4B or 4C	n = 11 (50%)
2nd degree A-V block Mobitz type I	n = 1 (4.5%)
Myocardial ischemia	n = 6 (27%)

4. Discussion

Mönckeberg's sclerosis (MS) is a degenerative and apparently non-inflammatory disease in which the media of small and medium-sized muscular arteries becomes calcified independently of atherosclerosis. The exact pathogenesis of this process is far from being understood, but it is frequently related to diabetes mellitus, aging, male gender, autonomic neuropathy, osteoporosis, chronic renal failure, hyperparathyroidism, smoking and hyperuricaemia (2). In medial calcinosis calcium salts are deposing in the media of arteries thus reducing their elasticity. Native X-ray of the affected limb arteries shows continuous tubular shadows of the media ("rail tracking") in contrast to the complicated calcified atherosclerotic plaques, in which native X-ray shows spotted intermittent drawings of the plaques in the intima. Medial calcinosis is also more frequently observed in patients with autonomic neuropathy. Similar calcifications, which develop in diabetics with autonomic neuropathy, are also found in non-diabetic patients after lumbar sympathectomy.

Morphological findings in medial calcinosis differ also from calcifications of the lamina elastica interna in Giant-cell arteritis. Typical histopathological finding in Giant-cell arteritis is a granuloma, focal inflammation in the media (3). Affected are all layers of the vessel wall but dominantly media. It leads to fissures and fragmentation of internal elastic membrane

with the findings of calcification, which is one of the typical features of Giant-cell arteritis (4).

Reduced ABI is a reliable warning sign of increased cardiovascular risk, with ABI values below 0.7 indicating a significantly worse prognosis from the aspect of survival compared to subjects with normal ABI values (range from 0.9 to 1.1) (5). Criqui et al. have pointed out that cardiovascular mortality during a 3-year follow-up was directly related to ABI values: in severe ischemia ABI below 0.7 and medial calcinosis ABI 1.3 and more. Similar results were also found in a 6-year mortality follow-up (6).

Coronary artery atherosclerosis in diabetic patients occurs much earlier than in non-diabetic patients and reaches a greater extent (7). 16 members of our group had diabetes mellitus. 50% of group members already had myocardial infarction or ischemic stroke. These findings are consistent with the occurrence of metabolic syndrome (MS) in our group. It is widely known that people with MS have a higher morbidity and mortality compared to people without MS (8).

There are also other factors that participate in the development of MS and its complications including proatherogenic dyslipoproteinemia and proinflammatory state. We cannot omit the factor of age that affects all levels of pathogenesis, explaining the increasing prevalence of MS with the age (9, 10). These factors could contribute to the occurrence of cardiac dysrhythmia and ischemia in our group of patients.

5. Conclusions

During Holter ECG monitoring in patients with medial arterial calcinosis we found high incidence of cardiac dysrhythmia and/or myocardial ischemia (together 91%). Patients with medial calcinosis are in risk of serious cardiac complications including sudden cardiac death. Therefore interdisciplinary approach to patients is crucial. ABI examination can reveal persons with increased cardiovascular risk. It is a simple, non-invasive and reproducible method which should be done routinely during overall cardiovascular risk estimation.

References

[1] Lamina C, Meisinger C, Heid IM et al. Association of ankle-brachial index and plaques in the carotid and femoral arteries with cardiovascular events and total mortality in a population-based study with 13 years of follow-up. *European Heart Journal*, 27 (21): 2580-2587, 2006.

[2] Couri CEB, Da Silva GA, Martinéz JAB et al. Mönckeberg's sclerosis – is the artery the only target of calcification? *BMC Cardiovascular Disorders*, 5 (1):34, 2005.

[3] Weyand CM, Goronzy JJ. Pathogenetic principles in giant cell arteritis. *International Journal of Cardiology*, 75 (Suppl 1): 9-15, 2000.

[4] Rovenský J, Tauchmannová H, Štvrtinová V et al. Polymyalgia rheumatica a obrovskobunková arteritída, príspevok ku klinicko-laboratórnej syndromológii a terapii. *Česká Revmatologie,* 14 (3): 135-143, 2006.

[5] Diehm C, Lange S, Darius H et al. Association of low ankle brachial index with high mortality in primary care. *European Heart Journal,* 27 (14): 1743-1749, 2006.

[6] Criqui MH, Ninomiya JK, Wingard DL et al. Progression of peripheral arterial disease predicts cardiovascular disease morbidity and mortality. *Journal of the American College of Cardiology*, 52 (21): 1736-1742, 2008.

[7] Gray RP, Yudkin JS. Cardiovascular disease in diabetes mellitus, in Textbook of diabetes. Pickup J, Wiliams G. Editors. 2nd edition. Blackwell Science Ltd, Oxford, 1997, 1-57.

[8] Isomaa B, Almagren P, Tuomi T et al. Cardiovascular morbidity and mortality associated with the metabolic syndrome. *Diabetes Care,* 24 (4): 683-689, 2001.

[9] Ford ES. Prevalence of the metabolic syndrome defined by the International Diabetes Federation among adults in the U.S. *Diabetes care,* 28 (11): 2745-2749, 2005.

[10] Abbasi F, Brown BW, Lamendola C et al. Relationship between obesity, insulin resistance, and coronary heart disease risk. *Journal of the American College of Cardiology*, 40 (5): 937-943, 2002.

Posters:
New Methods and Technologies in Electrocardiology

Assessment of AF Capture during Antitachycardia Pacing Using Largest Lyapunov Exponent Estimation. Insights From a Biophysical Model

[1,2]A. Luca, [1]J.-M. Vesin, [2]A. Vlad

[1]Applied Signal Processing Group, Swiss Federal Institute of Technology, Lausanne, Switzerland
[2]Applied Electronics and Information Engineering Department, University POLITEHNICA of Bucharest, Bucharest, Romania
Email: adrian.luca@epfl.ch

Abstract. *The present study investigates the potential of the Largest Lyapunov Exponent (LLE) for the quantification of AF complexity as a marker of antitachycardia pacing (ATP) effectiveness in a biophysical model of the human atria. From ongoing simulated atrial fibrillation, 20 transmembrane potential maps were used as initial conditions for a rapid pacing from the septum area (at pacing cycle length as a percentage of the AF cycle length). The LLE was separately computed during AF and ATP for the transmembrane potential time series recorded at a single site in the right atrial posterior wall. The averaged results over all 20 simulations show that the LLE decreases during ATP relative to AF. These results suggest that LLE may serve as an indicator of AF complexity and also as a discriminating metric in automatic assessment of AF capture during ATP.*

Keywords: atrial fibrillation, largest Lyapunov exponent, pacing therapies, biophysical model of the human atria

1. Introduction

Atrial fibrillation (AF) is the most common type of sustained arrhythmia which affects about 2% of the general population and 8-11% of those older than 65 years and its incidence is increasing. Important clinical issues in AF data processing are the discrimination between AF groups using the electrocardiogram, the efficient monitoring of AF catheter ablation and the quantification of the influence of antitachyarrhythmia pacing in AF termination. In this context, computer modelling has gained importance in the development of therapeutic strategies for atrial fibrillation, overcoming some of the limitations encountered in clinical research. Specifically, a computer model of AF gives access to the global atrial electrical activity, that is, it is possible to record the electrical activity on a grid covering the atrial tissue.

The three previously mentioned issues in AF data processing are in fact closely related: many research works point to a close relationship between the ability to terminate AF and the amount of disorder in atrial electrical activity during AF, revealing thus the potential of chaos theory based approaches for the quantification of atrial activity organisation in the context of AF treatment. Techniques derived from non-linear dynamics analysis have been used to characterize and to gain a deep insight into the behaviour of cardiac electrical activity, [1-4]. In this context, our study considers the Largest Lyapunov Exponent (LLE) for the quantification of the complexity of the atrial electrical activity during AF. The effectiveness of LLE in the assessment of AF capture during rapid atrial septal pacing was tested by using a biophysical model of the human atria [5].

2. Methods

Biophysical Modelling of Atrial Fibrillation

The biophysical model was based on a homogenous tissue in which the Luo-Rudy model was adjusted to mimic electrical remodelling as observed in patients with permanent AF. This was simulated by setting the channel conductance G_{Na}, G_K and G_{si} to 16, 0.423 and 0.55 mS/cm^2 respectively, [6]. A programmed stimulation protocol was used to initiate atrial fibrillation in the biophysical model. The simulated AF (SAF) dynamics revealed multiple wavelets continuously changing in size and duration due to functional or anatomical re-entries. Figure 1(a) illustrates a snapshot of the wavelet dynamics for simulated AF.

Modelling Pacing of Atrial Fibrillation

From 10 minutes of ongoing SAF, 20 instantaneous transmembrane potential maps were selected as initial conditions for the subsequent simulation of ATP. These maps correspond to different states of electrical activity in the atrial tissue. For each initial condition, a rapid pacing was applied from the whole septal area during 60 seconds at a pacing cycle length (PCL) as a percentage of the AF cycle length (AFCL). The AF cycle length computed out of 10 minutes of SAF was AFCL = 72 ms. The rapid pacing was simulated by injecting a stimulus current inside the cells located in the septal area. The pacing strategy (pacing site and PCL) was designed according to the results from [7, 8], in which the computer modelling was used to search for optimal pacing sites and pacing cycle length leading to a local capture of AF. Figures 1(b)-(c) show the snapshots of the dynamics during atrial septal pacing for two situations: PCL equal to 83% of AFCL and PCL equal to 91% of AFCL, respectively.

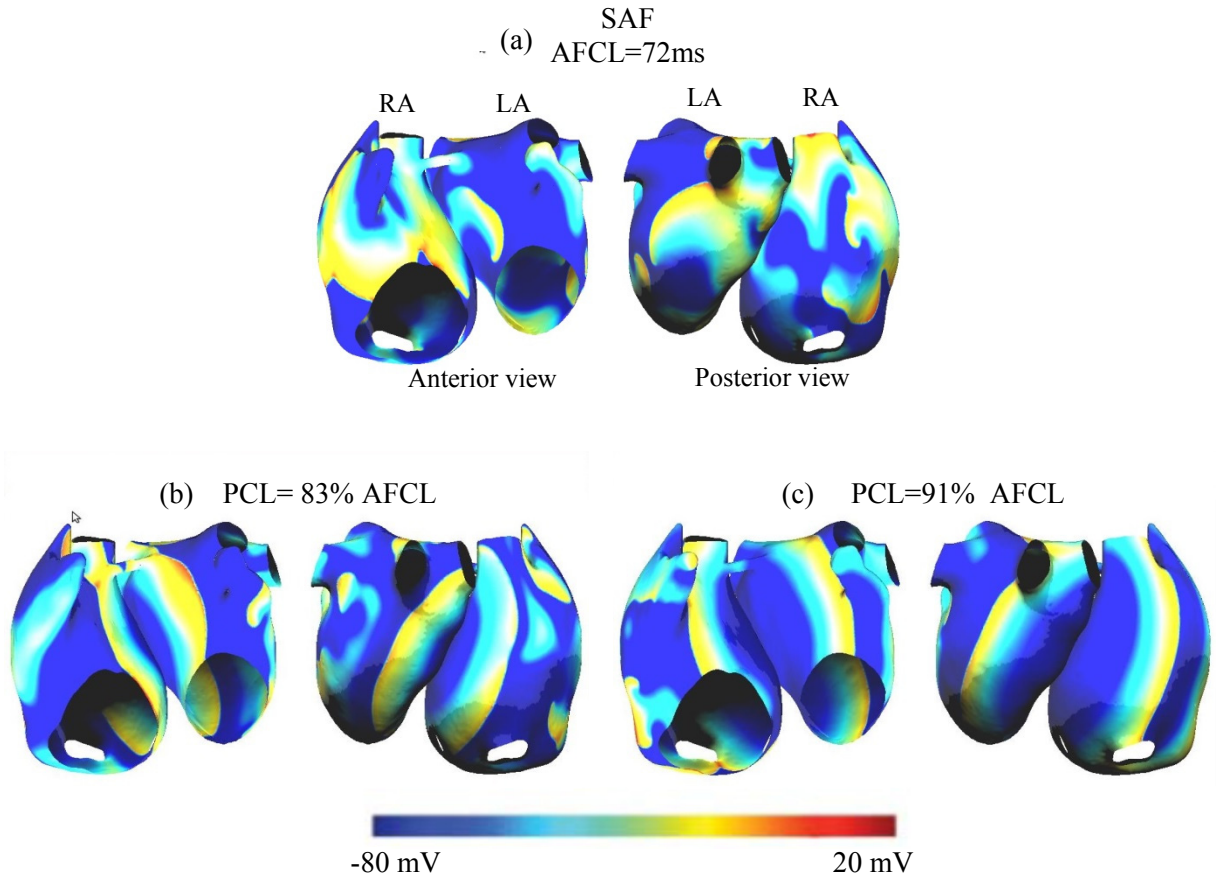

Fig. 1. Snapshots of the dynamics during simulated AF and during pacing for two PCLs. The time of snapshots during the pacing is the 50th second of the simulations.

Assessment of AF capture by using Largest Lyapunov Exponent

20 transmembrane potential time series from a single site in the middle of the right atrial posterior wall were separately recorded during SAF and during pacing. The 20 AF time series consist in non-overlapping segments of 30 seconds length obtained out of 10 minutes of ongoing SAF. The time series during the rapid pacing consist in the last 30 seconds of the pacing simulation. In each situation, the length of the time series was N=30000 samples (the sampling frequency was f=1kHz).

The Lyapunov exponents of a dynamical system are a quantitative measure of the sensitivity of the system to initial conditions (a positive exponent reflects exponential divergence of the trajectories and diagnoses chaos). Furthermore, in many applications it is sufficient to only refer to the largest Lyapunov exponent. The higher LLE is, more complex is the behaviour of the analysed time series (*i.e.* in the present study, a larger LLE means a less organized atrial electrical activity).

The first step in computing the LLE is the reconstruction of the attractor dynamic starting from a particular single time series. One can reconstruct the attractor from a single scalar time series $\{x_k\}$, $k = 1,2,\dots,\mathrm{N}$, using the time delay vectors $(x_k, x_{k+\tau}, \dots, x_{k+(m-1)\tau})$. For an infinite noise free data series one can almost find an embedding dimension *m* (and any delay time τ) for which the delay vectors yields a phase space that has the same properties as the one formed by the original variables of the system. As in practice we do not deal with infinite noise free data series, various methods have been suggested to estimate *m* and τ, but decisions are still often subjective and related to the investigated signals. In the present study, the time delay τ was taken as the time for the autocorrelation function dropped to (1-1/e) of its initial value and the embedding dimension *m* was chosen using Cao's method, [9].

The LLE was separately computed for all time series recorded during AF and during pacing for different PCL values. Based on Rosenstein's algorithm, [10], the LLE was calculated as the slope of the linear regression line defined by:

$$y(i) = \frac{1}{\Delta t} < ln[d_j(i)] >$$

where Δt is the sampling period of the time series, $d_j(i)$ is the distance between the j^{th} pair of nearest neighbours (neighbours from time delay embedding space) after *i* discrete-time steps, i.e. $i \cdot \Delta t$ seconds and $< \cdots >$ denotes the average over all values of *j*.

3. Results

Figure 2 shows the box-plot of LLE estimates during AF and during rapid pacing for two values of PCL (83% of AFCL and 93% of AFCL, respectively). Averaged over all 20 AF initial conditions, the LLE was 0.108±0.002 ms^{-1} (during AF), 0.105±0.003 ms^{-1} (PCL=83% of AFCL) and 0.078±0.009 ms^{-1} (PCL=91% of AFCL).

It can be observed that LLE decreases during pacing relative to AF ($p < 10^{-5}$, Kruskal-Wallis test). Also, the significant difference between LLE for the two values of PCL ($p < 10^{-7}$) indicates that LLE can guide the choice of PCL leading to appropriate AF capture (a smaller LLE means a more regular atrial activity, *i.e.* here a good AF capture by pacing).

4. Conclusions

As we move from AF to ATP, the decrease in the LLE is an evidence of the possibility to use LLE as a non-invasive discriminating metric in automatic assessment of AF capture during ATP. The results obtained in the present model-based study suggest that LLE can quantify the organisation of atrial activity during atrial fibrillation using, noteworthy, measurements from

a single site. These preliminary results motivate further applications of LLE to specific problems in the context of AF treatment, which will permit us to investigate the correlation of the LLE values with AF organization and termination.

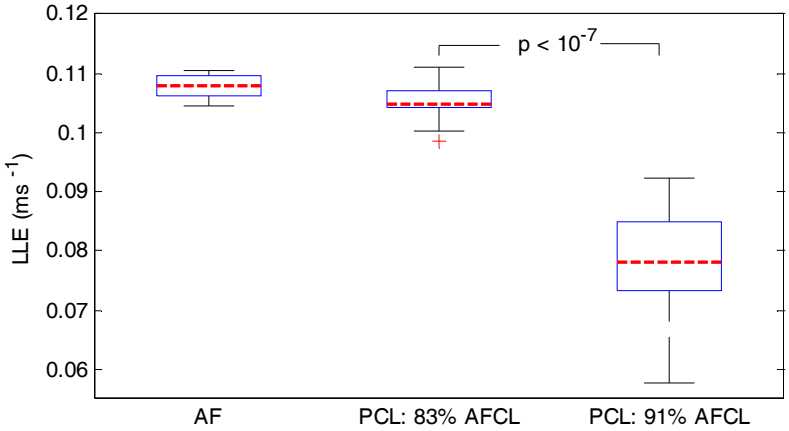

Fig. 2. Box-plot of Largest Lyapunov Exponent during AF and rapid septal pacing for two PCLs

Acknowledgement

The research has been supported by *The Scientific Exchange Programme between Switzerland and the New Member States of the EU* (Sciex-NMS^{ch}) , Project Code 12.363.

References

[1] Kaplan DT, Cohen RJ. Is fibrillation chaos? *Circulation Research*, 67: 886- 892, 1980.

[2] Babloyantz A., Destexhe A. Is the normal heart a periodic oscillator? *Biol. Cybern.*, 58: 203-211, 1988.

[3] Casaleggio A, Ranjan R, Thakor NV. Correlation dimension analysis of epicardial cell action potentials during different cardiac arrhythmias. Computers in Cardiology, IEEE Computer Society Press, 1994, 697-700.

[4] Perc M. Nonlinear time series analysis of the human electrocardiogram. *Eur. J. Phys.* 26: 757–68, 2005.

[5] Jacquemet V. A Biophysical Model of Atrial Fibrillation and Electrograms: Formulation, Validation and Applications. PhD Thesis, École Polytechnique Fédérale de Lausanne, 2004.

[6] Kim BS, Kim YH, Hwang GS, Pak HN, Lee SC, Shim WJ, Oh DJ, Ru YM. Action potential duration restitution kinetics in human atrial fibrillation. *J. Am. Coll. Cardiol.*, 39(8): 1329-1336, 2002.

[7] Udry L, Virag N, Lindemans F, Vesin JM, Kappenberger L. Atrial septal pacing for the termination of atrial fibrillation: study in a biophysical model of human atria. *Europace*, 14 (suppl. 5): v112-v120, November 2012.

[8] Virag N, Rusu A, Vesin JM, Kappenberger L. Modeling atrial pacing. In proceedings of the 35th Annual International Conference of the IEEE/EMBS, 2013, 1518-1521.

[9] Cao L. Practical method for determining the minimum embedding dimension of a scalar time series. *Physica D*, 110 (1–2) : 43–50, 1997.

[10] Rosenstein MT, Collins JJ, De Luca CJ. A practical method for calculating largest Lyapunov exponents from small data sets. *Physica D*, 65: 117–34,1993.

Derivation of McFee-Parungao Orthogonal Leads from Standard Electrocardiogram

[1]V. Trunov, [1]E. Aidu, [2]V. Fedorova, [3]E. Blinova, [3]T. Sakhnova

[1]Institute for Information Transmission Problems RAS, Moscow, Russia
[2]Ates Medica Soft, Moscow, Russia;
[3]Cardiology Research Complex, Moscow, Russia,
Email: trunov@iitp.ru

Abstract. *The study aim was to construct linear transformations for derivation of McFee-Parungao vectorcardiogram (VCG) from 12 standard ECG or Frank VCG and to assess the accuracy of derived electric cardiac signals (ECS) and secondarily derived VCG parameters. A large archive of VCG data recorded in the McFee-Parungao lead system have been accumulated and analyzed in the Cardiology Research Complex (Moscow). To apply this experience to ECSs recorded in the Frank system or standard 12-lead system, linear transformations were constructed basing on sequentially recorded McFee-Parungao VCGs and standard 12-lead ECGs. These transformations provide sufficiently accurate VCGs and secondary vectorcardiographic parameters derived from 12 standard leads.*

Keywords: derived orthogonal ECG, McFee-Parungao lead system, VCG, dipole electrocardiotopography

1. Introduction

For efficient use of clinical experience accumulated with various lead systems, algorithms of ECG transformation are being developed, significantly expanding the armamentarium of diagnostic tools for ECG analysis and integrating disparate facts.

Diagnostic criteria based on orthogonal ECG or VCG findings are widely used in clinical practice. For example, spatial ventricular gradient (SVG) and spatial QRS-T angle are used as indicators of serious pathological changes in the heart. Vectorcardiographic lead systems allow for visual dipolar electrocardiotopographic data presentation, where the time series of instantaneous spatial vectors are converted into time series of areas of activation on a spherical image surface enveloping the heart [1, 2, 3]. Synchronously measured standard ECGs allow for approximate derivation of VCGs and, hence, make benefit from additional possibilities provided by vectorcardiography and decartography.

Various algorithms of standard ECG transformation into the Frank VCG have been proposed [4, 5]. However, some medical centers use another system of corrected orthogonal leads, i.e., the McFee-Parungao system.

Burger et al. [6] compared various systems of orthogonal leads and calculated matrices of linear transformation from one orthogonal system to another, particularly from Frank to McFee-Parungao system. This study was conducted with the original McFee-Parungao lead placement scheme that was subsequently altered.

The aim of the present study was to construct linear transformations for derivation of McFee-Parungao VCG from standard 12-lead ECG or from Frank VCG.

2. Subject and Methods

The Cardiology Research Complex (Moscow) collected a large archive containing standard 12-lead ECGs and McFee-Parungao VCGs. This database contains 50,000 standard ECGs and 10,000 McFee-Parungao VCGs covering a wide range of cardiopathology. The study enrolled 215 patients with paired records of standard ECGs and McFee-Parungao VCGs made sequentially with electrodes replacement from one system to another. These paired records were used to derive approximate linear transformations between ECSs measured in different lead systems.

First of all, we aimed at the construction of linear transformations to derive McFee-Parungao VCGs from standard 12 leads and vice versa. Also of great interest are mutual linear transforms from McFee-Parungao VCGs and true or derived Frank VCGs.

ECSs for the two lead systems were recorded sequentially, therefore, for ECGs to be compared and regression methods to be applied, the measured signals were time-aligned. Functionally relevant time intervals (P, PQ, QRS, ST, and T) obtained via automatic ECG segmentation were aligned by piecewise time interpolation in such a way that the number of points in 12-lead ECG time intervals coincided with the number of points on the corresponding time intervals of VCGs. In some cases, such alignment was impossible due to essential differences in structural, time, and morphological characteristics of ECSs recorded in different lead systems. After exclusion of these cases, the sample contained 195 aligned pairs ($\mathbf{m}_i$, $\mathbf{s}_i$), $i = 1 \ldots 195$, where $\mathbf{m}_i = [\mathrm{x}_i\ \mathrm{y}_i\ \mathrm{z}_i]$ is McFee-Parungao VCG presented as matrix composed of X, Y, and Z components, and $\mathbf{s}_i = [\mathbf{l}_{\mathrm{I},i}\ \mathbf{l}_{\mathrm{II},i}\ \mathbf{v}_{1,i}\ \mathbf{v}_{2,i}\ \mathbf{v}_{3,i}\ \mathbf{v}_{4,i}\ \mathbf{v}_{5,i}\ \mathbf{v}_{6,i}]^{\mathrm{T}}$ is standard ECG presented as matrix composed of 8 linearly independent components.

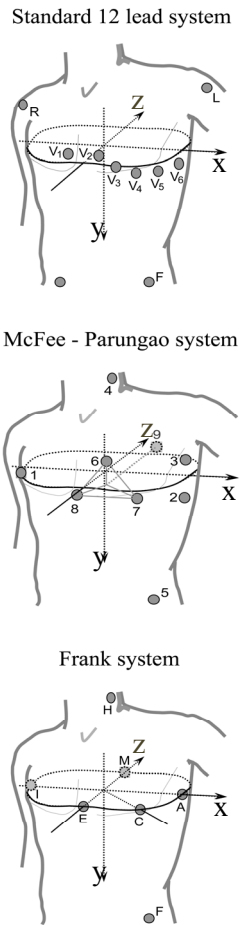

Fig. 1. Lead systems under investigation

The required linear transformation $\hat{\mathbf{T}}$ minimizes the mean squared distance between VCG $\mathbf{m}_i$ and their estimates $\hat{\mathbf{m}}_i = \hat{\mathbf{T}}\mathbf{s}_i$ for standard ECG $\mathbf{s}_i$ in the whole sample:

$$\hat{\mathbf{T}} = \arg\min_{\mathbf{T}} \left(\frac{1}{n} \sum_{i=1}^{n} \left\| \mathbf{m}_i - \mathbf{T}\mathbf{s}_i \right\|^2 \right), \qquad (1)$$

where || . || is Euclidean norm for discrete representation of the 3d vector function.

A different approach is possible, that is, first, we derive the Frank VCG from standard ECG using one of the previously proposed transformations ($\mathbf{T}^{\mathrm{S}\to\mathrm{F}}_{\mathrm{Bemmel}}$, $\mathbf{T}^{\mathrm{S}\to\mathrm{F}}_{\mathrm{Dower}}$, $\mathbf{T}^{\mathrm{S}\to\mathrm{F}}_{\mathrm{Kors}}$ [3, 4]) and then apply the correcting linear transformation of Frank VCG to McFee-Parungao VCG. Approximate transformation $\hat{\mathbf{T}}^{\mathrm{F}\to\mathrm{M}}$ is defined using the minimum mean square error estimator (MMSE):

$$\hat{\mathbf{T}}^{\mathrm{F}\to\mathrm{M}} = \arg\min_{\mathbf{T}:\,\mathrm{F}\to\mathrm{M}} \left(\frac{1}{n} \sum_{i=1}^{n} \left\| \mathbf{m}_i - \mathbf{T}^{\mathrm{F}\to\mathrm{M}} \cdot \mathbf{T}^{\mathrm{S}\to\mathrm{F}}_{\mathrm{A}} \cdot \mathbf{s}_i \right\|_2^2 \right) \qquad (2)$$

Unbiased estimates of ECS approximation accuracy were computed using Leave One Out cross-validation approach, where VCG approximation $\mathbf{m}_j$ was performed with the use of

transformation matrix $\hat{\mathbf{T}}_j$ obtained from MMSE analogous to (1), but on the sample with excluded j^{th} pair of ECS.

3. Results

Using the sample comprised of 195 aligned pairs $(\mathbf{m}_i, \mathbf{s}_i)$ of McFee-Parungao VCG and standard ECG and the least square method, we obtained estimates of linear transformation between $\mathbf{m}_i$ and $\mathbf{s}_i$ for some ECG intervals. Transformation from standard ECG to McFee-Parungao VCG for QT interval is given in the Appendix, and unbiased mean squared approximation errors are listed in Table 1. For the sake of comparison, approximation errors of transformation from standard ECG to Frank VCG with subsequent correcting transformation obtained from (2) are also presented. The correcting transformation from the Frank VCG, derived by Kors matrix, to McFee-Parungao VCG is given in the Appendix.

Accuracy of the secondary derived VCG parameters was assessed using Lin's concordance coefficient [7] (see Table 2). For correct estimation of Lin's concordance coefficients, the sample was randomly divided into training (98 cases) and testing (97 cases) subsamples.

Table 1. RMSE estimates of QRST interval approximation (mean and standard deviation in μV)

Transformation	X Lead	Y Lead	Z Lead	VCG
$\mathbf{T}_{\text{Dower}}^{\text{S}\to\text{F}} * \hat{\mathbf{T}}_{QT}^{\text{F}\to\text{M}}$	90.1 ± 46.1	59.2 ± 28.5	109.5 ± 51.2	91.2 ± 37.3
$\mathbf{T}_{\text{Bemmel}}^{\text{S}\to\text{F}} * \hat{\mathbf{T}}_{QT}^{\text{F}\to\text{M}}$	94.0 ± 47.8	50.8 ± 26.2	94.4 ± 50.1	84.9 ± 37.3
$\mathbf{T}_{\text{Kors}}^{\text{S}\to\text{F}} * \hat{\mathbf{T}}_{QT}^{\text{F}\to\text{M}}$	70.5 ± 37.4	51.4 ± 25.4	91.8 ± 47.8	75.1 ± 33.9
$\hat{\mathbf{T}}_{QT}$ (S→M)	69.3 ± 37.0	49.6 ± 25.9	84.7 ± 45.8	71.4 ± 33.1

Table 2. Lin's concordance coefficient [7] and 95% two-side confidence interval of agreement between true McFee-Parungao VCG parameters and those for derived VCG's (peak spatial QRS-T angle; SVGM, magnitude of spatial ventricular gradient; IRVH, Index of Right Ventricle Hypertrophy[3]; ILVH, Index of Left Ventricle Hypertrophy [2]).

Transformation	QRS-T angle	SVGM	IRVH	ILVH
$\mathbf{T}_{\text{Dower}}^{\text{S}\to\text{F}} * \hat{\mathbf{T}}_{\text{QT}}^{\text{F}\to\text{M}}$	0.89 (0.84, 0.92)	0.93 (0.90, 0.95)	0.93 (0.89, 0.95)	0.86 (0.81, 0.90)
$\mathbf{T}_{\text{Bemmel}}^{\text{S}\to\text{F}} * \hat{\mathbf{T}}_{\text{QT}}^{\text{F}\to\text{M}}$	0.86 (0.80, 0.90)	0.92 (0.88, 0.94)	0.95 (0.92, 0.96)	0.80 (0.73, 0.86)
$\mathbf{T}_{\text{Kors}}^{\text{S}\to\text{F}} * \hat{\mathbf{T}}_{\text{QT}}^{\text{F}\to\text{M}}$	0.94 (0.92, 0.96)	0.96 (0.94, 0.97)	0.97 (0.95, 0.98)	0.93 (0.90, 0.95)
$\hat{\mathbf{T}}_{\text{QT}}$ (S→M)	0.95 (0.93, 0.97)	0.96 (0.95, 0.97)	0.96 (0.95, 0.98)	0.92 (0.89, 0.95)

4. Discussion

All systems of vectorcardiographic leads are designed to evaluate the electric dipole moment of the heart, but the results of measurements are not equivalent due to different placement of leads, and correcting transformations allow for significant reduction of distance between VCG as spatial curves.

We have demonstrated that standard ECG to McFee-Parungao VCG transformations provide sufficiently accurate approximation of the components, spatial VCG loops, and secondarily derived vectorcardiographic parameters. Our study, however, had some limitations, including asynchronous data recording and lack of stratification by gender, age, and diagnosis, which will be the aim of our future investigations. Moreover, it is important to analyze special transformations for other cardiocycle phases, depending on specific cardiopathology.

Acknowledgements

This work was partially supported by RFBR grant 13-01-00521A.

Appendix

The linear transformation matrix to derive McFee-Parungao VCG from standard ECG for QT interval:

$$\hat{\mathbf{T}}_{QT}^{S\to M}=\begin{bmatrix} 0.555 & -0.265 & -0.137 & 0.054 & 0.118 & -0.098 & 0.498 & 0.411 \\ -0.275 & 1.213 & 0.155 & -0.060 & 0.032 & 0.009 & -0.082 & 0.088 \\ 0.140 & -0.251 & -0.324 & -0.157 & -0.452 & -0.319 & -0.112 & 0.292 \end{bmatrix};$$

$$[\mathbf{x}\ \mathbf{y}\ \mathbf{z}]^{T}=\hat{\mathbf{T}}_{QT}^{S\to M}\cdot[\mathbf{l}_{I}\ \mathbf{l}_{II}\ \mathbf{v}_{1}\ \mathbf{v}_{2}\ \mathbf{v}_{3}\ \mathbf{v}_{4}\ \mathbf{v}_{5}\ \mathbf{v}_{6}]^{\mathbf{T}}.$$

The correcting transformation matrix from the derived Frank VCG $[\mathbf{x}_F\ \mathbf{y}_F\ \mathbf{z}_F]^{\mathbf{T}}$ to McFee-Parungao VCG for QT interval:

$$\hat{\mathbf{T}}_{QT}^{F\to M}=\begin{bmatrix} 1.346 & -0.093 & -0.482 \\ -0.291 & 1.300 & 0.205 \\ -0.084 & -0.174 & 1.662 \end{bmatrix};\quad [\mathbf{x}\ \mathbf{y}\ \mathbf{z}]^{T}=\hat{\mathbf{T}}_{QT}^{F\to M}\cdot[\mathbf{x}_F\ \mathbf{y}_F\ \mathbf{z}_F]^{\mathbf{T}}.$$

$$[\mathbf{x}_F\ \mathbf{y}_F\ \mathbf{z}_F]=\mathbf{T}_{Kors}^{S\to F}\cdot[\mathbf{l}_{I}\ \mathbf{l}_{II}\ \mathbf{v}_{1}\ \mathbf{v}_{2}\ \mathbf{v}_{3}\ \mathbf{v}_{4}\ \mathbf{v}_{5}\ \mathbf{v}_{6}].$$

References

[1] Titomir LI, Ruttkay-Nedecky I. Chronotopography: a new method for presentation of orthogonal electrocardiograms and vectorcardiograms. *International Journal of Bio-Medical Computing,* 20: 275-282, 1987.

[2] Titomir LI, Trunov VG, Aidu EA, Sakhnova TA, Blinova EV, Kneppo P. Electrocardiographic diagnosis of left ventricular hypertrophy on the basis of dipole electrocardiotopography method. *Journal of Electrocardiology,* 41 (6): 697.e1-e6, 2008.

[3] Titomir L, Trunov V, Aidu E, Sakhnova T, Blinova E. New approaches to the diagnosis of left and right ventricular hypertrophy by means of dipolar electrocardiotopography. – *The Anatolian Journal of Cardiology,* 7 (Suppl. 1): 29-31, 2007.

[4] Macfarlane PW, Oosterom A, Pahlm O, Kligfield P, Janse MJ, Camm J (Eds.). Comprehensive Electrocardiology. Pergamon Press, UK, 2010.

[5] Kors JA, et al. Reconstruction of the Frank vectorcardiogram from standard electrocardiographic leads: diagnostic comparison of different methods. *European Heart Journal,* 11: 1083, 1990.

[6] Burger HC, van Brummelen AGW, van Herpen G. Compromise in vectorcardiography. II. Alterations of coefficients as a means of adapting one lead system to another: Subjective and mathematical comparison of four system of VGG. *American Heart Journal,* 64 (5): 666 – 678, 1962.

[7] Lin LI. A Note on the Concordance Correlation Coefficient. *Biometrics*, 56: 324–325, 2000.

Comparison of Dubois and Base-Apex Lead Methods to Calculate QRS Angle (Mean Electrical Axis) in Thoroughbreds

C.F. Costa, N. Samesima, C.A. Pastore

Heart Institute (InCor) –HCFMUSP, São Paulo, Brazil
CNPq-Brazil - Scholarship
Email: cassiafre@hotmail.com

Abstract. *This study evaluated electrocardiographic profile of 53 Thoroughbreds, clinically healthy, with ages ranging 2-7 years old, 38 males and 15 females, all reared at the São Paulo Jockey Club, Brazil. Two electrocardiograms were recorded in each horse, and the results of mean electrical axis in frontal plane, obtained by measuring QRS complexes amplitude, were compared using two electrode positioning methods, Dubois and the base-apex methodology. QRS axis in both methods was calculated using 2 different formulas. First, from Tilley's table and second, from α tangent. Values obtained through Dubois lead-system, over 2 different formulas, did not show any statistical difference between them. Additionally, this was the best method of ECG acquisition. In conclusion, base - apex is not adequate for horses because of the influence of body limb positioning and because of inadequate relationship between electrode positioning and the heart.*

Keywords: Equine, Electrocardiogram, Thoroughbreds, Mean Electrical Axis.

1. Introduction

The electrocardiogram (ECG) recording has proved to be a low cost, painless, specific examination for diagnosis of cardiac arrhythmia [1]. However, positioning of the electrodes on the animals is controversial in the literature. In the present study, two different techniques were used. The first, called Dubois method, was described by Ayala et al (2000) and Bello (2012) [2, 3]. The other, base - apex method, was described by some authors like Diniz et al (2008), Dumont et al (2010, 2011) and Manesh & Naghadeh (2010) [4-7].

This study has the objective of comparing results of two different methods of determining the QRS complex angles in Thoroughbreds, using two available methods for electrode positioning to obtain electrocardiographic recordings in horses.

2. Methods

Study subjects
We studied 53 (38 male and 15 female) Thoroughbreds, aged 2 to 7 years old (mean 4.0 ± 1.3 y), mean weight 474 ± 32 kg and 1.62 ± 0.04 m mean height, all reared at the São Paulo Jockey Club. Exclusion criterion was the presence of any health disorder, including cardiopathy, as checked by clinical examination.

The ECG recordings were acquired in quiet environment, with a rubber mat for electrical insulation. The horses remained in orthostatic position, standing with parallel limbs, and no chemical constraint. A portable TEB ECGPC VET 12-channel-electrocardiograph was used, displaying three sensitivities and a paper speed of 25 mm/s or 50 mm/s. The device was set at 25 mm/sec paper speed and sensitivity of 1 cm = 1 mV. Bipolar (DI, DII, DIII), augmented unipolar (aVR, aVL, aVF) and precordial (rV2, V2, V4 and V10) leads were recorded.

The electrodes were fixed to alligator metal clips, which were attached to the horse's skin after being moistened with alcohol. Two ECGs were obtained in sequence from each horse.

Dubois method was first, by placing electrodes (1) and (2) next to the spine tuberosity of the left and right scapulas, respectively; electrode (3) on the xiphoid process of the sternun, and electrode (4) on the proximal cranial region of the left anterior limb (see Figure 1).

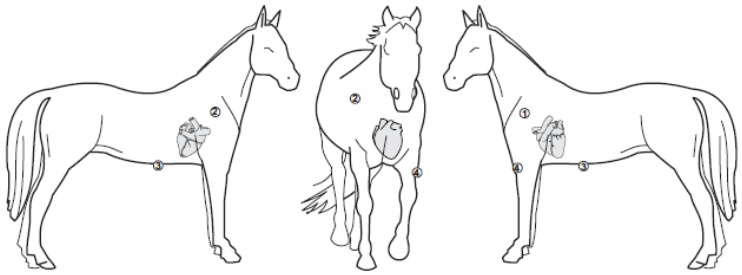

Legends:
(1) On the top of the left scapular spine.
(2) On the top of the right scapular spine.
(3) Over the xiphoid.
(4) Neutral.

Figure 1 – The illustration depicts the disposition of electrodes on the horse using the Dubois method.

The second ECG, using the base-apex method, consists in placing electrode (1) above the left cardiac apex, caudal to the olecranon; electrode (2), cranially to the right shoulder, next to the jugular vein; electrode (3), above the left tibiofemoral patellar joint, and electrode (4) on the proximal cranial region of the left anterior limb (Figure 2).

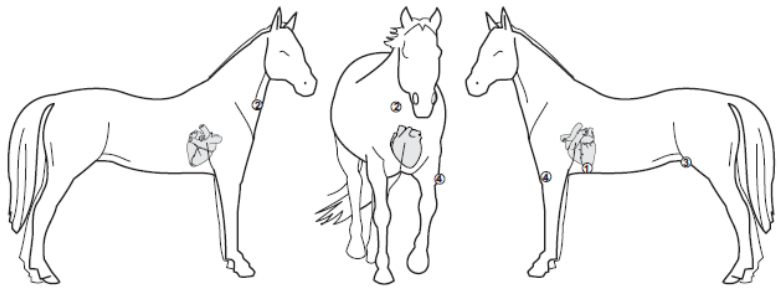

Legends:
(1) On the left chest, just caudal to the point of the elbow (about the 5th intercostal space).
(2) On the right side of the neck, next to the jugular vein (distal).
(3) Left hindleg, placed on the loose skin at the left stifle in the region of the patella.
(4) Neutral.

Figure 2 – The illustration depicts the disposition of electrodes on the horse using the base-apex method.

The parameters for evaluation were obtained by systematic analysis of the QRS complex amplitude values in millivolts (mV), which were semi-automatically measured in leads DI, DIII and aVF with the software of the electrocardiograph, by a sole observer (CFC).

Values of the QRS complex angles were obtained: first, using pre-defined tables, which were developed to be used in cats and dogs to determine the mean electrical axis in the frontal plane from QRS complex amplitudes measured in leads DI and DIII, according to the description by Tilley (1992)[8]; second, from trigonometric calculations (α tangent) of QRS complex amplitudes in leads DI and aVF. Both modes of calculation were applied to the two methods for ECG acquisition (Dubois and base-apex).

Continual variables were expressed as mean and standard deviation values; categorical variables in percent values. Paired *t*-test and Fisher's test were used to compare groups; significance level was set to be lower than 5%.

3. Results

ECGs were divided into two groups, A = base-apex, and B = Dubois, according to acquisition method. The cardiac axis values obtained from leads DI and DIII, as calculated according to Tilley method, composed subgroups A1 and B1. The trigonometric calculations obtained from the intersection of QRS amplitudes in leads DI and aVF, similar to those made for humans, composed subgroups A2 and B2. Figure 3 displays all these results.

Cardiac axis in the ECGs of group A (base-apex), as calculated by Tilley (A1), had mean

+135.1° ± 90.9°, and those trigonometrically calculated (A2) had -15.0° ± 11.3°, p < 0.0001. In the ECGs of group B (Dubois), Tilley (B1) method resulted in -81.1° ± 3.6°, while trigonometric calculation (B2) resulted in -79.9° ± 7.4°, p = 0.3128 (NS).

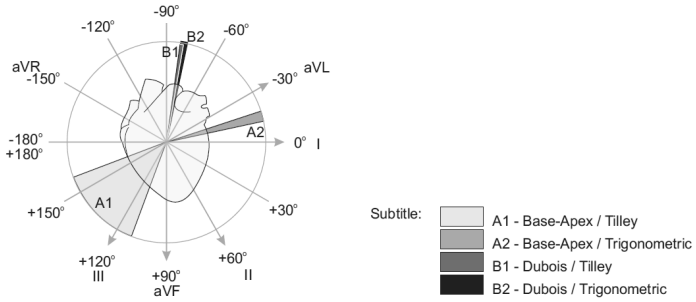

Figure 3 – Graphic representation of the cardiac axis (degrees) in the frontal plane measured in Thoroughbreds.

.

4. Discussion

Presently, there is no standardization for recording electrocardiograms in horses. Several studies came to different results using distinct methodologies. We worked on the assumption that the most reliable results are obtained after centralizing the heart inside the Einthoven triangle. Thus, we studied two methods for positioning the electrodes reported in literature, the base - apex and the Dubois methods. Their main difference relies in the localization of the caudal electrode: the base - apex places it on the tibiofemoral patellar joint, and the Dubois, on the xiphoid process. Given the extent of the animal's long axis, the distance of this electrode in the two approaches can range up to 70 centimeters, which can substantially modify the amplitude values of all ECG waveforms.

Calculation of the P-wave, QRS complex and T-wave angles are based on their voltage and duration; thus, the positioning of electrodes has a key role on results. In order to obtain the values for the QRS complex angles we tested both, the table developed by Tilley and the conventional trigonometric formula. The first, Tilley [8], is composed by values obtained from studies in small animals (cats and dogs). We can consider the results from Tilley´s table as made of values for animals with hearts centered inside the Einthoven triangle. For the second approach we used the conventional trigonometric formula for calculating the α tangent.

The overlapping results of QRS angles obtained by Dubois method, using either approach, the Tilley table or the α tangent, were vertically located in the left quadrant. This result was already expected, since positioning the caudal electrode on the xiphoid process tends to better center the heart, even considering the big dimensions of horses. On the other hand, the base-apex method revealed significantly different values when compared to those acquired by Dubois method, using either formula for QRS axis calculation. The axes are oriented in opposite directions, i.e., there is an axis in ventral and rightward direction (Tilley), and an axis in slightly dorsal and leftward direction (tangent).

The finding of an axis in rightward direction clearly proves that Tilley table cannot be used with the base - apex methodology, since it is inconceivable to have a QRS axis deviated to the right in healthy horses. On the contrary, the results obtained by α tangent calculation showed the QRS axis deviated leftward and dorsally. We understand that the caudal electrode positioned so far from the heart tends to minimize the QRS complex amplitudes, therefore with a smaller projection on the frontal plane leads, and consequently, a more horizontally located angle (Figure 4).

From the anatomical viewpoint, the equine heart is displaced, with 60 % of its volume on the left of the median plane between the 3rd and the 6th rib directly cranial to the diaphragm and quite protected by the forward limbs [9]. Therefore, it is expected that its axis is caudal-ventrally inclined and to the left [10]. This anatomical concept demonstrates that the results provided by the base-apex method (by Tilley) (axis in a ventral orientation and to the right) are incorrect, a fact that was also described by AYALA and col. [2].

Figure 4 – Electrocardiograms differences of a 5 years old male Thoroughbred acquired by the Dubois (left) and the base-apex (right) methods in the same animal.

5. Conclusions

In Thoroughbreds, the electrocardiogram should be performed only by the Dubois method, independent of the QRS complex calculation (Tilley table or α tangent). Otherwise, the heart in this breed will be decentralized in relation to the Einthoven triangle, thus providing significantly distinct and incorrect results.

6. References

[1] Fernandes WR, Larsson MHMA, Alves ALG, Fantoni DT, Belli CB. Características eletrocardiográficas em equinos clinicamente normais da raça Puro Sangue Inglês. [Electrocardiographic characteristics in clinically normal Thoroughbred equines] *Arq. Bras. Med. Vet. Zootec.,*56 (2): 143-149, 2004.

[2] Ayala I, Gutierrez-Panizo C, Benedito JL, Prieto F, Montes A. Morphology and amplitude values of the electrocardiogram of Spanish-bred horses of different ages in the Dubois leads system. *Veterinary Research,* 31: 347-354, 2000.

[3] Bello CAO, Dumont CBS, Souza TC, Palma JM, Lima EMM, Godoy RF, Neto GBP, Moreira M. Avaliação eletrocardiográfica de equinos após exercício de polo (baixo handicap*). Pesq. Vet. Bras.* 32 (1): 47-52, 2012.

[4] Diniz MP, Muzzi RAL, Muzzi LAL, Alves GES. Estudo eletrocardiográfico de equinos da raça Mangalarga Marchador. *Arq. Bras. Med. Vet. Zootec.*, 60 (3): 536-542, 2008.

[5] Dumont CBS, Leite CR, Moraes JM, Alves RO, Godoy RF, Lima EMM. Parâmetros eletrocardiográficos de equinos Puro Sangue Árabe submetidos a exercício prolongado de enduro. *Ciência Rural,* 40 (9): 1966-1973, 2010.

[6] Dumont CBS, Moraes JM, Leite CR, Alves RO, Moreira M, Moscardini ARC, Godoy RF, Lima EMM. Parâmetros eletrocardiográficos de equinos desclassificados por exaustão em competições de enduro. *Arq. Bras. Med. Vet. Zootec.,* 63 (1): 20-27, 2011.

[7] Manesh HT, Naghadeh BD. Electrocardiographic parameters in purebred kurd horse. *Journal of Animal and Veterinary Advances,* 9 (21): 2698-2703, 2010.

[8] Tilley LP. Essentials of canine and feline electrocardiography. 3 ed. Lea & Febiger, Philadelphia, 1992. 470p.

[9] Konig HE. Anatomia dos Animais Domésticos. Vol. 2. Porto Alegre: Editora Artmed, 2004. 787p.

[10] Dyce KM, Sack WO, Wensing CJG. Tratado de Anatomia Veterinária [Treatise on V40

[11] Veterinary Anatomy] 2nd ed. Rio de Janeiro: Ed. Guanabara Koogan, 1997. 856p.

Heart Rate Variability Expressed by Poincaré Plot in Metabolic Syndrome

[1]A. Drkošová, [1]J. Kozumplík, [2]Z. Nováková

[1]Department of Biomedical Engineering, FEEC, BUT, Brno, Czech Republic
[2]Department of Physiology, FM, MU, Brno, Czech Republic
Email: drkosova@phd.feec.vutbr.cz

Abstract. *Heart rate variability, considered as an indicator of autonomic nervous function shows differences between healthy persons and patients with metabolic syndrome. Data from 40 patients with metabolic syndrome and 48 healthy subjects were obtained. Poincaré plots and calculated indexes SD1 and SD2 were used to evaluate the differences between heart rate variability in these two groups. The SD1 and SD2 showed lower values during rest in patients with the metabolic syndrome and a smaller decrease of these parameters occurred during the tilt relative to the control group. This change can be expressed by the difference ΔSD1 and ΔSD2 before and during the tilt. In conclusion, the ΔSD1 obtained from a signal measured in tilt in controlled breathing of 20 times per minute may perhaps help to distinguish between healthy persons and patients with the metabolic syndrome if it is correctly used.*

Keywords: heart rate variability; metabolic syndrome; Poincaré plot

1. Introduction

The heart rate variability (HRV) is considered too be an important tool for the study of autonomic nervous functions. There are several methods for HRV analysis: linear and nonlinear, in time domain or in frequency domain. In this study was used the Poincaré plot, a graphical method belonging to time domain analysis. It stands on the border between nonlinear and linear methods as discussed in [1]. A typical Poincaré plot is constructed as a relationship between RR_i (x-axis) and RR_{i+1} (y-axis), which means that each point in the plot corresponds to two consecutive RR intervals [1], [2].

HRV analysis can be of help also in the study of the metabolic syndrome (MetS), which is defined by a set of multiple metabolic abnormalities associated with cardiovascular diseases [3], [4]. The main risk factors accepted as a part of this syndrome are central obesity, insulin resistance, hyperglycemia, hypertension, and dyslipidemia [3], [5]. There are many different approaches for common classification criteria of MetS [4]. The most used of them are the criteria defined by the U.S. National Cholesterol Education Program, often denoted just as ATP III (Third Adult Treatment Panel) [3]. This standard was also used in this study.

A significant aspect of MetS is a diminished autonomic cardiovascular control which is observed as lower HRV values [6-10]. In almost all of these studies HRV was measured using traditional linear parameters like the time domain statistical methods and spectral analysis, except of the study [8]. Here were used also non-linear parameters, like short-term fractal scaling exponent of detrended fluctuation analysis (DFA-1) and power law slope.

The data in this study were originally obtained in order to examine changes in autonomic functions in patients with MetS for the doctor thesis [10]. This study evaluated blood pressure, pulse pressure, change of pulsatile impedance signal, RR intervals, baroreflex sensitivity, heart rate and blood pressure variability. Hereby, HRV was only evaluated using frequency analysis.

2. Subject and Methods

Subjects
Data were obtained from 40 patients with MetS and from 48 healthy subjects in the First Internal Cardioangiology Clinic, St. Anna's University Hospital Brno. The measuring protocol included 5 min in a horizontal position, followed by an 8 min tilt (75°) and again 5 min in the horizontal position [10]. The controlled breathing of the subjects was 6 times per minute (tilt6) and 20 times per minute (tilt20) respectively.

Poincaré plot
The Poincaré plot was constructed from 5 min intervals before, during and after the tilt for all subjects in all measurements and the parameters SD1 and SD2 were calculated.

The typical shape of a Poincaré plot is an elongated cloud of points (see Fig. 1.) around the line-of identity (LoI).

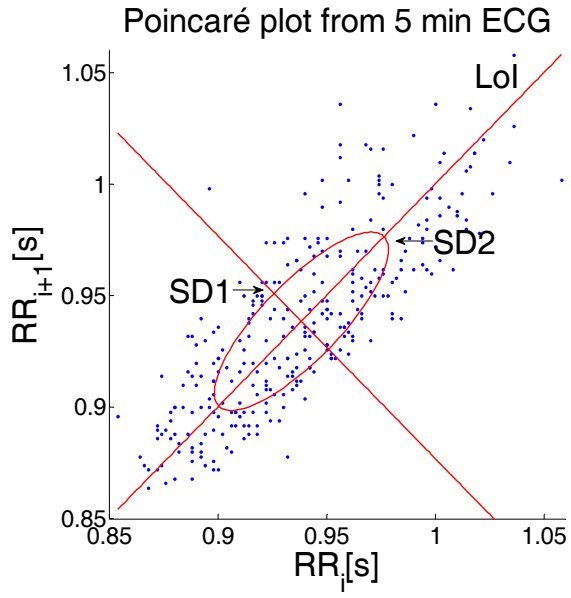

Fig. 1. Poincaré plot from a 5 min record of ECG signal from before tilt (tilt6) in a healthy person.

The shape of the plot can be evaluated visually or numerically. For the numerical evaluation in this study the popular ellipse fitting technique was used. The ellipse minor axis perpendicular to LoI is identical with the standard deviation SD1 and represents the short term variability [1], [2]. The major axis, which is represented by the standard deviation SD2, represents the long term variability. In this study, for the calculation of SD1 and SD2 the equations stated in [2] were used.

3. Results

The SD1 and SD2 showed lower values in rest by patients with MetS and also a smaller change of this parameters occurred during the tilt. In order to better express this change, the difference of SD1 and SD2 before and during the tilt was calculated for each subject. The average values of ΔSD1 and ΔSD2 are in Table 1.

Some values calculated from some subjects had to be omitted because of errors in Poincaré plots due to detection errors of the R wave or heavy ectopic activity. Another problem were also the not long enough stable sections before or during the tilt. To eliminate outliers the Grubbs` test and Dixon test was used on the $\Delta SD1_i$ and $\Delta SD2_i$ values. All the finally used groups for the computing of the average ΔSD1 (or ΔSD2) had statistically significant

differences between SD1i (or SD2i) before and during the tilt (Wilcoxon's matched-pairs signed-ranks, $p<0.05$).

Comparing the values from Table 1, the most visible contrast is between healthy persons and patients with MetS in the case of ΔSD1 in tilt20. In this case we found statistically significant differences $\Delta SD1_i$ (Mann Whitney, $p=0.03$) between healthy persons and patients with MetS.

Table 1. Average values of ΔSD1 and ΔSD2 for the selected set of the healthy control group (Control) and patients with the metabolic syndrome in tilt6 and tilt20 test.

	tilt6_ΔSD1 [ms]	tilt20_ΔSD1* [ms]	tilt6_ΔSD2 [ms]	tilt20_ΔSD2 [ms]
Control	5.69 (sd. 8.63) N = 25	12.15 (sd. 11.10) N = 30	7.81 (sd. 15.07) N = 25	5.01 (sd. 11.91) N = 30
Metabolic syndrome	4.19 (sd. 4.05) N = 22	5.58 (sd. 4.82) N = 33	6.49 (sd. 10.2) N = 22	4.02 (sd. 6.19) N = 31

sd. – standard deviation, N – number of subjects in group, * Mann-Whitney U test $p<0.05$

Calculation of SD1 in time (1 min intervals) showed that the short-term variability decreases faster and more in healthy persons than in the metabolic group when changing the position from horizontal to tilt and afterwards increases again faster when changing the position back to horizontal.

4. Discussion and Conclusions

From the results it is visible that the decrease of SD1 and SD2 in MetS is smaller than in healthy persons. Statistically significant were just the differences $\Delta SD1_i$ during controlled breathing 20 times in minute ($p=0.03$). This breathing frequency (approximately 0.33 Hz) intervenes with the high frequency area (HF 0.15-0.4 Hz) of the HRV spectrum. The parameter SD1 represents fast changes in HRV so it is connected to the HF, which could be a reason why ΔSD1 response in tilt20 so strongly. Further on, by comparing the values of SD1 of the individual subjects there was clearly noticeable that the dispersion of the values before tilt is much higher than during the tilt in tilt20 measure. In the case of tilt6 this phenomenon is not significantly visible.

The high values of standard deviations are most likely due to the interindividual variation of other parameters influencing the HRV, which were not taken in account and represent a limitation of this study.

In the doctor thesis [10] lower values of HRV were expressed by indicators in spectral analysis in patients with MetS than in healthy persons, which is in accordance with findings in this study. Further on, it is pointed out that the breathing frequency of 6 times per minute enhanced the difference between healthy persons and patients with MetS. By this breathing frequency the average values of HRV spectra in low frequency (LF 0.04-0.15 Hz) and HF increased very markedly in the case of healthy persons as compared to MetS instead of decreasing as by tilt20. In our study, a significant difference showed just by ΔSD1 tilt20. Also according to the average values there is just a decrease in the HRV indicators during the tilt and no increase as reported in [10]. But in individual cases there were some, where the HRV parameters increased instead of reducing. This happened in much more cases by SD1 during tilt6 than tilt20. This is probably also a reason why ΔSD1 was significant by tilt20 but not by tilt6. It is discussed in [10] that by the breathing frequency of 0.1 Hz (6 per minute) breathing influences the baroreflex by coming into a resonance with the internal baroreflex frequency of 0.1 Hz and invokes in this way a high response.

Other studies observed statistically significantly lower values in LF and HF in patients with MetS as compared to healthy persons [6] and [9]. In [7] the LF and HF were not significant instead lower values of SDNN (standard deviation of normal RR intervals) and very low frequency in patients with MetS were here significant. These studies used different lengths of recorded data (2-5 min) and diverse compositions of the studied groups. Study [8] cannot be accurately compared with this or the other mentioned studies because it was performed on long-term recordings.

In conclusion, ΔSD1 obtained from a signal measured in the tilt experiment using controlled breathing of 20 times per minute may perhaps help to distinguish between healthy persons and patients with MetS, if other interindividual parameters are also considered.

Acknowledgements

We would like to thank to the collective of the First Internal Cardioangiology Clinic, St. Anna's University Hospital Brno for recording the data used in this study and to the collective of the Institute of Scientific Instruments, Academy of sciences of Czech Republic for providing us with these data.

This work has been supported by the study project no. P102/12/2034 of the Grant Agency of the Czech Republic.

References

[1] Brennan M, Palaniswami M, Kamen P. Do existing measures of Poincare plot geometry reflect nonlinear features of heart rate variability? *IEEE Transactions on Biomedical Engineering*, 48(11): 1342-1347, 2001.

[2] Karmakar ChK, Gubbi J, Khandoker AH, Palaniswami M. Analyzing temporal variability of standard descriptors of Poincaré plots. *Journal of Electrocardiology*, 43(6): 719-724, 2010.

[3] Alberti KGMM, Zimmet PZ, Consultation WHO. Definition, diagnosis and classification of diabetes mellitus and its complications. Part 1: diagnosis and classification of diabetes mellitus. Provisional report of a WHO Consultation. *Diabetic Medicine*, 15(7): 539-553, 1998.

[4] Alberti KGMM, Zimmet P, Shaw J. Metabolic syndrome - a new world-wide definition. A Consensus Statement from the International Diabetes Federation. *Diabetic Medicine*, 23(5): 469-480, 2006.

[5] Shen B-J. Are Metabolic Risk Factors One Unified Syndrome? Modeling the Structure of the Metabolic Syndrome X. *American Journal Of Epidemiology*, 157(8): 701-711, 2003.

[6] Liao D, Sloan RP, Cascio WE, Folsom AR, Liese AD, Evans GW, et al. Multiple metabolic syndrome is associated with lower heart rate variability: The Atherosclerosis Risk in Communities Study. *Diabetes Care*, 21(17): 2116-2122, 1998.

[7] Kang MG, Koh SB, Cha BS, Park JK, Woo JM, Chang SJ. Association between Job Stress on Heart Rate Variability and Metabolic Syndrome in Shipyard Male Workers. *Yonsei Medical Journal*, 45(5): 838-846, 2004.

[8] Stein PK, Barzilay JI, Domitrovich PP, Chaves PM, Gottdiener JS, Heckbert SR, et al. The relationship of heart rate and heart rate variability to non-diabetic fasting glucose levels and the metabolic syndrome: The Cardiovascular Health Study. *Diabetic Medicine*, 24(8): 855-863, 2007.

[9] Koskinen T, Kähönen M, Jula A, Mattsson N, Laitinen T, Keltikangas-Järvinen L, et al. Metabolic syndrome and short-term heart rate variability in young adults. *Diabetic Medicine*, 26(4): 354-361, 2009.

[10] Plachý M. Changes in autonomic functions in patients with metabolic syndrome (language: Czech). 2011. Dissertation thesis. Masaryk University, Faculty of Medicine, Brno. Supervisor: Miroslav Souček.

Assessment of Number of Lesions from Integral Body Surface Potential Maps

M. Teplan, J. Švehlíková, M. Tyšler

Institute of Measurement Science, Slovak Academy of Sciences, Bratislava, Slovakia
Email: michal.teplan@savba.sk

Abstract. *In this simulation study various characteristics of difference STT integral body surface potential maps (DI BSPMs) were used to discriminate cases with single and double modelled lesions with changed repolarization. One or two lesions in different positions in the ventricular myocardium were modelled and corresponding BSPMs were calculated. DI BSPM was computed by subtraction of BSPM computed from normal activation from the BSPM computed from the activation with the presence of one or two lesions. Various morphological and statistical properties of DI BSPM were used as features for a discriminant analysis. Quadratic Fisher discriminant analysis with cross-validation was then used to determine the number of lesions in each case. Taking into account just one best performing feature, the overall error rate for distinguishing the number of lesions was 25.2%. Feature dimensionality was reduced by a feature selection algorithm resulting in 12 features as the optimal number for distinguishing DI BSPMs representing two lesions from maps representing a single lesion. The overall error rate was 4.1%, with partial errors 9.6% and 1.2% for misclassification of single or double lesions, respectively. Discriminant analysis based on exploitation of geometrical and statistical properties of integral BSPMs may be helpful in correct identification of the number of ischemic lesions.*

Keywords: body surface potential maps; discriminant analysis; morphological and statistical map properties; number of lesions

1. Introduction

Patients with ischemic heart disease and atherosclerosis may suffer from one or more simultaneously occluded coronary arteries. In [1] the method for localization of two simultaneous (double) lesions with changed repolarization from DI BSPMs was introduced. DI BSPMs from STT interval [2] were computed by subtracting the normal integral BSPM from an integral BSPM computed from the heart with one or two modelled lesions. However, for optimal use of this method it would be helpful to have preliminary information about the number of lesions in the examined heart.

Therefore in this study various characteristics of simulated DI BSPMs were employed to assess the information about the number of lesions. The aim of the presented paper is to suggest a method for discrimination between cases with single and double lesions with changed repolarization.

In our previous work [3] we suggested to distinguish the cases with two or one lesions from the features of the inverse solution results. Discriminant analysis was performed on both noiseless and noisy data. The best overall error rate for noiseless data was 5.9 % while employing 7 features derived from characteristics of dipoles that were obtained by the inverse solution. However, the inverse problem solution has appeared to be too complicated for the use in clinical praxis. Data for the discriminant analysis were prepared by a multiple step procedure.

Thus, we made an attempt to solve the same problem of distinguishing two from one lesion by a simplified procedure. The new procedure avoids rather demanding step of computing the

inverse solution and extracts characteristics for discrimination analysis directly from the modelled DI BSPMs.

The main idea was based on our expectations that two dipoles might create different DI BSPMs compared to single dipole in respect to maps' morphological and statistical properties. Projection of such disturbances through the body volume conductor should keep information about the number of disturbances. The philosophy is that this information is stored in DI BSPMs, regardless of the fact how we recover it - whether we use the inverse solution or a different approach. However, one may expect certain loss of this information especially in certain mutual positions and sizes of lesions, namely when positions of two lesions are in certain occultation.

2. Subject and Methods

One or two lesions in different positions in the ventricular myocardium were modelled and corresponding BSPMs were calculated on the surface of an inhomogeneous torso model using the multiple dipole cardiac generator. Details regarding heart and lesions simulation models were explained e.g. in [4]. Twelve combinations of two ischemic lesions were adopted, each with eight variations in size and shape. Together 96 pairs and 48 single lesions were modelled. BSPMs on an inhomogeneous torso model were computed using boundary element method [5].

DI BSPMs were used as input data for derivation and calculation of a number of features that were subsequently applied in the discriminant analysis task. The approach comes from an assumption that the maps might differ in both local and global properties. Various morphological and statistical properties of DI BSPMs were studied. The properties should not be dependent on absolute values of map potentials, thus in the first step DI BSPMs were scaled to fit into (-1,1) range of values.

Over 100 features were constructed and tested for performance in the discriminant analysis. Features were constructed in a systematic manner and covered much of all possible ways of measuring the map morphology. In the first step, from every single map representing normalized potential values, number of additional field maps was derived. The maps were constructed according to scalar and vector field operations: gradient (difference of neighbouring map values), divergence (subsequently from gradient field), Laplacian (representing second derivative). Moreover, in addition to construction of this new two-dimensional maps, one dimensional objects were created as well: Map projections in vertical and horizontal direction were processed in a form of mean values obtained from map columns or rows respectively.

Global statistical properties of the maps and their projections were then computed. Among them there were number of peaks (local extremes), minimum, maximum, mean, standard deviation, and central moments (extension of standard deviation into higher orders). Finally, distribution properties of map values were taken into account, being extracted from histogram shape and represented by a histogram based entropy and a length of histogram envelope. Mutual combinations of maps, projections, and statistical properties resulted in 112 different features.

In order to illustrate expected differences in selected features, double lesions might have, for example, higher number of local extremes in both maps and projections, higher mean gradient and mean laplacian in maps, and higher length of curves created by projection either in horizontal or vertical direction.

Two classes corresponding to one and two lesions were used in the discriminant analysis. Quadratic variant of Fisher discriminant analysis (QDA) suitable for unequal covariance matrices of multivariate normal distributions was applied [6]. The analysis was performed in the following testing mode: a cross-validation technique was applied in a form of repeated random sub-sampling validation. In 1000 trials 80% of available data was randomly chosen for training and remaining 20 % for validation. A Classification rule was obtained during the training. The classification outcome was obtained as the number of correctly and incorrectly classified single and double lesions. A feature selection was applied in order to reduce the data dimensionality and to simplify the data evaluation. Greedy forward selection algorithm was used by adding the best feature at each round [7].

3. Results

Taking into account just one best performing feature, the overall error rate for distinguishing number of lesions was as high as 25.2 %. Single most effective feature was *gradStdev*. Its discriminative potential in combination with the second feature *projCurveA* yielded error rate of 17.9 % (see Fig.1). Feature *gradStdev* was derived from the standard deviation of a gradient field map, while feature *projCurveA* is associated with the length of curves created by projections in both vertical and horizontal direction (curves' points are data means from corresponding columns or rows). Further increase of the number of involved features improved the discriminative performance up to the number of 12 (see Fig.2). The overall error rate for the best set of 12 features was 4.1 %, with partial errors of 9.6 % for misclassification of single lesions and 1.2 % for misclassification of double lesions.

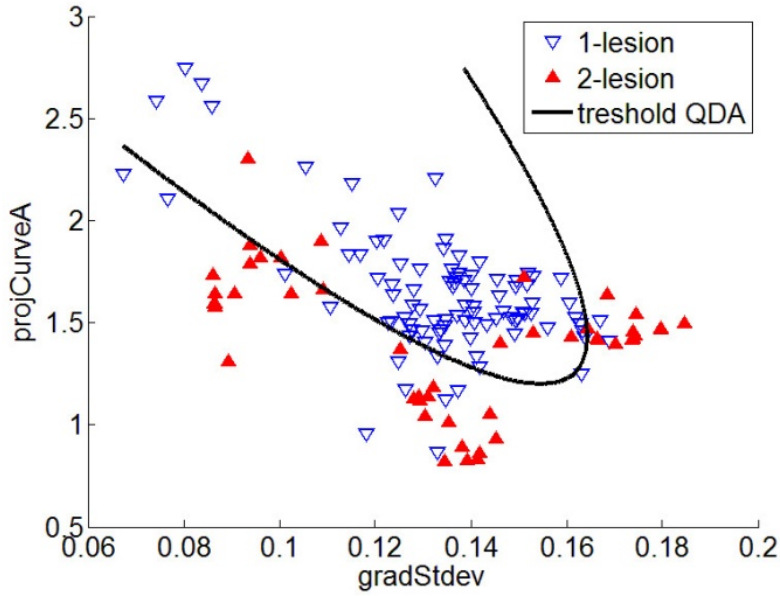

Fig. 1. Quadratic discriminant analyses. Two best performing features in 2 dimensional feature space with overall error 17.9 %.

4. Discussion and Conclusions

The method was applied on 144 cases of simulated data (96 cases of two lesions and 48 cases of one lesion). In distinguishing between one or two simultaneous lesions our newly proposed method over-performed our previous more complicated approach that employed inverse solution [3]. While for the set of 7 features both approaches obtained the same error rate of 5.9 %, only the new method further increased its accuracy and achieved 4.1 % error when 12 selected features were used.

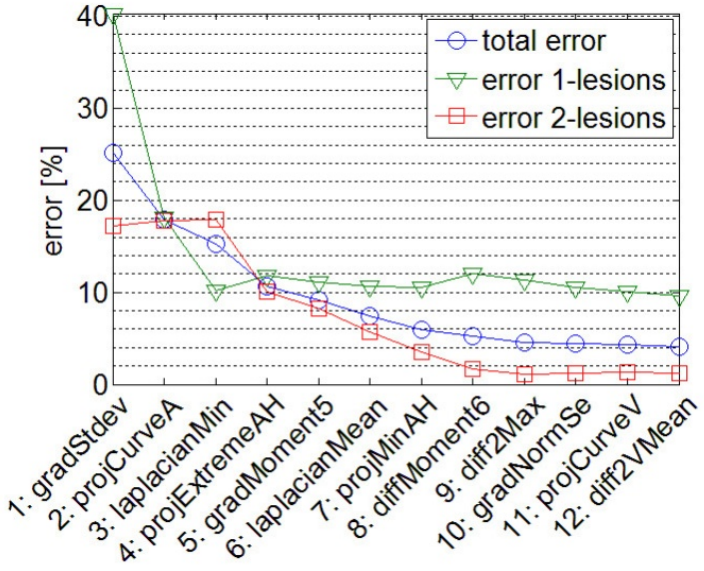

Fig. 2. Quadratic discriminant analyses. Performance of the most effective set of features according to the number of features used. Set of 12 features yielded minimal total error of 4.1 %.

Besides noiseless maps, discriminant analysis between maps with added 20 dB noise was performed as well. Discriminating accuracy remained at the same level of errors. For our future analysis we intent to apply different types of noise, namely noise derived from electrode position uncertainities and from dipole moments that represent the lesions. Discriminant analysis based on exploitation of morphological and statistical properties of integral BSPMs may be helpful in successful identification of number of local electrical sources in the heart ventricles.

Acknowledgements

This work was supported by research grants No. 2/0131/13 and 2/0043/13 from the Vega Grant Agency in Slovakia, by grant No. APVV-0513-10 from the Slovak Research and Development Agency and by project Biomedicine University Research Park Bratislava (ITMS code 26240220087).

References

[1] Svehlikova J, Lenkova J, Turzova M, Tysler M, Kania M, Maniewski R. Influence of individual torso geometry on inverse solution to 2 dipoles. *J Electrocardiol,* 45:7, 2012.

[2] Svehlikova J, Kania M, Turzova M, Heblakova E, Tysler M, Maniewski R. Identification of Ischemic Lesions Based on Difference Integral Maps, Comparison of Several ECG Intervals. *Meas Sci Rev,* 9:117–21, 2009.

[3] Svehlikova J, Teplan M, Tysler M. Classification of Inverse Solutions to Two Dipoles. *Computing in Cardiology,* 40:1127-1130, 2013..

[4] Svehlikova J, Tysler M. Noninvasive finding of local repolarization changes in the heart using dipole models and simplified torso geometry. *J Electrocardiol,* 46:4, 284-288, 2013.

[5] Barr RC et al.. Determining Surface Potentials from Current Dipoles, with Application to Electrocardiography. *Ieee Trans Biomed Eng*, 13:88, 1966.

[6] Therrien C. Decision, Estimation and Classification: an Introduction to Pattern Recognition and Related Topics. John Wiley and Sons, New York, 1989.

[7] Theodoridis S, Koutroumbas K. Pattern recognition. Academic Press, San Diego, 4th ed., 2006.

Analysis of the Ventricular Depolarisation Using Autocorrelation Maps in Young Adult Men and Women

K. Kozlíková, M. Trnka
Institute of Medical Physics, Biophysics, Informatics and Telemedicine,
Faculty of Medicine in Bratislava, Comenius University in Bratislava, Bratislava,
Slovak Republic
Email: katarina.kozlikova@fmed.uniba.sk

Abstract. *Voltage distributions over the whole chest surface can be displayed in form of a set of isopotential maps (IPMs) that can be analysed quantitatively using the Pearson´s correlation coefficient allowing the construction of autocorrelation maps (ACMs). The aim of this retrospective study was to analyse the autocorrelation maps in young adults in time standardised QRS complex. We constructed 21 isopotential maps at equidistant intervals form the QRS complex in 90 young adult controls (42 men). For each QRS complex, every IPM was compared with every IPM using Pearson's correlation coefficient r. These values were displayed in form of ACMs, squared graphs with values r = 1.000 on the main diagonal and symmetrical according to it. The mean QRS complex duration was (92 ± 12) ms. The mean correlation coefficients of single ACMs were 0.087 ± 0.044. The high positive correlation r ≥ 0.900 covered in average (26 ± 5) % of the whole ACM. Negative correlations occurred mainly parallel to the main axis with the mean value - 0.543 ± 0.054. We identified three basic types of ACMs according to the form of regions with positive and negative correlations. In the type I, high positive correlation at beginning of the QRS complex and along the main diagonal changed into a negative correlation reaching the borders of the ACM (15 men, 12 women). In the type II, the negativity was followed by a positivity at the borders of the ACM (23 men, 32 women). In the type III, the positivity was followed by a second negativity in the corners of the ACMs (4 men, 4 women). The ACMs display the large normal variability in ventricular depolarisation by eliminating the influence of the torso.*

Keywords: Body surface potential mapping; QRS complex; Autocorrelation maps; Time standardisation

1. Introduction

Voltage distributions over the whole chest surface can be displayed in form of a set of isopotential maps that can be analysed quantitatively using the Pearson´s correlation coefficient [1] allowing the construction of autocorrelation maps. These maps were firstly introduced in 1976 [2] to express the normal ventricular repolarization in the body surface distribution of T potentials. The autocorrelation analysis was used to analyze the effect of intra-thoracic heart position on electrocardiogram [3] or the beat-to-beat repolarization measurements [4].

The aim of this retrospective study was to analyse the autocorrelation maps in young adults in time standardised QRS complex.

2. Subject and Methods

We studied 90 young adults, 48 women, 42 men, mean age (18.6 ± 0.4) years. None of the subjects had signs of cardiovascular diseases or cardiovascular risk. All subjects had normal 12-lead standard electrocardiographic and echocardiographic findings as well as blood pressure values.

Unipolar electrocardiograms for body surface potential mapping were registered using the limited 24-lead system after Barr based on a grid of 10 rows and 15 columns and processed using the mapping system ProCardio [5, 6]. All data were registered in supine position during normal expiration. Linear baselines were taken through TP segments in each electrocardiogram. The onset and offset of the QRS complex were established manually from the root mean square signal. For time standardisation, the QRS complex duration of each subject was divided into 20 equidistant parts. We constructed 21 isopotential maps for each QRS complex [7]; the first map corresponded to the QRS complex beginning, the last map to its end (see Fig. 1). For each subject, every isopotential map (map A) of a single beat was compared with every isopotential map (map B) of the same beat using Pearson´s correlation coefficient r_{AB} [1]

$$r_{AB} = \frac{\sum_{i=1}^{150}(U_{Ai} - \bar{U}_A)\cdot(U_{Bi} - \bar{U}_B)}{\sqrt{\sum_{i=1}^{150}(U_{Ai} - \bar{U}_A)^2}\cdot\sqrt{\sum_{i=1}^{150}(U_{Bi} - \bar{U}_B)^2}}, \quad (1)$$

where

U_{Ai} (U_{Bi}) the value of electric potential in the i^{th} point of the map A (B),
$\bar{U}_A$ ($\bar{U}_B$) mean value of electric potential in the map A (B).

Comparisons were presented in form of autocorrelation maps, squared graphs displaying the correlation coefficients of every possible pair of potential distribution with values $r = 1$ on the main diagonal and symmetrical due to it (see Fig. 2). We analyzed the form of the regions with high positive correlation $r \geq 0.9$ where the potential distribution changed slowly.

3. Results

The isopotential maps of the QRS complex revealed typical features (see Fig. 1). At the beginning, an anterior maximum appeared that moved downwards and leftwards simultaneously with increasing value till the middle part of the QRS complex. Then its value decreased and the maximum moved to the back or to the upper part of the anterior chest. Low negative potential covered the lower part of the chest at the beginning of the QRS complex. Around its middle, a distinct negativity occurred in the upper right anterior chest (right epicardial breakthrough) and the minimum moved towards the maximum. During the last third of ventricular activation, low negative potential covered either the upper or the lower part of the chest.

The mean QRS complex duration was (92 ± 12) ms. The mean correlation coefficients of single autocorrelation maps were 0.087 ± 0.044 (range $0.011 - 0.207$). The high positive correlation $r \geq 0.900$ occurred predominantly along the main axis but also in other areas. It covered in average (26 ± 5) % of the whole autocorrelation map (mean 0.970 ± 0.004; 15 % – 40 %). Negative correlations occurred mainly parallel to the main axis with the mean value $- 0.543 \pm 0.054$ (down to $r = - 0.994$). No statistically significant differences were found between the groups of men and women in any analysed parameter.

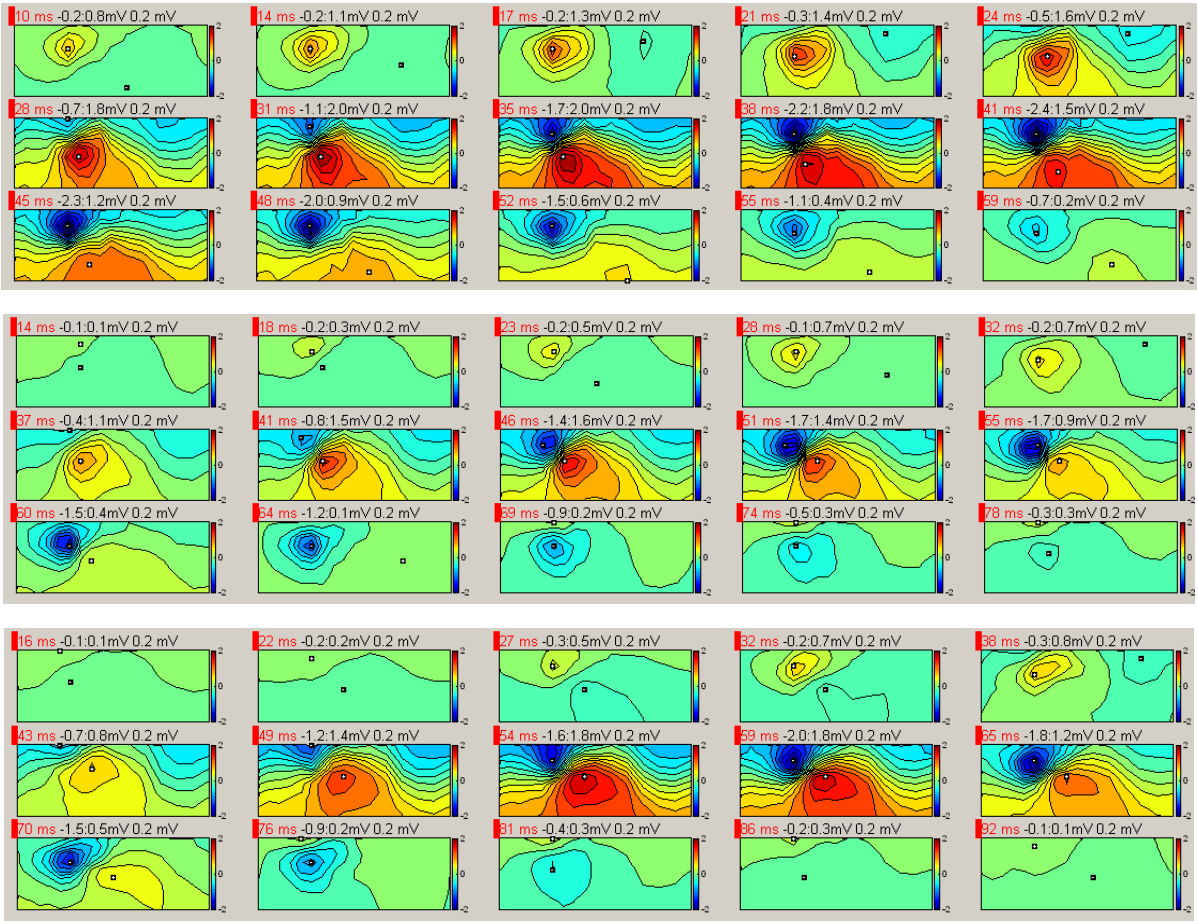

Fig. 1. Examples of isopotential maps of evaluated subjects W-I, W-II, W-III. The maps 4 to 18 are always displayed. The left half of the rectangles corresponds to the anterior chest, the right half to the back. Step between isopotential lines is 0.2 mV.

We identified three basic types of autocorrelation maps according to the form of regions with positive and negative correlations. In the type I, high positive correlation at beginning of the QRS complex and along the main diagonal changed into a negative correlation reaching the borders of the autocorrelation maps (15 men, 12 women; 30% of all maps). In the type II, the negativity was followed by a positivity at the borders of the autocorrelation maps (23 men, 32 women; 61%). In the type III, the positivity was followed by a second negativity in the corners of the autocorrelation maps (4 men, 4 women; 9%).

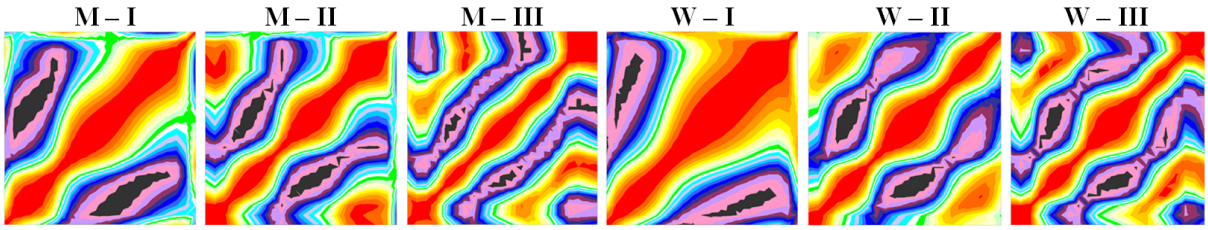

Fig. 2. Examples of 3 different types (I, II, and III) of autocorrelation maps in men (M) and in women (W). The time increases from bottom to top and from left to right. The autocorrelation maps W-I, W-II, and W-III correspond to the isopotential maps in Fig. 1.

4. Discussion And Conclusions

According to the experimental study concerning the QT interval [3], the autocorrelation maps reflect only phenomena taking place in the electric source (myocardium), are very little influenced by the geometry of the volume conductor (thorax) that connects it to the lead system, and are very sensitive to variations in the activation sequence. Comparing the QRS complex autocorrelation map with corresponding isopotential map sequence we found, that the wider is the area of high positive correlation area, the smaller is the change in shape of the activation sequence between successive instants (compare Fig. 1 and Fig. 2).
Great variety of shapes of autocorrelation maps occurred among the studied subjects. However, we could identify three main types of autocorrelation maps. Two types are similar to those identified earlier in [8] that were divided into 12 classes. The elimination of the thorax contribution to the body surface potential maps opens the possibility to evaluate the extent of the heart activation and recovery variability in a normal population.

Acknowledgements

This work was partially supported by the VEGA project 1/0727/14 from the Ministry of Education, Science, Research and Sport of the Slovak Republic.

References

[1] Kozlíková K, Martinka J. The Essentials of Biomedical Measurement Processing II (Slovak). Asklepios, Bratislava, 2009.

[2] Abildskov JA et al. The expression of normal ventricular repolarization in the body surface distribution of T potentials. *Circulation,* 1976; 54(6): 901 – 906.

[3] Corlan AD, MacLeod RS, DeAmbroggi, L. The effect of intrathoracic heart position on electrocardiogram autocorrelation maps. *Journal of Electrocardiology,* 2005; 38(2): 87 – 94.

[4] Kozmann G, Haraszti K. Importance of body surface potential field representation fidelity: analysis of beat-to-beat repolarization measurements. *The Anatolian Journal of Cardiology*, 2007; 7(Suppl 1): 5 – 7.

[5] Barr RC, Spach MS, Herman-Giddens GS. Selection of the number and positions of measuring locations for electrocardiography. *IEEE Transactions on Biomedical Engineering,* 1971; 18: 125 – 138.

[6] Rosík V, Tyšler M, Turzová M. Portable device of for ECG mapping, in Proceedings of International Conference of Measurement. Frollo I and Plačková A (Eds.). SAV, Bratislava, 1997, 367 – 370.

[7] Kozlíková K. Surface integral maps, their characteristics and methods of quantitative analysis. *Bratislavské lekárske Listy* 1990; 91 (11): 815 – 823 (Slovak).

[8] Corlan AD, DeAmbroggi L. The normal variability of the QRS autocorrelation maps, in Advances in Electrocardiology 2004. Hiraoka et al. (Eds.). World Scientific Publishing, Singapore, 2005, 507 – 511.

Quantitative VCG and BSPM Repolarization Parameters Evidence Increased Sympathetic Activation of the Ventricular Myocardium in Different Adrenergic Situations

V. Regecová, E. Kellerová

Institute of Normal and Pathological Physiology, Slovak Academy of Sciences, Bratislava, Slovakia
Email: valeria.regecova@gmail.com

Abstract. *Participation of the sympathetic nervous system (SNS) in normal or pathological regulations of the heart is in present studies documented mainly by blood pressure (BP) and heart rate (HR) derived indexes. The previously proposed parameters characterizing ventricular repolarization were used in this study to detect the presumed effect of SNS hyperactivity on the ventricular myocardium in prehypertensive subjects and in sympathergic situations. In 75 healthy boys and men, aged 15 – 35 years with optimal, normal and high normal BP and normal or increased body fat proportion (BF), the BP, HR, QTc index, rate pressure product (RPP), magnitude of the maximal spatial repolarization vector (sTmax) and amplitude of the isointegral repolarization map (RIMampl) were evaluated. Compared to subjects with optimal casual BP ≤120/80 mmHg, already in the class defined as normal and high normal BP (ESH/ESC 2013), the differences in repolarization parameters point to significantly higher sympathetic outflow to the ventricular myocardium at rest, similar to changes due to psycho-emotional or postural reactions. An additional factor – higher proportion of BF amplified the sTmax and RIMampl signs of the direct myocardial SNS effects.*

Keywords: Ventricular repolarization; VCG and BSPM; Sympathetic activation; Stress; Prehypertension; Obesity

1. Introduction

The first convincing evidence about the contribution of a permanently increased sympathetic drive of central origin to the onset of human primary hypertension came in the late 1950's, based on experimental studies by Brod et al.[1]. They documented in borderline hypertensives already at rest a cardiovascular pattern similar to that displayed in emotional defense reactions. Another study revealed a 70% prevalence of a hyperkinetic circulation in young hypertensives [2]. Increased HR, or low frequency components of the power spectral density of HR variability are the noninvasive, easily accessible parameters, most frequently used in clinical and physiological studies to estimate the enhanced sympathetic activation of the heart. However these measures reflect mainly the sympathetic and parasympathetic interaction in the control of the pacemaker activity, but not necessarily the specific sympathetic effect on ventricular myocardium. VCG and BSPM parameters characterizing ventricular repolarization - namely the magnitude of the maximal spatial repolarization vector (sTmax), the spatial angle between QRS and T vectors and the peak-to-trough amplitude of the integral STT BSPM (RIMampl) - have repeatedly been shown to carry information on the direct effect of sympathetic activation on the ventricular myocardium, in a variety of physiological situations involving autonomic cardiovascular control in normal subjects [3]. With the aim to assess the presumably increased sympathetic drive of the cardiac ventricles, these descriptors were analyzed in young subjects with optimal, normal and high normal BP

(according the ESH/ESC 2013 stratification) - at rest, as well as during sympathergic psycho-emotional and postural reactions, and with respect to different body fat proportion.

2. Subject and Methods

A total of 75 healthy boys and men, aged 15 – 35 years were enrolled in the study, divided in subgroups, to investigate the effect of high normal BP, increased body fat percentage and of sympathergic situations (psycho-emotional stress, head-up tilting,). There were 23 subjects with optimal BP ≤ 120/80 mmHg and body fat percentage (BF) ≤15%, 46 in the range of normal and high normal BP, according to the ESH/ESC (2013) stratification, 21 of them were with BF proportion ≤ 15% and 31 with increased BF >15%.

PC based electrocardiographic system CARDIAG 128.1 was used to record, and partly processed by the Frank lead system VCGs and body surface potential maps (BSPM) from 80 electrode sites. Simultaneously BP was measured oscilometrically by an OMRON M10 IT device. From a selected single beat the maximal spatial vector of ventricular depolarization (sQRSmax) and repolarization (sTmax), spatial angle between integral QRS and STT vectors (QRS-T angle), the peak-to-trough amplitude of the isointegral repolarization maps (RIMampl), the RR and QTc intervals were evaluated. For the detailed processing of isointegral maps see [4]. As an estimate of the major determinant of the cardiac oxygen consumption, the rate pressure product (*RPP = BPsyst * HR/100*) was calculated.

The recordings were performed in following situations: lying supine at rest (SUP), tilted head-up to 60^{o} (TILT), after an intermission sitting rest (SIT) and using stressful mental arithmetic as an emotional stimulus (MA). Chi-square, Student-t tests and / or two-way ANOVA were used for statistical evaluation and the minimal level of significance was set to $P < 0.05$.

3. Results

Comparing to the control subgroup with BP ≤ 120/80 mmHg and BF proportion ≤ 15%, already in the group of subjects with normal and high normal BP (median 131/85 mmHg and BF ≤ 15%), all seated at rest, a significantly decreased magnitude of the maximal spatial repolarization vector (sTmax) by 25%, of amplitude of the STT body surface map (RIM ampl) by 20%, shortened R-R by 14% and an increased rate pressure product (RPP) by 35% were found. (Table 1, subgroup 2). There was an expected trend for increased QRS-T angle by 4%.

When an additional risk factor - higher body fat proportion >15% was considered (Table1, subgroup 3), all above mentioned differences were amplified - decrement of sTmax was 39%, RIM ampl 40%, R-R 19%, increase of RPP 55% and of the QRS-T angle 10%.

The differences between subgroups 1 – 3 are evident also in horizontal and tilted body posture (Table 2) and in the MA test (Table 1).

Changes in the repolarization parameters due to the elevated BP and increased BF%, are similar to those, which were evoked by sympathergic test situations, namely by emotional stress induced by MA in sitting position (Table 1, subgroup 1 - 3), compared to rest supine, with significant diminution of sTmax by 17 - 24%, RIM ampl by 30 - 42%, R-R by 25 – 31%, an increase of RPP by 53% and of the QRS-T angle by 27– 49%

Tilting head-up (Table 2, subgroup 1 - 3) caused significant diminution of sTmax by 16 -25%, RIM ampl by 10 - 12%, R-R shortening by 16 -20%, change of RPP from –16 to +26% and an increase of QRS-T angle by 27 – 41%.

The sQRSmax vector as a parameter defining depolarization did not change meaningfully in any situation. Interestingly some correlations of sTmax and RIMampl, with BP and QTc significant at rest, decrease or disappear in reactive situations.

Table 1. Mean values of blood pressure, R-R and QTc intervals, magnitude of maximal spatial repolarization vector (sTmax) and amplitude of integral repolarization map (RIMampl), during the test of mental arithmetics (MA), compared with values sitting at rest (SIT).

	Blood pressure [mm Hg]		R-R interval [ms]		QTc interval [ms]		sTmax [μV]		RIMampl [μVs]	
	SIT	MA	SIT	MA	SIT	MA	SIT	MA	SIT	MA
1	112/75	**129/85**	959	**775**	392	**420**	588	**538**	162	**146**
2	132/81 *	**142/91** *	821 *	**648** *	403	**436**	442 *	**393** *	130 *	**114** *
3	132/83 *	**140/90** *	781 *	**652**	397	**416**	360 *	**329** *	98 *	**87** *
All	124/80	**135/88**	846	**694**	397	**423**	452	**415**	128	**115**

Table 2. Mean values of blood pressure, R-R and QTc intervals, magnitude of maximal spatial repolarization vector (sTmax) and amplitude of integral repolarization map (RIMampl), in head-up tilted position to 60° (TILT), compared with values at rest supine (SUP)

	Blood pressure [mm Hg]		R-R interval [ms]		QTc interval [ms]		sTmax [μV]		RIMampl [μVs]	
	SUP	TILT	SUP	TILT	SUP	TILT	SUP	TILT	SUP	TILT
1	118/72	**116/83**	1074	**861**	392	**417**	648	**542**	209	**188**
2	135/76*	134/**92** *	941 *	**792**	402	**416**	554*	**424** *	199	**181**
3	135/79*	**131/88** *	873 *	**715** *	395	**410**	433*	**326** *	149 *	**131** *
All	128/76	**125/87**	948	**786**	398	**414**	529	**424**	179	**159**

Subgroups: 1= BP ≤ 120/80 mmHg with BF ≤15 % (control)
2 = BP normal and high normal with BF ≤15 %
3 = BP normal and high normal with BF >15 %

Bold – significant change vs sitting / supine rest $p<0.05$

* significant vs control subgroup $p<0.05$

4. Discussion and Conclusion

The discriminative power of the VCG and BSPM repolarization parameters was strong enough to distinguish the changes in the cardiac electric field in adolescents and young adults with elevated BP - just above the limit of its optimal value, and in subjects with increased body fat proportion. Decreased sTmax as well as of the RIM ampl in these subgroups, are similar to changes registered during mental or postural reactions in this and earlier studies [3,5]. Comparable results in the repolarization pattern were described in patients with no

cardiovascular diseases but suffering from panic disorder [6] treated by antidepressant drugs [6], or in normal subjects under the infusion of dopamine [8]. These findings support our interpretation of the ventricular recovery pattern in young subjects with elevated BP and higher BF% as well as of its reactive changes in sympathergic situations as an effect of direct sympathetic nervous drive of ventricular myocardium.

Present data in agreement with a previous study [4] document, that the effect of the body fat percentage on the repolarization characteristics goes over the extend of the physiological interindividual variability, and as it differs from the negligible effect on depolarization, it cannot be explained only by physical reasons (increased distance of electrodes from the heart, impedance of the fat tissue, etc.), but indicates with a high probability the contribution of an augmented sympathetic activation of the ventricular myocardium in the obese.

As all these phenomena are related to some individual trait, characterized by predisposition to activate the sympathetic drive of ventricles, there is an intra-individual variability in their intensity and appearance.

Our conclusions hold true above all in subjects between the dividing lines for normotension, and hypertension, still with no clinical signs of some target organ damages, but – more often than not – with an autonomic imbalance, playing not only a primary pathogenetic part, but amplifying the adverse effects of other cardio-vascular risk factors as well. As in Slovakia 51% of the adolescent and young men are in the category of high normal BP and 22% are overweight or obese, present analysis may be of value in characterizing a certain individual state of the sympathetic regulation of the cardiac ventricles and also instrumental in studies of cardiovascular risk prediction.

Acknowledgement

This work was supported by grants APVV-0523-10, VEGA2/0084/14.

References

[1] Brod J, Fencl V, Hejl Z, Jirka J. Haemodynamics in essential hypertension. Nature, Nov 21;184 (Suppl 21): 1643-1644, 1959.

[2] Widimský J, Fejfarová MH, Fejfar Z. Changes in cardiac output in hypertensive disease. Cardiologia (Basel), (31):381-389, 1957.

[3] Ruttkay-Nedecký I: The effect of the autonomic nervous system on the heart. Electrocardiographic evaluation: Problems and concerns. Cardiol. (10): 42-48, 2001.

[4] Regecová V, Katina S, Kellerová E, Szathmáry V: Influence of subcutaneous fat on the variability of body surface integral maps. Slov. Antropol., 10(1):113-118, 2007 .

[5] Ruttkay-Nedecký I. Effect of emotional stress on cardiac repolarization vectors. Adv Cardiol (21):284-285,1978.

[6] Pišvejcová K, Paclt I, Slavíček J, Kittnar O, Dohnalová A, Kitzlerová A: Electrocardiogram, vectocardiogram and body surface maps in patients with panic disorder. Phys. Res (51): 401-406, 2002.

[7] Slavíček J, Paclt I, Hamplová J, Kittnar O, Trefný Z, Horáček BM: Antidepressant drugs and heart electrical field. Phys Res 1998; 47: 297-300.

[8] Kellerová E, Vigaš M, Kvetňanský R, Ježová D: the influence of dopamine on the maximal spatial repolarization vector of the human heart. In: Electrocardiology ‘83. Ruttkay-Nedecky I, Macfarlane PW (Eds.), Elsevier, Amsterdam, 1984; pp. 78-83.

Comparison of Propagation of Atrial Excitation with the Cardiopotential Distribution on the Body Surface of Fish

S. Smirnova, I. Roshchevskaya, M. Roshchevsky

Laboratory of Comparative Cardiology, Komi Science Centre, Russian Academy of Sciences, Syktyvkar, Komi Republic, Russia
E-mail: smirnova.sl@mail.ru

Abstract. *This research was aimed at studying the sequence of depolarization the atrial epicardium and formation of the cardioelectric field on the body surface (BSPM) of Atlantic cod Gadus morchua (n=9). The initial zone of depolarization appeared on the atrial epicardium of fish before the origin of the P-wave in the ECGII. During the ascending phase of the PII-wave the excitation wave evenly spread from the caudal part of the dorsal side to the cranial part in the right-lateral area of atria. At the peak of the PII-wave and during the first half of the descending phase of the PII-wave the dorsal side and the caudal part of the ventral side in the right-lateral area of atria were depolarized. Atrial depolarization during initial phases of are projected on BSPM by the distribution of zones of positive and negative cardiopotentials before the beginning of the P–wave in the ECG. The location of zones of positive and negative cardiopotentials and the movement of extrema on the BSPM reflect the propagation of the excitation wave along the atrium from the venous sinus to the heart ventricle of fish.*

Keywords: *atrial depolarization, body surface potential map, epicardium, Atlantic cod Gadus morchua*

1. Introduction

The heart of poikilotherms consists of one atrium and ventricle [1]. In the fish heart there is only one specialized system: the pacemaker [2]. The ring-shaped structure around the venous sinus can function as a pacemaker in Zebrafish [3].

In European grayling and pike, the depolarization wave successively spreads along atrial walls from the sino-atrial area to the atrioventricular opening providing a successive contraction of the heart walls from sino-atrial area to the atrioventricular opening [4].

In mammals, the sequence of atrial depolarization is reflected on BSMP by the location of areas of positive and negative cardioelectric potentials [5, 6].

The pattern of the sequence of atrial depolarization and regularities of the reflection of excitation on BSPM in fish is not described.

This research was aimed at studying the sequence of depolarization along the atrial epicardium and formation of the cardioelectric field on the body surface of Atlantic cod *Gadus morchua*.

2. Methods

Subject and Animals

Experiments were carried out on nine Atlantic cod *Gadus morchua* (a habitat of the White Sea, Republic of Karelia). Fish were caught by fixed nets and spinning. They were placed on a specially made table, a tube through which water was given to gills was inserted in a mouth (the water temperature was kept within the limits of natural habitat t = 12-11° C).

The investigation conforms with the Guide for the Care and Use of Laboratory Animals published by the US National Institutes of Health (NIH Publication No. 85–23, revised 1996) and was approved by an institutional ethical committee.

Experimental protocol
Body surface potential mappings (BSPM) were simultaneously recorded from 32 subcutaneous needle electrodes (registering surface-0.06 cm2), uniformly distributed on the torso surface of fish. After opening the thorax and cutting the pericardium, by using multipolar electrode with 40 leads (contacting electrode surface 0.004 cm2) unipolar epicardial electrograms (EG) were recorded from atria in the same fish (32 deferent electrodes were placed on the dorsal side of the atrium, and 8 discharging electrodes were placed on the ventral surface).

Electrocardiography
Simultaneous data acquisition was done by means of a custom-designed mapping system (16 bits; bandwidth 0.05 to 1000 Hz; sampling rate 4000 Hz) [7]. Unipolar epicardial electrograms EG and ECGs were recorded in reference to Wilson's central terminal. By unipolar ECGs from the body surface isopotential mappings were constructed. Sequence of spreading of the excitation wave was constructed through the first temporal derivative of epicardial EG. BSMP and sequence of epicardial depolarization were compared relative to R-peak in the ECGII in the limb leads. The data processing was carried out using the software of our development [7].

Statistical analysis
Data were analyzed using Statistica software version 6.0 for Windows statistical package (StatSoft, Inc., Tulsa, OK, USA). All results were expressed as mean±standard deviation. Statistical analysis was performed using an independent samples t-test. Differences were considered to be statistically significant if the p value was <0.05.

3. Results

Before the beginning of the P-wave in the ECG II from the limb leads, on the atrial epicardium of fish the initial zone of depolarization appears in the caudal part of the dorsal side (Fig. 1, D, - 269.00 ms). On BSMP in this period of time (Fig. 1, A, - 269.00 ms), the area of positive cardiopotentials occupies the largest part of the ventral and dorsal sides, the area of negative potentials occupies the caudal part of the dorsal side, the positive extremum is located left-laterally from the ventral side, the negative one – caudally in the middle part of the dorsal side.

During the ascending phase of the P_{II}-wave, the excitation (Fig. 1, D, - 246.00 ms) evenly spreads along the atrial epicardium from the caudal part of the dorsal side to the cranial part along the right-lateral area. On BSMP (Fig. 1, A, - 246.00 ms) the zone of negative potentials increases and occupies the left-lateral part of ventral and dorsal sides, while the zone of positive ones is situated right-laterally from the ventral and dorsal sides. Such location of the areas of positive and negative cardiopotentials remains up to the peak of the P_{II}-wave. During the ascending phase of the P_{II}-wave, on BSMP the extrema move cranially: the positive extremum – to the ventral side, the negative extremum – to the middle part of the dorsal side. Such location of the extrema remains in the peak and the descending phase of the P_{II}-wave.

In the peak and the first half of the descending phase of the PII-wave, on the atrial epicardium (Fig. 1, D, - 213.50 ms) the whole dorsal side and the caudal part of the ventral side in the right-lateral area are depolarized. During the first half of the descending phase of the PII-wave

on BSMP, (Fig. 1, A, - 213.50 ms) the area of positive cardioelectrical potentials increases and occupies the largest part of the ventral and dorsal sides, whereas the area of negative ones shifts and occupies the caudal part of the dorsal side.

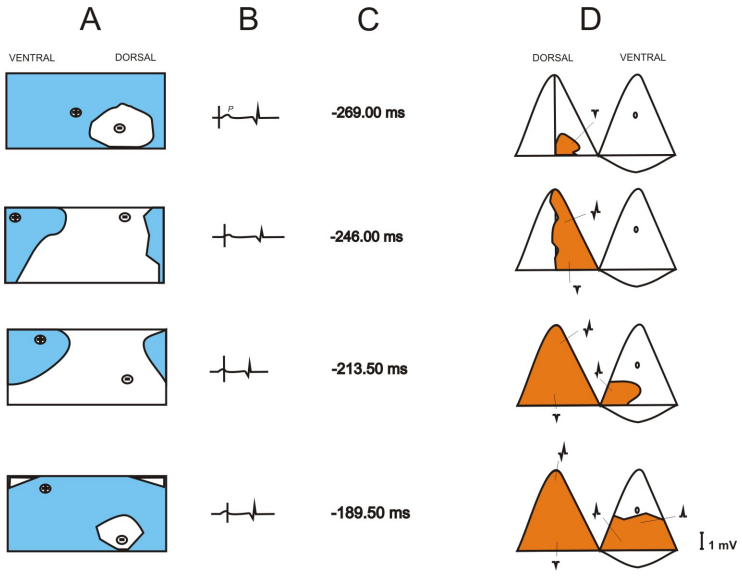

Fig. 1 Sequence of depolarization along the atrial epicardium and formation of the cardioelectric field on the body surface of Atlantic cod *Gadus morchua*.

By the end of the PII-wave (Fig. 1, D, - 189.50 ms) while spreading along the epicardium the excitation wave reaches the junction of the atrium and ventricle.

Isopotential body surface map (BSPM) on the fish's body surface (A). Shaded areas are positive potentials; «+» and «-» - locations of positive and negative extrema. ECG in the II limb lead with the time market (vertical line) (B). Time of time market relative to the peak RII (C) Scheme of sequence of the excitation wave on atrium epicardium of fish. (D) Near the map there are original electrograms registered in the areas marked with pointers.

4. Discussion

Before the beginning of the *P*-wave in the ECG II on the atrial epicardium of fish, the initial zone of depolarization appears which is reflected on BSMP by a characteristic location of areas of positive and negative cardioelectric potentials. On the body surface of mammals the inversion of mutual location of areas of positive and negative potentials is observed before the beginning of the *P*-wave in the ECG II [8]. On BSMP of fish during atrial depolarization, the inversion of mutual location of the areas of positive and negative potentials isn't observed before the beginning in the ECG II of the *P*-wave. It's connected with a simple organization of the conducting system of the fish heart [3]. The early zone of atrial depolarization in fish is located in the place of the junction of the sinous node and atrium. It is known that in African lungfish the pacemaker of the first order is located in the sinous node, under certain conditions the pacemaker can shift [9]. The distribution of the excitation wave through the atrium in zebrafish happens evenly, there is a small delay in excitation passing from the atrium to the ventricle [10].

On BSMP during ascending and descending phases of the PII-wave, there are no significant changes in the location of positive and negative cardiopotentials. During the ascending phase of the PII-wave, the excitation wave evenly spreads along the atrial epicardium from the caudal part of the dorsal side to the cranial part in the right-lateral area. At the peak of the PII-wave and during the first half of the descending phase of the PII-wave, on the epicardium the whole dorsal side and the caudal part of the ventral side in the right-lateral atrial area are depolarized. In mammals, the shift of positive and negative extrema on BSMP during the ascending phase of the P-wave is associated with the passage of the excitation wave from the right atrium to the left one [5, 11, 12]. In fish, on BSMP the movement of extrema reflects the passage of the excitation wave from the caudal part to the cranial one along the dorsal side and from the dorsal side to the ventral side along a single atrium.

Study limitations

Cold-blooded animals depend on the ambient temperature. During the experiment, we kept the temperature of the animal body within 10 - 12° C. Changing the temperature of fish will significantly influence the myocardial electrical activity.

5. Conclusion

Initial phases of atrial depolarization are projected on body surface potential map by the distribution of zones of positive and negative cardiopotentials before the beginning of the P–wave in the ECG. The location of zones of positive and negative cardiopotentials and the movement of extrema on the cardioelectric field on body surface reflect the propagation of the excitation wave along the atrium from the venous sinus to the heart ventricle of fish.

Acknowledgments

The work is supported by the grants 09-0498814-a, 12-P-4-1069 Russian Science Support Foundation, 14-4-TG-416.

References

[1] Simo˜es-Costa MS Vasconcelos M, Sampaio AC, Cravo RM, Linhares VL, Hochgreb T, Yan CYI, Davidson B, Xavier-Neto J. The evolutionary origin of cardiac chambers. *Developmental Biology,* 277: 1–15, 2005.

[2] Prosheva VI. Functional specificity of the pacemaker system of the heart // *Success Physiological Sciences,* 3: 79-91, 1998.

[3] Tessadori F, van Weerd JH, Burkhard SB, Verkerk AO, de Pater E, Boukens BJ, Vink, Christoffels VM, Bakkers J. Identification and functional characterization of cardiac pacemaker cells in zebrafish. *PloS ONE,* 7 (10): e 47644, 2012

[4] Roshchevsky MP, Shmakov DN. Excitation of the heart. Moscow: Nauka, 2003. 144.

[5] Roshchevsky MP, Chudorodova SL, Roshchevskaya IM. Expression of atrial epolarization on the body surface. *Doklad Biological Sciences*, 412: 15-17, 2007.

[6] Smirnova S, Ivanova L, Markel A, Roshchevskaya I, Roshchevsky M. Comparison of propagation of atrial excitation with the cardiopotential distribution on the body surface of hypertensive rats. *Anadolu Kardiyol Derg*, 12 (3): 195-199, 2012.

[7] Roshchevsky MP, Arteeva NV, Kolomeyets NL, Antonova NA, Kambalov MY, Shmakov DN, Roshchevskaya IM. The system “Cardioinform” for visualization and analysis of the heart electric field. *Medical Academic Journal,* 5: 74-79, 2005.

[8] Roshchevsky MP, Chudorodova SL, Shmakov DN, Roshchevskaya IM The cardioelectric field on tne pig body surface during initial atrial activity. *Doklad Biological Sciences,* 402: 174-175, 2005.

[9] Arbel ER, Liberthson R, Langendorf R, Pick A, Fishman AP Electrophysiologica and anatomical observations on the heart of the African lungfish. *American Journal of Physiology,* 232 (l): 24-34, 1977.

[10] Sedmera D, Reckova M, de Almeida A, Sedmerova M, Biermann M, Volejnik J, Sarre A, Raddatz E, Robert A, Mc Carthy R, Gourdie RG, Thompson RP. Functional and morphological evidence for a ventricular conduction system in zebrafish and Xenopus hearts. *Am. J. of Physiology - Heart and Circulatory Physiology,* l284: 1152–1160, 2003.

[11] Mirvis DM. Body surface electrocardiographic mapping. Boston: Kluwer Academic Publishers, 1988, 204.

[12] Kawano S., Hiraoka M., Yamamoto M., Sawanobori T., Sakamoto Y. Body surface maps of ectopic P waves originating in the left atrium in dog. *Journal Electrocardiology,* 22 (1): 27-43, 1989.

Decartographic and Echocardiographic Correlations in Patients with Pulmonary Arterial Hypertension

T. Sakhnova, E. Blinova, M. Saidova, A. Loskutova, O.Arkhipova, E. Yurasova, T. Martynyuk, I. Chazova

Cardiology Research Complex, Moscow, Russia
Email: tamara-sahnova@mail.ru

Abstract. *In patients with pulmonary arterial hypertension (PAH) decartographic parameters of "recovery acceleration" are helpful for the detection of right ventricular (RV) overload and assessment of its severity. The aim of the work was to study the interrelations of "recovery acceleration" and echocardiographic parameters in PAH patients. We examined 30 PAH patients (87% females; age 38.0±2.0 years). Echocardiographic parameters including systolic pulmonary artery pressure (SPAP); RV anterior wall thickness (AWT); anterior-posterior (APD) and middle (MD) RV dimensions; tricuspid annular plane systolic excursion (TAPSE), RV fractional area change (FAC), RV peak systolic annular velocity (TVI-S); RV mean peak early diastolic period velocity (TVI-E); longitudinal strain (LS) were assessed using comprehensive echocardiographic examination, including Tissue Doppler Imaging. Magnitude G and spatial components Gx, Gy, Gz of the "recovery acceleration" vector were calculated using the derived orthogonal-lead ECG. All patients had SPAP>50 mm Hg. G, Gx and Gy had statistically significant moderate negative correlations with SPAP, RV dimensions, TVI-E and LS (r from -0.4 to -0.6, $p<0.05$) and positive correlations with FAC and TVI-S (r from 0.4 to 0.6, $p<0.05$). In patients with severe PAH decartographic parameters of "recovery acceleration" correlate with RV dimensions and parameters of RV systolic and diastolic function.*

Keywords: pulmonary arterial hypertension, right ventricular overload, repolarization, echocardiography

1. Introduction

In patients with pulmonary arterial hypertension (PAH) ventricular gradient and decartographic parameters of "recovery acceleration" were shown to be helpful for the detection of right ventricular overload and for the assessment of its severity [1], [2]; ventricular gradient was shown to predict mortality [3]. The aim of the work was to study the interrelations of "recovery acceleration" and echocardiographic parameters in patients with PAH.

2. Subject and Methods

Patients

We examined 30 PAH patients (87% females; age 38.0±2.0 years) in whom the presence of PAH was verified with clinical and instrumental methods. There were 2 patients with systemic sclerosis, one patient with residual PAH after operated septal defect, one patient with portal hypertension and one patient with chronic thromboembolic disease, in 25 patients after comprehensive clinical and instrumental examination PAH was considered to be idiopathic.

Echocardiography
Comprehensive echocardiographic examination, including Tissue Doppler Imaging was performed using a high-quality ultrasound machine (Vivid 7; GE, USA) with the subjects in the left lateral recumbent position. All measurements were made in accordance with current recommendations of European Society of Cardiology/American Society of Echocardiography (ESC/ASE) [4]. The estimated systolic pulmonary artery pressure (SPAP) was defined as the right ventricular (RV) to right atrial pressure gradient added to the right atrial pressure. Right atrial pressure was estimated 5 to 15 mm Hg, according to the diameter and inspiratory collapse of the inferior caval vein. RV anterior wall thickness (AWT), anterior-posterior (APD) and middle (MD) RV dimensions were estimated using parasternal and apical 4-chamber conventional 2-dimensional grayscale images. RV systolic function was assessed by calculating RV fractional area change (FAC), tricuspid annular plane systolic excursion (TAPSE) and peak systolic annular velocity by pulsed tissue Doppler (TVD) on tricuspid annulus lateral wall (S). RV diastolic function was assessed by calculating peak diastolic early period velocity and peak diastolic later period velocity by pulsed wave Doppler (E/A) and mean peak early diastolic period velocity by TVD on tricuspid annulus lateral wall (E'). The speckle-tracking analysis was performed with calculation of global right ventricular longitudinal strain (LS).

Electrocardiograpy
Conventional 10-s digital electrocardiograms were recorded by certified ECG technicians using the standard 12-lead electrode configuration on commercially available electrocardiograph, averaged into 1 single beat that was subsequently converted into a derived orthogonal-lead beat and processed by means of software developed in Cardiology Research Complex and Institute for Information Transmission Problems. We studied the magnitude G (in ms) and spatial components Gx, Gy, Gz of the "recovery acceleration" vector (directed to the left, inferior, and anterior). Decartographic "recovery acceleration" map shows the distribution of the dipole component of the depolarized state duration over the heart surface, projected onto the image sphere which encloses the heart ventricles. The image sphere radius is taken equal to the maximum magnitude of the heart vector in the QRS period. The use of the maximal QRS vector as a scale helps to understand more clearly internal interrelationships between different parts of QRST complex. Concerning the electrophysiological meaning, "recovery acceleration" vector is close to the ventricular gradient vector.

Statistical analysis
Data were analyzed using MedCalc Statistical Software version 12.7.8 (MedCalc Software bvba, Ostend, Belgium). Results are presented as mean ± standard deviation. To identify the relationship between variables Pearson correlation coefficient was calculated. A value of $p<0.05$ was considered to be statistically significant.

3. Results

All patients had severe PAH (SPAP>50 mm Hg). Mean heart rate was 74.2±12.5 bpm. Echocardiographic and decartographic characteristics of the patients are presented in Table 1.

Correlation coefficients of decartographic and echocardiographic parameters are presented in the Table 2. For all presented correlation coefficients $p<0.05$.

Table 1. Echocardiographic and decartographic characteristics of the group.

Parameter	Mean±SD
SPAP, mm Hg	98.6±4.8
AWT, mm	0.801±0.200
APD, mm	3.89±0.72
MD, mm	4.37±0.94
TAPSE, cm	1.392±0.336
FAC, %	20.7±7.3
TVI-S, cm/s	7.11±1.92
TVI-E, cm/s	-5.25±3.19
LS, %	-15.2±8.3
G, ms	32.8±17.5
Gx, ms	5.2±19.2
Gy, ms	7.7±13.8
Gz, ms	2.7±13.5

Table 2. Correlation coefficients of decartographic and echocardiographic parameters.

	G	Gx	Gy
SPAP	-0.6	-0.6	
AWT		-0.6	-0.4
APD		-0.5	-0.5
MD	-0.5	-0.6	-0.6
TAPSE	0.4		
FAC	0.4	0.6	0.4
TVI-S	0.4	0.4	0.6
TVI-E	-0.6	-0.4	-0.4
LS		-0.4	-0.6

4. Discussion

The ECG-derived ventricular gradient and decartographic parameters of "recovery acceleration" in PAH patients were shown to be accurate in detecting chronic increase in RV pressure load, and distinguishing between normal RV pressure load, mildly to moderately increased RV pressure load, and severely increased RV pressure load. The ventricular gradient projection on the x-axis (VGx) correlated inversely with pulmonary pressure, a severely decreased VGx was related with increased mortality in patients with PAH [1], [3]. Reduced RV function in PAH patients is also an important predictor of mortality. Patients with changes of ventricular gradient are likely to have more impaired RV function. In the present study decartographic parameters of "recovery acceleration" had statistically significant but moderate correlations with RV dimensions and parameters of RV systolic and diastolic function. The limitation of the study was that only patients with severe PAH were included. Ventricular gradient and "recovery acceleration" vector changes in PAH patients are likely to reflect changes in ventricular action potential duration heterogeneity related to RV remodelling, which may be a result of not only increased RV pressure load, but also biochemical and molecular changes. Clarifying mechanisms of ECG changes in ventricular hypertrophy may potentially give additional information about the pathogenesis of the disease [5], [6], [7].

5. Conclusions

In patients with severe PAH decartographic parameters of "recovery acceleration" have moderate correlations with RV dimensions and parameters of RV systolic and diastolic function.

References

[1] Henkens IR, Mouchaers KT, Vonk-Noordegraaf A, et al. Improved ECG detection of presence and severity of right ventricular pressure load validated with cardiac magnetic resonance imaging. *Am J Physiol Heart Circ Physiol,* 294(5): H2150-H2157, 2008.

[2] Sakhnova T, Blinova E, Trunov V, et al. Decartographic detection of presence and severity of right ventricular overload in patients with pulmonary hypertension. *Journal of Electrocardiology*, 46: e9-e10, 2013.

[3] Scherptong RW, Henkens IR, Kapel GF, et al. Diagnosis and mortality prediction in pulmonary hypertension: the value of the electrocardiogram-derived ventricular gradient. *Journal of Electrocardiology*, 45(3): 312-318, 2012.

[4] Lang RM, Bierig M, Devereux RB, et al. Recommendations for chamber quantification: a report from the American Society of Echocardiography's guidelines and standards committee and the Chamber Quantification Writing Group, developed in conjunction with the European Association of Echocardiography, a branch of the European Society of Cardiology. *Journal of the American Society of Echocardiography,* 18(12): 1440-1463, 2005.

[5] Bacharova L, Estes H, Bang L, Mateasik A. The first statement of the Working Group on Electrocardiographic Diagnosis of Left Ventricular Hypertrophy. *Journal of Electrocardiology*, 43(3): 197-199, 2010.

[6] Bacharova L, Estes EH, Bang LE, et al. Second statement of the working group on electrocardiographic diagnosis of left ventricular hypertrophy. *Journal of Electrocardiology,* 44(5): 568-570, 2011.

[7] Hakacova N, Wagner G, Bacharova L. Right and left ventricular pressure overload as imaged by electrocardiogram. *Journal of Electrocardiology,* 47(2):273, 2014.

Relation of Sex and ECG on Cardiovascular Mortality Risk in 10 Years Follow Up

G. Muromtseva, A. Deev, S. Shalnova

National Research Centre for Preventive Medicine, Moscow, Russia
Email: gmuromtseva@yahoo.com

Abstract. *Follow up of randomly selected cohort from Moscow population (17821 subjects aged 35-72), baseline examined in 1975-2001 years, was carried out for 20 years on average. We evaluated the effect of the gender on cardiovascular disease mortality (CVD-M) with ECG variables. It is shown that atria fibrillation and left ventricular hypertrophy are more dangerous for females than for males, but on the contrary QQS major and ST-T abnormalities are more dangerous for males. The decrease of the obtained CVD-M RR, detected by ECG variables, with follow up (from 10 to 20 years) is not related to gender.*

Keywords: Standard 12-lead ECG, Relative Mortality Risk, Minnesota Code, Gender Effect

1. Introduction

Cardiovascular disease (CVD) remains the leading cause of mortality in the world [1, 2]. It is well known gender differences in mortality trends in developed countries especially in Russia. The difference between prevalence of ECG abnormalities in men and women was found in many studies [3, 4]. The aim of this analysis is to investigate the gender interaction between ECG variables and CVD mortality (CVD-M).

2. Subject and Methods

Study Population and Follow up
Mortality follow up of randomly selected cohort from Moscow population (17821 subjects aged 35-72, mean age 49.7±8.0 years, 4934 of them were females), baseline examined in 1975-2001 years, was carried out for 20 years on average. There were 9252 deaths from all causes including 4610 cases of CVD. 441 participants have been died due to CVD up to 5 years, 1153 persons – up to 10 years and 4610 persons – up to the end of follow up.

Statistical Analysis
Cox regression model to estimate relative risks (RR) and 95% confidence intervals (CI) for an association between ECG variables with sex- age- interaction and 5 years, 10 years and full CVD-M, with age and sex adjustment was done. 5 years and 20 years CVD-M were used for comparison purposes. We used SAS version 6.12.

ECG-variables
Standard 12-lead ECGs were recorded at baseline in the resting supine position using strictly standardized procedures in single clinical center, in National Centre for Prevention Medicine. ECG data were stored and analyzed by the Minnesota code (1982) by 2 independent ECG-experts. A third one was involved in the work for controversial cases. ECG abnormalities were divided into 6 following groups, including atria fibrillation (AF), left ventricular hypertrophy (LVH), QQS codes (QQSmajor and QQSminor) and ischemic codes (ISCH and ISCHE; see Table 1).

Table 1. Minnesota Codes Categories

Definitions of Minnesota Codes Categories	Description	Minnesota codes
AF (atria fibrillation)	Atria fibrillation or atria flutter	8-3
LVH (left ventricular hypertrophy)	High amplitude of R wave	3-1 or 3-3
QQS major ("definite Myocardial infarction")	Major Q and QS patterns in leads I, II, III, aVL, aVF or in any leads V1-5, V6	1-1-1 through 1-1-7 or 1-2-1 through 1-2-7
QQS minor ("possible Myocardial infarction")	Minor Q and QS patterns in leads I, II, III, aVL, aVF or in any leads V1-5, V6	1-2-8 or 1-3-1 through 1-3-6,
ISCH ("definite ischemia")	ST depression: ST-J and segments depression ≥1,0 mm in leads I, II, III, aVL, aVF or in any leads V1-5, V6 and/or T-wave changes: T wave inversion in lead I, II, III, aVL, V1-6 without LVH	4-1, 4-2, 5-1, 5-2 without 3-1 or 3-3
ISCHE ("possible ischemia")	Minor ST-T changes (borderline ST segment depression and T wave flattening)	4-3, 4-4 and/or 5-3, 5-4

To detect gender specifics of ECG variables on CVD-M we have introduced interactions between gender and ECG variables in a form (sex-1)*ECG variables. As males were coded "1", females – "2", so RR of CVD-M for males this terms were become 0. On this condition those interactions are additional indicators of increment of RR value for females relative to males. We used significant increments: sAF, sLVH, sQQSmajor, sQQSminor, sISCH and sISCHE, as additional to main affects in this analysis.

3. Results and Discussion

The RR of 10 years CVD-M for every of 6 ECG groups of abnormalities were assessed (see Fig. 1). The highest RR of CVD-M was found for AF (RR=4.32; 95% CI 2.88-6.48); ISCH (RR=4.32; 95% CI 3.33-5.61); QQSmajor (RR=3.05; 95% CI 2.24-4.14); the lowest – for LVH (RR=1.89; 95% CI 1.53-2.32).

CVD-M RR of every ECG variables decreased with a follow-up. The RR of AF and QQSmajor at the end of follow-up were approximately equal: 2.5 (95% CI 1.8-3.47) и 2.58 (95% CI 2.11-3.15), respectively (see Fig. 1).

CVD-M RR for "sex" was 0.28 (95% CI 0.21-0.40) in 10 years of follow-up and varied from 0.25 (95% CI 0.15-0.40) in 5 years to 0.31 (95% CI 0.27-0.40) in the end of follow-up.

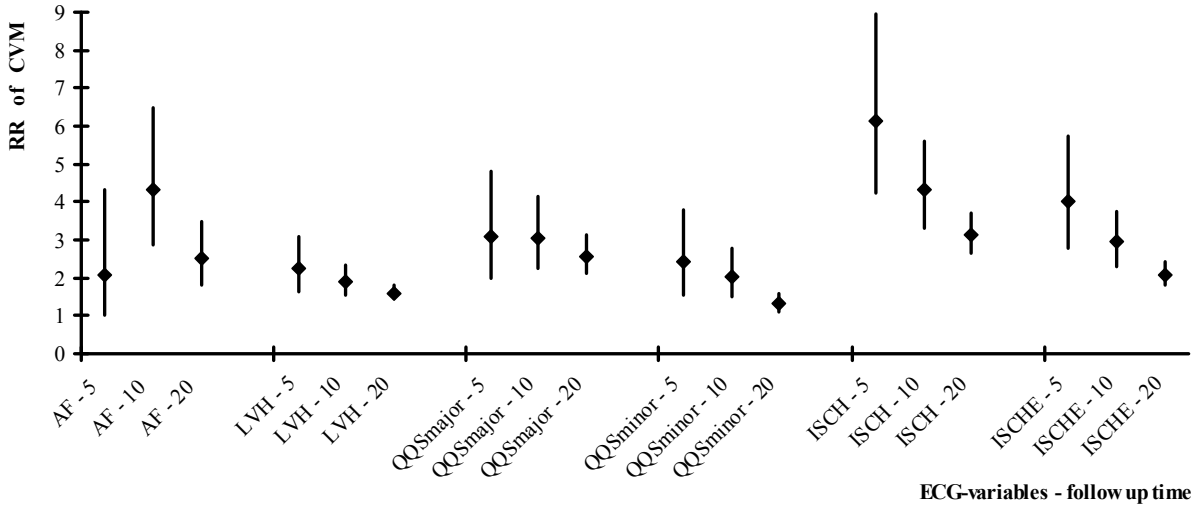

Fig. 1. RR of CVD-M dynamics predicted by 6 ECG variables (AF, LVH, QQSmajor, QQSminor, ISCH and ISCHE) in 5, 10 and 20 years follow up

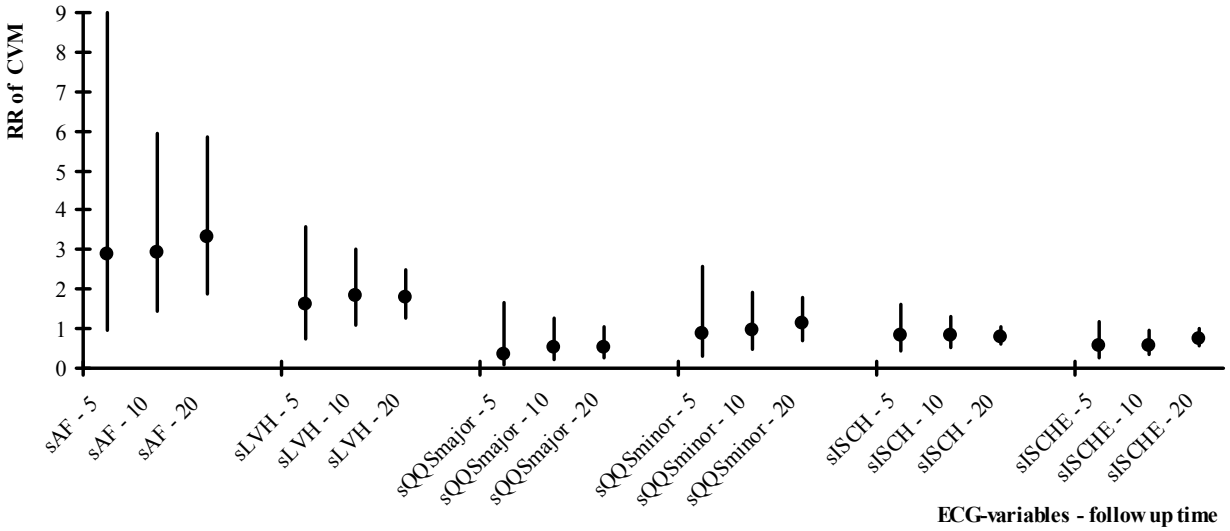

Fig. 2. RR of CVD-M dynamics, predicted by 6 ECG variables (sAF, sLVH, sQQSmajor, sQQSminor, sISCH and sISCHE), in 5, 10 and 20 years follow up

sECG variables analysis are shown on Fig.2 and Table 2. The 10 years RR of sAF detected in females, is about 3 times higher than in males 2.9 (95% CI 1.44-5.94; p=0.003). Also RR of sLVH detected in females is about 1.8 times higher than in men (the 10-years RR=1.82; 95% CI 1.11-3.00; p=0.02). But sQQSmajor, sISCHE and sISCH were more strongly associated with males: 10-years female's risks of CVD-M were 0.51, 0.58 and 0.83 of male's RR, respectively.

As shown in Fig. 2, a decrease of CVD-M RR of sECG variables with a follow-up time was not revealed.

Table 2 demonstrated β-coefficients in regression equation, which were related with impact of every sECG variables in CVD-M RR. The bilateral relations were found: impact of sAF and sLVH on CVD-M RR in females were higher than in males (β-coefficients were positive). Impact of some other interactions was opposite (β-coefficients for them were negative). For sQQSminor the β-coefficient was near zero and CVD-M RR was near "1" (in 10 years of

follow-up RR=0.95; 95% CI 0.47-1.92, Fig. 2). In other words there was not any clear gender predominance for this variable.

Table 2. Impact of sECG variables to prediction of RR of CVD-M

ECG variable	Values of β-coefficient (St.error), p<		
	5-	10-	20 years follow up time
sAF	1.07 (0.58), p<0.06	1.07 (0.36), p<0.003	1.19 (0.29), p<0.0001
sLVH	0.49 (0.40), *	0.60 (0.25), p<0.02	0.58 (0.17), p<0.0006
sQQS major	-1.05 (0.80), *	-0.67 (0.47), *	-0.61 (0.34), p<0.07
sQQS minor	-0.13 (0.55), *	-0.05 (0.36), p<0.02	0.12 (0.23), *
sISCH	-0.17 (0.34), *	-0.19 (0.22), *	-0.24 (0.15), p<0.1
sISCHE	-0.60 (0.40), *	-0.55 (0.25), p<0.03	-0.30 (0.15), p<0.04

* – p>0.05

4. Conclusions

Inclusion of the "Sex" as a significant independent variable in a Cox regression model showed that for females CVD-M RR is 0.25-0.31 RR of males.

There are more detailed gender specific effects for ECG variables on CVD-M. AF and LVH are more dangerous for females than for males, on the contrary QQSmajor and ST-T abnormalities (ISCH and ISCHE) are more dangerous for males in respect of CVD-M.

The decreased association between CVD-M RR and ECG variables with follow up (from 10 to 20-years; see Fig. 1) did not related to gender (see Fig. 2 and Table 2).

References

[1] Rautaharju P.M., Ge S., Nelson J.C., Marino Larsen E.K., Psaty B.M., Furberg C.D., Zhang Z.M., Robbins J., Gottdiener J.S., Chaves P.H. Comparison of mortality risk for electrocardiographic abnormalities in men and women with and without coronary heart disease (from the Cardiovascular Health Study). *Am.J.Cardiol*., 97 (3): 309-15, 2006.

[2] Menotti A., Seccareccia F. Electrocardiographic Minnesota code findings predicting short-term mortality in asymptomatic subjects. The Italian RIFLE Pooling Project (Risk Factors and Life Expectancy). *G.Ital.Cardiol*, 27 (1): 40-9, 1997.

[3] Saltykova M., Muromtseva G., Baum O., Ryabikina G., Lazareva N., Ataullachanova D., Popov L., Voloshin V., Shalnova S., Oshepkova E., Rogoza A. Effect of sex on informative power of various electrocardiographical criteria of left ventricular hypertrophy in patients with excessive body mass. *Kardiologia (in Russian)*, 48 (5): 23-26, 2008.

[4] Shalnova S., Konrady A., Karpov U., Kontsevaya A., Deev A., Kapustina A., Khudiakov M., Shlyachto E., Boytsov S. Analysis of mortality from cardiovascular disease in 12 regions of the Russian Federation, participating in the research on "Epidemiology of cardiovascular disease in various regions of Russia". *Russian Journal of Cardiology (in Russian)*, 5 (97): 6-11, 2012.

Automated ECG Delineation using Machine Learning Algorithms

[1]Indu Saini, [2]Dilbag Singh, [1]Arun Khosla

[1]Dept. of Electronics & Communication Engineering and
[2]Dept. of Instrumentation & Control Engineering,
Dr.B.R. Ambedkar National Institute of Technology, Jalandhar, India
Email: drdilbag@gmail.com

Abstract. *The aim of automated electrocardiogram (ECG) delineation system is the reliable detection of fundamental ECG components and from these fundamental measurements, the parameters of diagnostic significance, namely, P-duration, PR-interval, QRS-duration, QT-interval, are to be identified and extracted. In this work, two supervised machine learning algorithms, K-Nearest neighbour (KNN) and Support Vector Machine (SVM) have been applied for accurate and efficient delineation of ECG signals. The algorithms were evaluated on a standard database CSE DS-3. The mean and standard deviations of the basic intervals obtained by KNN and SVM algorithms have been calculated and compared with three 12-lead programs used in the CSE study from the combined program median. The results show that the proposed algorithms give a new direction of using KNN and SVM effectively for the identification and delineation of the ECG wave components.*

Keywords: ECG, KNN, SVM, gradient, classifier, durations, intervals.

1. Introduction

All ECG computer analysis programs are basically composed of two parts. The first part deals with the accurate identification and measurement of characteristic features of ECG signal whereas the second part deals with the diagnostic interpretation. The main task in the measurements is to find exact location of major reference points, i.e., onset and offset points of P, QRS and T-waves. In recent years, many algorithms have been developed for the detection and delineation of the ECG signals. Some of them are as:-

Li et al. in 1995 [1] proposed an algorithm based on Wavelet Transform (WT) for detecting ECG characteristic points. In [2] the authors used quadratic spline wavelet as prototype wavelet for detection of ECG significant points and the first four scales of the DyWT were analyzed. Martinez et al. in [3] have presented and validated a wavelet based ECG delineation system which performed QRS detection and provided the locations of the peak(s) of P, Q, R, S and T-waves, and their boundaries. Goutas et al. in 2005 [4] presented a new algorithm based on digital fractional order differentiation for P and T-waves detection and delineation. Mehta and Lingayat in [5] presented the application of SVM for QRS detection in single and 12-lead ECG using entropy and combined entropy criterion. Arzeno et al. in 2008 [6] analyzed traditional first-derivative based squaring function and Hilbert transform-based methods for QRS detection and proposed their modifications with improved detection thresholds. In [7], the authors presented an efficient method for detection of P and T-waves in 12-lead ECG using SVM. The authors in 2010 [8] proposed Bayesian inference to represent a priori relationships among ECG wave components.

This paper presents an application of KNN and SVM for delineation of ECG signal. The KNN method is an instance based learning method that stores all available data points (examples) and classifies new data points based on similarity measure [9].The goal of SVM is to produce a model which predicts target value of data instances in the testing set where only

the attributes are given [10]. The SVM classification is based on supervised learning, where known labels help indicate whether the system is performing in a right way or not.

This paper is organized as follows: section II presents a brief outline of KNN and SVM-classifiers. Section III explains the methodology adopted for delineation. Section IV presents the results and Section V draws the conclusion.

2. Outline of KNN and SVM algorithms

KNN Algorithm
KNN is a non-parametric algorithm that does not make any assumptions on the underlying data distribution. It is also a lazy algorithm means it does not use the training data points to do any generalization. More exactly, all the training data is needed during the testing phase. One of the advantages of the KNN method in classifying the objects is that it requires only few parameters to tune: K and the distance metric, for achieving sufficiently high classification accuracy [9].

SVM Algorithm
SVM is an algorithm of machine learning introduced by Vapnik based on the structural risk minimization principle from statistical learning [11]. SVM is a method for finding a hyperplane in high dimensional space that separates training samples of each class which maximizing the minimum distance between that hyperplane and the training samples. A decision plane is one that separates between sets of objects having different class memberships [10]. The solution gives rise to the decision function of the form.

$$f(x) = \mathrm{sgn}\left[\sum_{i=1}^{l} y_i \alpha_i (x.x_i) + b \right] \quad (1)$$

where α_i are Lagrange multipliers.

The accuracy of an SVM model is largely dependent on the selection of the kernel method applied. The input data are mapped to a higher dimensional space that a separating hyperplane is constructed to maximize the margin. There are number of kernel functions results in different kinds of SVMs with different performance levels. These include linear, polynomial, radial basis functions [10].

3. Methodology

In this section, we describe the proposed algorithm for the detection of P-wave, QRS-complex, T-wave, their onsets, offsets points, their durations and intervals in ECG signal using KNN and SVM classifiers.

Data Acquisition
The multi-lead ECG records have been acquired from CSE data libraries. All the data sets have been sampled at 500Hz. This dataset consists of ECG records of 125 patients whose record length is 10 seconds for each lead. The CSE committee has published measurement results of 25 records out of 125, hence proposed algorithm has been tested only for 25 records.

Method
Here, we describe the steps followed for developing the delineation algorithm;

In order to attenuate the noise in a raw ECG signal, the acquired signal is passed through a band-pass filter which is composed of cascaded high-pass and low-pass filters. The band-pass

filter reduces the influence of muscle noise, baseline wander, 50 Hz and T-wave interferences [12].

For the feature extraction of filtered signal, the gradient of the signal is used as feature vector. Slope or gradient of the signal at every sampling instant is calculated. These slope values are then squared for normalization.

After obtaining the feature vector, the KNN and SVM classifiers are trained. In this phase a training matrix is formed, consisting of m training instances of n features. The number of training instances (m) is equal to the number of samples of selected portions of ECGs and the value of n is the normalized gradient value of each lead of the ECG at a training instance. If the training instance belongs to QRS region, the training label vector is set to 1 and if it belongs to non-QRS region it is set to -1.

After training of KNN and SVM, 25 number records of the CSE are tested for the detection of the QRS-complex. Here, testing labels are unknown; hence any random value can be used.

After testing, a train of 1's is obtained at the output of KNN and SVM classifiers. Then this train of 1's is picked and by using their duration, average pulse duration of 1's is evaluated. Those trains of 1's, whose duration turns out to be more than the average pulse duration are detected as QRS-complex and the other are discarded. The starting and end instances of QRS-complex are depicted as QRS-onset and QRS-offset points. QRS-complex duration has been calculated by using their onset and offset points.

The obtained QRS-complexes are removed from ECG signal by replacing them by baseline. The slope at every sampling instant of QRS less ECG signal is calculated and normalized. The KNN and SVM are again trained and tested for T-wave as explained above. The starting and end instances of T-wave are depicted as T-on and T-end points. QT-interval has been calculated from the onset point of QRS-complex and offset point of T-wave.

The obtained T-waves are removed from QRS less ECG signal by replacing them by baseline. The slope at every sampling instant of ECG signal without QRS and T-wave is calculated and normalized. The KNN and SVM are again trained and tested for P-wave as explained above. The starting and end instances of P-wave are depicted as P-onset and P-offset points. P wave duration is calculated by using onset and offset point of P-wave. PR-interval has also been calculated from onset of P-wave and onset of QRS-complex.

Mean and standard deviation of P-duration, PR-interval, QRS-duration and QT-interval for 25 records of CSE database has also been computed using KNN and SVM algorithms.

4. Results and Discussions

The quantitative values of the P-on, P-peak, P-off, QRS-on, R-peak, QRS-off, T-peak and T-end using KNN and SVM algorithms for 25 records of CSE database are computed and compared with referee results. The most of the values are well within the tolerance limits suggested by the CSE working party and the overall accuracy in the measurement of five wave fiducials is about 92.8 % and 94.4% for KNN and SVM algorithms respectively [13,14].

Based upon the onsets and offsets of P, QRS and T-wave, the important diagnostic parameters P-duration, PR-interval, QRS-duration and QT-interval have been calculated. The mean and standard deviations of the basic intervals obtained by KNN and SVM algorithms and three 12-lead programs used in the CSE study [15] from the combined program median is given in Table I.

Table 1. Comparison of Mean and Standard deviation of ECG wave intervals using KNN and SVM algorithms on CSE database.

Method	P-duration m±std(ms)	PR-interval m±std(ms)	QRS-duration m±std(ms)	QT-interval m±std(ms)
KNN based delineator	-2.5±9.3	5.4±9.9	-2.3±7.2	5.0±13.4
SVM based delineator	-0.1±7.9	2.3±7.1	-1.1±7.0	3.9±11.8
CSE Prog. 2 Marquette)	-12.0±17.6	-8.7±12.1	-0.8±7.2	6.2±15.4
CSE Prog. 11 Glasgow)	-2.4±12.6	5.1±12.5	-1.4±7.1	3.9±14.8
CSE Prog. 13 (Padova)	2.8±10.1	-2.8±8.3	1.8±7.3	-1.1±9.2

5. Conclusion

KNN and SVM based ECG delineators has been presented here for ECG delineation. Both the algorithms of delineation may be capable of enhancing specific rhythms in ECG signals, which may in turn, proves helpful in accurately detecting the P, QRS and T-wave components. These algorithms have been validated on 25 records of CSE DS-3 database. Mean and standard deviation has also been calculated and compared with the results of referees and tolerance limits accepted by cardiologists for CSE.

References

[1] Li C, Zheng C, and Tai C. Detection of ECG characteristic points using wavelet transforms. *IEEE Transactions on Biomedical Engineering*, 42 (1): 21–28, 1995.

[2] Martinez J P, Olmos S and Laguna P. Evaluation of a wavelet-based ECG waveform detector on the QT database. *Computers in Cardiology*, 27: 81-84, 2000.

[3] Martinez J P, Almeida R S, Olmos S, Rocha A P and Laguna P. A Wavelet-based ECG delineator: Evaluation on standard databases. *IEEE Transactions on Biomedical Engineering*, 51 (4): 570–581, 2004.

[4] Goutas A, Ferdi Y, Herbeuval J P, Boudraa M, Boucheham B. Digital fractional order differentiation-based algorithm for P and T-waves detection and delineation. *ITBM-RBM*, 26: 127–132, 2005.

[5] Mehta S S and Lingayat N S. Comparative study of QRS detection in single lead and 12-lead ECG based on entropy and combined entropy criteria using support vector machine. *Journal of theoretical and applied information technology*, 3(2): 8-18, 2007.

[6] Arzeno N M, Deng Z D, and Poon C S. Analysis of first-derivative based QRS detection algorithms. *IEEE Transactions on Biomedical Engineering*, 55(2): 478-484, 2008.

[7] Mehta S S and Lingayat N S. Application of support vector machine for the detection of P- and T-waves in 12-lead electrocardiogram. *Computer methods and programs in Biomedicine*, 93 (1): 46-60, 2009.

[8] Lin C, Mailhes C, and Tourneret J Y. P- and T-wave delineation in ECG signals using a bayesian approach and a partially collapsed gibbs sampler. *IEEE Transactions on Biomedical Engineering*, 57(12): 2840-2849, 2010.

[9] Thirumuruganathan S. A detailed introduction to K-Nearest Neighbor algorithm. 2010.

[10] Vikramaditya J. Tutorial on Support Vector Machine. School of EECS, Washington State University, Pullman, 2010.

[11] Vapnik V. The nature of statistical learning theory. New York: Wiley, 1988.

[12] Pan J and Tompkins W J. A real time QRS detection algorithm. *IEEE Transactions on Biomedical Engineering*, 32: 230-236, 1985.

[13] Saini I, Singh D, Khosla A. P- and T-wave Delineation of ECG signal using Support Vector Machine. *IETE Journal of Research*, 59(5): 615-623, 2013.

[14] Saini I, Singh D, Khosla A. K-Nearest Neighbor-based algorithm for P and T-waves detection and delineation. *Journal of Medical Engineering and Technology*, 38 (3): 115-124, 2014.

[15] Willems JL. The CSE Multilead atlas manual-measurement results dataset-3. Printed in Belgium by ACCO, Brusselsestraat-118a, 3000 Leuven, Belgium, 1988.

Detection of Time-Intervals in Biomedical Signals Using Template Matched Filter

[1]S. Kumar, [2]S. Anand, [2]A. Sengupta

[1]National Institute of Technology, Jalandhar, India
[2]AIndian Institute of Technology, Delhi, India
Email: pahujas@nitj.ac.in

Abstract*. Fetal Heart Rate Variability (FHRV) is a reliable quantitative marker of autonomic nervous system (ANS) activity of the fetus and its analysis has gained importance in medical research and clinical applications. Fetal Electrocardiograph (FECG) is clinically used to help doctors diagnose various diseases. One of the popular measurements is FHR and other physiological parameters. World wide, the standard method of monitoring the fetus during labor is the display of continuous fetal heart rate (FHR) and the uterine activity with the help of cardiotocogram (CTG). By analysis and appropriate interpretation of changes in the CTG obstrician hope to prevent the delivery of dead or impound babies who had suffered as a result of a lack of oxygen during labor and delivery. These signals are analyzed using an automatic PC-Based virtual instrument in LabVIEW. A template matching technique works well in the calculation of R-R interval of the ECG/FECG data and peaks of the biomedical signals.*

Keywords: FHRV, ECG, uterine contractions, fetal movements, R-R interval

1. Introduction

Fetus in situ initiates compensatory protective mechanism to sustain pregnancy, which enables fetus in utero and mother to adapt and acclimatize to an altered state of pregnancy. Therefore it is imperative to monitor vital parameters at a regular interval and at times continuously (fetal autonomic nervous system, fetal movement and uterine contractions) throughout pregnancy and labor for an optimal pregnancy outcome. There for continuously monitoring of fetal and maternal activities antenatal and intra-partum is important to detect in advance fetal problems that could result in irreversible neurological damage or even fetal death during labor. The FECG signal was obtained by measuring (invasively) differentially between an electrode on the fetal scalp and a standard skin electrode placed on the maternal thigh, and a second maternal electrode was used a earth [1]. Non-invasively, the ECG and FECG signals are commonly measured at two locations; the chest and the abdomen. The analysis of the electrocardiogram (ECG) signal has been known as a fairly reliable technique for cardiac disease diagnosis. ECG, recorded from maternal abdomen, can in principle be used to monitor the electrical activity of the fetal heart during pregnancy period. In abdominal FECG recording, the mother ECG (MECG) represents an additional and predominant source of interference. Numerous attempts have been made to detect the FECG in abdominal recording. To this and ,the authors have mainly focused on the removal of the MECG using classical filtering techniques (Bemmel and van der Weide 1966) or estimating technique , such as adaptive filtering (Windrow et al 1975) , subtraction (Meijer 1981) and averaging (Abboud and Sadeh 1989, Cerutti et al 1986). However none of these proposed methods have been validated on a large database of real abdominal ECG measurements. This limited reproducibility of the measurement may suggest a scarce performance due to the inaccurate removal of the MECG and to presence of other significant interference signals.

Recently, a completely different approach for FECG detection has been considered. Some authors formulated the FECG detection as a blind source separation (BSS) problem (Callaerts

et al 1986, Zarzoso et al 1997, Lathauwer et al 2000). BSS method e.g., principal component analysis (PCA) and independent component analysis (ICA), are algebraic methods for the estimation of unobserved component from multidimensional data. The alterations of the heart beat or HRV is a useful tool for assessing the status of the ANS non-invasively. These concepts were successfully used for separating mutually independent signals in biomedical signal processing. On the other hand, Barros and Ohnishi proposed a new method called heart instantaneous frequency (HIF) which showed to be an efficient estimator of HRV using the spectral response of the cardiac signal. The most common approach for HRV calculation is based on QRS complex detection. HRV is calculated from an electrocardiogram (ECG), after detecting the QRS complex (Fig. 1), and then computing the time difference between two successive R-waves. The spectral analysis of HRV signal (R-R time series) allows quantitatively evaluating and distinguishing between the different activities of the ANS such as high frequency component, a low frequency component and a very low frequency [2-4].

2. Algorithm

The various techniques are used to detect QRS complex like linear digital filters, nonlinear transformations, decision processes, and template matching. Typically, two or more of these techniques are combined together in a detector algorithm. The most common approach for QRS detection is based on template matching. A model of the normal QRS complex, called a template, is extracted from the filtered ECG [5]. This template is compared with the subsequent incoming real-time ECG to look for a possible match, using a mathematical criterion. A close enough match to the template represents a detected QRS complex. If a waveform comes along that does not match but is a suspected abnormal QRS complex, it is treated as a separate template, and future suspected QRS complexes are compared with it. From the QRS detector, the RR intervals are determined [7]. The ECG signal is then classified based on the QRS duration and the RR interval, hence HR. The same way the peaks are identified from the fetal movements and uterine contractions for finding their intervals.

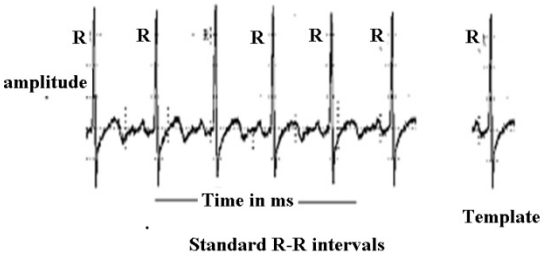

Fig. 1. A standard ECG signal with R-R intervals and template

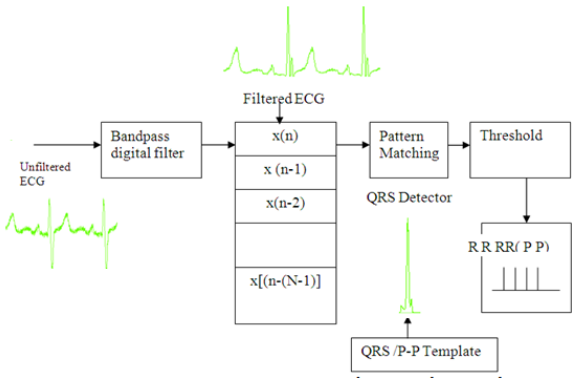

Fig. 2. General Block Diagram of QRS complex and P-P detection from unfiltered ECG / biomedical signal

A general block diagram of the QRS/P-P detection process is shown in figure 2. The unfiltered biomedical signal is first passed through a band pass filter/ Notch filter (as shown in Figure 3) to reduce the effect of noise. The filtered data samples are stored in the file for comparison with the QRS template in the QRS detector. When it is matched, the output of the QRS detector is then one (unit impulse signal for each matching) [7].

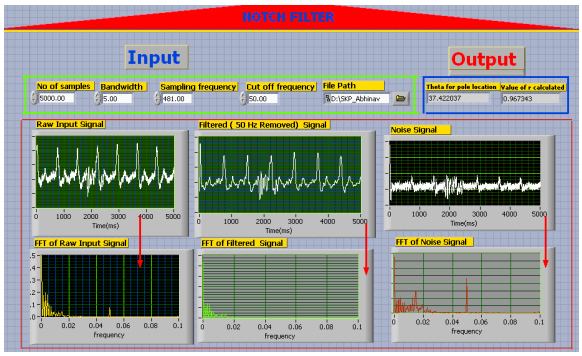

Fig. 3. Snap shot of the real time notch filter

Fig. 4. Fetal movement and uterine contractions

3. Data Recording

Signals were recorded non-invasively using BIOPAC with sampling frequency was 1000 samples per seconds while the ECG and FECG are recorded by Ag-Ag/Cl electrodes on the thoracic region and abdomen region. Uterine and fetus movements were recorded non-invasively by pressure sensors placed on various positions on the abdomen of the subjects as shown in figure 4 while some phantom data was also recorded to depict fetal movements with the help of IPG instrument. The instrument records the signal and any variations inside the phantom/abdomen as shown in figure 5.

4. Implementation Of The Algorithm And Result

The algorithm discussed here is designed in LabVIEW, a graphical programming system with a large built-in library for data acquisition, processing, analysis, and display. Bandpass filter reduces the influences of muscle noise, power line frequency, baseline wander, and T-wave interference. The desirable pass band to maximize the QRS energy is approximately 5-15 Hz [6]. The unfiltered ECG (fig.6 (a) and pulse signals are passed through the band pass or notch filter. The filtered output is shown in fig 6(b). The reference signal (fig.6(c)) is compared with the subsequent incoming ECG samples for a possible match, using a mathematical criterion. A close match to the template represents an impulse of unity gain as shown in fig 6(d). It shows the time interval of 830ms and HR of 72.29 between 2 and 3 R-R interval as shown in fig.6 (e). Figure 7 shows the result of fetal movements.

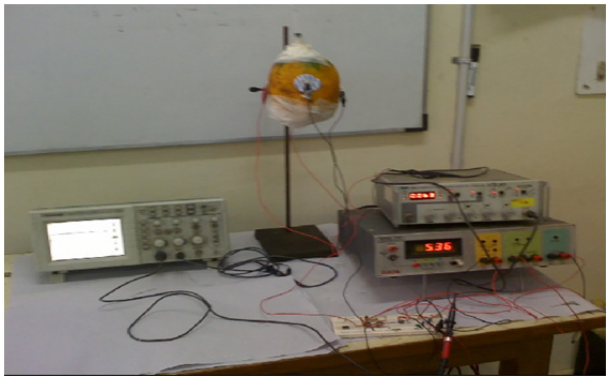

Fig. 5. Phantom for recording changes inside the papaya to depict fetal movements

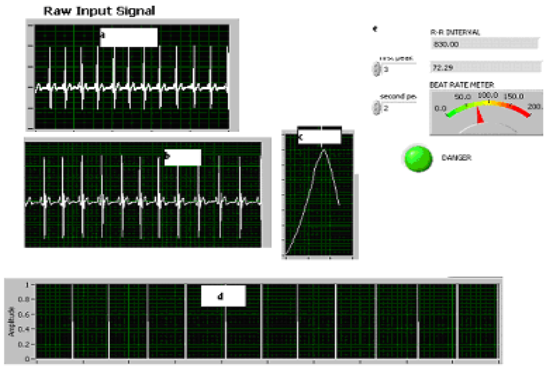

Fig. 6. (a) Unfiltered ECG, (b) filtered signal, (c) ref. signal, (d) matched signal, (e) R-R interval and HR

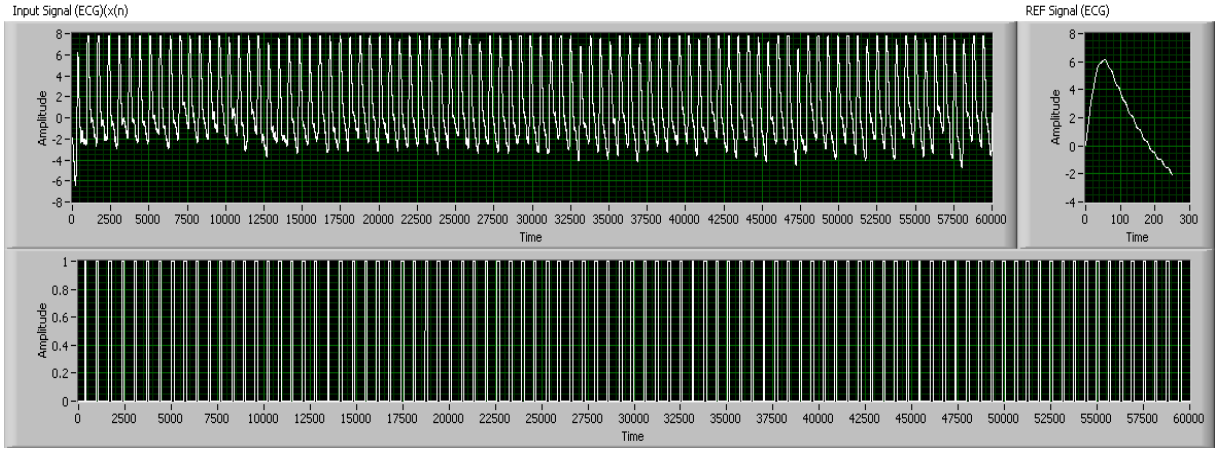

Fig.7. Result of fetal movements using template matching.

5. Conclusions

If conclusions are stated in a separate section, they should be clear and concise. In this paper we have tested a template matching algorithm for QRS complex detection on the different signals, i.e. ECG, FECG, and fetal movements. ECG has been extensively studied because of its great clinical significance in diagnosing heart diseases. QRS complex detection is the most important problem in ECG signal analysis. A number of QRS detectors have been designed for measurement of R-R interval. ECG signal is an electrical signal while the radial artery signal is a mechanical signal. Here, a template matching method is used for the determination of QRS complex of the ECG signal, hence R-R interval and P-P interval from the fetal movements. ECG signals showed heart rate of various signals. Future research will concentrate on the diagnosis of disease using the system designed and in various feto-maternal well being studies.

References

[1] Jafari MG and Chambers JA. Fetal Electrocardiogram Extraction by Sequential Source Separation in the Wavelet Domain. IEEE Transactions on Biomedical Engineering. 2005; 52: 390-400.

[2] Holger G. A. Design of a PC-Based System for Time-Domain and Spectral Analysis of Heart Rate Variability. Computers and Biomedical Research 32, 77–92, 1999.

[3] Barros AK, Wisbeck J, Ohnishi N. Extracting the Heart Rate Variability from an Electro-cardiogram Sampled at a Very Low Frequency. Computers in Cardiology, 335-338, 1999.

[4] Task Force of The European Society of Cardiology and The North American Society of Pacing and Electrophysiology. Heart rate variability Standards of measurement, physiological interpretation, and clinical use. European Heart Journal, 354–381, 1996.

[5] Bifulco P, Cesarelli M, Bracale M. HRV Adaptive Spectral Estimation for Transient Detection. Proceedings of the 22nd Annual EMBS International Conference, 2000, Chicago, IL.

[6] Pan J, Tompkin W. A real-Time QRS Detector Algorithm. IEEE Transactions on Biomedical Engineering. 32(3):, 230-236, 1985.

[7] Jervis, DSP A practical approach, Second Edition, Pearson Education, 2003.

Design of Very Precise and Miniature Low Power ECG Holter

[1]E. Vavrinsky, [1]M. Daricek, [2]D. Moskalova, [1]F. Horinek [1,3]M. Donoval

[1]Institute of Electronics and Photonics, Slovak University of Technology, Bratislava, Slovakia
[2] Department of Psychology, Comenius University, Bratislava, Slovakia
[3] NanoDesign ltd., Bratislava, Slovakia
Email: erik.vavrinsky@stuba.sk

Abstract. *This paper presents design of very precise and miniature low power ECG Holter, which is enriched with sensitive 3D accelerometer, impedance measurement circuit, real-time clock, trigger etc. Total power consumption is optimized with respect to the best balance between performance and operating time. The work presents selected results demonstrating the high quality and universal usability of the proposed system.*

Keywords: ECG, Miniature, Low Power, Accelerometer, Integrated Respiration Impedance

1. Introduction

Human healthcare is intensively dependent on prevention and early diagnostics. Hectic lifestyle of today's world however pushes people to overcome these health problems. The repercussions of hasty life style will be delivered years later and will also impact the average health of people living in modern world. In order to improve the overall home healthcare and peoples interest in their condition improvement, new smart systems and promising automated diagnostics methods are broadly being researched. Raising computing power of new microprocessors, production of novel low price integrated chips and continual development of measurable health parameters sensing technics influence the expansion of new integrated medical devices very positively. Devices for daily health monitoring are important for the end consumer, but also for many research groups [1, 2]. This paper introduces design of ECG Holter which uses latest advances in high-tech electronics. Except for very precise measurement features, which characterize this device (high gain, low noise, multi-probe measuring), some special features as low voltage and ultra-low power consumption were reached in order to achieve its longer performance for daily use. Following the requests of practice the Holter was enhanced by precise accelerometer, respiration measurement circuits, real-time clock, trigger button and optical and acoustic signalization. For online monitoring it is possible to build in a ZigBEE module and connect Holter wireless to PC or mobile phone.

2. Subject and Methods

The system (Fig. 1) is primary designed for 24 hour daily monitoring of ECG. It can be useful in many clinical applications including diagnosis of arrhythmias, ischemia, or heart failure. Thanks to built-in accelerometer and respiration monitor it can be also very helpful in telemedicine, sports and fitness, including event, stress and vital signs monitoring. The Holter is based on analog font-end ADS1292R, microcontroller ATxmega128A3 and acceleration sensor LIS3DH. The ADS1292R is 2-channel, 24-bit, delta-sigma analog-to-digital converter with a built-in programmable gain amplifier, internal reference, an on-board oscillator and respiration impedance measurement function [3]. The ADS1292R incorporate all features commonly required in portable, low-power medical electrocardiogram, sports, and fitness applications. Power consumption of one channel is only 335 μW. The ATxmega 128A3 is low power, high performance 16-bit μ-controller featuring 128KB flash program memory, 2048-Byte EEPROM, and up to 32 MIPS throughput at 32MHz. The device is capable of achieving extremely low power consumption, which is required by both portable electronics

and battery-powered applications [4]. The LIS3DH is an ultra low-power high performance 3D linear accelerometer belonging to the "nano" family. The device features ultra low-power operational modes that allow advanced power saving and smart embedded functions [5].

All components were chosen on top state of the art with respect to the lowest power consumption while retaining the highest possible performance. Total power consumption of designed ECG Holter is 3 mA (on 250 SPS). By using standard 120 mAh Li-Pol battery the system allows operating time of 40 hours. Ideal working time (25 hours) can be achieved on 500 SPS. Thanks to microcontroller implemented HRV detection algorithms, ECG Holter can be switched in HRV mode (only HRV peaks are detected) for extended operation time of few days. Data is stored in CSV format to built-in 4 GB SD card, with possibility of conversion to +EDF format. The Holter is fixed to the human body using pre-gelled disposable Ag/AgCl electrodes. Optical signalization and trigger button is installed on the top of Holter. Acoustic signalization and micro USB connector for recharging, data transfer and parameter set is located on the reverse side. Holter is equipped with real-time clock for time-log management. The ECG Holter offers two low-noise, high resolution ECG channels, where one channel can be used for respiration monitoring, so the system allows simultaneousness multichannel signal acquisition of ECG, acceleration and respiration. The acceleration is measured 3D with 16 bit data output (standard system use mostly 8-bit only), where the sample rate is identical to sampling rates of ECG sensing. Respiration circuits are primarily concerned for monitoring of chest impedance, but as you will see, it can be easily modified for electro-dermal activity (EDA) monitoring. To get versatile system, gain and sample rate of Holter are selectable.

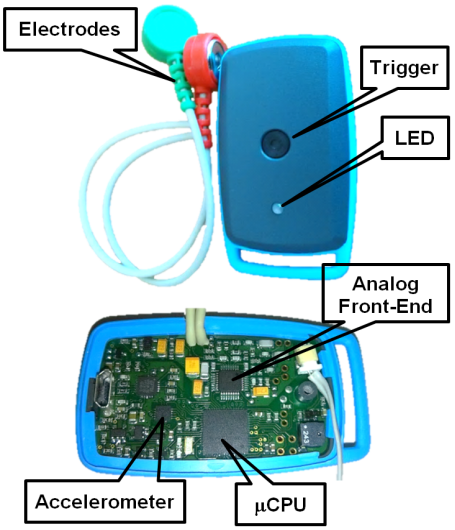

TECHNICAL PARAMETERS OF ECG HOLTER

Number of Channels	2
Programmable Gain	1, 2, 3, 4, 6, 8 or 12, Low-noise
ADC resolution	2x 24-bit, no data missing
Sample rate	125 SPS - 8 kSPS
MCU	16 bit AVR, 32 MHz SRAM 8 Kbytes EEPROM 2048 bytes
Built-In	Respiration
Acceleration sensor	3D, 16 bit data output, ±2g/±4g/±8g/±16g
Supply voltage	1x Li-Pol 120 mAh, over 24h stamina (on 500 SPS) charging time: 20min
Temperature range	0 – 70 °C
Electrodes	Disposable Ag/AgCl
Connectivity	Micro USB
Data storage	Integrated 4 GB SD card
Output data format	CSV, EDF+
Weight	20 g
Dimensions	37 x 25x 15 mm

Next features: RGB LED and acoustic signalization, trigger button, real-time clock

Fig. 1. ECG Holter design.

3. Results

Designed sensor system was tested on a wide range of experiments, where ECG parameters like: P, Q, R, S, T amplitudes, RR, PR, JT, QT, QTc time intervals, T wave symmetry, HRV spectrum and EDR algorithm were analysed in detail. As an example, simultaneous testing of designed ECG Holter to a reference device is presented in this paper. As reference device in all experiments NeXus-10 MKII from MindMedia was used. NeXus-10 is a versatile portable and advanced system for physiological research [6]. In Fig. 2 you can see ECG and respiration signal without any additional filtering or postprocessing. The electrode configuration is shown in Fig.2. During this phase of experiment, proband was in siting position. Both ECG signals offer high quality - clear QRS segment, P, T wave etc. The respiration signals are very similar. Small differences may be based on different physical

principles. ECG Holter uses evaluating of impedance between two electrodes on chest top and reference system uses evaluating of the rib cage volume using standard chest belt.

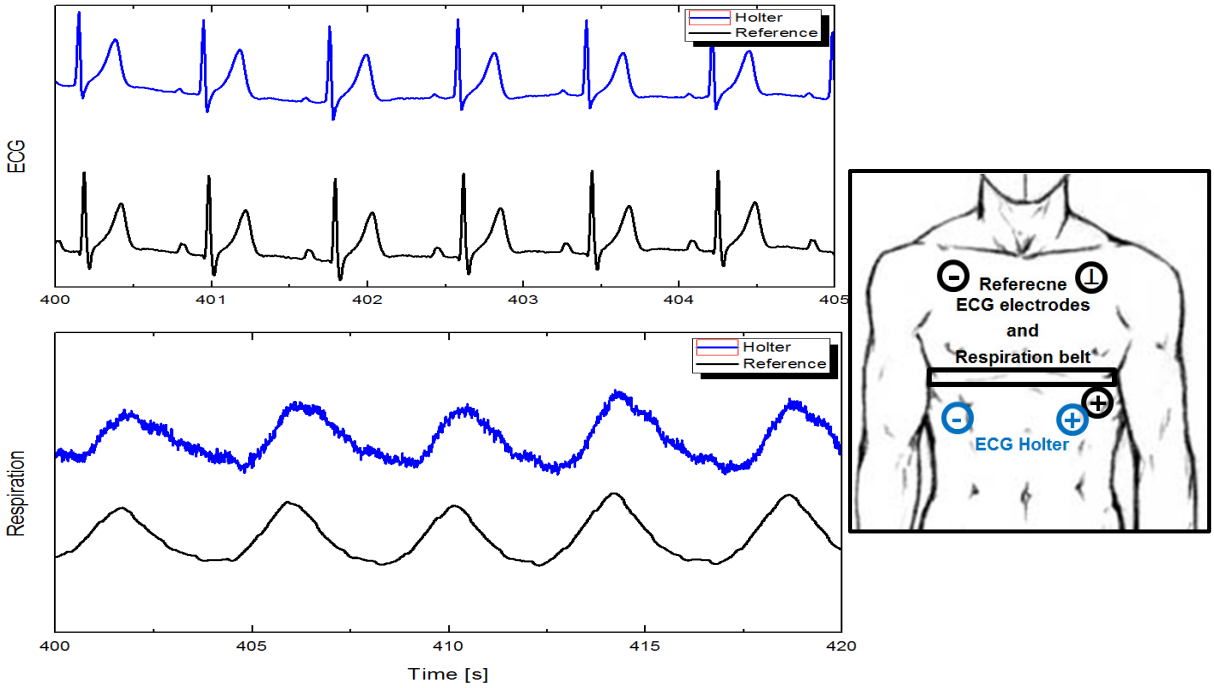

Fig. 2. Simultaneous testing: ECG and respiration signal.

As mentioned earlier, our ECG Holter has built in very precise 3D accelerometer. We can apply it for classical measurement of probands body movement and activity (Fig. 3). Using 16-bit accelerometer we can even measure more sophistic parameters, like cough pass and some brand new physiological parameters, like amyostasia monitoring (so called mechanomyography). If we measure ECG in chest area we can even monitor mechanical heart activity with implemented accelerometer (Fig. 3 - zoom). For example we found that time-shift between ECG and acceleration signal corresponds to physical or mental excitation of proband.

Integrated respiration impedance measurement function can be easy modified for EDA monitoring. We need only to remove DC signal part (Fig. 4). Using this simple method, when we use 2 separate channels (4 cable configuration), we can simultaneously monitor ECG and EDA, which is very often requested by psychology researchers. In Fig. 5 you can see our implementation of such system in SMART clothes. In the system we used commercial conductive fabrics and threads.

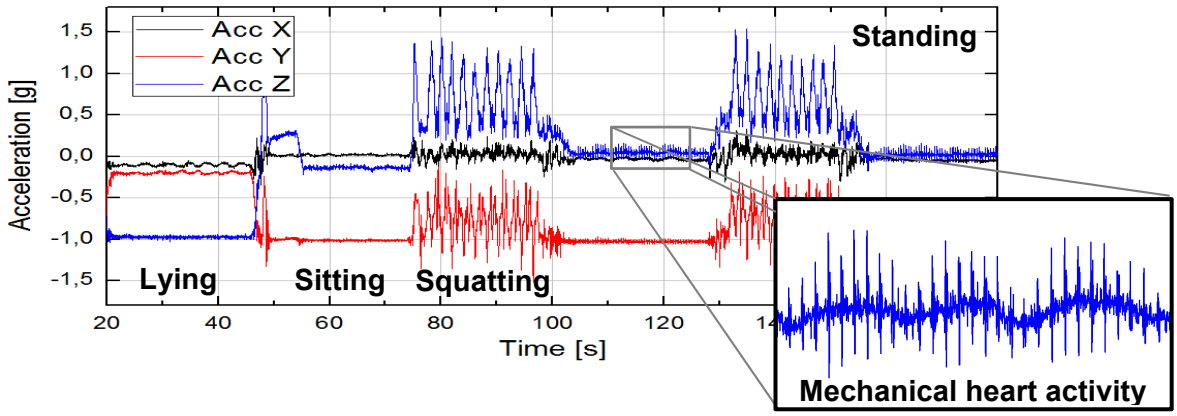

Fig. 3. Acceleration experiment with ECG Holter.

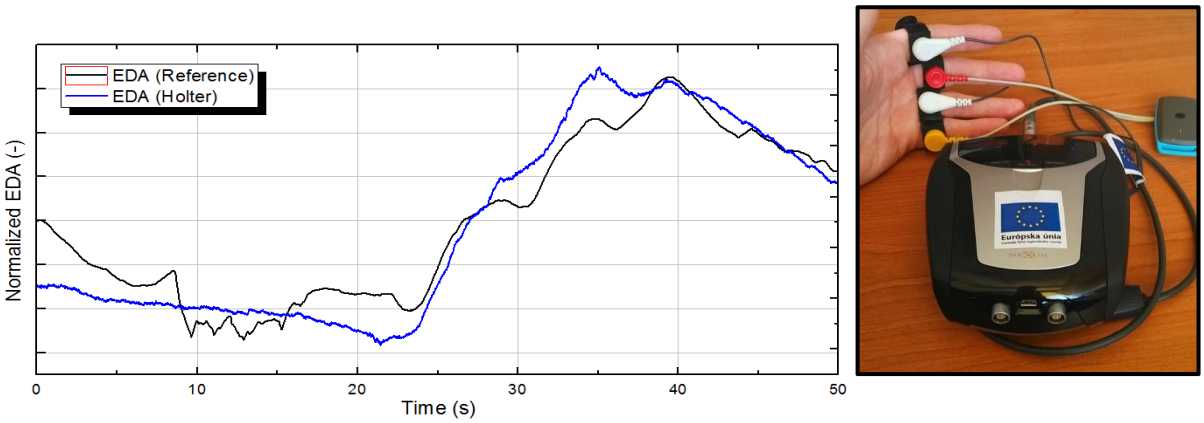

Fig. 4. Application of ECG Holter in EDA measurement.

4. Conclusions

Fig. 5. Smart T-shirt.

High quality and scientific potential of designed smart system was experimentally proven. Obtained results clearly proved high stability. Thanks to implementation of precise accelerometer, impedance circuit, real-time clock etc. is possible to use the Holter in more complex physiological experiment like standard Holters. Together with ultra-low power consumption the novel device is very suitable and promising for long-term testing and medical monitoring. There is also possibility of development of new healthcare diagnostic methods using developed ECG Holter. Integrated medical electronic system field provides great opportunities and continual developing potential for life quality enhancement.

Acknowledgements

This work was supported in part by the Ministry of Education, Science, Research and Sport of the Slovak Republic under grant VEGA 1/0459/12 and by the Slovak Research and Development Agency under the contracts APVV-0819-12 and APVV-0496-12.

References

[1] Penders J, Altini M, van de Molengraft J, Romero I, Yazicioglu F, Van Hoof C. A low-power wireless ECG necklace for reliable cardiac activity monitoring on the move. In proceeding of the 33rd Annual International IEEE EMBS Conference, Boston, 2011.

[2] Chuo Y, Marzencki M, Hung B, Jaggernauth C, Tavakolian K, Lin P, Kaminska B. Mechanically Flexible Wireless Multisensor Platform for Human Physical Activity and Vitals Monitoring. *Biomedical Circuits and Systems*, *IEEE Transactions on*, 4(5): 281-294, 2010.

[3] Texas Instruments (2012). Low-Power, 2-Channel, 24-bit Analog Front-End for Biopotential Measurements (Rev. B). [Online] Available: http://www.ti.com

[4] Atmel (2014). Datasheet - 8/16 bit Atmel XMEGA A3U Microcontroller. [Online] Available: http://www.atmel.com

[5] STMicroelectronics (2010). MEMS digital output motion sensor, ultra low-power high performance 3-axes “nano” accelerometer. [Online] Available: http://www.st.com.

[6] MindMedia (2012). NeXus-10 MKII
[Online] Available: http://www.mindmedia.info/CMS2014

AUTHORS INDEX

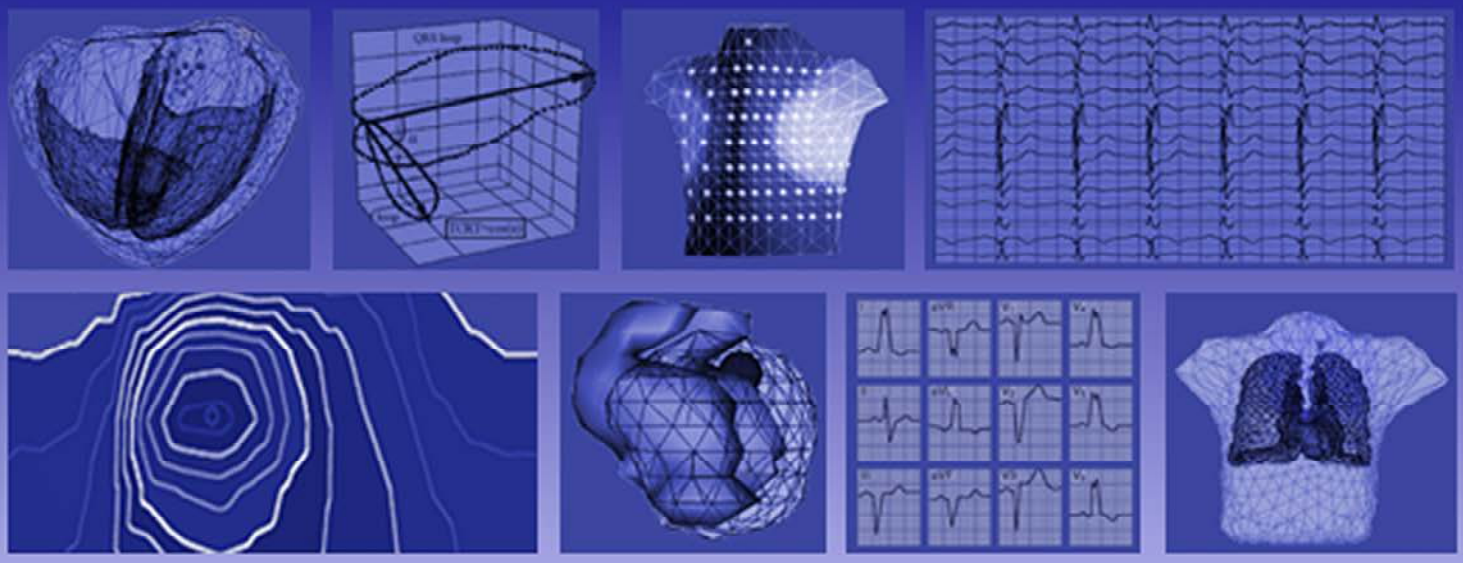

ISBN 978-80-969-672-7-8